CD95R-Fc coated Microparticle Delivery to Cancer Cells

Heather Alice Ruth Baldie

A thesis submitted for the degree of
Doctor of Philosophy

2018

Centre for Cutaneous Research

The Blizard Institute

Barts and The London School of Medicine and Dentistry

Queen Mary, University of London

Acknowledgements

I would like to thank my supervisor, Professor Kenny Linton, for his teaching, patience, constant support and guidance throughout my PhD. Thank you for keeping me on track. I am grateful to my second supervisor, Dr Davidson Ateh, for his guidance and for allowing me to study the technology he developed.

To past and present members of the Linton Lab, Dave and Ouma especially, thank you for everything. I have been incredibly lucky to have such wonderful people work beside me as Postdocs, who I can call friends for life. To my 'Bay Babes' – Ouma, Deb, Joanna, Viviana, Clare, Hephzi and Emily, thank you for being such inspirational, intelligent and hardworking women. I am so grateful that I got to sit, work and laugh beside you all. Thank you to everyone at the Blizard and my best friends, Anke, Hannah, Elly & Emma for your never-ending support. Thank you to my support at home, Muzz and Nick, for putting up with me, my constant moaning and for always being there. Also, my best friend Anna, for putting a smile on my face at the most difficult of times and for always believing in me, even when you are hundreds of miles away. To Mon, Nish, Nicole, Katie, Ashleigh and Claire, for being there and for your patience when I couldn't be around.

Finally, and most importantly, I dedicate this thesis to my amazing Mum. I am so lucky to have grown up with such an inspirational female role model. It is the strength you show in such difficult times that has carried me forward and allowed me to finish this piece of work. I'm so grateful to be able to share this milestone in my life with you. Dad, thank you for watching over me and for believing in me from day one. I hope I have made you proud.

Statement of Originality

I, Heather Alice Ruth Baldie, confirm that the research included within this thesis is my own work or that where it has been carried out in collaboration with, or supported by others, that this is duly acknowledged below and my contribution indicated. Previously published material is also acknowledged below.

I attest that I have exercised reasonable care to ensure that the work is original, and does not to the best of my knowledge break any UK law, infringe any third party's copyright or other Intellectual Property Right, or contain any confidential material.

I accept that the College has the right to use plagiarism detection software to check the electronic version of the thesis.

I confirm that this thesis has not been previously submitted for the award of a degree by this or any other university.

Signature: Heather Baldie

Date: 24/11/2018

This work was supported by the Medical Research Council, grant number RRPF-QMICMN1.

Abstract

Triple-negative breast cancers lack the three main breast cancer biomarkers; oestrogen-, progesterone- or HER2-receptors and chemotherapy is the only established treatment option for patients. Chemotherapies are associated with physically debilitating, off-target toxicities and tumours often develop resistance to cytotoxic compounds. Nanomedicine has the potential to improve chemotherapy efficacy and has enabled the development of small, therapeutic carriers such as microparticles (MPs). These can be made from biodegradable polymers, loaded with (sometimes poorly soluble) chemotherapeutic agents and their surfaces coated in tumour targeting proteins. CD95L has been reported to be upregulated in cancer cells identifying it a promising target. In this study, the CD95 receptor, CD95R, was fused to the Fc region of human IgG1, and baculoviral-mediated expression was optimised in Sf21 and Hi5 insect cells. The protein was purified by affinity chromatography and used to coat microparticles. CD95R-coated MPs improved the uptake into triple-negative, MDA-MB-231 cells, ostensibly via a mechanism involving CD95L. Anti-CD95L antibodies were validated following expression of CD95L-Myc-DDK in otherwise naïve HEK293T cells. The expression of supposed target ligand CD95L was then tested in MDA-MB-231 cells and found to be undetectable. Furthermore, the CD95R-coated particles were efficiently taken up by non-cancerous primary fibroblasts. The reasons for the enhanced uptake of CD95R-coated MPs were explored in MDA-MB-231 cells. Differences in the surface charge of the coated-MPs, characterised by dynamic light scattering (DLS) and electrophoresis, were ruled out as a cause. However, inhibition of the common endocytic pathways did suggest that coated-MP uptake likely occurs via macropino- or phagocytosis. The use of this system for targeted cancer treatment or for wider applications are discussed.

Contents

List of Figures

List of Tables

List of Equations

Abbreviations

12His	12xHistidine
Å	Angstrom
AA	Antibiotic/Antimycotic
aa	Amino Acid
AcMNPV	*Autographa californica* multiple nucleopolyhedrovirus
ADAM10	A Disintegrin and metalloproteinase domain-containing protein 10
AFU	Arbitrary Fluorescence Units
AICD	Activation-induced Cell Death
ALPS	Autoimmune Lymphoproliferative Syndrome
APS	Ammonuium Persulphate
AU	Airy Unit
BAC	Bacterial Artifical Chromosome
BAR	Bin, Amphiphysin and Rvs
BRCA1	Breast Cancer Type 1 Susceptibility Gene
BRCA2	Breast Cancer Type 2 Susceptibility Gene
BSA	Bovine Serum Albumin
BV	Budded Virions

CD36	Cluster of Differentiation 36
CD59	Cluster of Differentiation 59
CD63	Cluster of Differentiation 63
CD95L	Cluster of Differentiation 95 Ligand
CD95R	Cluster of Differentiation 95 Receptor
CDC42	Cell Division Control Protein 42
CHO	Chinese Hamster Ovary
cm	Centimetres
CMV	Cytomegalovirus
CT	Chemotherapy
Daoy	Desmoplastic Cerebellar Medulloblastoma
DAPI	4’,6-diamidino-2-phenylindole
DcR3	Decoy Receptor 3
DCIS	Ductal Carcinoma in situ
DD	Death Domain
dH_2O	Distilled Water
DICE	Death Induced by CD95R/L Elimination
DISE	Death Induced by Survival gene Elimination
DISC	Death-inducing Signalling Complex

DLPs	Dynamin-like Proteins
DLS	Dynamic Light Scattering
DMEM	Dulbecco's Modified Eagle's Medium
DMSO	Dimethyl Sulfoxide
DNA	Deoxyribonucleic Acid
cDNA	Complementary DNA
DOC	Deoxycholate
E1 – 4	Elution 1 – 4
EC_{50}	Half-maximal Effective Concentration
ECD	Extracellular Domain
ECL	Enhanced Chemiluminescence
EDTA	Ethylenediaminetetraacetic acid
EGF	Human Epidermal Growth Factor
ELISA	Enzyme-linked Immunosorbent Assay
ELMO1	Engulfment and Cell Motility Protein 1
Endo-H	Endoglycosidase-H
ERP	Enhanced Permeability and Retention
ER	Oestrogen Receptor
Erk1/2	Extracellular Signal-related Kinase 1/2

ET	Endocrine Therapy
EVs	Extracellular Vesicles
Fab	Fragment antigen-binding
FAC	Fluorouracil, Doxorubicin and Cyclophosphamide
FADD	Fas-associated Death Domain
FBS	Fetal Bovine Serum
Fc	Fragment Crystallisable Region
FcR	Fc Receptos
FEC	Fluorouracil, Epirubicin and Cyclophosphamide
FITC	Fluorescein Isothiocyanate
FT	Flow Through
GDP	Guanosine Diphosphate
GFP	Green Fluorescence Protein
Gld	Generalised Lymphoproliferative Disease
Grb2	Growth Factor Receptor-bound Protein 2
GTP	Guanosine Triphosphate
HEK	Human Embryonic Kidney
HER2	Human Epidermal Growth Factor Receptor 2
HMVECs	Microvascular Endothelial Cells

HPLC	High Performance Liquid Chromatography
HRP	Horseradish Peroxidase
IBC	Inflammatory Breast Cancer
ICD	Intracellular Domain
IGF-1	Insulin like Growth Factor 1
IgG1	Immunoglobulin G1
IF	Immunofluorescent
IL	Interleukin
IMAC	Immobilised-metal Affinity Chromatography
JNK1/2	c-Jun N-terminal Kinase 1/2
Jun	Transcription Factor AP-1
Kbp	Kilobase pair
kDa	Kilodalton
KIM-1	Kidney Injury Molecule 1
LacCer	Lactosylceramide
Lamp-1/2	Lysosomal-associated Membrane Protein 1/2
LB	Lysogeny Broth
LCIS	Lobular Carcinoma in situ
LDS	Lithium Dodecyl Sulphate

Lpr	Lymphoproliferation
M	Molar
mA	Milliamps
mAb	Monoclonal Antibody
MARCO	Macrophage Receptor with Collagenous Structure
MAP	Mitogen-Activated Protein
ml	Millilitre
mm	Millimetre
mM	Millimolar
MMP	Matrix Metalloproteinases
MOI	Multiplicity of Infection
MPs	Microparticles
mV	Millivolts
MVBs	Multivesicular Bodies
MWCO	Molecular Weight Cut-off
NA	Numerical Aperture
NF-κβ	Nuclear Factor kappa-light-chain-enhancer of activated B cells
ng	Nanograms
NK	Natural Killer

nm	Nanometres
NPs	Nanoparticles
NSO	Mouse Myeloma cells
OET	Oxford Expression Technologies
ORF	Open Reading Frame
OV	Occluded Virions
PAGE	Polyacrylamide Gel Electrophoresis
PBS	Phosphate Buffered Saline
PBS-T	PBS-Tween
PCR	Polymerase Chain Reaction
PDI	Polydispersity Index
PEI	Polyethyleneimine
PFA	Paraformaldehyde
PGE	Prostaglandin E_2
PGP	P-glycoprotein
pH	Potential of Hydrogen
PIP2	Phosphatidylinositol-4,5-biphosphate
PLGA	Poly(lactic-co-glycolic acid)
PM	Plasma Membrane

PNGase-F	Peptide-N-glycosidase-F
PR	Progesterone Receptor
PVDF	Polyvinylidene Fluoride
RAC	Ras-related C3 Botulinum Toxin Substrate
Ran	RAs-related Nuclear protein
RCC1	Regulator of Chromosome Condensation 1
RhoA	Ras Homolog gene family, member A
RNA	Ribonucleic acid
RPM	Rotations Per Minute
RT	Radiation therapy
RT-qPCR	Real-time Quantitative PCR
sCD95L	Soluble CD95L
SDS	Sodium Dodecyl Sulphate
SFM	Serum Free Media
SH3	Src Homology 3
shRNA	Short Hairpin RNA
siRNA	Small Interfering RNA
SM	Starting Material
SOC	Super Optimal broth with Catabolite repression

SPA/Protein-A	Staphylococcal Protein A
SPPL2A	Signal Peptide Peptidase Like 2A
SV40	Simian Virus 40
TCA	Trichloroacetic Acid
TEMED	Tetramethylethylenediamine
TLP	Templated Lipoprotein Nanoparticles
TNBC	Triple Negative Breast Cancer
TNF	Tumour Necrosis Factor
UTR	Untranslated Region
VEGF-A	Vascular Endothelial Growth Factor A
W1 – 3	Wash 1 – 3
WASP	Wiskott-Aldrich Syndrome Protein
X-gal	5-bromo-4-chloro-3-indolyl ß-D-galactopyranoside
µg	Microgram
µl	Microlitre
µM	Micromolar
µm	Micrometre

1. Introduction

1.1. Breast cancer

1.1.1. Breast cancer epidemiology

Breast cancer is the most common form of cancer among women, impacting 2.1 million women in 2018, accounting for almost 1 in 4 female cancer cases (Bray et al., 2018). In 2018, it is estimated that 627,000 women died from breast cancer, representing 15% of all cancer deaths among women (Bray et al., 2018). Breast cancer incidence rates are highest in Australia/New Zealand, Northern Europe (such as the UK, Sweden, Finland and Denmark), Western Europe, Southern Europe and Northern America (Bray et al., 2018). While breast cancer rates are higher among women in more developed countries, rates are increasing in nearly every region globally.

1.1.2. Risk factors for breast cancer

Hereditary and genetic factors, including a personal or family history of breast or ovarian cancers, and inherited mutations (in *BRCA1*, *BRCA2* and other breast cancer susceptibility genes) account for only 5 – 10% of breast cancer cases (Bray et al., 2018). Studies of migrants have shown that non-hereditary factors are the major drivers of breast cancer incidence and comparisons of low-risk populations migrating to high-risk populations have revealed that breast cancer incidence rates rise in successive generations (Ziegler et al., 1993). Elevated incidence rates are attributed to higher prevalence of known risk factors related to menstruation (early age at menarche, later age at menopause), reproduction (nulliparity, late age at first birth, fewer children), exogenous hormone intake (oral

contraceptive use and hormone replacement therapy), nutrition (alcohol intake) and anthropometry (greater weight, weight gain during adulthood and body fat distribution); whereas breastfeeding and physical activity are known protective factors (Bray et al., 2018, Schottenfeld and Fraumeni Jr, 2006).

1.1.3. Breast cancer types

Breast cancer can be classified in a number of ways to assist the clinical diagnosis and management of patients. Histologically, breast cancer is classified depending on whether the cancer has arisen from the ducts or the lobules of the breast. Ductal carcinoma in situ (DCIS) arises from clonal proliferation and atypical hyperplasia of cells from the terminal and lactiferous (glandular) ducts of the breast tissue, confined within the epithelial basement membrane. Invasive ductal carcinoma arises once the cells have invaded through this basement membrane (Harris et al., 2004). The majority of invasive forms of breast cancer (80%) arise from the ducts of the breast. The remaining cases of breast cancer evolve from the terminal duct-lobular apparatus; lobular carcinoma in situ (LCIS), which can also break through the basement membrane and become invasive (Frykberg, 1999). In contrast to ductal carcinoma, lobular carcinomas tend to be slower growing (Korkola et al., 2003). Inflammatory breast cancer (IBC) arises when cancer cells grow along and block the lymph vessels of the breast. IBCs are the most virulent form of breast cancer, characterized by involvement of the skin and rapid progression of the disease (Woodward and Cristofanilli, 2009).

Another important form of classification for breast cancers is their hormone receptor status. Breast cancers are routinely tested for the presence or absence

of three key proteins; the oestrogen receptor (ER), the progesterone receptor (PR), and the human epidermal growth factor (EGF) receptor 2 (HER2). The presence of these receptors provides tumourigenic benefits and, crucially, they are targeted by endocrine therapies (see section 1.1.5). Luminal ER-positive, HER2-negative (ER+HER2–) breast cancer, which is characterised by expression of the ER but absence of *HER2* amplification, accounts for 70% of all breast cancers (Turner et al., 2017). HER2 positivity accounts for about 15 – 20% of breast cancers (Loibl and Gianni, 2017). The other ~15 – 20% of breast tumours express none of these three markers and are collectively referred to as triple-negative breast cancers (TNBCs; ER−, PR−, HER2−) (Kalimutho et al., 2015). TNBCs are a heterogeneous subtype of breast cancer which are prevalent in younger women (under 40 years of age), and have a poor clinical outcome (Kalimutho et al., 2015).

1.1.4. Breast cancer treatments

The aim of treating in situ or locally invasive breast cancer is ultimately curative and directed towards preventing recurrence. The main types of treatment for breast cancer are surgery, radiation therapy (RT), chemotherapy (CT) and endocrine (hormone) therapy (ET) (Nounou et al., 2015). Breast conservation surgery is the trending approach for the treatment of localised breast cancer (DCIS) (Matsen and Neumayer, 2013). Surgery can be preceded by neoadjuvant therapy to shrink the tumour, and followed by adjuvant therapy to minimize the risk of metastases (Nounou et al., 2015). RT, where cancer cells are exposed to a high level of radiation directly, can then be utilised to kill cells that are missed during surgery (Dhankhar et al., 2010). For other types of breast cancer, a

mastectomy is recommended, followed by a mix of RT, ET or CT after surgery, as required.

1.1.5. Endocrine and HER2-directed therapy

Oestrogen is the main hormone involved in the development and growth of breast tumours (Smith and Dowsett, 2003). The purpose of ET is to balance or block oestrogen and is indicated in all patients with detectable ER expression (Nounou et al., 2015). The choice of medication is determined by a patient's menopausal status, differences in drug efficacy and side effect profile. For example, premenopausal women are usually prescribed Tamoxifen, which is an ER antagonist. Postmenopausal women however, are normally offered aromatase inhibitors which suppress plasma oestrogen levels by inhibiting aromatase, the enzyme responsible for the synthesis of oestrogens from androgenic substrates (Smith and Dowsett, 2003). Breast cancers which express the HER2 receptor can be treated with targeting drugs such as Trastuzumab (Herceptin®). This is a monoclonal antibody that inhibits ligand-independent HER2 signalling, inhibits the shedding from the extracellular domain and can trigger antibody-dependent cellular cytotoxicity (Loibl and Gianni, 2017). Trastuzumab is often given in combination with CT (such as taxanes), or given as an antibody-drug conjugate, such as Kadcyla (Trastuzumab-Emtansine); Emtansine is a cytotoxic, microtubule-inhibitory agent (Loibl and Gianni, 2017). For TNBC patients however, no targeted therapies are available, and CT will be recommended in the vast majority of cases.

1.1.6. Chemotherapy for breast cancer

The benefit from CT in breast cancer is more pronounced in ER-negative tumours. CT will be recommended for TNBC, HER2-positive or metastatic breast cancers. Adjuvant CT for treating breast cancer usually involves anthracycline-containing combinations of drugs. These combinations include Fluorouracil, Doxorubicin and Cyclophosphamide (FAC) or Fluorouracil, Epirubicin and Cyclophosphamide (FEC). More recently however, taxane based chemotherapeutics, such as paclitaxel and docetaxel, are used in combination with anthracycline regimes to reduce the chance of cancer metastasis. A meta-analysis of 13 randomised trials concluded that administration of paclitaxel resulted in a 5% absolute reduction in recurrence of breast cancer (disease-free survival) in contrast to 3% with the use of anthracyclines (De Laurentiis et al., 2008). Paclitaxel (commercially known as Taxol) exerts its anti-cancer activity in a unique way, by polymerising and stabilising microtubules and inducing apoptosis. It is used to treat a wide range of cancers, including breast cancer.

1.2. Chemotherapy

1.2.1. Limitations of chemotherapies

Adjuvant CT, used to treat breast cancer and many other types of cancer, are commonly associated with major and debilitating physical side effects. The side effects of Paclitaxel therapy for example, include neutropenia, alopecia and neurotoxicity (de Weger et al., 2014). This systemic toxicity is due to the non-specific nature of chemotherapeutic agents affecting both normal and cancerous cells (Danhier et al., 2010). Additionally, paclitaxel is very poorly soluble in aqueous solutions which makes drug delivery challenging. As a result, Taxol

preparations contain toxic cremophor and ethanol to solubilise the drug for clinical applications (Ateh et al., 2011). Cremophor causes further side effects in patients such as serious hypersensitivity reactions (Wang et al., 2012) and patients often require premedication with steroids and antihistamines (Wood et al., 1995, Ateh et al., 2011). Cytotoxic drug treatment is also limited by drug metabolism and clearance mechanisms often involving the overexpression of drug transporter proteins, which can efflux drugs from cancer cells (Fletcher et al., 2010). These issues highlight the need for treatments which target directly to cancer cells to ensure delivery of the optimum dose of drug, in order to improve patient survival and quality of life.

1.2.2. Targeted cancer treatments

Nanomedicine has the potential to improve the efficacy of CT treatments. By combining nanotechnology and medicine, this field of research has enabled the development of small particle, therapeutic carriers such as microparticles (MPs) (Wang et al., 2012). MPs can be made from biodegradable polymers such as poly(lactic-co-glycolic acid) (PLGA), loaded with chemotherapeutic agents and their surfaces functionalised by coating or opsonising with targeting proteins (Kohane, 2007). These targeting proteins are selected to bind to tumour-specific markers, allowing uptake and internalisation of MPs into tumour cells (Wang et al., 2012). Upon internalisation, PLGA MPs degrade into lactic and glycolic acids which can be readily excreted or metabolised by the body, making them biocompatible (Jain et al., 2000). This drug delivery system has been shown to result in higher drug concentrations within solid tumours and lower off-target toxicity (Wang et al., 2012). MPs can be loaded with drugs including those that

are too toxic to be administered intravenously or those that are poorly soluble (Wang et al., 2012) removing the need for toxic additives in the formulation to overcome the solubility issue. MPs therefore offer the potential advantages of improved bioavailability and sustained and controlled drug release within the target cell (Kohane, 2007).

1.3. The TNF family

The tumour necrosis factor (TNF) family of proteins consist of more than 20 proteins with a broad range of functions including control of cell death, immune differentiation and regulation (Fulda and Debatin, 2006). Members of this family are trimeric ligands which bind their corresponding trimeric receptors. The TNF receptors share similar cysteine-rich extracellular domains (ECD) and a cytoplasmic death domain (DD) (Fulda and Debatin, 2006). The cysteine-rich domains are thought to fold independently and are stabilised by extensive, intra-chain disulphide bonding (Orlinick et al., 1997). The DDs are required to transduce death signals from the cell surface to intracellular signalling pathways (see section 1.4.2) (Fulda and Debatin, 2006).

1.4. CD95R

1.4.1. CD95R topology

Human CD95R (Fas/APO-1/TNFRSF6) belongs to the TNF receptor family and is localised to the plasma membrane, where is has been shown to assemble into homotrimers even in the absence of ligand (Siegel et al., 2000). CD95R mediates apoptosis when bound to its natural ligand, CD95L (CD178/TNFSF6) (section

1.4.2). It is ubiquitously expressed in the body, but is particularly abundant in the thymus, liver, heart and kidney (Peter et al., 2015). Human, full length CD95R is a 45kDa, type I transmembrane protein with 335 amino acids (Orlinick et al., 1997). It has a 25 amino acid (aa) signal peptide, a 148 aa ECD (rich in cysteine residues), a 17 aa transmembrane alpha-helix, and a 145 aa cytoplasmic death domain. There are two N-linked glycosylation sites in the ECD (N118 and N136) (Shatnyeva et al., 2011). N-linked glycosylation is introduced upon entry of the polypeptide into the lumen of the endoplasmic reticulum and involves the transfer of a carbohydrate moiety to an asparagine residue within a specific amino acid consensus sequence (N-X-S/T) (Shatnyeva et al., 2011). As a type I transmembrane protein, the N-terminal region of CD95R is extracellular. Full length CD95R has not been crystallised however, a part of the ECD (corresponding to amino acids 52 – 129 in full length CD95R; Figure 1.1) has been crystallised in complex with Fab fragment E09 (PDB; 3THM); the structure was resolved to 2.1Å and shows extended loops and turns with anti-parallel β-strands, with no helices (Chodorge et al., 2012).

1.4.2. CD95R and apoptosis

The CD95R death receptor is well known for its involvement in programmed cell death and tissue homeostasis by the immune system (Chen et al., 2010). Apoptosis is a regulatory mechanism of programmed cell death, which is vital for maintaining tissue homeostasis. Apoptosis can proceed through two main pathways (extrinsic/receptor-mediated and intrinsic/mitochondrially mediated) (Iverson and Orrenius, 2004). Upon activation by its ligand CD95L, CD95R can trigger apoptosis via the extrinsic pathway (Shatnyeva et al., 2011). A CD95L

trimer binds three CD95R molecules, resulting in the conformational change of the receptors' DDs (Nisihara et al., 2001). The DDs then recruit the adaptor protein Fas-associated death domain (FADD) to which procaspase-8 can bind (Sayers, 2011). The resulting complex of proteins is called the death-inducing signalling complex (DISC). Caspase-8 is released from DISC, which goes on to activate effector caspase-3, caspase-6 and caspase-7 (Ashkenazi, 2008). This cascade of reactions subsequently leads to apoptosis. This pathway is one that is activated indirectly by chemotherapeutic agents such as doxorubicin, methotrexate and bleomycin (Meza-Lamas et al., 2006) upregulating CD95R expression and inducing autocrine or paracrine expression of CD95L (Meza-Lamas et al., 2006, Wesselborg et al., 1999).

Figure 1.1. Crystallised fragment of human CD95R ectodomain.
The structure of the crystallised fragment of CD95R ECD, corresponding to amino acids (aa) 52 - 129 in full length human CD95R. The fragment was crystallised in complex with Fab fragment E09 (not shown). Arrows represent ß-strands, C129 is the C-terminal aa and L52 is the N-terminal aa. Structure was resolved to 2.1 Å (PDB; 3THM) (Chodorge et al., 2012).

1.4.3. CD95R/L and the immune system

The CD95L/R system also plays an important role in immune system homeostasis (Voss et al., 2008). Activation-induced cell death (AICD) is a homeostatic mechanism used by the immune system to control T-cell responses and prevent autoimmunity by promoting tolerance to self-antigens (Askenasy et al., 2005). After activation, T cells express CD95R and CD95L and with repeated antigenic stimulation become sensitive to CD95R/L-mediated autocrine and paracrine apoptosis (Dhein et al., 1995). This serves to regulate immune responses and control the pool of antigen-activated T cell clones (Askenasy et al., 2005). CD95R- and CD95L- deficient mice (*lpr/lpr* and *gld/gld,* respectively) suffer autoimmune diseases (Takahashi et al., 1994a). A lpr (lymphoproliferation) mutation in mice causes defective CD95R expression, resulting in lymphadenopathy and systemic lupus erythematosus-like autoimmune disease (Watanaba et al., 1992). Gld (generalised lymphoproliferative disease) mice express a mutant form of CD95L, suffering from a phenotype similar to lpr mice, including lpr and autoimmune disease (Peter et al., 2015). Additionally, a genetic disorder in humans is caused by mutations in CD95R/L, called autoimmune lymphoproliferative syndrome (ALPS), resembling mice with lpr and gld mutations, respectively (Peter et al., 2015).

1.4.4. CD95R and cancer

CD95R is often downregulated during cancer progression (Chen et al., 2010) and it is thought that this may be a cancer-specific mechanism for survival, in order to avoid apoptotic-induced cell death. However, complete loss is rarely seen and reducing CD95R expression has also been found to have a growth inhibiting

effect in many cancer cell lines (colon, renal, breast and liver) (Chen et al., 2010) suggesting the involvement of CD95R in non-apoptotic activities. For example, CD95R, via a pathway involving JNK and Jun, promotes growth of ovarian and liver cancer in mouse models (Chen et al., 2010). Once cancer cells acquire resistance to CD95R-mediated apoptosis, further stimulation of CD95R is tumorigenic (Peter et al., 2015). CD95R signalling has been shown to increase the motility and invasiveness (migration through Matrigel-coated membranes) of 22 apoptosis-resistant cancer cell lines (Barnhart et al., 2004). This occurs via three signalling pathways resulting in activation of NF-κB and Erk1/2, and involves active caspase-8 and urokinase plasminogen activator (Barnhart et al., 2004). In a study using cells from ALPS patients, as well as cellular and mouse model systems, non-apoptotic signalling through CD95R involved activation of NF-κß and the three MAP kinases, Erk1/2, JNK1/2 and p38 (Barnhart et al., 2004, Legembre et al., 2004a, Legembre et al., 2004b). The elimination of CD95R/L was previously reported to kill cancer cells via a unique form of cell death, labelled DICE (death induced by CD95R/L elimination) (Ceppi et al., 2014). However, more recent publications suggest this effect is not due to loss of CD95R or CD95L, but the result of unique off-target effects from the siRNAs and shRNAs designed against CD95R and CD95L (Putzbach et al., 2017). This is discussed in more detail in Chapter 4 (section 4.1.5).

1.5. CD95L

1.5.1. CD95L structure

Human CD95L is a 40kDa protein with 281 amino acids belonging to the TNF superfamily (Takahashi et al., 1994b, Suda et al., 1993). It has an 179 aa ECD,

a 22 aa transmembrane alpha-helix, an 80 aa cytoplasmic domain (Takahashi et al., 1994b) and as a type II transmembrane protein, the C-terminal region of CD95L is extracellular. The protein has 3 N-linked glycosylation sites in the ECD (N184, N250 and N260) and one intramolecular disulphide bond (C202 – C233) (Voss et al., 2008) and self-associates to form homotrimers. CD95L can be released from the cell surface producing a soluble form of the protein which remains trimeric. The topology and features of CD95L are discussed in more detail in Chapter 4 (section 4.1.1).

A fragment of the CD95L ECD (amino acids 143 - 281) has been crystallised as a trimer, in complex with the decoy receptor DcR3 (PDB; 4MSV); the structure was resolved to 2.5Å (Figure 1.2 and 1.3) (Liu et al., 2014). In Figure 1.2A, a monomer of the crystallised fragment of CD95L ECD is shown. The structure shows eleven β-strands, arranged in two anti-parallel β-sheets. The positions of the three N-linked glycosylation sites are indicated with the asparagine side chains shown in stick format and coloured elementally on the monomeric CD95L ECD fragment in Figure 1.2B, which is shown interacting with a monomer of DcR3. Decoy receptor 3 is a secreted member of the TNF family, which is typically expressed at low levels in healthy individuals but is highly elevated in various cancers, likely serving as a mechanism for tumour immune evasion (Bai et al., 2000). DcR3 has been shown to prevent the induction of apoptosis of cancer cells by CD95L-expressing immune cells, by blocking CD95L interaction with CD95R (Strasser et al., 2009).

There are two points of interaction between CD95L and DcR3 (Figure 1.2B), which may provide insight into the CD95L:CD95R recognition surface, which is yet to be co-crystallised. For Figure 1.2B, the sequences of the crystallised fragment of the CD95R ECD (Figure 1.1) and the crystallised DcR3 were aligned and the region of homology is shown in orange, indicating a similar CD95L binding region. The homologous region of the crystallised fragment of CD95R ECD aligns to amino acids 14 – 83 in the crystallised DcR3 and amino acids 46 – 115 in full length, human DcR3. In Figure 1.3, the functional complex/hexamer (Liu et al., 2014; personal communication; PDB; 4MSV) that forms between trimeric CD95L and DcR3 is shown. Figure 1.3A shows a side view of the complex and Figure 1.3B shows a view of the complex, looking down onto the CD95L expressing cell. This may be a similar arrangement to the CD95L:CD95R functional complex, with two trimeric forms of the proteins interacting.

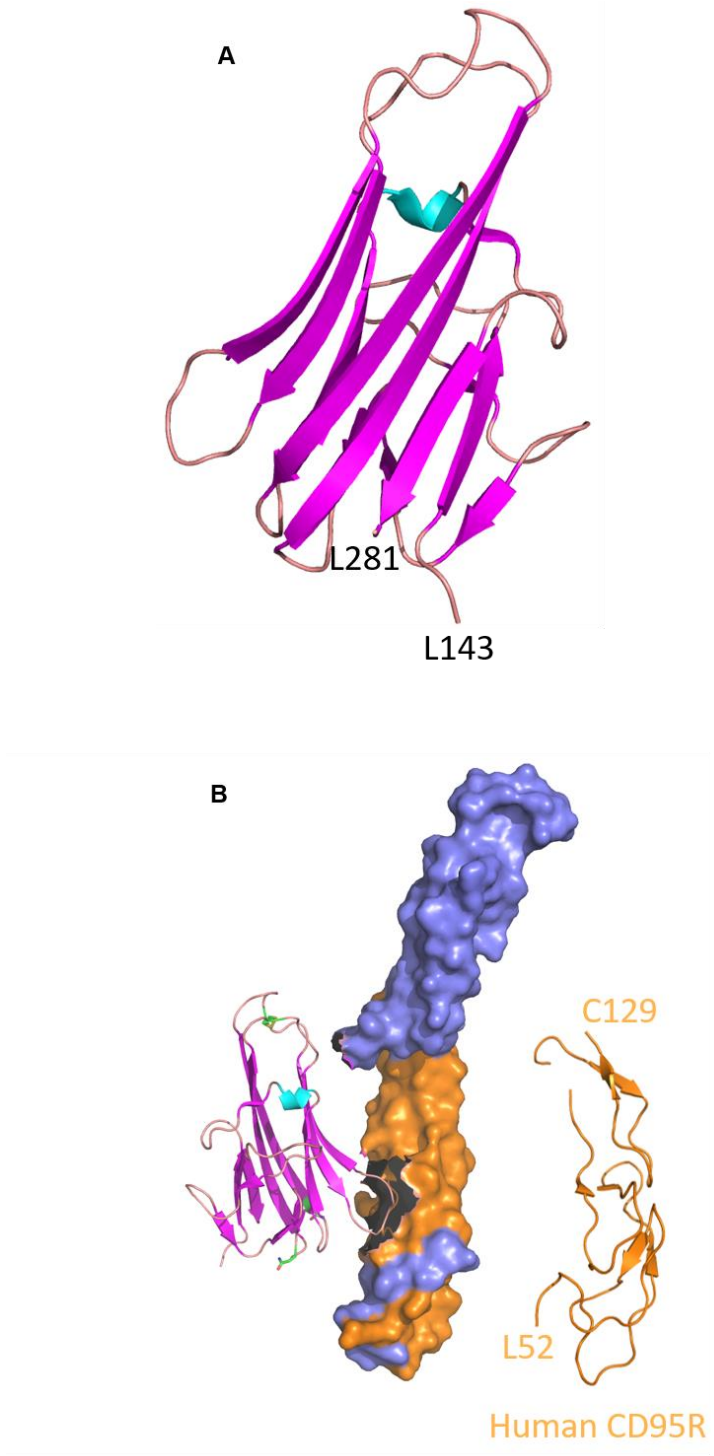

Figure 1.2. Crystallised fragment of human CD95L ectodomain in complex with DcR3. (**A**) The structure of a monomer of the crystallised fragment of CD95L ECD, corresponding to amino acids (aa) 143 - 281 in full length human CD95L is shown in cartoon format. Pink arrows represent ß-strands, while the only helical secondary structure is shown in cyan. L143 is the N-terminal aa and L281 is the C-terminal aa. (**B**) The CD95L ECD fragment was crystallised in complex with DcR3 (Decoy Receptor 3). A monomer of CD95L ECD (shown in cartoon format) is shown here interacting with a monomer of DcR3 (shown with surface rendering in slate and orange). The asparagines of the 3, N-linked glycosylation sites of CD95L (N184, N250 and N260) are shown in stick format and coloured elementally. The region of DcR3 that is homologous with the crystallised fragment of CD95R ECD (Figure 1.1 and aligned here on the right) is coloured orange in the surface rendered cartoon. The homologous region of the crystallised fragment of CD95R ECD aligns to aa 14 – 83 in the crystallised DcR3 and aa 46 – 115 in full length, human DcR3 (PDB; 4MSV) (Liu et al., 2014).

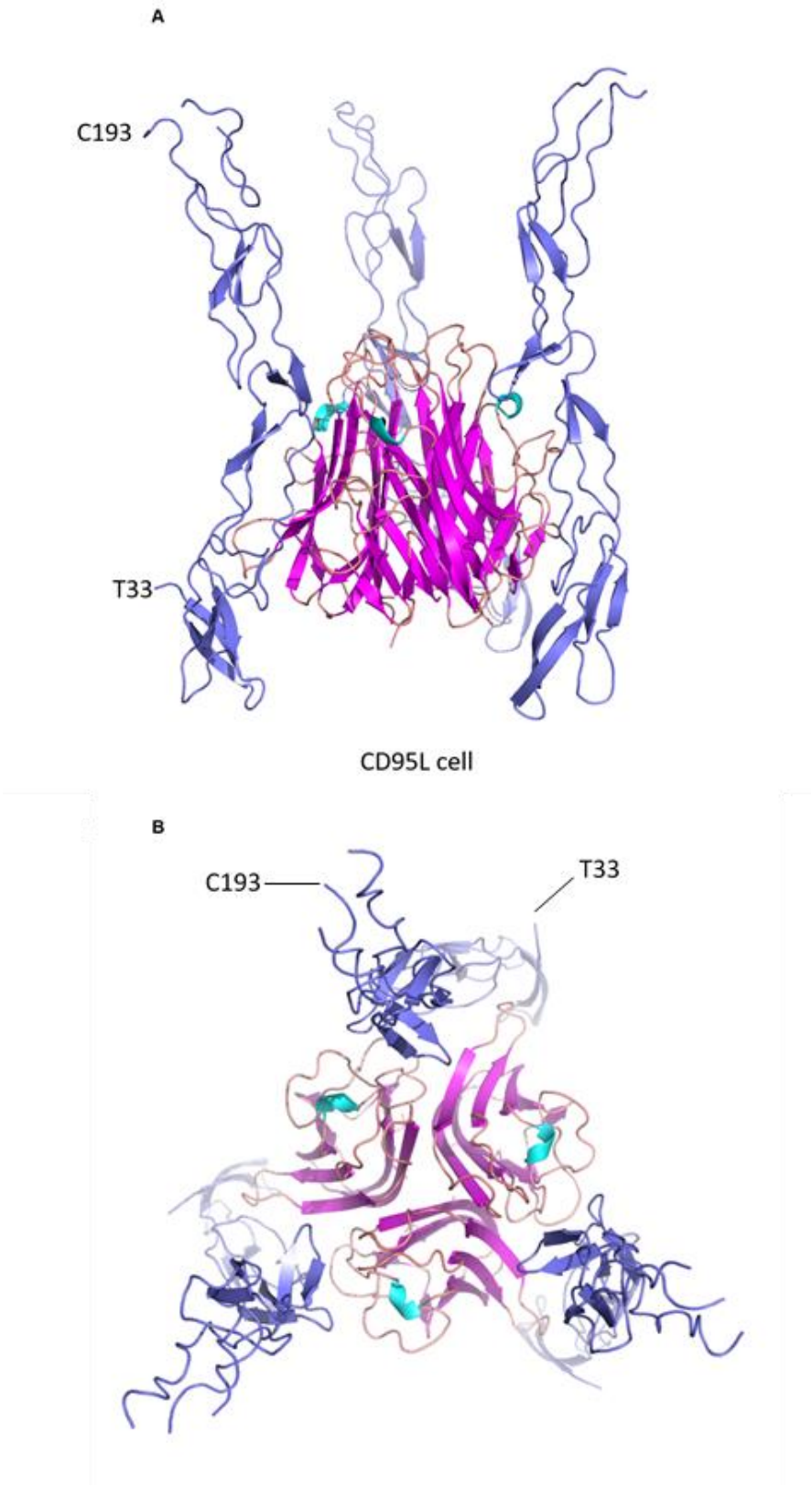

Figure 1.3. The functional complex of trimeric, crystallised CD95L ectodomain and DcR3. (**A**) A side view of the complex between the trimeric, crystallised fragments of CD95L ECD interacting with DcR3. The bottom of the image demonstrates the location of the CD95L expressing cell. CD95L is shown coloured by secondary structure (predominantly pink), while DcR3 is coloured blue (**B**) The complex viewed from above, looking down onto the CD95L expressing cell. C193 is the N-terminal amino acid (aa) of DcR3 and T33 is the C-terminal aa (Liu et al., 2014; personal communication; PDB; 4MSV) (Liu et al., 2014).

1.5.2. CD95L and the concept of immune privilege

CD95L is expressed in immune-privileged sites such as epithelial cells in the eye, neurons and astrocytes of the central nervous system and Sertoli cells in the testis (Griffith et al., 1995, Voss et al., 2008). The purpose of this is to prevent inflammation, by inducing apoptosis of CD95R-positive cells which may invade such tissues (Griffith et al., 1995, Linkermann et al., 2005).

1.5.3. CD95L and cancer

CD95L is normally expressed by immune cells such as natural killer (NK) cells to induce apoptosis (Ateh et al., 2011), however its expression has been linked to tumour cells. The expression of CD95L by tumours has long been thought to provide a counterattack against the immune system, killing infiltrating T cells and preventing apoptosis. However, the counterattack theory has been subject to debate, as CD95L-expressing tumours are rapidly rejected and induce inflammation in mice (Igney and Krammer, 2005). Recently, CD95L expression has been detected in the endothelium of vascularised solid human and mouse tumours, but not in normal vasculature, suggesting a role in immune tolerance of the tumour similar to the immune privilege of the CNS, testes and the eye (Motz et al., 2014). The expression of CD95L in the endothelial cells of the vasculature is thought to be induced by common factors in the tumour microenvironment such as tumour-derived vascular endothelial growth factor A (VEGF-A), interleukin 10 (IL-10) and prostaglandin E_2 (PGE). The evidence for and against expression of CD95L by tumour cells has changed drastically since a key paper was published in 2017 (Putzbach et al., 2017) and warrants careful reappraisal of the literature.

This paper and the complex issues surrounding this topic are explained in more detail in Chapter 4.

1.7. The CD95R ECD for targeted chemotherapeutic delivery

A paper published in 2011 by Ateh et al., found a novel use for CD95R in a chemotherapeutic, drug delivery system using microparticles. By coating or opsonising the surface of MPs (>0.5 µm in diameter) with the extracellular domain of CD95R fused to the Fc region of human IgG1 (CD95R-Fc) they could enhance the uptake of MPs in a range of cells including neurones, medulloblastoma, breast and ovarian cancer cells, *in vitro* (Ateh et al., 2011). Initially, 0.5 and 1µm, fluorescent polystyrene particles were coated with commercially available CD95R-Fc and uptake was tested using flow cytometry and confocal microscopy in these different cell types. In each case, CD95R-Fc opsonisation led to increased uptake in comparison to non-coated particles or IgG (to control for the -Fc domain) coated particles. For example, in MDA-MB-231 cells (a highly invasive, triple-negative, breast adenocarcinoma cell line) the uptake of 0.5µm MPs increased from 15% to around 70% when coated with CD95R-Fc (Ateh et al., 2011). Interestingly, increased uptake of CD95R-Fc coated particles could be prevented in Daoy (desmoplastic cerebellar medulloblastoma) cells by preincubating the cells with CD95R-Fc for a minimum of 15 minutes (Ateh et al., 2011). Uptake was also tested using PLGA, biodegradable MPs, loaded with ethidium homodimer, a membrane impermeable nucleic acid dye. Coating in CD95R-Fc increased ethidium homodimer uptake by Daoy cells by nearly 10-fold compared to excess dye added directly to cell cultures (Ateh et al., 2011). Paclitaxel-loaded, PLGA particles were then tested, and with a CD95R-Fc

coating, they were cytotoxic to Daoy cells to a similar extent as dose-matched, free Paclitaxel.

Drug delivery, using the paclitaxel-loaded PLGA particles, was then investigated in two different *in vivo* models. The first used a subcutaneous xenograft of Daoy medulloblastoma cells in NOD/SCID (a type of immunodeficient) mice. PLGA MPs with or without a paclitaxel cargo and with or without CD95R-Fc coating were injected directly into the tumour and the percentage change in tumour volume was recorded for 7 days. An equivalent dose of free paclitaxel was also injected to compare to the MP treatments. Paclitaxel-loaded PLGA particles, regardless of coating, inhibited tumour growth to a greater extent than paclitaxel alone after a single intratumoural injection (Ateh et al., 2011). There was also an effect with placebo PLGA particles (CD95R-Fc coated PLGA particles without paclitaxel) which was attributed to CD95R-Fc interfering with CD95R/L mediated tumour proliferation. The result observed with uncoated, drug-loaded particles was thought to be due to the large MPs being retained within the tumour, enabling local release of the paclitaxel. In this experiment, the CD95R-Fc coating did not provide any measurable benefit to the reduction in tumour volume. However, the same MPs were tested in a murine model of peritoneal ovarian cancer dissemination (IGROV1-luciferase expressing cancer cells), a more clinically relevant cancer model (Ateh et al., 2011). All treatments were administered via intraperitoneal injection. Live imaging showed a >65-fold reduction in tumour bioluminescence by week 4 with the CD95R-Fc coated, paclitaxel-loaded MP treated group, compared with an equivalent dose of Taxol (paclitaxel dissolved in

Cremophor and ethanol) (Ateh et al., 2011). In this case, non-coated, drug-loaded MP treatment matched Taxol, and both placebo treatments were ineffective.

1.7.1. Proposed mechanism and benefits of CD95R-coated MPs for drug delivery

Since there was a large database of evidence for the expression of CD95L by cancer cells (but rebutted in Chapter 4), it was hypothesised that the enhanced uptake of CD95R-Fc coated MPs was due to a CD95R:CD95L interaction. More specifically, the CD95R on the surface of the MP was thought to bind to the CD95L on the surface of the cancer cell initiating an internalisation mechanism, possibly phagocytosis. Phagocytosis is commonly associated with professional phagocytes of the innate immune system, such as macrophages and neutrophils (Rabinovitch, 1995). However “non-immune” cells including cancer cells, also have phagocytic capacity which is regulated by poorly understood cell membrane signals (Rabinovitch, 1995, Ateh et al., 2011). This could explain why pre-incubating cells with CD95R-Fc prevented MP uptake, since free CD95R-Fc would bind to and block the cell surface CD95L, preventing interaction with the coated particles. If this mechanism is correct, CD95R-Fc coated particles could provide a targeted, chemotherapeutic, drug delivery method, improving intracellular drug concentrations and removing the need for toxic paclitaxel preparations (as described in section 1.2.2). However, there was very little, direct evidence to demonstrate the tumour expression of CD95L in the *in vivo* models used to test uptake in the 2011 study. Immunofluorescent (IF) staining of CD95L in the cancer cell lines used *in vitro* was presented. However, the anti-CD95L antibody used for IF was not stated nor validated. A more detailed investigation

was therefore warranted to seek evidence of CD95L expression and determine the route of uptake of the CD95R-Fc coated MPs.

1.8. Objectives of the current study

The exact mechanism of CD95R-coated particle uptake is not known. More evidence is needed to demonstrate the involvement of CD95L, and whether it is expressed by cancer cells. Characterising the pathways involved in MP uptake and the CD95R/CD95L targeting mechanism will be important for optimising the delivery of chemotherapeutics to their intended site of action. For this study, uptake mechanisms will be investigated primarily in MDA-MB-231 cells, a triple-negative, breast cancer cell line. TNBC is not only prevalent in younger women with a poor clinical outcome but no targeted therapies are available, and chemotherapy is the front-line treatment option. An improved drug delivery system for chemotherapeutics, such as targeted PLGA MPs, would be well suited for these patients to reduce major and debilitating physical side effects.

The primary objectives of this study were to develop an expression and purification system to purify significant amounts of CD95R-Fc suitable for uptake studies in MDA-MB-231 cells (Chapter 3), to determine the expression level of CD95L by this cell line (Chapter 4) and to investigate potential mechanisms of uptake (Chapter 5).

1.9. Project aims

- Express and purify CD95R-Fc
- Formulate CD95R-Fc coated microparticles to test targeted delivery to cancer cells
- Understand the efficacy of the targeting mechanism by investigating CD95L expression in the cancer cells of interest
- Characterise the mechanisms involved in coated microparticle uptake

2. Materials and Methods

2.1. Bacteria culture medium

Lysogeny Broth (LB):	1% tryptone, 0.5% yeast extract, 1% NaCl
LB Agar:	1% tryptone, 0.5% yeast extract, 1% NaCl
SOC Medium:	2% tryptone, 0.5% yeast extract, 0.05% NaCl, 0.02% KCl, 0.04% glucose, 0.01M $MgCl_2$, 0.01M $MgSO_4$

Solid or liquid growth media were supplemented with ampicillin to a final concentration of 100µg/ml or kanamycin to final concentration of 50µg/ml.

2.2. Bacterial culture and storage

Bacteria were grown in liquid growth media with shaking (230rpm), or on plates in an incubator set to 37°C. Bacteria were frozen for long term storage at -80°C in a mixture of LB medium and 15% glycerol.

2.3. Molecular biology

2.3.1. Plasmids

The baculovirus transfer vector, Mouse CD95R/Fc_pOET1, was provided by OET, encoding mouse CD95R ectodomain (residues 1 - 169), linker region (residues 170 - 177), and Fc portion of human IgG (residues 178 - 407) (see Figure 3.2 for amino acid sequence). Briefly, the cDNA sequence for Mouse CD95R-Fc fusion protein was optimised for expression in insect cells with additional 5' *Xba*I, 5' UTR (AACTCCTAAAAAACCGCCACC), stop codon (TAA) and 3' *Sma*I sequences. The gene was synthesised and the sub-cloned into pOET1 transfer plasmid.

The mammalian expression plasmid pCMV6-FasLG, coding for CD95L with a C-terminal, Myc-DDK tag, was provided by BioMoti and purchased from OriGene (RC204894; Figure 2.1).

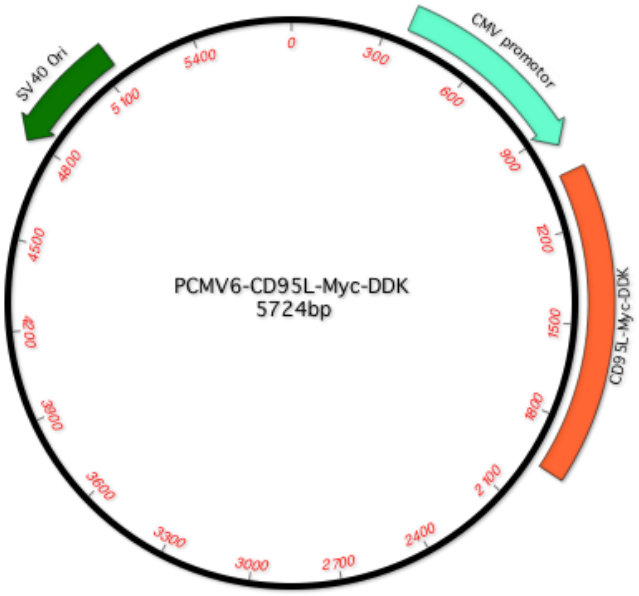

Figure 2.1. pCMV6-CD95L-Myc-DDK plasmid map
Map of the pCMV6, mammalian expression plasmid (Origene) which expresses CD95L-Myc-DDK. Map displays the Simian Virus 40 (SV40) origin of replication (ORI), the cytomegalovirus (CMV) promotor and the CD95L-Myc-DDK gene.

The pCMV6 vector (OriGene) permits high level and efficient expression of recombinant proteins in mammalian cells, under the control of the strong cytomegalovirus (CMV) promoter (Schmidt et al., 1990). Additionally, it contains the Simian Virus 40 (SV40) origin of replication, which enables the vector to replicate in cells which express the SV40 T antigen (such as HEK293T cells) (Gluzman, 1981).

Plasmids were also used as controls. pTracer-CD36 (which expresses human CD36 attached to a green fluorescent protein, GFP) and pCINeoCD36-12His (which expresses human CD36 ECD with a C-terminal 12 histidine tag and an N-

terminal honeybee melittin secretory signal) were used as transfection controls and provided by Kenneth Linton.

2.3.2. Preparation of plasmid DNA

Plasmid DNA preparations were generated using the QIAGEN plasmid midi kits (for up to 100µg of plasmid DNA) following the manufacturer's protocol (QIAGEN). 100µl of bacteria (from a 3ml overnight culture) were used to inoculate a 100ml culture and grown overnight at 37°C with vigorous shaking. Cells from the 100ml culture were harvested by centrifugation for 15 minutes at 6000xg at 4°C. The cell pellet was resuspended in 4ml Buffer P1 (resuspension buffer; 50mM Tris-Cl, pH 8.0, 10mM EDTA, 100ug/ml RNase A). Once the cell pellet was completely resuspended, 4ml of Buffer P2 (lysis buffer; 200mM NaOH, 1% SDS) added to the solution, mixed by inversion and incubated at room temperature for 5 minutes. Nucleic acids and proteins within the lysate were subsequently denatured due to the alkalinity of the Lysis buffer. Following incubation in Lysis Buffer, 4ml of Buffer P3 was added (neutralisation buffer; 3.0M potassium acetate, pH 5.5), the solution mixed and incubated on ice for 15 minutes, causing the aggregation of insoluble genomic DNA and high molecular weight RNA as well as the precipitation of protein-SDS complexes. To remove these aggregates, the lysate was centrifuged at ≥20,000xg for 30 minutes at 4°C, for two rounds. QIAGEN-tip 100 columns were prepared by adding 4ml of Buffer QBT (equilibration buffer; 750mM NaCl, 50mM MOPS, pH 7.0, 15% isopropanol, 0.15% Triton X-100). The supernatant from the cell lysate was then added to the prepared columns. The QIAGEN-tip was then washed with 2 x 10ml of Buffer QC (wash buffer; 1.0M NaCl, 50mM MOPS, pH 7.0, 15% isopropanol) before eluting

DNA with 5ml of pre-warmed, Buffer QF (elution buffer; 1.25M NaCl, 50mM Tris-Cl, pH 8.5, 15% isopropanol). DNA was precipitated by adding 3.5ml of isopropanol to the eluted DNA and the mix was centrifuged at ≥ 15,000xg for 30 minutes at 4°C. The supernatant was decanted, and the DNA pellet washed with 70% ethanol and centrifuged again at ≥ 15,000xg for 10 minutes. The supernatant was decanted, and the pellet left to air-dry for 5 minutes before re-dissolving in a suitable buffer, such as TE buffer (10mM Tris-Cl, pH 8.0, 1mM EDTA). Recovered plasmid DNA was quantified using a NanoDrop (ND-100, Thermo Scientific), measuring the optical density at a wavelength of 260nm. Estimation of purity of the plasmid DNA was achieved through measuring the A260:A280 ratio; a ratio of 1.8 - 2.0 was indicative of a pure sample.

2.4. Insect cell culture

2.4.1. Insect cell culture medium and reagents

For virus propagation and protein production, Sf21 cells were cultured in suspension, in Sf-900™ II Serum Free Media (SFM; Thermo Fisher Scientific) and Hi5 cells in Ex-cell 405 media (Sigma). For plaque assay, Sf21 cells were grown in TC-100 media (Thermo Fisher Scientific) supplemented with 10% Fetal Bovine Serum (FBS, Thermo Fisher Scientific). Both conditions included 1% antibiotic/antimycotic (AA; HyClone) to a final concentration of 100units/ml penicillin G, 100µg/ml streptomycin sulphate, and 25µg/ml amphotericin B. Cells were cultured at 27°C in a 311DS, Labnet obital shaker at 120rpm.

2.4.2. Insect cell co-transfection and baculovirus generation

Sf21 cells were co-transfected with the transfer vector (CD95R/Fc_pOET1) and *flash*BAC GOLD (Oxford Expression Technologies, OET) genomic DNA as instructed by the manufacturer. 1 x 10^6 cells/2mls were seeded onto a 3.5cm tissue culture dish (BD Biosciences) in TC100 medium without FBS or antibiotics.

For the co-transfection, the following reagents were mixed:

100ng	Baculoviral genomic DNA (*flash*BAC GOLD*)*
500ng	Transfer Plasmid (CD95R/Fc_pOET1)
1.2µl	baculoFECTIN II transfection reagent (OET)
100µl	TC100 media without FBS or antibiotics

The solution was gently mixed and incubated at room temperature for 15 - 20 minutes. Medium was then aspirated from the monolayer of insect cells and the baculoFECTIN II:DNA complex mixture added drop-wise to different areas of the dish. Each dish was then incubated overnight at 27°C in a humidified sealed box containing (lined with paper soaked in 50mM EDTA). After 24hrs, 1ml TC100 containing 10% FBS and antibiotics was added to each dish and incubated for a further 4 days, as before. Following incubation, the medium containing the recombinant virus p0 stock was harvested into sterile tubes.

Generation of FlashBAC ULTRA-CD95R-Fc was outsourced to OET. Recombinant virus was produced by co-transfection of flashBACULTRA viral

DNA and CD95R/Fc_pOET1 construct with baculoFECTIN liposome forming agent in Sf9 insect cells following a similar procedure as described above (OET; personal communication). A p1 stock was received from OET and amplified into a working stock (as described in section 2.4.4).

2.4.3. Plaque assay to determine baculovirus titre

Plaque assays were used to assess the titre of recombinant baculoviruses. Sf21 (1×10^6) cells, grown in TC-100 media, were seeded onto 3.5cm dishes to give 50% confluency. Media was aspirated and 200µl of virus stock diluted to 10^{-4}, 10^{-5} and 10^{-6} was added to duplicate dishes. The dishes were incubated for 1 hour at room temperature. The supernatant was aspirated and replaced with 1.5ml 1% seaplaque, low meting temperature agarose in 75% TC-100. The agarose was left at room temperature to set and then overlaid with 1ml TC-100. The dishes were incubated in a sealed box lined with tissue soaked in 10mM EDTA. After 3 days incubation, 1ml of 0.03% neutral red in phosphate-buffered saline (PBS) was added to each dish and incubated at 27°C for 2 hours. The media and stain were then aspirated, the dishes inverted and left at room temperature in the dark overnight. Neutral red stains live cells, allowing the visualisation of virus plaques of lysed or dying cells as clear regions within the red background monolayer.

2.4.4. Amplification of baculovirus stocks

To obtain working stocks, baculovirus was amplified over a number of stages. At each stage the premise remains the same; with a low ratio of virus particles to insect cells (multiplicity of infection; MOI) used to permit cell growth to continue whilst allowing multiple cycles of viral infection, replication and budding to occur.

p0 to p1 stock amplification (flashBAC GOLD virus)

A suspension culture containing 25ml Sf21 insect cells at a density of 2 x 10^6 cells/ml in Sf900 II SFM media was infected with 500µl p0 viral stock. The cells were incubated overnight, before being diluted with 25ml of fresh Sf900 II SFM media. After a total of 5 days, the cells were removed by centrifugation at 2060xg for 10 minutes at 4°C. The supernatant was recovered and stored at 4°C as p1 stock. The baculovirus titre was calculated by plaque assay.

p1 stock to working stock amplification (flashBAC GOLD and ULTRA viruses)

100ml of Sf21 cells, at a density of 2 x 10^6 cells/ml in Sf-900™ II SFM, were infected with p1 virus stock resulting in a multiplicity of infection (MOI) of 0.1 virus particle per cell, according to the viral titre determined by plaque assay. The cells were incubated overnight, before being diluted with 100ml of fresh Sf900 II SFM media. After incubation for 5 days at 27°C, the cells were removed by centrifugation at 2060xg for 10 minutes at 4°C. The supernatant was recovered and stored at 4°C as a working stock (WS).

2.4.5. Small-scale infection for protein production

In order to determine the time course and MOI required for CD95R-Fc expression, 10ml cultures of Sf21 cells in Sf-900™ II SFM or Hi5 cells in Ex-cell 405 media, at a density of 1 x 10^6 cells/ml, were infected with WS at different MOI, 0.1, 1 and 3 (with one uninfected, control culture), and incubated for 5 days at 27°C. 500µl of each culture was sampled every 24 hours over the 5 day period, spun at 9600xg in a microcentrifuge to remove the insect cells, and the

supernatant recovered for analysis by western blot (see section 2.7.7, 2.7.8 and 2.7.11).

In order to produce protein which would go on to be purified, 10ml cultures of Sf21 cells in Sf-900™ II SFM or Hi5 cells in Ex-cell 405 media, at a density of 1 x 10^6 cells/ml, were infected with WS. Sf21 cells were infected at a MOI of 0.1 and incubated for 5 days, whereas Hi5 cells were infected at a MOI of 3 and incubated for 3 days, at 27°C. Cells the cells were removed by centrifugation at 2060xg for 10 minutes at 4°C. The supernatant was recovered and bound directly to protein-A resin (see section 2.7.1).

2.5. Mammalian Cell Culture

2.5.1. Cell lines, medium and reagents

Monolayers of triple negative, human breast adenocarcinoma cell line MDA-MB-231 were cultured in Dulbecco's Modified Eagle's Medium (DMEM, Thermo Fisher Scientific) with high glucose (4.5 g/L) supplemented with 5% (v/v) FBS (Sigma). MDA-MB-231 cells were kindly provided by Cleo Bishop.

Monolayers of human embryonic kidney (HEK293T) cells were cultured in DMEM (Thermo Fisher Scientific) with high glucose (4.5 g/L) supplemented with 10% (v/v) FBS (Sigma). HEK293T cells were kindly provided by Kenneth Linton.

Monolayers of primary dermal fibroblasts (isolated from a 42 year old female, facelift patient) were cultured in DMEM (Thermo Fisher Scientific) with high glucose (4.5 g/L) supplemented with 10% (v/v) FBS (Sigma). Primary dermal fibroblasts were kindly provided by Cleo Bishop.

All cells were cultured with additional penicillin-streptomycin (Sigma; diluted to a final concentration of 100 units penicillin and 0.1 mg/ml streptomycin) at 37°C with 5% CO_2 in a water saturated atmosphere. Adhered MDA-MB-231 cells were removed using Versene (Thermo Fisher Scientific). All other adhered cells were removed using TrypLE Express or trypsin EDTA (Thermo Fisher Scientific). All cells were washed with sterile-filtered, phosphate buffered saline (PBS), pH 7.4 (Sigma). All manipulations were performed in a sterile environment, with disposable plastic ware and glassware.

2.5.2. Transfection reagents

Cells were transfected with the cationic polymer polyethyleneimine (PEI) (Sigma). PEI was prepared by dissolving 45mg PEI in 8ml sterile water, corrected to pH 7.2 with dilute HCl, filtered through a sterile filter (0.2µm) and kept at RT. Glucose, 5% (w/v) was prepared by dissolving 2.5g glucose in sterile water, passed through a sterile filter (0.2µm) and kept at room temperature.

2.5.3. Inhibitor preparation and storage

The inhibitors used to block CD95L-sheddases were GM1006 (Merck), a cell permeable, broad spectrum MMP inhibitor (of MMP - 1, 2, 3, 7, 8, 9, 12, 14, 26)

and GI254023X (Sigma), which is marketed as selective ADAM10 inhibitor. Both inhibitors were resuspended in dimethyl sulphoxide (DMSO), an organic solvent, and aliquots stored at -20°C. Both inhibitors were used at a working concentration of 20µM.

Inhibitors were also used to block endocytic pathways. Inhibitors of macropinocytosis were Cytochalasin D (Santa Cruz) used at 20µM and 5-(N,N-dimethyl)-Amiloride hydrochloride (Amiloride; Cayman Chemical) used at 50µM. Inhibitors used to block clathrin-dependent endocytosis were Chlorpromazine (Santa Cruz) used at 15µM and Dynasore monohydrate (Santa Cruz) used at 50 µM. Inhibitors of caveolin-dependent endocytosis were Nystatin (Sigma) and Filipin III, from *Streptomyces filipienensis* (Sigma); both used at 50nM. Mannan, from *Saccharomyces cerevisiae* (Sigma) was used at 1mg/ml to block mannose-receptor mediated endocytosis and Nocodozole (Sigma) was used at 5µM to block microtubule involvement in particle internalisation. All inhibitors were solubilised in DMSO and aliquots stored at -20°C, except Mannan, which was dissolved in H_2O and stored at 4°C.

2.6. Mammalian cell (HEK293T) transfection

2.6.1. For western blot and flow cytometric analysis

HEK293T cells (3 x 10^5) were seeded as a monolayer on 6-well plates (Nunclon) in 2ml DMEM, 24 hours prior to transfection. The transfection mixture included 5µg DNA (pCMV6-FasLG (CD95L); Origene) at a concentration of 1 µg/µl, with 0.5% glucose (w/v) adjusted to a final volume of 8.5µl with sterile water. Then

1.5µl PEI was added followed by DMEM (2ml), before applying to cells. The cells were harvested 48 hours post transfection and either lysed (see section 2.7.6) or analysed by flow cytometry (see section 2.9.3). For inhibitor experiments, 24 hours post transfection, the media was aspirated from cells, they were washed with 2ml PBS and then incubated with 20µM GM1006 or 20µM GI254023X, or both inhibitors in combination, for 24 hours, in 2ml, FBS-free DMEM with high glucose (4.5 g/L; Thermo Fisher Scientific). 24 hours later, the cells were harvested and analysed by flow cytometry (see section 2.9.3).

2.6.2. For immunofluorescent staining

HEK293T cells (3 x 10^5) were seeded as a monolayer on 6-well plates (Nunclon) in 2ml DMEM. Before seeding, sterile 18mm coverslips were placed into each well and treated with 1ml Poly-L-Lysine (Sigma) for 1 hour at room temperature. Cells were transfected 24 hours later (see section 2.6.1). Cells were fixed 48 hours post transfection (see section 2.10) and immunostained. For inhibitor experiments, cells were treated as previously described (see section 2.6.1) and then immunostained.

2.7. Protein Biochemistry

2.7.1. Batch purification of CD95R-Fc

12ml of spent insect culture was incubated with 125, 250 or 500µl MabSelect, protein-A resin (slurry in 20% ethanol; GE Healthcare) overnight, at 4°C. The resin was spun at 228xg using a swing out rotor, to form a pellet and then washed three times by resuspension in 5ml sterile PBS (pH 7.4), spinning each time to

pellet the resin before the next wash. The protein was eluted in 4 x 1ml, 100mM citric acid (pH 3) spinning between each elution to pellet the resin.

2.7.2. Dialysis

CD95R-Fc protein from the first elution fraction was buffer exchanged into PBS (pH 7.4) using a Slide-A-Lyzer Dialysis Cassette (10K MWCO) (Thermo Scientific), following the manufacturer's protocol. Briefly, the elution was added to the dialysis cassette and dialysed against 300x the volume of sample with dialysis buffer (PBS), in a beaker at 4°C for 1 hour with gentle stirring. The process was repeated for another hour with fresh dialysis buffer and then allowed to dialyse overnight in a third batch of dialysis buffer.

2.7.3. PD-10 column for buffer exchange

Buffer exchange was performed using a PD-10 desalting column (GE Healthcare), following the manufacturers protocol. The column was equilibrated with 25ml PBS (pH 7.4) only or PBS with additional BSA (50ug BSA for every 1ug CD95R-Fc) and the first elution (E1) fraction added. A following 7 x 1ml of PBS only or PBS & BSA was added, collecting each fraction separately. 25ml of PBS only was then run through the column to wash it, and it was stored in 20% ethanol at 4°C.

2.7.4. Trichloroacetic acid precipitation of protein samples

Protein solutions were precipitated using trichloroacetic acid (TCA) prior to separation by SDS-PAGE (see section 2.7.7 and 2.7.8). 0.15% DOC was made

by dissolving 75mg sodium deoxycholate in 50ml H_2O. The solution was stirred to give a uniform slurry. 0.8M NaOH was added drop-wise until the solution cleared. On ice, DOC was added to the protein sample (10% of the protein sample volume) and incubated for 5 min. 72% TCA was added (10% of the protein sample volume) and incubated on ice for 10 minutes. The sample mixture was spun at 14000xg in a microcentrifuge for 20 minutes and the supernatant removed. The protein pellet was resuspended in 4% SDS, 0.2M Tris (pH 7.5), 0.15M NaOH (pH 10) and loading buffer added (see section 2.7.7) before separation by SDS-PAGE (section 2.7.8).

2.7.5. MDA-MB-231 and primary dermal fibroblast, whole-cell extracts

MDA-MB-231 cells or primary dermal fibroblasts (2 x 10^6 or otherwise specified) were pelleted at 3000xg, media aspirated and cells washed in 1ml PBS. A 5x stock of lysis buffer was made (5% sodium dodecyl sulphate (SDS) in PBS, 750mM NaCl, 50mM HEPES). Cells were resuspended in 250µl PBS and 250µl 2x lysis buffer (consisting of 400µl 5x lysis buffer, 40µl, 20x protease inhibitor cocktail (Roche), 20µl EDTA (0.5M, pH 8), 1µl (25 U/µl) Benzonase® Endonuclease (Novagen) and made up to 1ml with PBS). The endonuclease was allowed to act for 15 min at room temperature before DNA was sheared using a 21-gauge then a 25-gauge needle. Samples were centrifuged at 17,000xg for 15 minutes at 4°C to remove any insoluble material. The supernatant was collected in fresh tubes and stored at -80°C.

2.7.6. HEK293T whole-cell extracts

48 hours post transfection (see section 2.6.1), HEK293T cells (1 x 10^6) were pelleted at 3000xg, media aspirated, and cells washed in 1ml PBS. Whole-cell extracts were then prepared as previously described (see section 2.7.5).

2.7.7. Preparation of protein samples for SDS-polyacrylamide gel electrophoresis (SDS-PAGE)

Protein samples or whole-cell extracts were mixed with 4 x LDS sample buffer (Life Technologies) plus 4% (CD95R-Fc protein samples) or 8% (whole-cell extracts) 2-mercaptoethanol and incubated at 75°C for 5 minutes prior to loading the gel. For expression tests (Figure 3.3 and 3.4) samples were heated to 90°C for 3 minutes.

2.7.8. SDS-PAGE

Proteins were separated by electrophoresis through vertical 1.0mm thick polyacrylamide gels (0.1% SDS, 10% or 8% acrylamide), using the procedure described by Laemmli (Laemmli, 1970). The required reagents and volumes to make the resolving (8% and 10%) and stacking gels, along with SDS-PAGE running buffer are described in Table 2.1. The stacking gel was overlaid onto polymerised separating gel after addition of tetramethylethylenediamine (TEMED) and ammonium persulphate (APS) to initiate polymerisation. Gels were run at 120 volts (V) in SDS-PAGE running buffer for 2 hrs or until the dye front had reached the bottom of the gel.

Resolving gel (8%/10% - 5ml):	2.3ml/1.9ml H_2O
	1.3ml/1.7ml acrylamide mix (30% acrylamide/bis-acrylamide mix (37.5:1 ratio); National Diagnostics)
	1.3ml 1.5M Tris (pH 8.8)
	50µl 10% SDS
	50µl 10% ammonium persulphate
	3µl/2µl TEMED
Stacking gel (3ml):	2.1ml H_2O
	500µl acrylamide mix (National Diagnostics)
	380µl 1.5M Tris (pH 8.8)
	30µl 10% SDS
	30µl 10% ammonium persulphate
	3µl TEMED
SDS-PAGE running buffer:	25mM Tris-HCl
	190mM Glycine
	1% SDS

Table 2.1. SDS-PAGE stacking and resolving gels and SDS-PAGE running buffer
The required reagents and volumes to make 8% or 10% resolving gels and stacking gels along with SDS-PAGE running buffer.

2.7.9. Colloidal blue staining

Following separation by SDS-PAGE, proteins were visualised by fixing the gel (50% methanol, 7% acetic acid) for 15 minutes. The gels were then washed 3 times for 5 minutes with dH_2O and stained in GelCode® Blue Stain Reagent (Thermo Scientific) o/n. Gels were then destained by washing 3 times for 5 minutes, and overnight in dH_2O.

2.7.10. Protein quantification and purity

For BSA protein quantification, BSA standards (1, 0.8, 0.6, 0.4 and 0.2 µg) were made in PBS (pH 7.4) and run alongside protein samples using SDS-PAGE and stained with colloidal blue. The gel was scanned and the density of the BSA standards were measured using ImageJ software (NIH) and the standard curve plotted using GraphPad Prism software (version 5). Using the BSA standard curve, the linear equation (Equation 2.1.) was used to measure the concentration of protein based on the density of protein bands.

$$y = mx + c$$

Equation 2.1. The Linear Equation
m = gradient of the straight line and c = the y intercept

Percentage purity of a protein sample was calculated after SDS-PAGE and staining of the gel, using ImageJ. The pixels in a lane containing a protein sample was compared to a blank lane, to account for any background signal on the gel (Figure 2.2A).

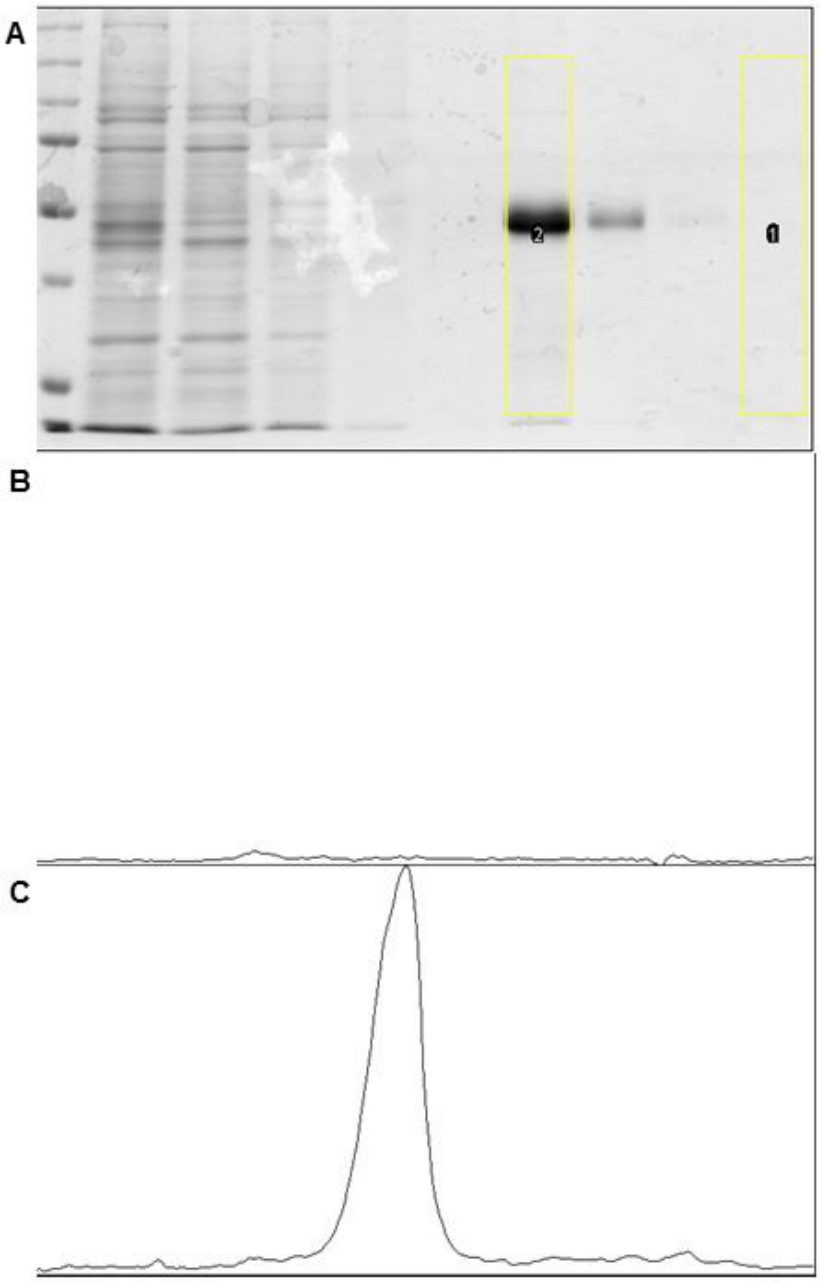

Figure 2.2. Calculating percentage purity using ImageJ.
(**A**) Example gel with a blank lane (yellow box 1) and a lane containing a protein sample (yellow box 2). (**B**) Total amount of pixels in the blank lane of the gel, representing background noise. (**C**) The total amount of pixels in the lane containing the protein sample. The large peak demonstrates the protein of interest which is calculated as a percentage in comparison to the total pixels in the lane, minus the background noise.

The pixels in the peak for the protein of interest (Figure 2.2C) are then calculated as a percentage in comparison to pixels in the rest of the lane (minus any background pixilation in the blank lane (Figure 2.2B)), which describes the presence of contaminating proteins. The resulting percentage is the level of purity of the protein of interest.

2.7.11. Western Blot

Samples were separated by SDS-PAGE (see section 2.7.8) and transferred onto a polyvinylidene fluoride (PVDF) membrane (Roche Diagnostics). The PVDF membrane is activated by soaking in 100% methanol followed by washing in dH_2O. The membrane along with 3mm filter paper (Whatman) was then soaked in transfer buffer (25 mM Tris-HCl, 190 mM Glycine and 5% Methanol). Electroblotting was carried out at 400 mA for 1 hour using a Mini Trans-blot cell (Biorad) with an ice pack, according to manufacturer's protocols. Following transfer, the membrane was blocked for 1 hour at room temperature in blocking buffer containing 5% w/v skimmed milk powder in PBS-tween (PBS-T, 0.1% v/v Tween 20 in PBS (pH 7.4)). Membranes were washed in PBS-T and then incubated overnight at 4°C with the required primary antibody (see table 2.2. for primary antibodies and dilutions) in 5% milk, PBS-T. Membranes were washed 3 times in PBS-T for 10 minutes and incubated for 1 hour at room temperature with secondary antibody polyclonal goat anti-mouse immunoglobulins-HRP (Dako) at a 1:10,000 dilution for HEK293T whole-cell lysates and at a 1:2000 dilution for MDA-MB-231 and primary dermal fibroblast whole-cell lysates, for detection of CD95L. For detection of CD95R-Fc, no primary antibody was used; membranes were incubated for 1 hour at room temperature with 1:100,000 dilution (in 5%

milk, PBS-T) of anti-human IgG (Fc specific)-Peroxidase (Sigma). Membranes were washed 3 times in PBS-T for 10 minutes, and bound antibody was detected using Immobilon™ Western, Chemiluminescent HRP Substrate (Millipore) and visualised on ECL Hyperfilm™ (GE Healthcare).

Primary Antibody	**Supplier**	**Dilution**
Mouse, anti-human CD178 (CD95L) clone G247-4	BD Pharmingen	1:1000
Mouse, anti-c-MYC	Sigma	1:4000
Mouse, anti-FLAG, clone M2	Sigma	1:4000
Monoclonal anti-β-tubulin, produced in mouse	Sigma	1:4000
Mouse, anti-human PI3-Kinase C2β	BD Biosciences	1:1000

Table 2.2. Primary antibodies used for protein detection via Western Blot.
Antibody names, suppliers and dilutions used.

2.7.12. Glycosidase digestion of glycoproteins

Proteins were deglycosylated using Peptide-N-glycosidase-F (PNGase-F) or Endoglycosidase-H (Endo-H) (New England Biolabs) according to manufacturer's protocol. Briefly, 1 – 20µg of protein was incubated for 10 minutes with denaturing buffer (0.5% SDS, 1% 2-mercaptoethanol) at 100°C, and then on ice for 2 min. 500U of PNGase-F was added with G7 buffer (50mM Sodium Phosphate, pH 7.5) supplemented with 1% NP40, or 1000U of Endo-H was

added with G5 buffer (0.5M Sodium Citrate, pH 5.5). Samples were incubated at 37°C for 2 hours. Control samples were also prepared in the same way, without PNGase-F or Endo-H in order to compare any shift in protein mobility following SDS-PAGE.

2.8. Microparticle opsonisation (coating)

Dragon Green fluorescent, 0.53µm polystyrene microparticles (MPs; 530nm; FS03F/5069) were pre-formed by Bangs Laboratories, USA. Spherical polystyrene microparticles (MPs) were pulse-vortexed for one minute before use. They were coated by physical adsorption with 0.5µg CD95R-Fc protein (expressed in-house, with or without additional BSA, or commercially-sourced from OET or Sigma) or human IgG – Fc fragment (Abcam) per 1µg MP, or sham coated in PBS (negative control). For BSA (Sigma), an excess was used for coating (80µg BSA: 1µg MP). Coating mixtures were made up to 100µl using PBS and incubated at 37°C for 90 minutes with mixing every 20 minutes.

2.9. Flow cytometric analysis

2.9.1. Flow cytometric analysis of microparticle uptake

MDA-MB-231 cells or primary dermal fibroblasts (1.4 x 10^5) were seeded in 6-well plates (Nunclon) in DMEM (Thermo Fisher Scientific) supplemented with 2% (v/v) FBS (Sigma) and cultured for 24 hours. MPs were coated (see section 2.8) and were added to the cells (4.05 x 10^6 per well) and incubated for a further 24 hours. Unbound MPs were removed by washing each well of cells 3 times with 2ml PBS, and gently tapping the sides of the 6-well plate to dislodge any particles.

Cells were harvested by adding 0.25% TrypLE™ Express (Thermo Fisher Scientific), neutralised with 2ml DMEM (Thermo Fisher Scientific) supplemented with 2% (v/v) FBS (Sigma), centrifuged at 228xg for 5 minutes and resuspended in 100µl PBS. Suspensions were analysed by flow cytometry (FACScan; Becton Dickinson). Data was acquired for 10,000 cells, gating on cells with normal size but including a large range of granularity (since MP uptake makes the cells appear more granular), using CellQuest™ Pro Software. Data were analysed using the FlowJo software package (Tree Star).

2.9.2. Flow cytometric analysis of microparticle uptake with endocytic inhibitors

MDA-MB-231 cells were seeded as previously described (section 2.9.1). 24 hours later, cells were pre-treated with each inhibitor for one hour (see section 2.5.3) in FBS free DMEM (Thermo Fisher Scientific), prior to incubation with coated MPs (see section 2.8) for 12 hours. Cells were then washed, harvested and analysed by flow cytometry as previously described (section 2.9.1).

2.9.3. Flow cytometric analysis of CD95L expression

HEK293T cells were transfected as described in section 2.6.1. Additionally, one well was transfected with 5µg P-tracer, full-length CD36 (GFP expressing) at a concentration of 2µg/µl, as a control for transfection efficiency, or with pCINeoCD36-12His (which expresses human CD36 ECD with a C-terminal 12 histidine tag and an N-terminal honeybee melittin secretory signal) at a concentration of 1µg/µl, as a "mock transfection" control. All cells were harvested 48 hours post-transfection using 1ml Versene (Thermo Fisher Scientific).

Versene was neutralised with 2ml DMEM (Thermo Fisher Scientific) supplemented with 10% (v/v) FBS (Sigma). Cells were counted and 1 x 10^6 transfected, untransfected and mock-transfected cells, and all harvested GFP-expressing cells, were pelleted at 220xg for 5 min and media aspirated. GFP-expressing cells were resuspended in 400µl phenol-red free DMEM (Sigma) supplemented with 1% (v/v) FBS (Sigma) in polypropylene FACS tubes (5ml; BD Biosciences) and stored at 4°C in the dark, ready for flow. Transfected, mock-transfected and untransfected cells were resuspended in 100µl phenol-red free DMEM (Sigma) supplemented with 1% (v/v) FBS (Sigma). 1µg of the primary antibody used (mouse anti-human CD178 (CD95L) NOK-1 clone (BioLegend), mouse, anti-human CD178 (CD95L) clone G247-4 or mouse, anti-c-MYC (Sigma)) was incubated with 1 x 10^6 cells in 100µl for 30 minutes at 4°C. The tubes were agitated every 5 minutes to maintain cells in suspension. Cells were then washed 3 times with 1ml, phenol-red free DMEM (Sigma) supplemented with 1% (v/v) FBS (Sigma), spinning at 220xg between washes to pellet the cells. 1µg of secondary antibody, goat, anti-mouse Alexa Fluor® 488 (Invitrogen) was incubated with 1 x 10^6 cells in 100µl for 30 minutes at 4°C. The tubes were agitated every 5 minutes to maintain cells in suspension. Cells were then washed 3 times with 1ml phenol-red free DMEM (Sigma) supplemented with 1% (v/v) FBS (Sigma), spinning at 220xg between washes to pellet the cells. Cells were resuspended in 400µl phenol-red free DMEM (Sigma) supplemented with 1% (v/v) FBS (Sigma) in polypropylene FACS tubes (5ml; BD Biosciences) and stored at 4°C in the dark. Suspensions were analysed by flow cytometry (FACscan; Becton Dickinson). Data was acquired for 10,000 cells of normal size and granularity using CellQuest™ Pro Software. Data were analysed using the FlowJo software package (Tree Star).

2.10. Immunofluorescent staining

HEK293T cells were cultured and transfected 24 hours post-seeding (see section 2.6.2). MDA-MB-231 cells (1.4 x 10^5) were seeded as a monolayer on 6-well plates (Nunclon) in 2ml DMEM. Before seeding, sterile 18mm coverslips were placed into each well and treated with 1ml Poly-L-Lysine (Sigma) for 1 hour at room temperature. For inhibitor treatment on MDA-MB-231 cells, 24 hours after seeding, the media was aspirated from cells, they were washed with 2ml PBS and then incubated with 20µM GM1006, for 24 hours, in 2ml, FBS-free DMEM with high glucose (4.5 g/L; Thermo Fisher Scientific). Forty-eight hours post transfection (HEK293T cells) or post-seeding (MDA-MB-231 cells), all the medium was aspirated from the wells and cells washed in 2ml PBS (with calcium and magnesium). Cells were fixed with 3.7% (w/v) paraformaldehyde (PFA) with 5% (w/v) sucrose for 15 minutes at room temperature. Cells were washed 3 times with 2ml PBS for 2 minutes. Cells which required permeabilisation were then incubated with 2ml, 0.1% (v/v) Triton X-100, which had been previously chilled to 4°C, for 5 minutes. Cells were washed again 3 times with 2ml PBS for 2 minutes. All cells were then blocked in 5% (v/v) goat serum (Sigma) in PBS for 1 hour at room temperature. Coverslips were then incubated with 200µl of primary antibody (mouse, anti-human CD178 (CD95L) NOK-1 clone (BioLegend) at a 1:100 dilution (in the block buffer), mouse, anti-human CD178 (CD95L) clone G247-4 at a 1:100 dilution or mouse anti-c-MYC (Sigma) primary antibody at a 1:200 dilution) for 90 minutes at room temperature. Following 3 washes with 2ml PBS for 2 minutes, the coverslips were incubated with 200µl secondary antibody, goat anti-mouse Alexa Fluor® 488 (Invitrogen) at a 1:1000 dilution (in the block buffer) along with DAPI (4',6-diamidino-2-phenylindole; Invitrogen) at a 1:1000 dilution, for 1 hour at room temperature, in the dark. The final 3 washes were with 2ml,

0.05% (v/v) PBS-T for 2 minutes. Coverslips were mounted onto microscope slides using FluorSave™ Reagent (Calbiochem) overnight at room temperature and stored in the dark at 4°C. MDA-MB-231 cells were viewed on a Leica DFC365, epi-fluorescent microscope, with a 63x oil immersion objective with a numerical aperture of 1.25. Images were processed and analysed using ImageJ (NIH). HEK293T cells were viewed using a Zeiss LSM710 confocal laser scanning microscope based on an Axiovert inverted microscope (Carl Zeiss) with a 40x oil immersion objective with a numerical aperture of 1.3. Laser lines 488nm and 405nm were used to excite Alexa Fluor® 488 and DAPI, respectively. The pinhole was set to 1 airy unit. Images were acquired with sequential scanning and image processing and analyses were performed using Zen 2010 software and ImageJ (NIH).

2.11. RNA extraction, cDNA conversion and RT-qPCR analysis

2.11.1 Isolation of total RNA from human cells

Small-scale (µg quantities) preparation of total RNA from human cells was carried out using the QIAGEN RNeasy® Mini Kit (QIAGEN) as described by the manufacturer. Transfected (see section 2.6.1) or untransfected HEK293T cells, or MDA-MB-231 cells were harvested, counted and 1 x 10^7 cells pelleted by centrifugation at 300xg for 5 minutes. Media was aspirated, and cells were lysed by the addition of 600µl Buffer RLT (supplemented with 1.0% 2-mercaptoethanol) with vortexing to disrupt the cell pellet. The lysate was homogenised by centrifuging through a QIAshredder spin column (QIAGEN) for 2 minutes at 14,000xg. One volume of 70% ethanol (Sigma) was added to the homogenised

lysate and mixed by pipetting six times. The sample, including any precipitate formed, was transferred to a RNeasy spin column (in a supplied 2ml collection tube) and was centrifuged for 15 seconds at 8,000xg, after which the flow-through was discarded. The column with bound RNA was subsequently washed with 700µl Buffer RW1 by centrifuging for 15 seconds at 8,000xg followed by two further 500µl washes with Buffer RPE using the same spin conditions. In each case the flow-through was discarded. The column was transferred to a fresh 2ml collection tube and spun for a further minute at 14,000xg to remove any residual Buffer RPE from the last wash. Subsequently, the column was transferred to a new 1.5ml Eppendorf microcentrifuge tube and 50µl RNase-free water was added directly to the spin column before being centrifuged for 1 minute at 14,000xg to elute the bound RNA. The concentration and purity of the eluted RNA was determined by spectrophotometric analysis as described in Section 2.11.2 and stored at -80°C.

2.11.2 Determination of RNA quality

RNA concentrations in nucleic acid preparations were determined by spectrophotometry by measuring the absorbance at 260nm (A_{260}) using the NanoDropND-1000 (ThermoFisher Scientific). The quality of nucleic is indicated by the ratio between the absorbance at 260 and 280nm. For pure RNA the A_{260}/A_{280} ratio should be ~2.0. Smaller ratios usually indicate contamination by protein or organic chemicals. As a secondary measure of nucleic acid purity, the A_{260}/A_{230} ratio was also measured which should be in the range of 2.0 to 2.2 for RNA. Only nucleic acids that passed these criteria were used in downstream applications.

2.11.3 Reverse-transcription of mRNA to cDNA

cDNA synthesis was carried out using the GrandScript cDNA synthesis Kit (PCR Biosystems) as per the manufacturer's instructions. Briefly, 1µg RNA (see section 2.11.1) was mixed with 4.0µl, 5x cDNA synthesis mix (proprietary), 1.0µl reverse transcriptase (RTase; proprietary) and nuclease-free H_2O to a total volume of 20µl before incubation at 42°C for 30 minutes, followed by incubation at 70°C for 10 minutes to denature the RTase. cDNA was stored at -20°C for up to one week or used immediately for downstream applications.

2.11.4. RT-qPCR of cDNA using SYBR® Green

cDNA from the reverse transcription of 1µg mRNA extracted from cells (see section 2.11.3) was diluted to 200ng/µl in RNase-free water and used in the reaction, as detailed in table 2.3, using SYBR® Green PCR master mix (Thermo Scientific) and 20µM of forward and reverse primers for either CD95L or GAPDH. Primer sequences were generated using the Harvard Primer Bank (found at: http://pga.mgh.harvard.edu/primerbank/) and were purchased from Eurofins Genomics (GAPDH) or Sigma (CD95L). A list of primer sequences used is found in table 2.4. Each condition was run in triplicate and each 10µl reaction mixture was transferred to a well of a 96-well reaction plate (Life Technologies) and the plate was sealed using optical adhesive film (Life Technologies).

Reagent	Volume (µl)
SYBR® Green PCR master mix (2x)	5.5
RNase-free H_2O	2.5
Forward Primer (20 µM)	0.5
Reverse Primer (20 µM)	0.5
cDNA (200 ng/µl)	1
Total Volume	**10**

Table 2.3. RT-qPCR reaction mixture (10 µl total volume)

Target Gene	Forward Primer (5' - 3')	Reverse Primer (5' - 3')
GAPDH	GGCTGCTTTTAACTCTGG	GGAGGGATCTCGCTCC
CD95L	TGCCTTGGTAGGATTGGGC	GCTGGTAGACTCTCGGAGTTC

Table 2.4. A list of the forward and reverse primer sequences used.

Stage	Temperature	Time	Number of cycles
Initial denaturation	95°C	10 minutes	1
Denaturation Annealing/Extension	95°C 60°C	15 seconds 1 minute	40
Hold	72°C	5 minutes	1
Melt Curve	95°C 60°C 95°C 60°C	15 seconds 1 minute 15 seconds 15 seconds	1 1 1 1

Table 2.5. RT-qPCR reaction conditions.

The plate was kept on ice before being loaded onto the qPCR machine (7500 Real Time PCR system, Applied Biosystems) and run with the conditions outlined in table 2.5. Ct values were generated using the 7500 software version 2.3 (Applied Biosystems) using the 'Auto threshold' function.

2.12. siRNA transfection

2.12.1. siRNA transfection protocol

MDA-MB-231 cells (3 x 10^5) were seeded as a monolayer on 6-well plates (Nunclon) in 2ml DMEM (Thermo Fisher Scientific) with 5% FBS (Sigma). 24 hours post seeding, siRNA sequences (see table 2.6) at 20µM, were made up to 200µl using Opti-MEM (Thermo Fisher Scientific) - mixture A. For the oligofectamine (transfection reagent) only control condition, no siRNA was used. Oligofectamine transfection reagent (Invitrogen) was mixed in a 1:1 ratio with Opti-MEM (equal to the volume of siRNA used) - mixture B. Each mixture was incubated at room temperature for 10 minutes. The contents of mixture B was then added to mixture A for each condition and incubated at room temperature for 25 minutes. Media was aspirated from each well and cells washed with 2ml PBS. 800µl Opti-MEM was added to each well (1ml to the non-treated well), and the siRNA mixture carefully added to each well. The cells were incubated for 4 hours at 37°C before adding 500µl of Opti-MEM supplemented with 30% FBS (Sigma). 12 hours later, the siRNA mix was aspirated from cells and 2ml DMEM added, supplemented with 5% FBS (Sigma). 48 hours following transfection, cells were harvested and whole cell extracts prepared (see section 2.7.5). Transfection reagent and siRNA against PI3-Kinase C2β were kindly provided by Tania Maffucci.

siRNA name	siRNA target	Supplier	siRNA target sequence (5' - 3')
si-CD95L 07	CD95L	Dharmacon	GCCCUUCAAUUACCCAUAU
si-CD95L 08	CD95L	Dharmacon	GGAAAGUGGCCCAUUUAAC
Non-targeting si	N/A (control)	Dharmacon	UGGUUUACAUGUCGACUAA UGGUUUACAUGUUGUGUGA UGGUUUACAUGUUUUCUGA UGGUUUACAUGUUUUCCUA
si-C2ß	PI3-Kinase C2β	Qiagen	AAGAATGCGACGCCTGGCAAG

Table 2.6. siRNA target sequences.

2.12.2. Western Blot analysis for siRNA knockdown

Whole cell extracts were prepared and analysed by Western blot as detailed in sections 2.7.5, 2.7.7, 2.7.8 and 2.7.9. Primary antibodies used were mouse, anti-human CD178 (CD95L) clone G247-4, anti-β-tubulin (Sigma) and mouse, anti-human PI3-Kinase C2β (BD Biosciences). Secondary antibody polyclonal goat anti-mouse immunoglobulins-HRP (Dako) was used at a 1:2000 dilution for CD95L detection, 1:10,000 for β-tubulin detection and 1:10,000 for C2β detection.

2.13. IN Cell analysis of microparticle uptake

2.13.1. Endpoint analysis of particle uptake

MDA-MB-231 cells (1.4 x 10^5) were seeded in 6-well plates (Nunclon) in DMEM (Thermo Fisher Scientific) supplemented with 2% (v/v) FBS (Sigma) and cultured for 24 hours. MPs were coated (see section 2.8) and were added to the cells (4.05 x 10^6 per well) and incubated for a further 24 hours. Unbound MPs were removed by washing each well of cells 3 times with 2ml PBS, and gently tapping the sides of the 6-well plate to dislodge any particles. Two hours prior to imaging, live, adhered cells were stained with 1µg/ml Hoescht (Thermo Fisher Scientific), diluted into DMEM (2% FBS). After two hours, cells were washed with 2ml PBS to remove any excess stain and then incubated with CellMask™ deep red plasma membrane stain (Thermo Fisher Scientific), at a 1:1000 dilution in DMEM (2% FBS), for 20 minutes. Cells were washed again with 2ml PBS and DMEM supplemented with 5% FBS was added before imaging on the IN Cell Analyser 6000 (GE Healthcare). Nine fields of view were imaged in each well, using a 40x objective with a numerical aperture of 0.6, covering an area of 0.966mm^2 and capturing ~200 cells per well. The plasma membrane of each cell was imaged using the confocal aperture (the pinhole was set to 1 airy unit, (AU)) and a 3-D, Z-stack of 6 x 1.7µm slices (excluding the top of the cells) was taken in order to capture all particles within the cell. Image processing and analyses were performed using the developer software version 1.9.1 (GE Healthcare). The software identifies the nucleus and cell membrane based on size and fluorescence (blue pixels for the nucleus and red for the membranes). The two are linked together to determine the number of cells per well. MPs are identified using similar parameters and the number of cells with particles determined by linking particles (or foci) to the nucleus and membrane of a cell. Each particle is

counted separately, allowing the analyses to calculate the number of particles internalised by each distinct cell. Stringencies were introduced to ensure only internalised particles were counted including that a particle should be 100% surrounded by the cell membrane; even if one pixel of a particle is not, the particle is not counted. The outer edge of the membrane was excluded during processing, so particles close to outside of the cell were also excluded from the count.

2.13.2. Live-cell imaging of particle uptake

MDA-MB-231 cells were seeded and then stained as described in section 2.13.1. CD95R-Fc coated MPs (section 2.8) were added to cells, 30 minutes prior to imaging. The plate was sealed with a breathe-easy® sealing membrane (Sigma) and cells supplied with 5% CO_2 and kept at 37°C whilst the cells were imaged on the IN Cell Analyser 6000. Nine fields of view, which equate to an area of 0.966mm^2, were imaged every 15 minutes for 5 hours. Image processing and analyses were performed using the developer software version 1.9.1 (GE Healthcare).

2.14. Dynamic light scattering and ζ- potential measurements

MPs were coated (see section 2.8) and samples made up to 1ml PBS. Measurements were made using a Zetasizer Nano ZS (Malvern), using a disposable folded capillary zeta cell, DTS1070 (Malvern). Measurement settings included material selection of polystyrene latex, dispersant of PBS and measurements were made at 37°C. Triplicate measurements were made with 10

runs, 30 seconds per run per measurement. Size measurements were made prior to zeta potential measurements, and particle diameter data are represented using the z-average diameter function. The Zetasizer utilises dynamic light scattering (DLS) and the Brownian motion of particles for characterisation. The Brownian motion of particles or molecules in suspension causes laser light to be scattered at different intensities. Analysis of these intensity fluctuations yields the velocity of the Brownian motion and hence the particle size using the Stokes-Einstein relationship (see equation 2.2).

$$d_H = \frac{kT}{3\,\pi\,\eta\,D}$$

Equation 2.2. The Stokes-Einstein equation
d_H = hydrodynamic diameter, k = Boltzmann's constant, T = absolute temperature, η = viscosity and D = diffusion coefficient.

Velocity of the Brownian motion is defined by the translational diffusion coefficient (D). The translational diffusion coefficient can be converted into a particle size (d_H), tracking particles in a vehicle of known viscosity at a known temperature, using the Stokes-Einstein equation.

2.15. Statistical analyses

Mean values are shown, with standard error of the mean (SEM) represented by error bars. To compare two groups of data, a Welch's t test (comparing mean), a paired t test (comparing means of paired samples) or Mann-Whitney U (nonparametric) test was performed using GraphPad prism 7 (GraphPad

Software Inc.). A one-way analysis of variance (ANOVA) was used to analyse the differences between the means of three of more independent groups, with Bonferroni's test, to compare every mean with every other mean; this was also completed using GraphPad prism 7 (GraphPad Software Inc.). Unless otherwise stated, at least three independent experiments were performed before statistical analysis.

3. Expression and Purification of CD95R-Fc Fusion Protein

3.1. Introduction

The ability to express and purify large quantities of recombinant protein with a high level of purity is important for numerous fields including biomedical study, the pharmaceutical industry and biotechnological applications. Well defined expression systems involve the use of bacterial, yeast, insect and mammalian cells for protein expression. Each system has its benefits and limitations, the choice of which usually depends on biochemical properties of the target protein (He et al., 2014).

The use of *Escherichia coli* (*E. coli*) for protein expression is a popular choice, with a large range of vectors and strains available which have been modified for successful expression. This system is convenient, inexpensive and it is possible to produce high yields of protein. However, due to a lack of some molecular chaperones and post-translational modification pathways, many proteins, especially eukaryotic proteins misfold when overexpressed, forming cytosolic inclusion bodies (Sodoyer, 2004). Protein recovered from these inclusion bodies must be denatured, purified and then refolded which adds extra, complicated steps to the purification process. Yeast systems are also cost effective and the cells can grow to a high density and express large quantities of intra- or extracellular recombinant protein (Sodoyer, 2004). Yeast cells can add post-translational modifications such as disulphide bonds and O- and N-linked

glycosylation (Macauley-Patrick et al., 2005). Still, differences in glycosylation patterns of higher eukaryotic proteins expressed in yeast systems are observed with over-glycosylation being a common problem. This is important since the correct glycosylation patterns of recombinant proteins may be important for their biological activity and help to prevent immune responses when used as pharmaceuticals (Macauley-Patrick et al., 2005).

Mammalian and insect cell expression systems are typically described as expensive and time-consuming as these cells have longer doubling times and high maintenance. However, they are popular choices for expressing very complex proteins or proteins which require precise post-translational modifications. Using a baculoviral/insect cell system for expression presents numerous advantages over a mammalian system. Insect cells are easy to grow on well-defined culture media and the system is safe to use. Yet, the adaptability of insect cells lines to large-scale procedures, such as microcarriers, can be troublesome (Sodoyer, 2004). Despite this, the insect cell system is the most prevalent for obtaining eukaryotic membrane proteins and has been used to express a large number of integral membrane proteins (He et al., 2014). Eukaryotic membrane proteins are of particular importance as they are key players in numerous biological processes and targets of therapeutic drugs and antibodies.

CD95R (Fas/APO-1/TNFRSF6) is a death receptor found on the surface of all cells (section 1.4). It is best known for its involvement in apoptosis and tissue homeostasis by the immune system (Chen et al., 2010). This chapter describes

the use of a baculovirus, insect cell expression system to express and purify large quantities of mouse CD95R ECD fused to the Fc region of human IgG1. The aim is to produce milligram quantities of highly purified CD95R for coating MPs, to allow investigation of the mechanism involved in particle uptake.

3.1.1. Baculovirus expression system

The *Baculoviridae* are a large family of insect viruses which primarily infect insect larvae of the order *Lepidoptera*, which includes moths and butterflies (van Regenmortel et al., 2000). The Baculovirus genome consists of a double-stranded covalently closed circular DNA that can be 80 to 180 kbp in size (Contreras-Gómez et al., 2014). The genomes of sequenced baculoviruses have identified 31 core genes which are conserved, the functions of which can be divided into DNA replication and transcription, virion packaging and assembly, cell cycle arrest and the primary infection of the insect host midgut cells (oral infectivity) (Yang and Zhang, 2012, Contreras-Gómez et al., 2014).

The life cycle of baculoviruses has been characterised and found to be biphasic, with 2 infectious phenotypes: Occluded Virions (OV) and Budded Virions (BV) (Yang and Zhang, 2012). Typically, infection of an insect host will begin with ingestion of OV, coated in a polyhedrin and P10 protein occlusion body which protects the virus from environmental stressors. In the insect midgut, this protective coating is degraded by the alkaline environment, releasing baculoviral capsids which fuse to and enter the midgut cells; the primary infection. The virus then replicates within the midgut cells, and new baculoviral capsids translocate to the plasma membrane, budding to form BVs which consist of a single

nucleocapsid enclosed in host plasma membrane modified with glycoprotein (gp)64 (Jehle et al., 2006) which infect cell to cell; the secondary infection. In the second round of infection, BVs will form OVs, which is triggered long after initial infection by the very late phase of gene expression, which leads to production of polyhedron and p10 in large amounts (Contreras-Gómez et al., 2014). The secondary infection results in release of the OVs after cell lysis and death of the insect, which is an important stage in horizontal transmission of infection (Contreras-Gómez et al., 2014).

For gene expression in insect cells, the most commonly used baculovirus vector is *Autographa californica* multiple nucleopolyhedrovirus (AcMNPV) and many insect cell lines are highly susceptible to infection by this virus (Contreras-Gómez et al., 2014). The ability of baculoviruses such as AcMNPV to produce large quantities polyhedrin and P10 for occlusion body formation is exploited for heterologous gene expression. Usually in OV synthesis, the level of polyhedrin protein is produced abundantly, accounting for some 50% of the total cell protein (Merrington et al., 1997). In cell culture, OV forms of virus for horizontal transmission are redundant (budded virus being the key infectious agent) and polyhedrin and P10 protein expression is therefore not essential because it is not required to produce BVs. Because of this, these redundant genes can be replaced by a gene-of-interest under the control of *polh* and *p10* promoters. These promoters are ‘very strong’ promoters allowing high expression levels of the recombinant protein at the late stage of infection (Merrington et al., 1997). However, as these promoters are active in the very late phase when cells undergo lysis and release OVs, intracellular proteases are also released which

can cause proteolytic degradation of the expressed recombinant protein (Brondyk, 2009). Expressing a protein at the early stages of infection or use of protease inhibitors can help to prevent this from happening (Contreras-Gómez et al., 2014). In conclusion, baculoviruses such as AcMNPV are engineered to replicate as highly infectious BVs which infect cell-to-cell in insect cell culture, expressing large quantities of the recombinant protein under the control of strong promoters.

3.1.2. Generation of recombinant baculovirus

The AcMNPV has a circular genome of 130 kbp (Kuzio et al., 1999), which is large and difficult to insert a gene-of-interest into. To overcome this, the target gene is first cloned into a transfer vector with sequences that flank the redundant polyhedrin gene in the baculovirus genome. There are two main systems used to generate a recombinant baculovirus. In the first system, the baculovirus and transfer vector are co-transfected into insect cells and homologous recombination occurs between the sequences of the polyhedrin gene in the viral DNA, and the homologous sequences flanking the gene-of-interest in the transfer vector (Merrington et al., 1997). In the recombinant virus genome, the gene-of-interest then sits in place of the polyhedrin gene, under control of the strong *polh* promotor. The second system uses a 'bacmid', a recombinant baculovirus modified so that it can be maintained in *E. coli* cells. Introduction of a transfer vector, containing the target gene, results in the transposition of the target gene into the bacmid genome (Je et al., 2001). Selection for the required recombinant DNA is carried out in *E. coli* (Je et al., 2001). The Linton lab uses insect cell

recombination systems, the first system described, since some cDNAs have been found to be unstable in *E. coli* (Byrne et al., 2009).

As with all homologous recombination systems, it is necessary to separate the recombinant virus from parental virus. A few methods are available to do this. Plaque-assays or plaque-purifications are one method, however they are generally inaccurate and time consuming due to a low frequency of recombination events (which in the first vector systems could be < 1%) (Kitts and Possee, 1993). Another method of separation involves the insertion of the *E. coli lacZ* gene, which encodes the ß-galactosidase enzyme which breaks down lactose, into the polyhedrin locus under control of the *polh* promotor (Possee and Howard, 1987). Recombination with the gene-of-interest in the transfer vector then removes the *lacZ* gene from the viral genome. Recombinant virus plaques would then be colourless when X-gal (5-bromo-4-chloro-3-indolyl ß-D-galactopyranoside) is added, since they lack the enzyme to break it down, thus can be differentiated from the blue parental plaques. However, issues still arise using this method as recombinant plaques can be masked by blue parental plaques (Merrington et al., 1997).

In order to improve recombination frequency, a unique restriction site (*Bsu*36I) was added at the polyhedron locus to linearize the virus. Double stranded breaks are highly recombinogenic and when a transfer vector based on the polyhedrin locus is co-transfected with the linear virus, a higher proportion of recombinant viruses (30%) are produced (Kitts et al., 1990). Linearization of the baculovirus however, decreases transfection efficiency by 15 - 150 fold compared to the

circularized virus (Kitts et al., 1990). Further modifications produced 90% recovery of recombinant viruses, using the BacPAK6 system (Kitts and Possee, 1993). This involves the *lacZ* gene insertion as described earlier, with *Bsu*36I restriction sites flanking genes either side of *lacZ*. Digestion of BacPAK6 with *Bsu*36I causes linearization and disrupts ORF 1629, which is an essential gene for AcMNPV replication (Possee et al., 1991). A transfer vector can be constructed containing ORF 1629 and the recombinant gene under the *polh* promotor, restoring infectivity only to the recombinant virus via homologous recombination. *Bsu*36I digestion however, is not always 100% efficient and there will still be a mix of recombinant and parental viruses which require purification.

3.1.3. The *flashBAC* baculovirus expression system

The *flash*BAC system (Oxford Expression Technologies; OET) removes the need to isolate recombinant from parental virus. The system has similarities to the BacPAK6 technology described above. The AcMNPV genome of *flash*BAC lacks part of ORF 1629 and the polyhedron gene is replaced with an origin of replication for a bacterial artificial chromosome (BAC) (Hitchman et al., 2009). The BAC allows the viral DNA to be propagated within bacterial cells, from which it can be isolated and purified.

As before, lack of ORF 1629 prevents virus replication in insect cells. After co-transfection of the *flash*BAC DNA and the transfer vector into insect cells and homologous recombination, ORF 1629 functionality is restored only to recombinant viruses and generation of a wild-type virus is impossible. Furthermore, the gene-of-interest in placed under control of the *polh* promoter,

simultaneously removing the BAC sequence (Hitchman et al., 2009). Non-recombinant virus is unable to replicate and recombinant virus will replicate to produce BV which can be harvested from culture medium of transfected insect cells for amplification and use.

3.1.4. The *flash*BAC GOLD expression system

An improvement on the original *flash*BAC expression system is *flash*BAC GOLD (OET), which has some further modifications. Genes have been identified in the baculovirus genome, which are not necessary for replication in insect cells. These include chitinase (*chiA*) which produces an enzyme with exo- and endochitinase activity, responsible (along with cathepsin) for the breakdown of the host cuticle for the release of virus for horizontal transmission (Hawtin et al., 1995, Hawtin et al., 1997). Using microscopy, chitinase has been found to be targeted to and densely packed in a para-crystalline array in the endoplasmic reticulum, of AcMNPV infected insect cells (Thomas et al., 1998). As a result, chitinase interferes severely with the function and efficacy of the insect cell secretory pathway (Saville et al., 2004) which is necessary for the secretion of recombinant proteins. Additionally, v-*cath*, which encodes V-cathepsin, has also been removed. V-cathepsin is a protease which is synthesized as an inactive proenzyme that accumulates in the endoplasmic reticulum, and is activated by chitinase upon cell death (Kaba et al., 2004, Hom et al., 2002). The deletion of both *chiA* and *v-cath* from the *flashBAC Gold* baculovirus genome is therefore designed to free up more processing space within the endoplasmic reticulum, improving the secretory pathway efficacy and yield of recombinant proteins.

3.1.5. The *flash*BAC ULTRA expression system

The genes *p10*, *p26* and *p75* have been deleted from *flash*BAC ULTRA (OET) DNA, along with the modifications already described. Deletion of *p10* increases *polh* promoter activity, leading to higher production of recombinant protein over a longer timeframe (Hitchman et al., 2010). The removal of both *p74* and *p26* has no effect on viral replication; P74 plays a role in oral infectivity of OV and midgut attachment (Faulkner et al., 1997) and *p26* codes for a protein of unknown function, but has the same 5′ terminus as *p10* (Rankin et al., 1986). These further modifications remove an unnecessary genetic burden from the recombinant viral genome (Hitchman et al., 2010), resulting in a more productive baculovirus expression vector.

3.1.6. Insect cells

Insect cells have the capability to introduce most post-translational modifications to recombinant proteins as found in mammalian cells. Asparagine, (N)-linked glycosylation occurs at the same site on the recombinant protein in insect and mammalian cells (N-X-S/T) (Schwarz and Aebi, 2011). However, glycosylation is less complex in insect cells, which add simple oligo-mannose sugar chains (Harrison and Jarvis, 2006) compared to complex sugar groups with terminal sialic acids in mammalian cells (Contreras-Gómez et al., 2014). These differences can alter the biological characteristics of a recombinant protein (Contreras-Gómez et al., 2014) and potentially cause allergenic reactions in humans (Harrison and Jarvis, 2006). However, human CD95R fused to human Fc domain has previously been expressed successfully using a baculovirus in Sf9 cells, and shown to bind CD95L (Muraki and Honda, 2010). This suggests

that the glycosylation is sufficient for functional human CD95R to be expressed, folded, trafficked and secreted by insect cells.

The two most common cell lines used for membrane protein expression are *Spodoptera frugiperda* (Sf9/Sf21) and *Trichoplusia ni* (Hi5) derived from pupal ovarian tissue from the fall armyworm and ovarian cells of the cabbage looper, respectively (Vaughn et al., 1977, Wickham et al., 1992). Sf9 cells are a clonal isolate of the Sf21 cell line and both cell lines exhibit similar properties. Sf21 and Hi5 cells are capable of growing in suspension to produce high yields of recombinant protein when infected with baculovirus. However, there are often differences between the yield and behaviour of heterologous proteins when expressed in these two cell lines (He et al., 2014). For example, Hi5 cells have been found to be superior to Sf21 cells in producing recombinant ß-galactosidase (Wickham et al., 1992). However, this can be variable depending on factors such as the protein being expressed (Taticek et al., 2001) and the multiplicity of infection (MOI). It is therefore necessary to test expression of a recombinant protein empirically in multiple insect cells lines in order to optimise protein production using the baculoviral system.

3.1.7. Affinity Chromatography

Affinity chromatography is a form of liquid chromatography that utilises biological-like interactions for the separation and specific analysis of sample components (Hage, 1999). Affinity chromatography has several advantages since it is an easy, fast and selective for capturing a target protein (Hober et al., 2007). Staphylococcal protein A (SPA; Protein-A) was one of the first discovered

immunoglobulin-binding molecules which has been developed for use in affinity chromatography systems (Hober et al., 2007). SPA is a cell wall associated protein domain exposed on the surface of *Staphylococcus aureus*, a Gram-positive bacterium (Hober et al., 2007). Protein-A has an affinity for IgG from various species such as human, rabbit and guinea-pig (Richman et al., 1982) and the protein contains a region of five homologous binding domains which are independently capable of binding the fragment crystallisable region (Fc region) of IgG (Hober et al., 2007). Recombinant proteins which are expressed with an Fc tag can exploit this specific affinity for purification purposes. Other forms of affinity chromatography such as IMAC (immobilised-metal affinity chromatography) makes use of interactions that can occur between immobilized metal ions and proteins, for example, nickel ions (Ni^{2+}) and histidine-tagged recombinant proteins (Hage et al., 2012). IMAC may not be as specific if other proteins in the sample contain naturally occurring histidine residues. These will have an affinity for the IMAC matrix and may co-elute with the recombinant protein, resulting in significant contamination of the final product (Bornhorst and Falke, 2000). A further advantage of using an Fc-tag is that the Fc portion is likely to fold independently, and can therefore aid solubility and stability of its partner molecule (Czajkowsky et al., 2012, Carter, 2011) potentially improving the yield of fusion proteins expressed in *E. coli*. In the past, some drawbacks of using protein-A have been the low binding capacities (below 40mg/ml) and high costs of Protein-A resins, however, resins are now available with reported dynamic binding capacities of over 60mg/ml (GE Healthcare) (Ghose et al., 2014).

3.1.8. Functionality of expressed CD95R

Previous literature has demonstrated that CD95R expressed in insect cells (Sf9) can form a stable complex with CD95L expressed in yeast, therefore maintaining its functional activity (Muraki and Honda, 2010). Another commonly used assay to measure recombinant CD95R functionality, tests its ability to inhibit a well-described biological function of CD95L, the induction of apoptosis of Jurkat cells (Cheng et al., 1994). The functionality of recombinant human CD95R fused to Fc (CD95R-Fc) expressed in Chinese hamster ovary (CHO) cells (BioMoti), mouse CD95R-Fc expressed in Sf21 insect cells and human CD95R-Fc expressed in mouse myeloma (NSO) cells (both sourced from Sigma), was tested by BioMoti (Figure 3.1). Briefly, CD95L was incubated with different concentrations of CD95R-Fc, and then added to Jurkat cells for 3 hours at 37°C. The Jurkat cells are then lysed and the cleavage of caspase substrate Ac-DEVD-AFC was used to determine the extent of apoptosis, since apoptosis is paralleled by an increased activity of caspases (e.g. caspases 3 and 7). Furthermore, caspase activity correlates with the percentage of apoptotic cells determined morphologically after staining the cells with propidium iodide and Hoechst-33342. EC_{50} (half-maximal effective concentration) values for each protein were calculated and the potency of the three proteins were in the same order of magnitude (human CD95-Fc prepared from NSO cells, 807ng/ml, human CD95R-Fc prepared from CHO cells, 380ng/ml, and mouse CD95-Fc prepared from Sf21 cells, 447ng/ml).

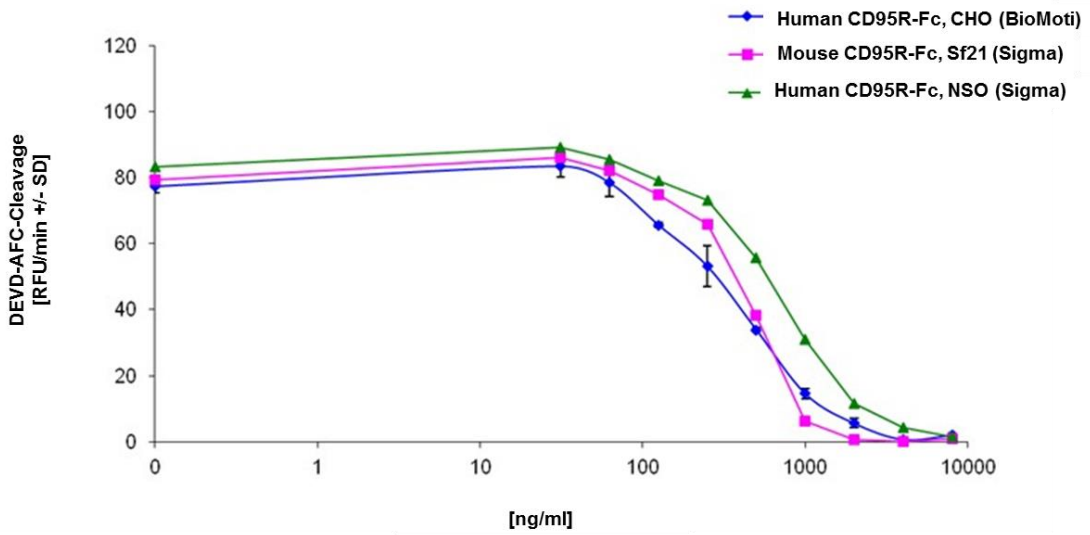

Figure 3.1. Human and mouse CD95R-Fc prepared from rodent and insect cells behaves similarly to inhibit CD95L-dependent induction of apoptosis in Jurkat cells (BioMoti). 250ng/ml of CD95L was incubated with increasing concentrations of CD95R-Fc purified from different host cells: Human CD95R-FC from Chinese hamster ovary cells (CHO; BioMoti), mouse CD95R-Fc from Sf21 cells (Sigma) and human CD95R-Fc from mouse myeloma cells (NSO; Sigma). The CD95L/CD95R-Fc mix was then added to Jurkat A3 cells. Cells were lysed and the cleavage of the caspase substrate Ac-DEVD-AFC (+/- standard deviation) was measured for each protein to determine the extent of apoptosis. EC_{50} values were calculated as follows: Human CD95-Fc, NSO (Sigma), EC_{50}: 807ng/ml; human CD95R-Fc, CHO (BioMoti), EC_{50}: 380ng/ml and mouse CD95-Fc, Sf21 (Sigma), EC_{50}: 447ng/ml.

Via its interaction with CD95R, CD95L induces apoptosis, which is the key physiological feature of death signalling by CD95R/CD95L. This shows that across a range of expression systems, mouse and human CD95R-Fc can specifically block the CD95R/CD95L interaction, strongly suggesting that the recombinant protein is correctly folded, maintains its natural binding ability and functionality in a physiologically relevant assay.

In this chapter I describe the use of a baculovirus, insect cell expression system to express and purify large quantities of secreted mouse CD95R ECD fused to the Fc region of human IgG1. The aim is to produce milligram quantities of highly purified CD95R for coating MPs, to allow investigation of the mechanisms involved in particle uptake.

3.1.9. Aims of Chapter 3

- Test expression and secretion of CD95R-Fc in Sf21 and Hi5 cells
- Determine the optimal MOI of baculovirus to insect cells to maximise the yield of CD95R-Fc
- Optimise batch purification conditions for CD95R-Fc using protein-A resin
- Optimise buffer exchange of CD95R-Fc for downstream applications
- Confirm glycosylation of secreted CD95R-Fc
- Test functionality of CD95R-Fc to coat microparticles (MPs) for uptake into MDA-MB-231 cells
- Test stability of CD95R-Fc and optimise conditions for long term storage

3.2. Results

3.2.1. Generation of baculovirus FlashBAC Gold-CD95R-Fc

A gene encoding a chimeric fusion protein of the mouse CD95R ectodomain fused to the Fc portion of human IgG was sub-cloned into pOET1 transfer plasmid by OET (for a description of the construct see Figure 3.2). The recombinant virus 'FlashBAC Gold-CD95R-Fc' was produced through homologous recombination in insect cells as described in section 2.4.2. The recombinant baculovirus was used in a series of Sf21 insect cell infections to amplify the baculovirus titre (section 2.4.4). Each infection was performed using a low multiplicity of infection (MOI; 0.1 = 1 virus per 10 cells) to produce intermediate (p1) and then working stocks of baculovirus. The titre of the working stock was measured by plaque assay (detailed in section 2.4.3) and determined to be 6 x 10^7 plaque-forming units (pfu) per ml.

3.2.2. Amplification of baculovirus FlashBAC Ultra-CD95R-Fc

Generation of FlashBAC ULTRA-CD95R-Fc was outsourced to OET due to potential improvements in protein expression levels. FlashBac Ultra-CD95R-Fc was amplified into a 200ml working stock (section 2.4.4) and the virus titre determined by plaque assay (section 2.4.3) as 1.3 x 10^8 pfu per ml. Both baculoviruses were used to express protein under the same conditions (section 2.4.5). When purified using affinity chromatography (section 2.7.1; Figure 3.5C & D) a similar yield and purity of protein was achieved, therefore there was no apparent advantage in using the ULTRA virus (section 3.2.4). The baculoviruses were used interchangeably for expression, unless specified.

CD95R-Fc Protein Sequence
10 20 30 40 50 MLWIWAVLPL VLAGSQLRVH TQGTNSISES LKLRRRVRET DKNCSEGLYQ 60 70 80 90 100 GGPFCCQPCQ PGKKKVEDCK MNGGTPTCAP CTEGKEYMDK NHYADKCRRC 110 120 130 140 150 TLCDEEHGLE VETNCTLTQN TKCKCKPDFY CDSPGCEHCV RCASCEHGTL 160 170 180 190 200 EPCTATSNTN CRKQSPRNRD IEARMDPKSC DKTHTCPPCP APELLGGPSV 210 220 230 240 250 FLFPPKPKDT LMISRTPEVT CVVVDVSHED PEVKFNWYVD GVEVHNAKTK 260 270 280 290 300 PREEQYNSTY RVVSVLTVLH QDWLNGKEYK CKVSNKALPA PIEKTISKAK 310 320 330 340 350 GQPREPQVYT LPPSRDELTK NQVSLTCLVK GFYPSDIAVE WESNGQPENN 360 370 380 390 400 YKTTPPVLDS DGSFFLYSKLT VDKSRWQQGN VFSCSVMHEA LHNHYTQKS LSLSPGK

Figure 3.2. Protein sequence for recombinant mouse CD95R-Fc.
In red – CD95R ectodomain, residues 1 to 169 (corresponding to residues 1 to 169 in the native mouse CD95R) with the signal sequence underlined (residues 1 to 21), green – peptide linker, residues 170 to 176 and blue – Fc region of human IgG, residues 177 to 407. It is unknown whether the signal sequence is uncleaved in mature CD95R-Fc; this would need to be determined by N-terminal sequencing.

3.2.3. Determining the time course and multiplicity of infection required for CD95R-Fc expression

To optimise the MOI for expression and secretion of CD95R-Fc from Sf21 and Hi5 insect cells, three 10ml cultures of each cell type (at 1 x 10^6 cells/ml) were infected with the working stock of FlashBAC Ultra-CD95R-Fc baculovirus at a MOI of 3, 1 and 0.1 virus particles per cell (section 2.4.5). An uninfected, control culture for each cell type was also cultured alongside the infected cells. The cultures were sampled over a 5-day period and the spent media containing the secreted fusion protein was analysed by western blot (section 2.7.11; Figure 3.3 and 3.4). Equal volumes of harvested media were loaded to allow direct comparison of secreted CD95R-Fc protein levels (section 2.7.7).

Figure 3.3 demonstrates the presence of CD95R-Fc migrating with an apparent molecular weight close to that predicted for the peptide chain; the expected molecular weight of 45.7kDa (Figure 3.2). Increasing levels of CD95R-Fc were detected as MOI increases. At a higher MOI, more protein is expressed in Hi5 cells and for Sf21 cells. This is true until day 4, when expression levels remain similar across MOIs. At a lower MOI of 0.1, Sf21 cells are more efficient at producing CD95R-Fc protein than Hi5 cells, which can clearly be seen by Day 5 of expression (Figure 3.3E).

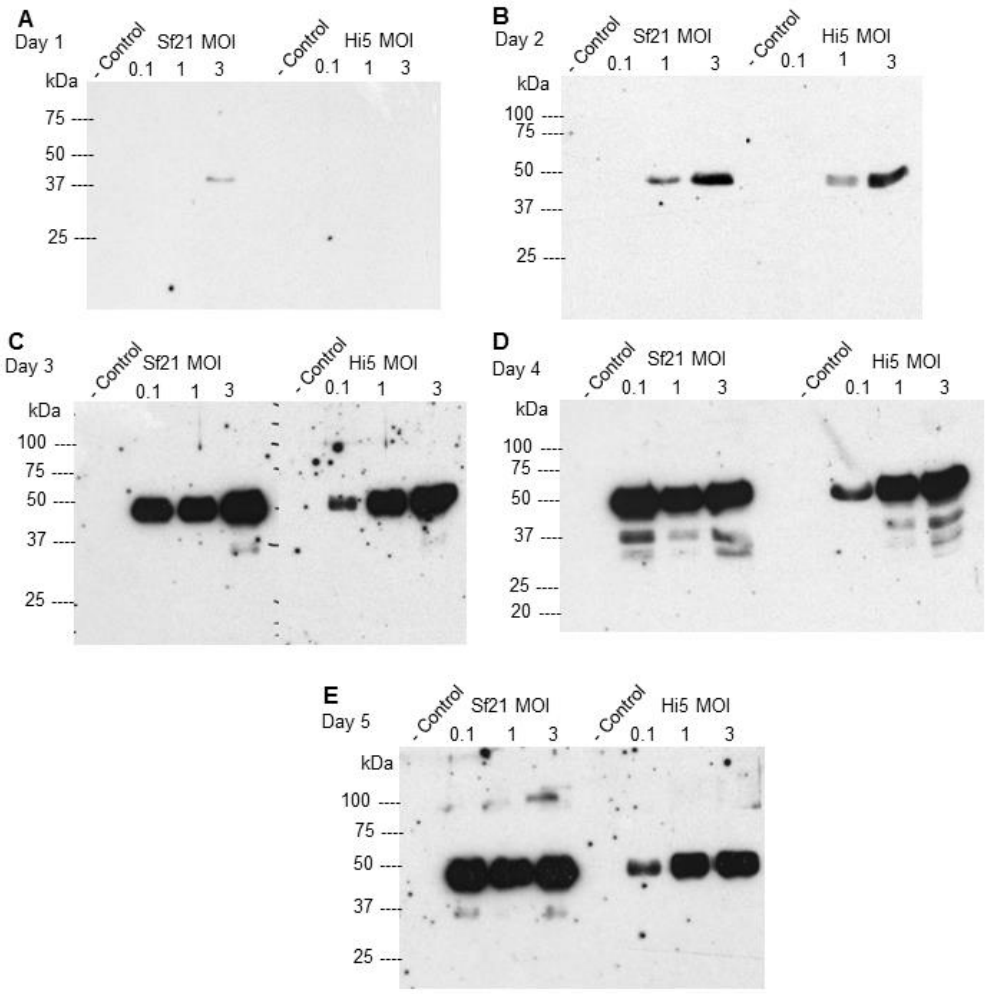

Figure 3.3. Effect of MOI on the expression and secretion of CD95R-Fc from Sf21 and Hi5 insect cells.
Sf21 and Hi5 cells were infected with working stock of FlashBAC Ultra-CD95R-Fc baculovirus at a range of MOIs. Samples were collected on days 1 – 5, post infection and subjected to western analyses (**A** – **E**). Samples from uninfected Sf21 and Hi5 cell cultures were also loaded as negative controls. 0.02% of total volume was loaded onto a SDS polyacrylamide gel and proteins separated by electrophoresis. The blot was prepared on a PVDF membrane and probed using anti-human IgG-Peroxidase (Sigma-Aldrich).

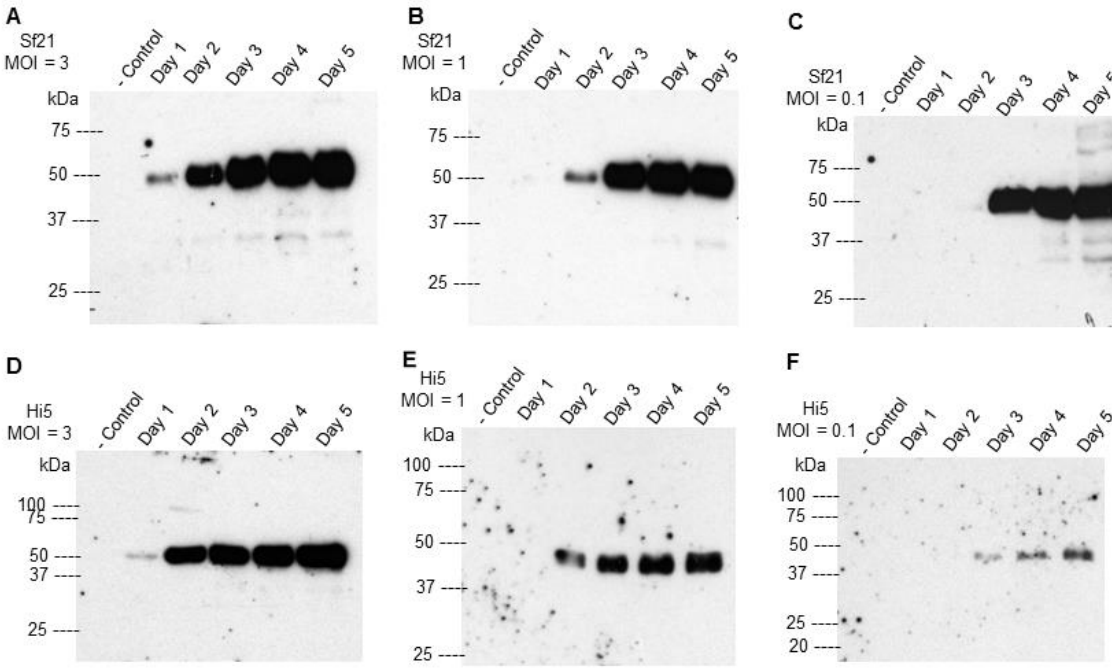

Figure 3.4. Effect of time on the expression and secretion of CD95R-Fc from Sf21 and Hi5 insect cells.
Sf21 and Hi5 cells were infected with working stock of FlashBAC Ultra-CD95R-Fc baculovirus, over 5 days, at a range of MOIs. MOI = 3 for **A** and **D**; MOI = 1 for **B** and **E**; and MOI = 0.1 for **C** and **F**. Samples from uninfected Sf21 and Hi5 cell cultures were also loaded as negative controls. 0.02% of total volume was loaded onto a SDS polyacrylamide gel and proteins separated by electrophoresis. The blot was prepared on a PVDF membrane and probed using anti-human IgG-Peroxidase (Sigma-Aldrich).

Figure 3.4 shows that with a higher MOI, detectable protein expression begins earlier and reaches maximal expression a shorter time period. For example, with Hi5 cells at MOI = 3, near maximal expression is reached by day 2 (although small increments are apparent on day 3 – 5; Figure 3.4D) but with an MOI = 1, maximal expression is reached on day 3 (Figure 3.4E). Together these data demonstrate that a lower MOI is sufficient to express maximal levels of protein, but a longer incubation time is required to reach this level. This is true of both cell lines, except for Hi5 cells at a MOI of 0.1, where maximal levels of protein are not reached (Figure 3.3E). This demonstrates that a higher MOI is favourable for maximum CD95R-Fc yield in Hi5 cells. Sf21 cells however, can produce maximal levels of protein using a lower MOI, as long as the incubation time is extended.

In conclusion, both cell types are suitable for protein expression under differing conditions. Using Sf21 cells and infecting at a low MOI (0.1) is suitable for conservative use of the baculovirus working stock. However, the longer expression times required result in the lower molecular weight bands present on Figure 3.2 and 3.3 at around 37 and 30 kDa. These are likely degradation products of CD95R-Fc and their presence is more noticeable in older cultures when the recombinant protein is more likely to encounter proteases released from lysed insect cells. When using a low MOI, it is therefore important not to leave cultures to grow for unnecessary long periods of time to prevent protein degradation. When using Hi5 cells however, a higher MOI (MOI = 3) and therefore more baculovirus is required for expression but high yields can be recovered after 72 hours. Since a high MOI results in a synchronous infection, higher protein yields are produced and can be recovered in a shorter time, reducing protein degradation.

3.2.4. Batch purification of CD95R-Fc

CD95R-Fc was purified on a test scale from 12ml of spent Sf21 culture medium by incubation with 500µl protein-A resin (slurry in 20% ethanol; section 2.7.1). The resin consists of a ligand complex based on protein-A, embedded in a cross-linked, agarose matrix (Hober et al., 2007) which allows purification of CD95R-Fc since it binds specifically to the Fc region of the fusion protein (Figure 3.2; residues 177 – 407). The resin was washed 3 times with 10 bed volumes of PBS. Bound CD95R-Fc was eluted in four fractions using 100mM citric acid (pH 3). Samples from each stage of the purification process were separated by SDS-PAGE, fixed and stained with colloidal blue to show total protein present (section

2.7.7, 2.7.8 & 2.7.9; Figure 3.5A). Eluates (E) 1 and 2 show CD95R-Fc at 46kDa, with few other proteins present, indicating pure samples with a good level of protein recovered. The percentage purity of E1 was estimated as 90% using ImageJ (detailed in section 2.7.10). To identify protein losses in the purification process, a sample from each fraction was analysed by western blot (section 2.7.11; Figure 3.5B). Some protein is lost, primarily in the flow through (FT) and the first wash (W1), however these were minimal compared to the yield. The amount of protein in E1 was estimated using densitometry in comparison with a BSA standard curve (Section 2.7.10). 1ml of E1 was found to contain 144µg of CD95R-Fc, representing a potential yield of 1.2mg per 100ml culture. Protein expressed by both FlashBAC Gold and Ultra viruses in Hi5 cells were also purified as described previously. Samples from the first elutions (E1) were separated by SDS-PAGE, fixed and stained with colloidal blue (Figure 3.5C) and analysed by western blot (Figure 3.5D). The elutions show CD95R-Fc at 46kDa on both the gel and western, with no difference in the molecular weight of protein expressed by each different baculovirus. The purity of protein recovered along with the yield demonstrates an efficient purification process, with both baculoviruses producing protein at the same molecular weight.

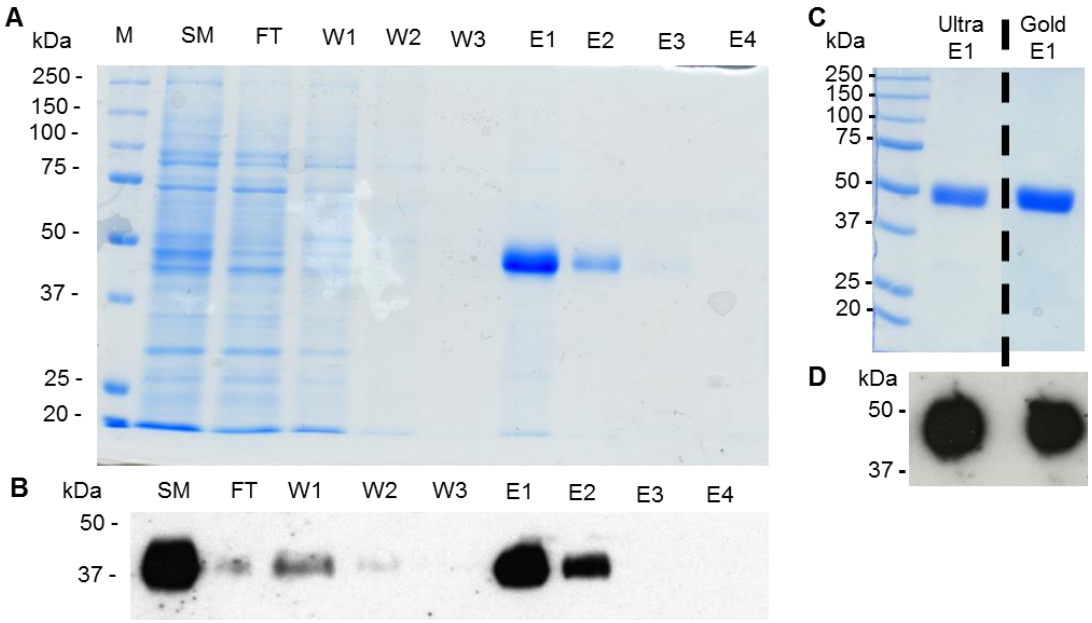

Figure 3.5. Purification of CD95R-Fc.
(**A**) 12ml of spent Sf21 cell culture was incubated with 500µl resin. Resin was washed in 3 x 5ml PBS and eluted in 4 x 1ml of 100mM citric acid (pH 3). Samples from each fraction were TCA precipitated and loaded onto a SDS polyacrylamide gel and the proteins separated by electrophoresis, fixed and stained with colloidal blue. SM: Starting Material (0.16% of total volume loaded), FT: Flow Through (0.16% of total volume), W1-W3: Wash 1 – Wash 3 (2% of total volume), E1-E4: Elution 1 – Elution 4 (2% of total volume), M: Marker. (**B**) Fraction samples were TCA precipitated and loaded onto a SDS polyacrylamide gel and proteins separated by electrophoresis. The blot was prepared on a PVDF membrane and probed using anti-human IgG-Peroxidase (Sigma-Aldrich). SM: 0.016% of total volume loaded, FT: 0.016% of total volume, W1-W3: 1% of total volume, E1-E4: 0.04% of total volume. (**C**) Hi5 cells were infected with either FlashBAC Ultra-CD95R-Fc or FlashBAC Gold-CD95R-Fc and 12ml of spent media from each culture were purified as in (**C**). Samples from each E1 were loaded onto a SDS polyacrylamide gel and the proteins separated by electrophoresis, fixed and stained with colloidal blue. E1: 1% of total volume. (**D**) Samples from each E1 were loaded onto a SDS polyacrylamide gel and proteins separated by electrophoresis. The blot was prepared on a PVDF membrane and probed using anti-human IgG-Peroxidase (Sigma-Aldrich). E1: 0.05% of total volume. Dashed line on (**C**) indicates other lanes of the same gel which were removed for convenience.

In order to optimise resin volume to spent culture media volume, batch purification was also carried out using 125µl and 250µl resin using the same method. Yield of protein recovered in the first elution for each resin volume, was estimated using densitometry in comparison with a BSA standard curve (section 2.7.10 and equation 2.1). As described previously, using 500µl resin gave a yield of 144µg of CD95R-Fc in the first elution. Using 125µl resin gave a yield of 132µg of CD95R-Fc and 250µl gave a yield of 152µg of CD95R-Fc. Using a larger resin volume does not therefore lead to increased recovery of protein. Similarly, using more resin does not lead to more non-specific binding since using 500µl gave an E1 fraction with 90% purity (Figure 3.6A). It is therefore possible to use a smaller volume of resin when batch purifying protein from small volumes of spent insect cell culture.

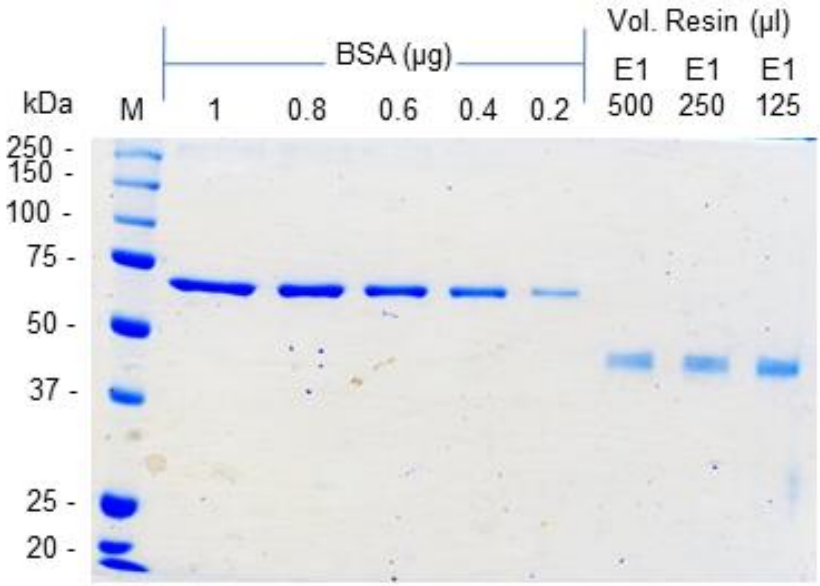

Figure 3.6. BSA protein quantification of E1 following purification with different resin volumes.
Samples from the first elution fraction following purification of 12ml spent insect cell culture with 125, 250 and 500µl resin were loaded onto an SDS polyacrylamide gel alongside known quantities of BSA. The proteins were separated by electrophoresis, fixed and stained with colloidal blue.

3.2.5. Optimisation of buffer-exchange following batch purification

In order to use CD95R-Fc in downstream applications (e.g. deglycosylation by PNGase F or coating of MPs for incubation with cancer cells), the protein may need to be buffer exchanged from 100mM citric acid (pH 3) into a more suitable condition such as PBS (pH 7.4). CD95R-Fc in spent insect cell culture (12ml) was purified as described previously (section 2.7.1), using 250µl resin, and the first elution fraction buffer-exchanged into PBS using a dialysis cassette (section 2.7.2; 10K MWCO; Thermo Scientific). The protein in the E1 was quantified by densitometry in comparison with a BSA standard curve (section 2.7.10 and equation 2.1) before dialysis (Figure 3.7A) and after dialysis (Figure 3.7B). The 'E1 2µl' value was used for quantifying CD95R-Fc before dialysis (Figure 3.7A) as the relative units for this protein band was within the linear range of BSA standards. 1ml of E1 was found to contain 270µg of CD95R-Fc before dialysis however, after dialysis E1 was found to contain 150µg of CD95R-Fc representing a loss of 44% after dialysis.

In order to optimise the recovery of protein during buffer exchange another method was investigated. Protein was purified using the same method as previously described, then the E1 fraction was buffer exchanged into PBS using a PD-10 desalting column (section 2.7.3; GE Healthcare). Samples from each 1ml fraction collected after buffer exchange were separated by SDS-PAGE (section 2.7.8; Figure 3.8A). CD95R-Fc was present in fractions 4 and 5.

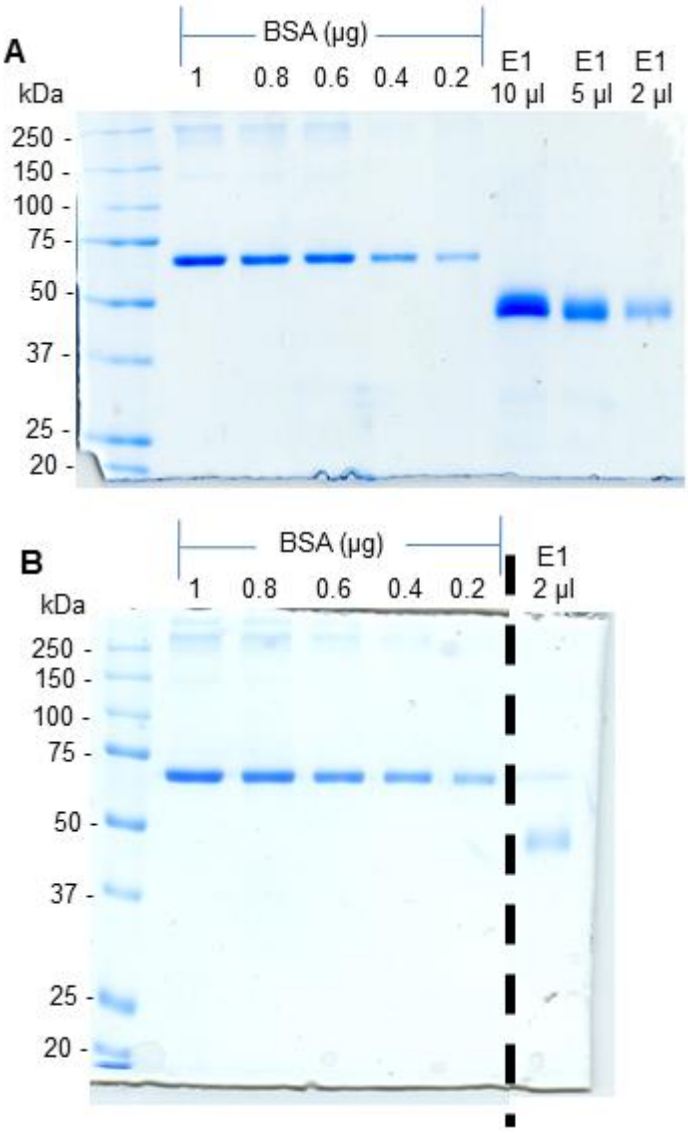

Figure 3.7. BSA protein quantification of E1 before and after dialysis.
Samples from the first elution fraction following purification of 12ml spent insect cell culture were loaded onto a SDS polyacrylamide gel alongside known quantities of BSA, before (**A**) and after (**B**) dialysis. The proteins were separated by electrophoresis, fixed and stained with colloidal blue. Dashed line on (**B**) indicates other lanes of the same gel which were removed for convenience.

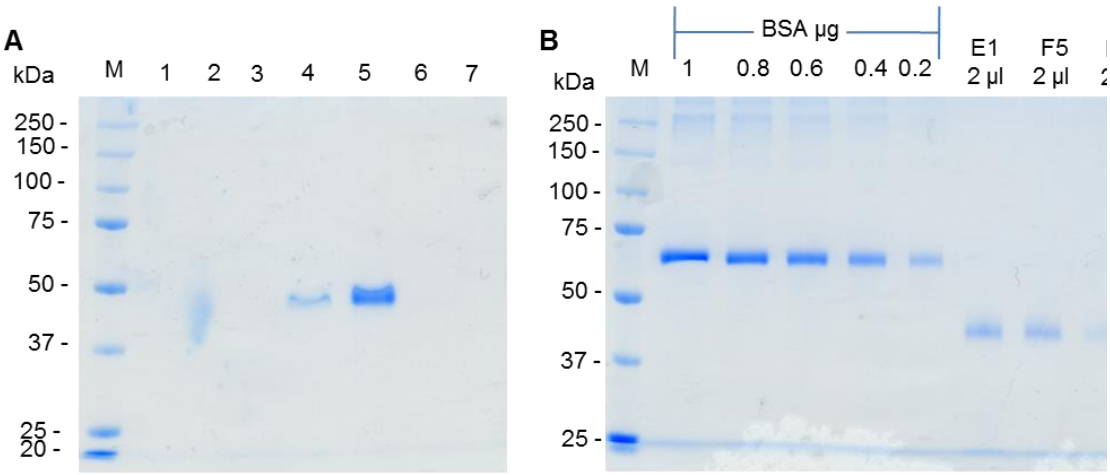

Figure 3.8. Buffer exchange using a PD-10 desalting column.
(**A**) Samples from each fraction collected throughout buffer exchange were loaded onto a SDS polyacrylamide gel, separated by electrophoresis, fixed and stained with colloidal blue. 1 – 7: Fraction 1 to Fraction 7 and M: Marker. Protein is present in fraction 4 and 5. (**B**) Samples from the first elution (E1) after purification and the fractions containing protein after buffer exchange (F4, F5; fractions 4 and 5) were loaded onto a SDS polyacrylamide gel alongside known quantities of BSA. The proteins were separated by electrophoresis, fixed and stained with colloidal blue.

The protein in E1 before buffer exchange and in fractions 4 and 5 after buffer exchange using a PD-10 column, was estimated using densitometry in comparison with a BSA standard curve (section 2.7.10 and equation 2.1; Figure 3.8B). 1ml of E1 was found to contain 142µg of CD95R-Fc before buffer exchange. Fraction 5 was found to contain 120µg of CD95R-Fc and fraction 4, 20µg. The recovery of protein after buffer exchange using a PD-10 desalting column is 98%, compared to 56% by dialysis. To buffer exchange small volumes of elution from batch purification into PBS, a PD-10 column will therefore be used to minimise loss of protein.

3.2.6. The recombinant CD95R-Fc expressed by Sf21 and Hi5 cells is glycosylated

Differences in glycosylation have been observed when the same recombinant protein is expressed in Sf21 and Hi5 cells. For example, when the heavily glycosylated, scavenger receptor CD36 is expressed in these two cell lines, heterogeneity in glycosylation is observed not only at different sites, but also between glycans occupying the same site (Sanders, 2015). To compare the glycosylation status of CD95R-Fc expressed in Sf21 cells and Hi5 cells, spent culture media from each cell line infected with the working stock of baculovirus, was denatured and treated with PNGase F and analysed by western blot (section 2.7.12 & 2.7.11; Figure 3.9A). PNGase F is an endoglycosidase capable of removing all N-linked glycans (Tretter et al., 1991). Digestion of CD95R-Fc secreted from both insect cell lines with PNGase F resulted in a slight increase in electrophoretic mobility indicating that CD95R-Fc is glycosylated in both cell lines.

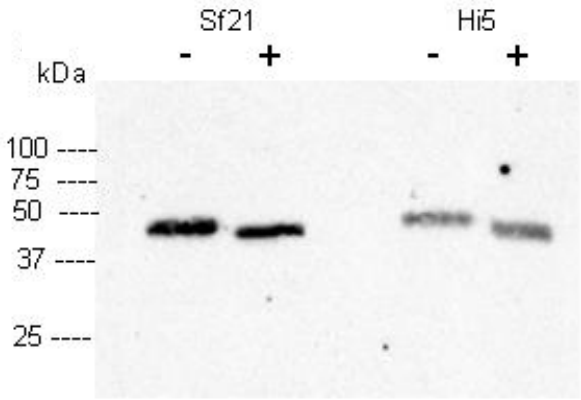

Figure 3.9. Deglycosylation of CD95R-Fc secreted from Sf21 and Hi5 insect cells using PNGase F.
3µl and 1µl of spent media containing CD95R-Fc from Sf21 and Hi5 insect cells, respectively, was treated with 500U of PNGase-F (+ samples) for 2 hours at 37°C. Control samples were also loaded, without any PNGase-F (- samples). Samples were loaded onto a SDS polyacrylamide gel and the proteins separated by electrophoresis. The blot was prepared on PVDF membrane and probed using anti-human IgG-Peroxidase (Sigma-Aldrich).

3.2.7. The purified CD95R-Fc can induce microparticle uptake in MDA-MB-231 cells

Purified CD95R-Fc from Sf21 cells was used to coat fluorescent 0.5µm polystyrene microparticles (MPs) via passive adsorption (section 2.8). Briefly, proteins are incubated with particles at a ratio of 0.5µg CD95R-Fc protein:1µg MP, for 90 minutes at 37°C, with mixing every 20 minutes. Adsorption occurs based on hydrophobic attractions between the hydrophobic portions of the adsorbed ligands and the polymeric surface of the microspheres (Bangs, 2008a). The coated particles are then added to MDA-MB-231 cells for 24 hours and unbound particles washed off before analysis using flow cytometry (section 2.9.1). Cells were also incubated with no particles (PBS only, negative control), non-coated particles and OET CD95R-Fc expressed in Sf21 cells (commercially-sourced protein as a positive control). The population of cells was analysed by flow cytometry, gating on cells with normal size but including a large range of granularity because polystyrene particle uptake will make the cells appear more granular (Figure 3.10A). Fluorescence emitted by the fluorescein label of the MP was detected in the FL-1 channel. Efficiency of MP uptake was determined by measuring the percentage of the gated cells with a fluorescence level above the autofluorescence of cells in the absence of particles (Figure 3.10B - E). Patterns of fluorescence from representative experiments were overlaid on a histogram (Figure 3.11) with distinct peaks which likely represent different numbers of internalised MPs per cell. The percentage uptake over the gated population for each condition, along with commercially available CD95R-Fc expressed in Sf21 cells from Sigma, was analysed by ANOVA for 3 independent repeat experiments (section 2.15; Figure 3.12).

The percentage uptake (the percentage of cells in the population with fluorescence levels above the negative control) for the CD95R-Fc purified in-house was 56 +/- 5% (Figure 3.12A) and was statistically different ($P \leq 0.0001$) to the mean uptake of non-coated particles, 7 +/- 3%. The mean uptake for the positive controls (OET, 60 +/- 4%; Sigma, 61 +/- 3%) were also statistically different, $P \leq 0.0001$, to non-coated particles. The percentage uptake of MPs opsonised with commercially-sourced CD95R-Fc (OET & Sigma) and CD95R-Fc made in-house was not statistically different ($P > 0.05$) suggesting all proteins improve uptake with the same efficiency. Uptake of cells incubated with non-coated particles and with no particles was not statistically different ($P > 0.05$).

Cells had the highest median fluorescence when coated with the CD95R-Fc made in-house (Figure 3.11), indicating a higher number of internalised MPs per cell. This is also demonstrated by a larger spread of events and increased side scatter (correlating to increased cell granularity as MPs are absorbed) on the scatter plot when comparing uptake of in-house CD95R-Fc coated MPS (Figure 3.10E) to OET coated CD95R-Fc (Figure 3.10D). The median fluorescence of cells with particles from 3 independent, repeat experiments was analysed to explore this further (Figure 3.12B). Cells incubated with in-house CD95R-Fc coated MPs, had a median fluorescence of 72 +/- 12 AFU. Cells incubated with MPs opsonised with the Sigma and OET protein had a median fluorescence of 73 +/- 7 AFU and 52 +/- 2 AFU, respectively.

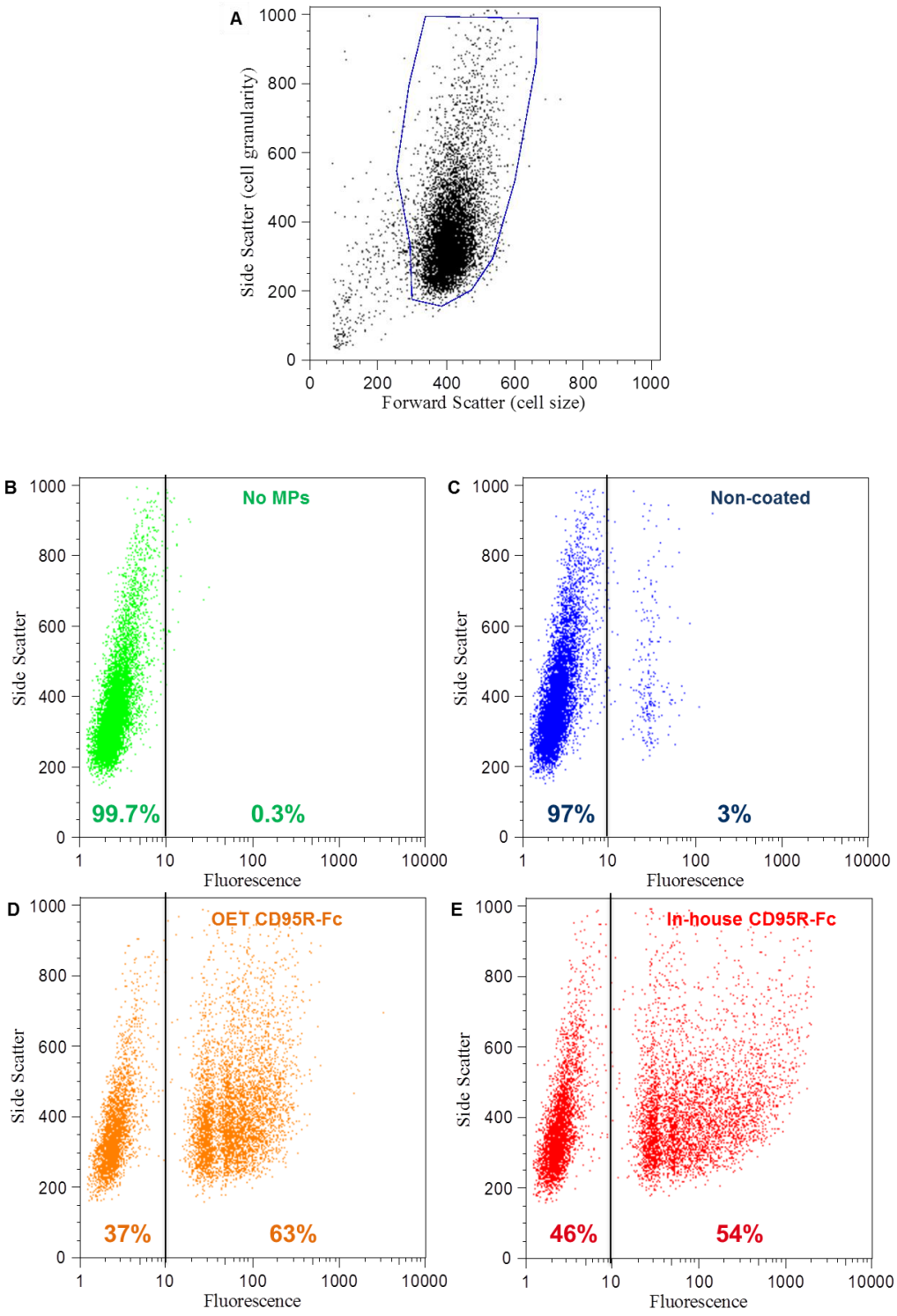

Figure 3.10. CD95R-Fc coating improves uptake of MPs in MDA-MB-231 cells.
MDA-MB-231 cells were incubated with fluorescent, 0.5µm MPs for 24 hrs and analysed by flow cytometry. Results from one representative experiment. (**A**) Scatter plot showing forward scatter and side scatter correlating with cell size and granularity, respectively. Cells were gated (blue line) to eliminate cell debris. 10,000 gated cells were analysed. (**B**) A scatter plot of cell fluorescence (arbitrary fluorescence units) against side scatter (cell granularity, arbitrary units) for cells incubated with PBS. (**C**) A scatter plot of cell fluorescence against side scatter for cells incubated with non-coated particles. Percentage of events in the left-hand panel indicates cells with no particles and the right-hand panel indicates of cells with particles. (**D**) A scatter plot of cell fluorescence against side scatter for cells incubated with OET (positive control – commercially available) CD95R-Fc coated particles. (**E**) A scatter plot of cell fluorescence against side scatter for cells incubated with in-house CD95R-Fc coated particles.

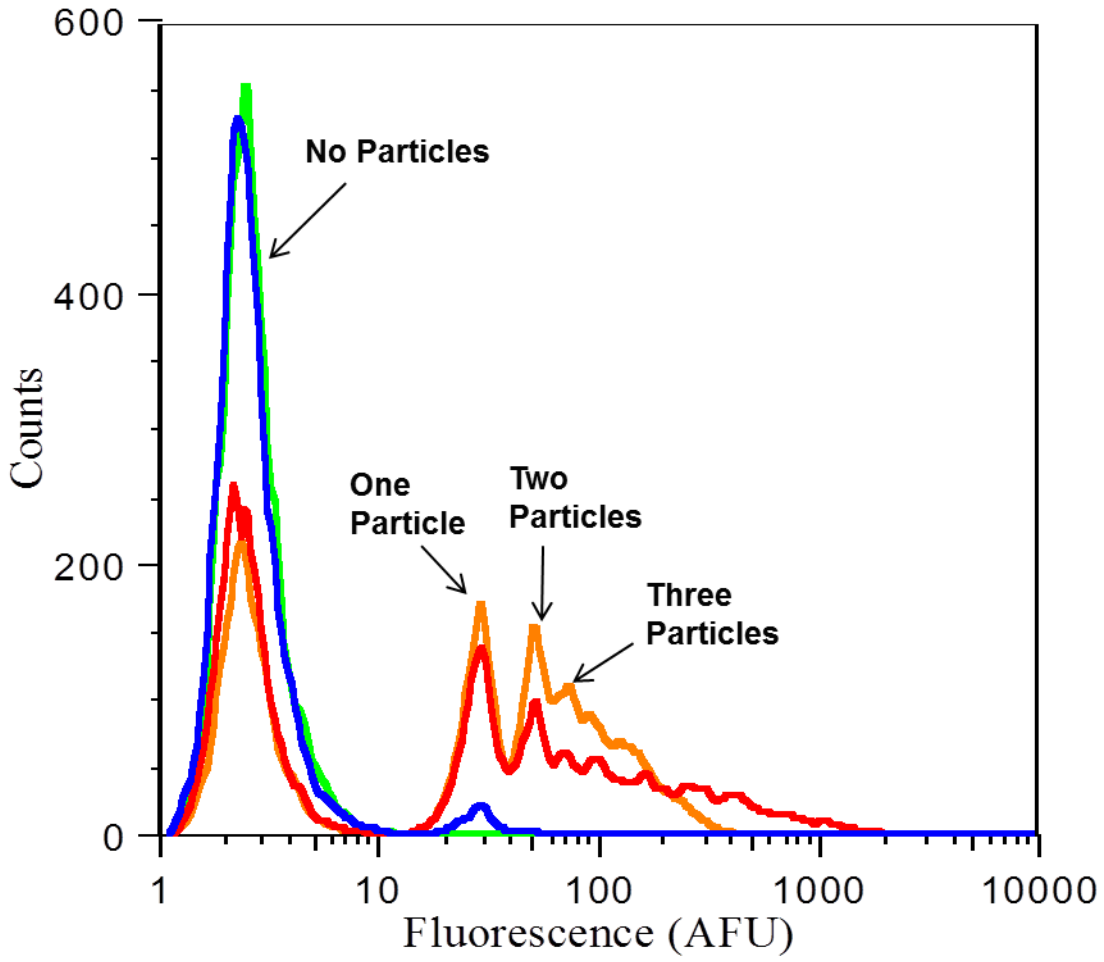

Figure 3.11. Histogram displaying uptake of CD95R-Fc opsonised MPs.
MDA-MB-231 cells were incubated with fluorescent, 0.5µm MPs for 24 hrs and analysed by flow cytometry. Cells were gated to eliminate cell debris. 10,000 gated cells were analysed. Results were overlain on a histogram, displaying distribution of fluorescence against number of cells (counts) for all conditions. Peaks on left, under 10 arbitrary fluorescence units (AFU) represents the auto-fluorescence of the cells without particles (green), and peaks to the right indicate cells which have taken up particles. Median fluorescence for cells with particles (i.e. above the background autofluorescence cut-off of 10 AFU) was 28 AFU for non-coated particles (blue), 55 AFU for OET CD95R-Fc coated particles (orange), and 64 AFU for the in-house CD95R-Fc coated particles (red). The series of peaks on the right likely reflect the number of particles in the cell, as labelled.

However, there was no statistical difference between the median fluorescence of cells incubated with the positive control proteins and in-house CD95R-Fc coated MPs. Therefore, the protein made in-house is as effective as commercially available CD95R-Fc at inducing efficient uptake with a similar number of particles internalised per cell.

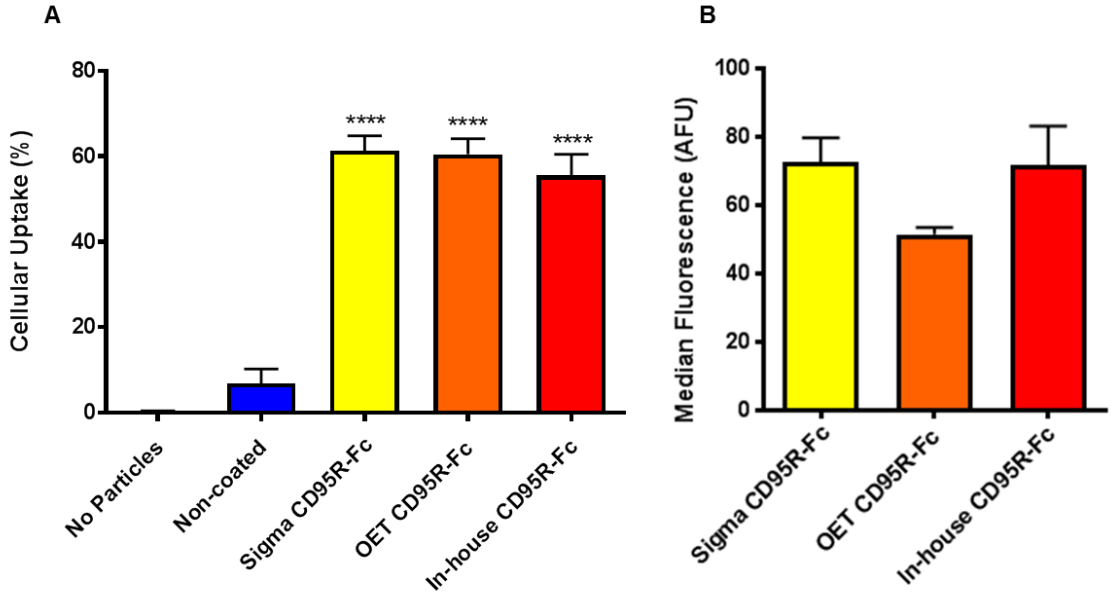

Figure 3.12. Statistical analysis of uptake of CD95R-Fc opsonised MPs.
MDA-MB-231 cells were incubated with fluorescent, 0.5µm MPs for 24 hrs and analysed by flow cytometry. Cells were gated to eliminate cell debris. 10,000 gated cells were analysed. Mean and SEM values are from three independent, repeat experiments (n=3). Significance was calculated by one-way ANOVA; **** $P \leq 0.0001$. (**A**) Mean percentage uptake of cells incubated with no particles (negative control), non-coated, Sigma and OET CD95R-Fc (commercially available proteins – positive controls) and in-house CD95R-Fc coated particles. In-house, Sigma and OET CD95R-Fc coated MP uptake was statistically different to non-coated MPs. (**B**) Mean median fluorescence of cells with particles, incubated with Sigma, OET and in-house CD95R-Fc coated particles. There was no statistical difference between these conditions ($P > 0.05$).

Important coating controls were tested to confirm that the CD95R ectodomain was the key moiety of the CD95R-Fc fusion protein for cellular uptake (Figure 3.13A). Particles were coated with either human IgG – Fc fragment (Abcam), to control for the Fc portion of CD95R-Fc, or an excess of bovine serum albumin (BSA), as this is present in the preparations of CD95R-Fc sourced from Sigma and to control for the effect of a non-specific protein coat (section 2.8). These additional control samples were run alongside previous conditions for direct comparison; no particles (PBS only, negative control), non-coated particles and CD95R-Fc expressed and purified in-house. MPs were prepared as described

before and incubated with MDA-MB-231 cells before measuring uptake using flow cytometry (section 2.9.1). Furthermore, protein expressed in Hi5 cells by either the recombinant FlashBAC Ultra-CD95R-Fc or FlashBAC Gold-CD95R-Fc baculoviruses, was purified (Figure 3.5C & D), used to coat particles and incubated with MDA-MB-231 cells (Figure 3.13B), in order to elucidate any differences between protein expressed by each different virus. The percentage uptake for each condition was analysed by ANOVA for 3 independent, repeat experiments (section 2.15; Figure 3.13A & B).

The percentage uptake for the expressed, in-house CD95R-Fc was 63 +/- 3% (Figure 3.13A) and was found to be statistically different ($P \leq 0.0001$) to the mean uptake of 7 +/- 2% for non-coated particles, 9 +/- 3% for BSA coated particles, and 7 +/- 2% for Fc coated particles. The percentage uptake of MPs opsonised with BSA or Fc protein was not statistically different to each other ($P > 0.05$), and neither of these proteins was statistically different to non-coated particles. Uptake of MPs by cells incubated with non-coated particles was not statistically different ($P > 0.05$) to the level of cellular fluorescence recorded in the absence of particles. This suggests that the CD95 portion of the CD95R-Fc fusion protein is responsible for the increased uptake seen.

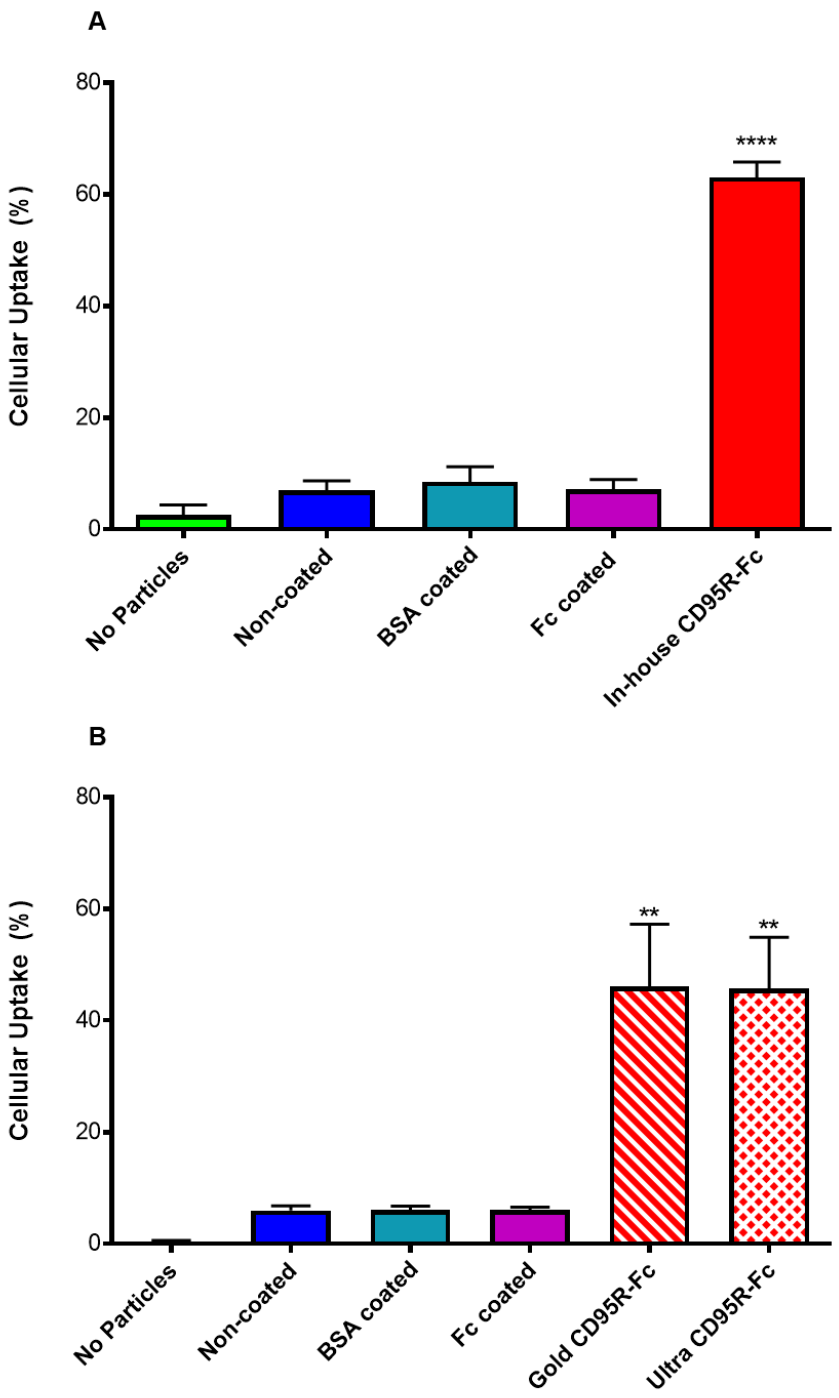

Figure 3.13. CD95R is responsible for increased uptake of CD95R-Fc modified particles, irrespective of the baculovirus used for expression.
MDA-MB-231 cells were incubated with fluorescent, 0.5µm MPs for 24 hrs and analysed by flow cytometry. Cells were gated to eliminate cell debris. 10,000 gated cells were analysed. Mean and SEM values are from three independent, repeat experiments (n=3). Significance was calculated by one-way ANOVA; **** $P \leq 0.0001$ and ** $P \leq 0.01$. (**A**) Mean percentage uptake of cells incubated with no particles (negative control), non-coated particles, BSA, Fc and in-house-purified CD95R-Fc coated particles. In-house-purified CD95R-Fc coated MP uptake was statistically different to non-coated MPs, BSA and Fc coated MPs. (**B**) Mean percentage uptake of cells incubated with no particles (negative control), non-coated particles, BSA, Fc and CD95R-Fc coated particles expressed using FlashBAC Ultra-CD95R-Fc or FlashBAC Gold-CD95R-Fc baculoviruses. Uptake of CD95R-Fc coated MPs, expressed using GOLD or ULTRA, were statistically different to non-coated MPs, BSA and Fc coated MPs. No difference was observed between the CD95R preparations from GOLD or ULTRA viruses.

For Figure 3.13B, a similar trend is seen. Percentage uptake for CD95R-Fc expressed by the GOLD virus, 46 +/- 11%, and the ULTRA virus, 46 +/- 9%, was found to be statistically different ($P \leq 0.01$) to the mean uptake of non-coated particles, 6 +/- 0.3%, BSA coated, 6 +/- 1% and Fc coated particles, 6 +/- 0.5%. There is no statistical difference in uptake when particles have been coated in CD95R-Fc which has been expressed using the GOLD or the ULTRA baculoviruses ($P > 0.05$).

3.2.8. Stability and storage of CD95R-Fc prepared in-house

Following buffer exchange, CD95R-Fc was stored at 4°C in PBS (pH 7.4). In order to optimise storage conditions, two batches of protein were expressed by Hi5 cells at an MOI of 3, for 72 hours (section 2.4.5). Spent insect cell media was collected and CD95R-Fc was purified (as in section 3.2.4) and buffer exchanged into PBS. The batches of protein were stored at 4°C for different lengths of time and then analysed by Western blot (Figure 3.14A). There is a distinct increase in Fc-containing proteins migrating at 30 kDa after 12 weeks storage (lane 1), compared to 3 weeks storage (lane 2), indicating a level of protein degradation. Sodium azide is not added to the protein samples, since this protein is used to coat MPs which are added directly to cells. Therefore, it is possible that contamination or bacterial growth are responsible for this degradation. The presence of a signal, migrating at around 90kDa in the 12-week sample, may also suggest a small amount of aggregated protein on prolonged storage.

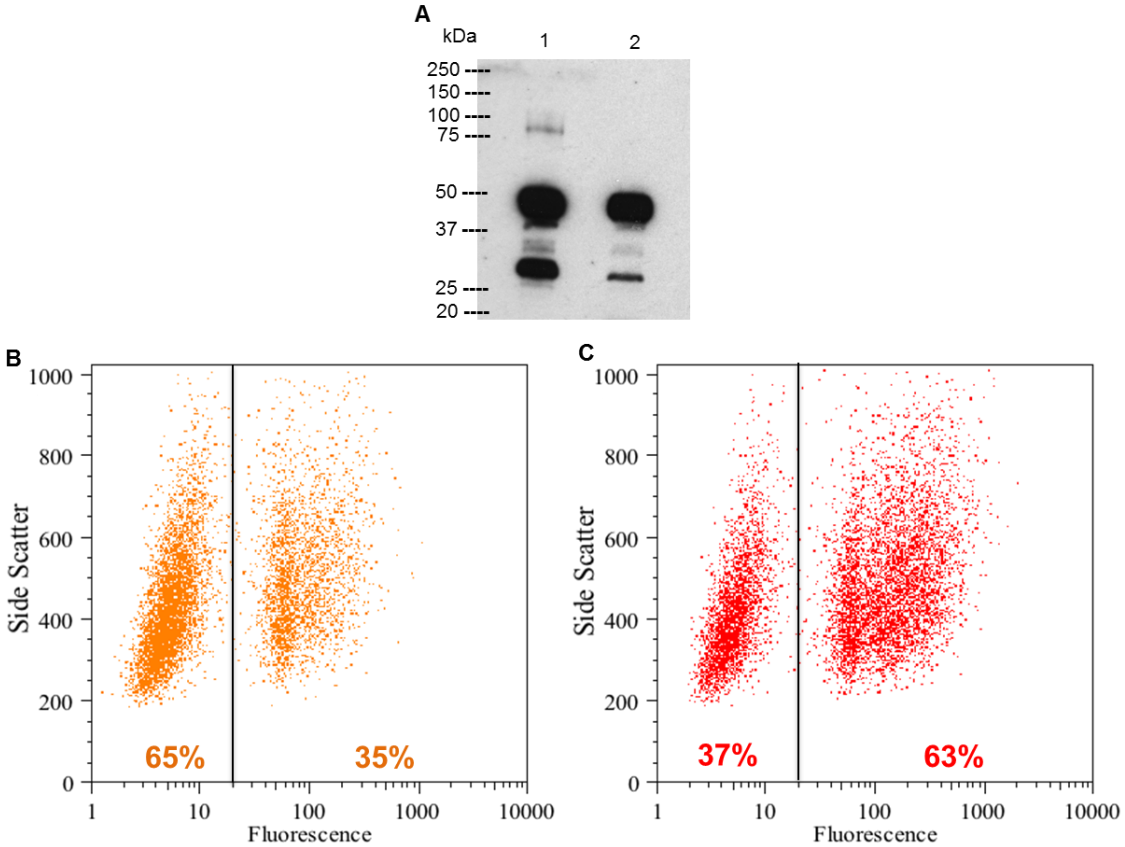

Figure 3.14. Long-term storage at 4°C leads to CD95R-Fc degradation which impacts uptake efficiency.
(**A**) Purified and buffer exchanged CD95R-Fc was stored at 4°C for 12 weeks (lane 1) and 3 weeks (lane 2). Equal weights of each sample (0.05ug) were loaded onto a SDS polyacrylamide gel and the proteins separated by electrophoresis. The blot was prepared on PVDF membrane and probed using anti-human IgG-Peroxidase (Sigma-Aldrich). (**B**) Microparticles (MPs) were coated in each protein, incubated with MDA-MB-231 for 24 hrs and cells analysed by flow cytometry. Cells were gated to eliminate cell debris. 10,000 gated cells were analysed. Results from a single experiment are shown. A scatter plot of cell fluorescence (arbitrary fluorescence units) against side scatter (cell granularity, arbitrary units) for cells incubated with MPs coated in CD95R-Fc stored at 4°C for 12 weeks. Percentage of events in the left hand panel indicates cells with no particles and the right hand panel indicates of cells with particles. (**C**) A scatter plot of cell fluorescence against side scatter for cells incubated with MPs coated in CD95R-Fc stored at 4°C for 3 weeks. Percentage of events in the left hand panel indicates cells with no particles and the right hand panel indicates of cells with particles.

The effect of storage time on protein quality was noticeable when the proteins analysed in Figure 3.14A, were used to coat MPs, and incubated with MDA-MB-231 cells (section 2.9.1). Results from a single experiment show that percentage uptake for CD95R-Fc after 12 weeks storage at 4°C was 35% (Figure 3.14B), representing a decrease in uptake by 44%, in comparison to CD95R-Fc after 3

weeks storage at 4°C (uptake 63%, Figure 3.14C). For short-term storage (up to 3 weeks) of CD95R-Fc, 4°C in PBS (pH 7.4) appears to be reasonably stable, with similar rates of uptake to fresh material (56 +/- 5%, Figure 3.12A).

However, for longer term storage, a different solution was required and freezing at -20°C was tested with added BSA to act as a cryoprotectant (Koda et al., 2001), and as a “carrier” or “filler” protein, protecting dilute protein solutions (under 1mg/ml) against degradation and loss. Protein was expressed and purified as previously described and half was buffer exchanged into PBS (Figure 3.15A; lane 1) and the other half was buffer exchanged into PBS and BSA (50ug BSA per 1ug CD95R-Fc, lanes 2 and 3). Lanes 1 and 2 were both stored at 4°C for 3 weeks after buffer exchange. The presence of smaller molecular weight proteins in lane 1 suggest degradation, however the addition of BSA has a protective effect for small amounts of time at 4°C. Lane 3 demonstrates protein which was frozen after buffer exchange and thawed 3 weeks later, suggesting that protein integrity is maintained through a round of freeze-thaw.

These proteins were then used to coat MPs and incubated with MDA-MB-231 cells, to test the effect of storage and added BSA on particle uptake (Figure 3.15B & C). Results from two repeat experiments are similar to previous results, that CD95R-Fc-coated MPs improve uptake (PBS, 4°C; 66 +/- 2%) compared to the controls: cells only, 0.8 +/- 0.2% and non-coated particles, 5 +/- 0.6%.

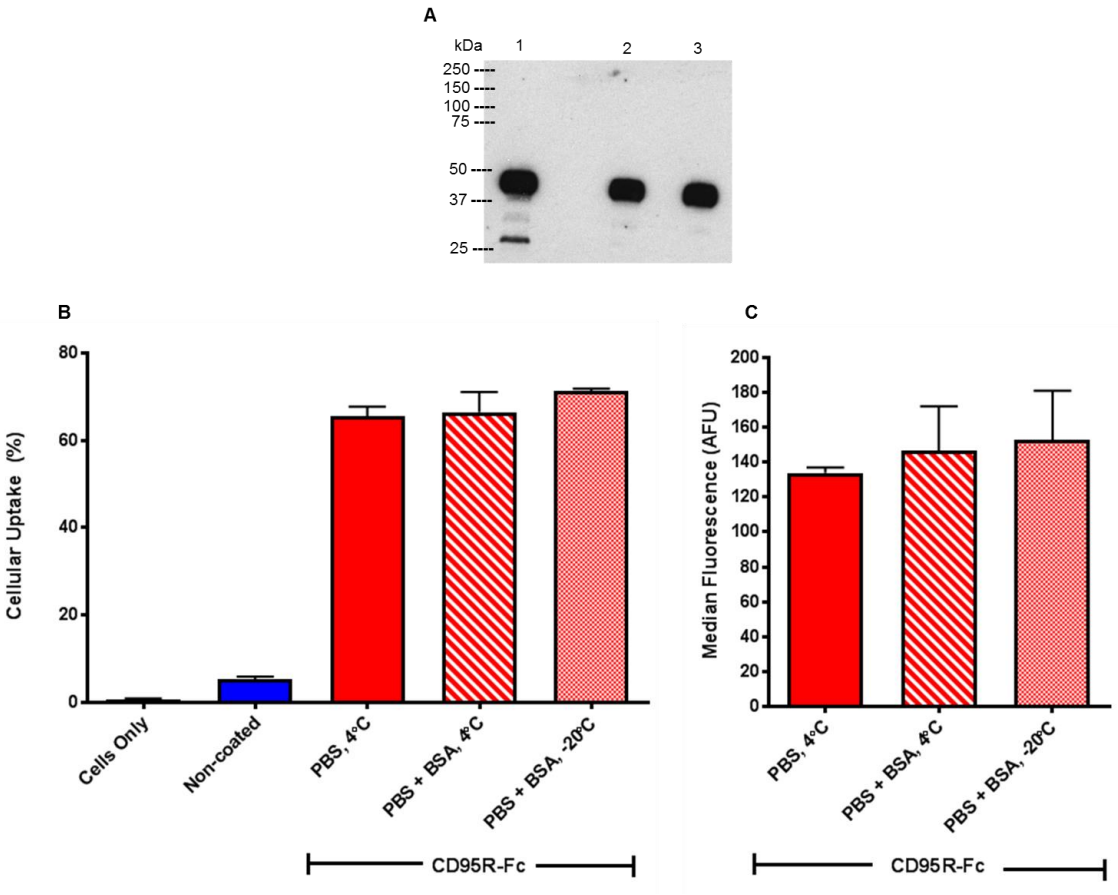

Figure 3.15. Additional BSA improves CD95R-Fc stability enabling long term storage. (**A**) Purified CD95R-Fc was buffer exchanged into PBS (lane 1) or PBS & BSA (50ug BSA:1ug CD95R-Fc; lanes 2 & 3). Protein was stored at 4°C (lane 1 & 2) or -20°C for 3 weeks (lane 3). Equal weights of each sample (0.05ug) were loaded onto an SDS polyacrylamide gel and the proteins separated by electrophoresis. The blot was prepared on PVDF membrane and probed using anti-human IgG-Peroxidase (Sigma-Aldrich). (**B**) Microparticles (MPs) were coated in each protein, incubated with MDA-MB-231 for 24 hrs and cells analysed by flow cytometry. Cells were gated to eliminate cell debris. 10,000 gated cells were analysed. Mean and SEM values are from two independent, repeat experiments (n=2). Mean percentage uptake of cells incubated with no particles, non-coated particles, or CD95R-Fc coated particles, stored in PBS at 4°C, PBS & BSA at 4°C or PBS & BSA at -20°C. (**C**) Mean median fluorescence of cells with particles, incubated with CD95R-Fc coated particles, stored in PBS at 4°C, PBS & BSA at 4°C or PBS & BSA at -20°C.

The addition of BSA to CD95R-Fc does not cause a noticeable change in percentage uptake of CD95R-Fc coated particles, nor does a round of freeze-thaw lead to any detrimental effects (PBS & BSA, 4°C; 67 +/- 5%, -20°C; 71 +/- 0.5%). When the median fluorescence levels are analysed to assess the number of MPs taken up per cell, there is a trend toward increased uptake following the

addition of BSA to CD95R-Fc and immediate storage at -20°C but there is sufficient difference in the two data sets to suggest that these differences represent random variability. The median fluorescence for CD95R-Fc in PBS & BSA, 4°C was 147 +/- 26 AFU and at -20°C, 153 +/- 28 AFU compared to CD95R-Fc in PBS only at 4°C, 134 +/- 3 AFU. Therefore, for long-term storage, CD95R-Fc was buffer exchanged into PBS and BSA, and kept at -20°C.

3.3. Discussion

The baculovirus/insect cell expression system is a useful tool for the expression of recombinant protein. In comparison to bacterial, yeast or mammalian cell expression, this system is an appealing alternative especially since insect cells are capable of post-translational modifications ensuring correct folding. Human CD95R ECD fused to human Fc domain has previously been expressed successfully using a baculovirus in Sf9 cells and in *Bombyx mori* (silkworm) larvae (Muraki and Honda, 2010). In this chapter, the successful expression and purification of mouse CD95R ECD fused with the Fc region of human IgG1, expressed in Sf21 and Hi5 cells, is described. The purified CD95R-Fc was used to coat MPs that may offer a novel therapeutic method for targeting and delivering cytotoxic drugs to cancer cells, reducing the debilitating side effects of current chemotherapy regimens. Via an undescribed mechanism, CD95R-Fc coated poly(lactic-co-glycolic) acid (PLGA) MPs are internalised and degraded, resulting in the release of loaded, cytotoxic compounds. The future development of this system is dependent on the production of recombinant CD95R-Fc to characterise and optimise therapeutic delivery.

Recombinant virus generated using the *flash*BAC GOLD system and an ULTRA version outsourced to OET were compared as vehicles for expression of CD95R-Fc. As CD95R-Fc is a type I membrane protein (see section 1.4.1), the N-terminal part of the protein is extracellular therefore, the truncated ECD (with no transmembrane domain (TMD) to anchor the protein to the membrane) is targeted to be secreted by eukaryotic cells. No differences in yield or purity of expressed CD95R-Fc from each virus was observed, therefore the two viruses

were used interchangeably. CD95R-Fc expression was also tested in Sf21 and Hi5 cells. At a lower MOI, the infected cultures require a longer incubation time to reach maximal protein expression. This is because at a high MOI, synchronous infection can be achieved (Licari and Bailey, 1991) to produce more protein in less time. At a low MOI, a smaller fractions of cells are initially infected (Wong et al., 1996) and so a small amount of protein is expressed in the same time frame. However, the infected insect cells will produce progeny virus budded from the plasma membrane resulting in a second round of infection of remaining cells (Wong et al., 1996). This requires more time, hence the time delay for maximal protein expression. For infection at low MOI, less 'working stock' virus is used with the advantage of cost efficiency and, time because there is a reduced requirement for rounds of baculovirus amplification. Conversely, baculoviral infection causes cell lysis, releasing cellular proteins including proteases into the surrounding media. Cruz *et al.* have suggested that at low MOI, with fewer cells infected, higher levels of active proteases may be present in the media since cell infection decreases protease synthesis (Cruz et al., 1999). It is possible that with a low MOI, CD95R-Fc secreted into the surrounding media could be degraded by proteases released from lysed insect cells. This may explain the presence of lower molecular weight bands on the western blots that appear in the older cultures. They are likely degradation products of CD95R-Fc; a disadvantage of using a low MOI and longer incubation time. Sf21 cells were found to be superior to Hi5 cells at expressing maximal levels of protein with the lowest MOI (0.1). A higher MOI is favourable for maximum CD95R-Fc yields in Hi5 insect cells. Hi5 cells have been found to be 100-fold less efficient at budding baculoviruses in comparison to Sf9 cells (Wilde et al., 2014). As use of a low MOI relies on production of the progeny virus and a second round of infection, this likely

explains why Hi5 cells do not produce maximal levels of protein at a low MOI. Hi5 cells are generally considered superior for secreting proteins resulting in high product yields (Wilde et al., 2014). However, no noticeable difference was observed in maximal yields of protein produced by Sf21 and Hi5 cells by day 5 of expression. In conclusion, both cell types are suitable for protein expression under differing conditions. Using Sf21 cells and infecting at a low MOI is suitable for conservative use of the baculovirus working stock, saving time and cost of amplifying baculovirus to replenish stocks. This is especially important when using the baculovirus/insect cell system for possible large-scale protein production in the future. With Hi5 cells, a higher MOI is necessary but high yields can be recovered after 72 hours. Since a high MOI results in a synchronous infection, higher protein yields are produced and can be recovered in a shorter time, reducing protein degradation. Both cell lines were used interchangeably to express CD95R-Fc for future work, with appropriate MOIs and incubation times to ensure good protein quality.

For purification of the secreted, recombinant protein from the spent culture medium, affinity chromatography was used. MabSelect resin (GE Healthcare) consists of a highly cross-linked, agarose matrix with a recombinant protein A ligand that has a binding specificity similar to native protein-A. The recombinant protein-A is specifically engineered to favour an orientated coupling that gives an affinity medium with enhanced binding capacity for IgG (Teng et al., 2000). Recombinant proteins which are engineered with an in-frame Fc tag can exploit this affinity for purification purposes. CD95R-Fc was purified in this manner, in batch, with a highly efficient yield and purity of >90%. The yield with 500µl resin

was found to be 1.2mg per 100ml culture with minimal losses after buffer exchange, which compares favourably with the previously reported yield of 215µg per 100ml culture when human CD95R ECD was expressed with an Fc tag via baculovirus in Sf9 cells (Muraki and Honda, 2010). Different resin volumes were tested and found little difference in the recovery of protein from the same volume of culture media. For 12ml culture, 125ul of resin was sufficient, with only a small loss of yield compared to 500ul and would ensure conservative use of the MabSelect (GE Healthcare). There was little non-specific binding when a large excess (500 ul per 12ml culture volume) of resin was used, testament to the avidity of the MabSelect for Fc and demonstrating that the washing conditions were adequate.

In order to use CD95R-Fc for downstream applications, two buffer-exchange protocols were tested to exchange from the elution buffer into PBS. Using a dialysis cassette, only 56% of protein was recovered. This is most likely due to a combination of factors including hydrophobic regions of the protein interacting with the dialysis membrane, and pipetting losses when working with small volumes. A PD-10 desalting column, which uses a Sephadex matrix rather than a membrane to buffer exchange protein solutions (Healthcare, 2007) gave much higher percentage of recovery. This will prove useful in future batch purifications to buffer exchange volumes up to 2.5ml. For a larger elution volume, a different method will need to be investigated for buffer exchange. Furthermore, the PD-10 desalting column dilutes the protein from a 1ml elution, to two 1ml fractions. However, these fractions could be pooled and concentrated using a spin column if necessary. These columns contain a membrane with a pore size that is chosen

to ensure the protein cannot pass through but that will allow excess solution through.

In humans, CD95 is glycosylated at two sites in the ECD at N118 and N136 (Shatnyeva et al., 2011). The mouse sequence of CD95R (Figure 3.2) has a conserved sequence for glycosylation at N114 (due to a 4 amino acid deletion compared to the human sequence); the site at N136 is not conserved. *In silico* computer modelling has predicted that N136 may play a role for CD95R/CD95L interactions since this glycan is in close proximity to CD95L when bound and could form an extensive hydrogen bond network with residues 200–204 of CD95L (Shatnyeva et al., 2011). However, this is concluded only from modelling; there is no crystal structure of CD95R bound to its ligand to verify this. There are two other possible N-glycosylation sites in the mouse CD95R-Fc sequence at N43 in the ECD and N257 in the Fc region (Figure 3.2). Deglycosylation experiments showed that the fusion protein expressed in both Sf21 and Hi5 was glycosylated and the protein mobility shifted on deglycosylation with PNGase F to similar molecular weights, suggesting no disparity in glycosylation between these 2 cell lines. It was not investigated whether all available sites for glycosylation on purified CD95R-Fc have glycans attached. The effect of these glycans on protein function has yet to be determined here, however, previous experiments have shown that both human and mouse CD95R-Fc expressed using cells from different organisms (insect, CHO or NSO) are functional and can bind to CD95L, neutralising its apoptotic activity in Jurkat cells (BioMoti; Figure 3.1). Since glycosylation of recombinant proteins is less complex in insect cells than

mammalian cells, this suggests that any disparity in complexity does not result in a change of functionality.

As a measure of the functionality of the purified CD95R-Fc, its ability to coat and induce uptake of MPs was measured. MDA-MB-231 human breast cancer cells were incubated with MPs coated in CD95R-Fc, or non-coated MPs. A small percentage of cells were able to internalise non-coated particles. Polystyrene particle uptake has been shown to involve a macrophage receptor with collagenous structure (MARCO), one of several scavenger-type receptors expressed on the cell surface of macrophages (Kanno et al., 2007). When COS-7 cells were transfected with either MARCO cDNA or an empty vector, the MARCO-transfected cells were able to internalise three sizes of polystyrene particles; 20nm, 200nm or 1µm, while no obvious uptake of particles occurred to the empty vector–transfected cells (Kanno et al., 2007). It is unknown whether MDA-MB-231 cells express MARCO however other scavenger-receptors present on the cell surface may be responsible for the polystyrene MP uptake seen. This background level of internalisation may also be due to hydrophobic interactions between the MPs and the surface of the cell which initiates phagocytosis (Ofek et al., 1995). However, uptake of CD95R-Fc coated particles in 56 +/- 5% of cells was strikingly and significantly enhanced compared to non-coated particles which were taken up by only 7 +/- 3% of cells, strongly suggesting that the CD95R-Fc coating is responsible for increased uptake. The increase in CD95R-Fc-coated MP uptake compared to non-coated MPs, suggests that a targeting mechanism may be responsible. However, while flow cytometry is an excellent tool for analysis of thousands of cells in a short space of time, one limitation (at least for

the FACScan) is that it does not discriminate between surface bound and internalised particles. Steps were taken in the procedure to ensure that surface particles were washed from cells before flow cytometry (by repeatedly washing adhered cells with PBS and tapping the sides of each plate to dislodge any unbound particles) but this is difficult to control. A more precise approach to investigate whether the particles have been internalised and not simply bound to the cell surface was provided by confocal analysis. These data are described in Chapter 5.

The uptake of MPs coated with CD95R-Fc purified in-house was not statistically different from the uptake of MPs coated with commercially-sourced CD95R-Fc (OET & Sigma). The protein provided by OET was expressed from the same *Flash*BAC ULTRA-CD95R-Fc as used here and was purified using a HiTrap Protein-A HP column (OET). The Sigma protein is mouse CD95R-Fc and was also expressed in Sf21 cells. The amino acid sequence of the Sigma protein is similar to the protein expressed in-house (Figure 3.2) but includes a few minor differences in the linker region and an extra 6x histidine tag on the Fc portion. When analysed by Western blot, the Sigma protein therefore migrates more slowly compared to the protein made in-house. The Sigma CD95R-Fc analysed in Figure 3.12 was also used in experiments undertaken by BioMoti, to test the functionality and ability of CD95R-Fc to block induction of apoptosis in Jurkat cells (Figure 3.1). In this experiment the Sigma protein was found to block CD95L-induced apoptosis in a dose dependant manner (with an EC50 of 447ng/ml). The efficacy to block CD95L-induced apoptosis suggests that the Sigma protein is correctly folded. It is therefore likely that the protein made in-house, which is

>98% identical and also expressed in, and purified from, Sf21 cells, is correctly folded because both proteins significantly improve the uptake of MPs in MDA-MB-231 cells.

The Fc portion of human IgG1 is fused to mouse CD95R to provide a convenient mechanism for purification, since protein-A in the MabSelect resin used binds Fc with high avidity and specificity. However, it is also possible that the Fc region will confer other properties and may also influence the behaviour of the fusion protein in the cancer clinic. The Fc domain could improve the plasma half-life and so therapeutic activity of the fusion protein since it binds to the salvage neonatal receptor (FcRn) which normally protects IgG from degradation (Czajkowsky et al., 2012). As seen via live cell imagining in vascular endothelial cells, when IgG is taken up it binds to FcRn in sorting endosomes which mature to multi-vesicular bodies (MVBs) (Ober et al., 2004). These return to the cell surface where exposure to physiological pH of the bloodstream triggers release of ligands back into the circulation in prolonged release or 'kiss-and-run' exocytosis (Andersen and Sandlie, 2009) thereby explaining the long half-life of this class of antibody in the serum (Roopenian and Akilesh, 2007). Conversely, the Fc portion may have a negative effect on targeting. The Fc portion of human IgG1 can bind to Fc-receptors (FcR), which are present on the surface of specialised phagocytes. When activated, FcR receptors transduce signals to the cytoplasm, causing internalisation of IgG-coated particles (Swanson and Hoppe, 2004). The presence of the Fc portion on the surface of MPs could cause uptake of MPs by specialised phagocytes *in vivo*, an off-target effect which should be considered and prevented. In the experiments described herein, it is also possible that the

Fc portion of the fusion protein contributes to the induction of uptake of coated MPs in the MDA-MB-231 cells. There is conflicting evidence as to whether MDA-MB-231 cells also express Fc receptors. Adams *et al.* have suggested the presence of FcR receptors in MDA-MB-231 cells using flow cytometry (Adams et al., 2006) but proteome analysis of this breast cancer cell line did not identify FcR (Strande et al., 2009). It was important therefore to control for this possibility. Human IgG - Fc fragment (Abcam) was therefore used to coat MPs and their uptake into MDA-MB-231 cells was measured. The uptake of Fc-coated particles was not statistically different to the uptake of non-coated particles, suggesting that it is not responsible for the uptake observed with CD95R-Fc. This is not entirely consistent with previous data which showed that mouse IgG-coated MPs does give significant uptake (around 55%) in comparison to non-coated MPs (around 15%) in MDA-MB-231 cells (Ateh et al., 2011). Although IgG is a larger, more complex protein (around 150 kDa) with variable regions, its interactions with receptors leading to internalisation are usually via its Fc region (as previously discussed; (Swanson and Hoppe, 2004)). Furthermore, the human Fc fragment of human IgG is a more relevant control for the mouse-CD95R/human-Fc chimera used herein.

Long term storage of the in-house purified CD95R-Fc in PBS at 4°C is not recommended due to protein degradation and aggregation. This is not uncommon for recombinant proteins as they are often unstable outside their native environments. The direct cause for the degradation is uncertain but could be due to low level protease contamination from the insect cells or perhaps bacterial contamination since sodium azide is not added to the protein samples.

The proteolysis of CD95R-Fc had a negative effect on the uptake of coated particles. This is could be because the mix of degradation products in the protein solution results in inefficient coating of the particles. The particles are coated using passive adsorption, a commonly used coating procedure in which the CD95R-Fc is attached to the microsphere by incubating the two together. Adsorption occurs based on hydrophobic attractions between the hydrophobic portions of the adsorbed ligands and the polymeric surface of the microspheres (Bangs, 2008a). Impurities or degradation products will compete with the ligand for space on the particle surface through relative affinity and relative concentration effects, therefore if the concentration of the impurity is very high, it could become the principle coating (Bangs, 2008a). The degradation product migrating at 30 kDa on Figure 3.14 is the correct size for the Fc portion (and is recognised by the anti-IgG antibody), which when used to coat MPs alone, does not statistically improve uptake but it could compete for adsorption sites on the MP with the full length or CD95R moiety. To prevent proteolysis of the purified CD95R-Fc it was frozen in aliquots at -20°C with the stabilising agent, BSA. This was shown to be protective against protein degradation for short periods (days) at 4°C, and at least 12 weeks at -20°C.

3.3.1. Limitations and possible future directions

In this chapter I have used passive adsorption to coat polystyrene particles with CD95R-Fc and measured their uptake into triple-negative breast cancer cells. The main limitations are the use of a chimeric fusion protein, the polystyrene particles are not the final delivery vehicle and the method of coating could be improved.

Passive adsorption is a simple and flexible method of protein attachment, which is commonly used. However, it is not easy to measure the efficiency of coating before testing MP uptake. Covalent attachment of proteins to the surface of functionalised microspheres is another method of coating that could be investigated, which means that the proteins are permanently bound in a favoured orientation. A microsphere can be functionalised with a carboxyl or amino acid group, and then incubated with an activating agent allowing the ligand or other coating material to bind directly to the particle surface (Bangs, 2008b). The effect of different protein coats on the MPs will be explored further in Chapter 5.

The IgG antibody heavy chain naturally forms a dimer through the hinge regions' cysteine residues and as a result, most Fc-fusions are expressed as disulphide-bonded homodimers (Czajkowsky et al., 2012). Via SDS-Page analysis, the disulphide bonds are reduced so only the monomer can be seen, although the presence of band which could correspond to a dimer was noticed after long term storage at 4°C (Figure 3.14A). The presence of different oligomeric forms of expressed, in-house CD95R-Fc was not investigated. Different oligomers could be isolated using size exclusion chromatography, whereby species of different molecular weights (i.e. monomeric CD95R-Fc 46 kDa and dimeric 92 kDa) can be eluted separately. The effect of the oligomeric forms of CD95R-Fc on particle coating and uptake could then be investigated, as they may affect any cell surface interactions involved in uptake. Additionally, the Fc region could be cleaved from the CD95R-Fc fusion protein post-purification since it does not have a significant effect on particle internalisation. For this, it would be necessary to engineer a cleavage site into the linker sequence, to allow efficient and specific removal. The

tobacco etch virus (TEV) protease for example, can recognise a specific cleavage site (Dougherty et al., 1989) and remove a tag from a fusion protein if it is linked by this sequence. Furthermore, the purified CD95R cleaved from the –Fc region could be incubated with cells, before testing CD95R-Fc coated MP uptake in MDA-MB-231 cells, as was done previously in medulloblastoma cells and found to block uptake (Ateh et al., 2011). The targeting mechanism of this system will be investigated in the next chapter.

In order to test how the in-house CD95R-Fc affects uptake, polystyrene MPs have been used here. Further work could involve formulation of PLGA microparticles. PLGA is a biocompatible, biodegradable polymer (Anderson and Shive, 2012) which can be loaded with drugs to deliver high drug concentrations within solid tumours and lower off-target toxicity (Wang et al., 2012). As with polystyrene MPs, CD95R-Fc-coated PLGA particles are also preferentially internalised by cancer cells (Ateh et al., 2011). PLGA MPs could be formulated to incorporate a fluorophore (in order to follow the particle in cell uptake experiments) and to deliver a compound that becomes fluorescent on exposure to the cytosol (in order to follow drug delivery).

3.4. Summary

A baculoviral/insect system was optimised for expression of recombinant CD95R, fused to the Fc region of human IgG1, in Sf21 and Hi5 cells. The protein was purified by affinity chromatography with a potential yield of 1.2mg per 100ml culture and a purity of 90%. The purified CD95R-Fc was used to coat microparticles (MPs) and found to be significantly taken up by MDA-MB-231 (breast cancer) cells, in comparison to non-coated particles. Stability of the in-house CD95R-Fc was tested, and long-term storage conditions were optimised. The development of this expression system is a crucial first step towards characterising the mechanisms involved in uptake.

4. Detecting expression of CD95L

4.1. Introduction

CD95L (FasL, APO-1L, CD178) is a TNF family member and type II transmembrane protein (Locksley et al., 2001). It binds to its receptor CD95R, resulting in a pro-apoptotic signalling cascade and cell death. CD95L function allows immune cells such as natural killer (NK) cells or activated T lymphocytes, to apoptose virally-infected cells. However, CD95L expression has also been reported in tumour endothelial cells, which is thought to be a “tumour counterattack” against the immune system (Voss et al., 2008). Very recently however, there has been a shift in knowledge regarding CD95L expression in cancerous cells, by a leading group in the field. They show evidence that the cell-death observed in cancer cells was not specifically due to the knockdown of CD95L, but due to an off-target RNAi mechanism (Putzbach et al., 2017). This puts into question some of the previous conclusions made on the expression of CD95L in cancer cells and warrants a careful reappraisal of the literature.

4.1.1. CD95L topology

Human CD95L is a 40kDa protein with 281 amino acids (Figure 4.1; Supplementary Figure 7) (Takahashi et al., 1994b, Suda et al., 1993). It has an 179 amino acid (aa) ECD, an 22 aa transmembrane alpha-helix, an 80 aa cytoplasmic domain (Takahashi et al., 1994b) and as a type II transmembrane protein, the C-terminal region of CD95L is extracellular. The protein has 3 N-linked glycosylation sites in the ECD, one intramolecular disulphide bond and a unique proline rich domain (PRD), which is not found in other TNF family ligands

(Voss et al., 2008). The PRD is involved in CD95L sorting and trafficking via protein-protein interactions with different Src homology 3 (SH3) or WW domain (named because of the presence of two tryptophan residues in a certain spacing) proteins (Lettau et al., 2014). The protein exerts its action as a non-disulphide linked homo-trimer, as with other TNF family members, and its oligomerisation is dependent on a “self-assembly” region spanning amino acids 137 to 183 (Voss et al., 2008). Human CD95L has 76.9% amino acid sequence identity with mouse CD95L and there is cross-reactivity of CD95L with CD95R in both human and mouse (Takahashi et al., 1994b). CD95L ECD (amino acids 143 - 281) has been crystallised as a trimer, in complex with the decoy receptor DcR3; the structure was resolved to 2.5 Å (Liu et al., 2014) (see section 1.5.1).

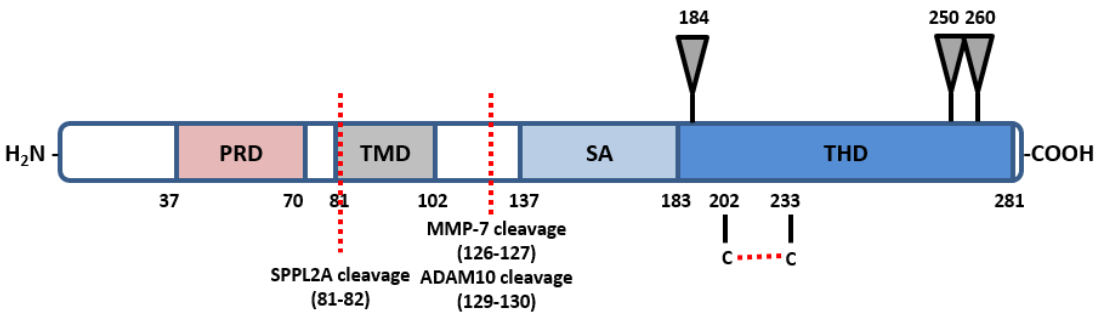

Figure 4.1. Human CD95L structure.
Schematic representation of CD95L structure. The proline rich domain (PRD) is found before the transmembrane domain (TMD). The self-assembly region (SA) is thought to be essential for CD95L trimerisation. The C-terminal moiety is characterised by its homology to other TNF ligand ectodomains (THD). Cleavage sites have been mapped. CD95L contains three putative glycosylation sites (N184, N250, N260) and one intramolecular disulphide bridge in the ectodomain. Diagram modified from Voss et al., 2008. For protein sequence, see Supplementary Figure 7.

CD95L can be released from the cell surface producing a soluble, 26kDa form of the protein which remains trimeric. The soluble form of CD95L (sCD95L) exerts reduced cytotoxic capacity in comparison to membrane bound CD95L (which is referred to here as CD95L, unless stated otherwise) (Tanaka et al., 1998, Schneider et al., 1998). However, there is some evidence to suggest that sCD95L competes with the membrane form, to bind CD95R without apoptotic activation, dampening down the apoptotic response (Chen et al., 1998, Schneider et al., 1998). The pro- or anti-apoptotic functions of sCD95L depend on other mediators in the environment (Askenasy et al., 2005). The proteases responsible for shedding of CD95L are matrix metalloprotease 7 (MMP7), ADAM10 and SPPL2A (Figure 4.1) which liberates both the CD95L ectodomain and the intracellular domain (ICD) (Voss et al., 2008, Kirkin et al., 2007). In T-cells, CD95L shedding by ADAM10 is a prerequisite for the intramembrane cleavage by SPPL2A (Kirkin et al., 2007). The intracellular domain can translocate to the nucleus and act as a transcriptional regulator in a process known as reverse signalling (Kirkin et al., 2007). This signalling impairs activation-induced proliferation in B and T cells and is involved in negative fine-tuning of certain immune responses, such as production of antigen-specific immunoglobulin antibodies (Lückerath et al., 2010). The deletion of the ICD has been shown to reduce localisation of CD95L to lipid rafts, suggesting a role in targeting to or maintenance within the membrane rafts (Cahuzac et al., 2006, Glukhova et al., 2018) (section 4.1.4).

Despite being well known for its role in apoptosis, the role of CD95L can vary depending on the cellular microenvironment (Voss et al., 2008). Several

derivatives of membrane CD95L have been shown to induce inflammation for example (Askenasy et al., 2005) (see section 1.5.3).

4.1.2. CD95L expression in immune cells

CD95L expression can be constitutive or inducible in hematopoietic cells such as NK cells and cytotoxic T-lymphocytes (Voss et al., 2008). Due to its cytotoxic activity, the expression of CD95L must be tightly controlled to prevent unwanted damage. Prior to induction, immune cells were thought to retain CD95L in secretory lysosomes via their PRD domains (Blott et al., 2001). When activated, for example, by T cell receptor engagement, CD95L is rapidly transported and released into the cytotoxic immunological synapse, referred to as the "kiss of death" (Voss et al., 2008). However, some studies have not found co-localisation of CD95L with classical markers or components of secretory lysosomes, suggesting its storage in other cellular compartments (Lückerath et al., 2010, Kassahn et al., 2009). Furthermore, in Schwann cells, the adaptor protein Grb2 has been found to link CD95L to adaptin β and regulate surface expression, suggesting a different mechanism for CD95L trafficking and PM expression (Thornhill et al., 2008).

4.1.3. N-linked glycosylation of CD95L

The three putative, N-glycosylation sites in CD95L have been experimentally modified but not found to alter receptor binding or trimerization (Voss et al., 2008) which could be due to the glycosylation sites being distant from the binding interfaces of CD95R (Liu et al., 2014). However, mutations of the putative N-linked glycosylation sites correlates with reduced CD95L expression in COS-1

cell transfectants (Orlinick et al., 1997) suggesting that glycosylation positively affects CD95L maturation and/or stability. Additionally, when expressed in HEK293T cells, the presence of all N-linked glycans seem to be essential for secretion of sCD95L (Schneider et al., 1998) and glycosylated sCD95L has a greater potency for the induction of Jurkat cell apoptosis, in comparison to non-glycosylated CD95L (Liu et al., 2014). On SDS-PAGE, non-glycosylated CD95L was found to experience significant aggregation, perhaps suggesting that glycosylation enhances the biological activities of sCD95L by reducing aggregation (Liu et al., 2014). Glycosylation of CD95L ectodomain may have a further protective effect against degradation of the protein, since it is localised to secretory lysosomes in immune cells and so exposed to a hydrolytic environment (Voss et al., 2008). This protective effect of N-linked glycosylation has been shown for other lysosomal proteins such as Lamp-1 and Lamp-2, where deglycosylating the proteins (using endoglycosidase H) leads to rapid degradation whereas the glycosylated proteins are stable (Kundra and Kornfeld, 1999).

4.1.4. CD95L localisation in lipid rafts

Exogenously expressed and endogenous CD95L has been found to constitutively partition into lipid rafts (Cahuzac et al., 2006); dynamic assemblies of cholesterol and sphingolipids in the outer-leaflet of the lipid bilayer of the plasma membrane that are thought to be important for signal transduction (Simons and Toomre, 2000). CD95L has been found to associate with caveolin-1, a major protein component of rafts, likely via the two caveolin-binding sites in the N-terminal domain of CD95L (Glukhova et al., 2018). The deletion of these binding sites

impairs CD95L distribution between cellular membranes, reducing its cytotoxic activity (Glukhova et al., 2018). This could be because the raft environment favours the formation of CD95L oligomers, a prerequisite for triggering CD95R-mediated cell death (Cahuzac et al., 2006). Lipid rafts are considered to be important for signal transduction and with binding of CD95L to CD95R, it was found that the amount of raft-associated CD95L increases, indicating increased CD95L translocation (Cahuzac et al., 2006). However, the mechanism controlling this is unclear; whether CD95L must be in the rafts for optimal contact with CD95R or whether its interaction with the receptor results in raft localisation.

4.1.5. The history of CD95L expression in cancer cells

The CD95R/CD95L system has been linked to multiple tumour-promoting activities (Peter et al., 2015) (see sections 1.4 and 1.5). It therefore seemed consistent that multiple shRNAs and siRNAs targeting CD95L mRNA slowed down cancer cell growth (Chen et al., 2010) and caused cell death, via a mechanism involving multiple cell pathways labelled ‘death induced by CD95R/L elimination (DICE)’ (Hadji et al., 2014). Additionally, CD95L was identified as a gene critical for the survival in multiple cancer cell line screens (Hadji et al., 2014). However, a more recent publication has found that these phenotypic effects were not due to the loss of CD95L, but due to unique off-target effects, predominantly from the siRNAs and shRNAs designed specifically against CD95L (Putzbach et al., 2017). These si/shRNAs were found to target 3’UTR of critical survival genes causing the observed cell death and this effect has now been labelled ‘death induced by survival gene elimination’ (DISE) (Putzbach et al., 2017). The authors suggest that CD95R and CD95L are not unique in this effect and that there may

be many other coding and also noncoding genes that contain sequences which, when expressed as si/shRNAs, will be toxic to cells (Putzbach et al., 2017). These conclusions are far reaching and raise questions about the previous experiments supposedly demonstrating the presence of CD95L in cancer. For example, the MCF-7 cells used to show the effect of CD95L knockdown were engineered to express a low amount of human CD95L, due to 'difficulties in detecting CD95L by Western blotting' (supplementary information; (Hadji et al., 2014)). This engineered cell line is the only one used to demonstrate successful CD95L knockdown using Western blot; other cell lines tested simply show an increase in the percentage of sub G1 cells, indicating apoptosis. In fact, the group have stated recently that CD95L expression in most cancer cells is barely detectable, yet they hypothesised that elimination of the protein induces death more effectively in cells that express less CD95L perhaps because it becomes rate limiting more easily (Peter et al., 2015).

Technical difficulties with antibodies have added to the problems, with many of the antibodies used to detect CD95L lacking specificity (Sträter et al., 2001). When 12 commonly used antibodies were tested for their reliability in immunocyto/histochemistry, only 5 did not significantly bind to controls and only one was recommended for immunohistochemistry (clone G247-4) (Sträter et al., 2001). It is therefore important to validate CD95L antibodies with appropriate controls and critically re-interpret the literature in light of antibody usage, although more recent CD95L publications do use the G247-4 clone. Additionally, many of the ELISA kits used to detect CD95L, whether in cell lines or the blood sera of

cancer patients, have been discontinued which may also relate to antibody validity.

A recent study has reported that tumour endothelium creates an immune barrier by expressing CD95L to induce apoptosis in T-cells thus preventing their infiltration into the tumour environment (Motz et al., 2014). In this rigorous study, they have used the recommended antibodies for Western blot (G247-4), flow cytometry (NOK-1) and tissue staining (G247-4) and have also validated these antibodies and presented the control data. Evidence of tumour endothelial expression of CD95L is shown, but little or no expression of CD95L was evident in most tumours; cancer cell lines were not tested. In fact, the authors extended the study to test expression of CD95L in tissue microarrays containing over 600 samples of human breast, colon, renal, bladder, prostate or ovarian carcinomas, but in the vast majority of tumours, the tumour cells expressed no or low levels of CD95L (Motz et al., 2014). There were a few exceptions, primarily metastatic ovarian cancer (as has been previously reported (Abrahams et al., 2003)) and colon cancer (CC) tumours, although no p value is stated for CC (Motz et al., 2014). The authors reached the conclusion that tumour endothelial tissue expression is promoted by tumour-derived vascular endothelial growth factor A (VEGF-A), interleukin 10 (IL-10) and prostaglandin E_2 (PGE) suggesting the tumour microenvironment is favoured for expression, since very little CD95L is expressed in normal endothelial cells (HMVECs). Although not tested in this study, CD95L has also found to be expressed by brain tumours (Kleber et al., 2008, Gratas et al., 1997). The presence of CD95L was also demonstrated via IHC staining of clinical samples of glioblastoma (GBM), using G247-4 (with

appropriate staining controls) although expression was not uniform in the tissue with increased staining around tumour vessels but small amounts inside the tumour (Kleber et al., 2008). This raises further questions regarding expression of CD95L by cancer cell lines alone, and potential need of the tumour microenvironment for expression of this protein.

4.1.6. The form of CD95L found in tumour cells

In the few types of tumours and cancer cell lines where CD95L has found to be expressed, the form of CD95L found can differ. In addition to the membrane form of CD95L and sCD95L, CD95L also appears to be stored and released via microvesicles, within multivesicular bodies (MVBs) with CD95L potentially being a transmembrane component of the "inner vesicles" (Voss et al., 2008).

CD95L has also been found in the cytoplasm of melanoma cells, confined to MVBs which contain melanosomes (Andreola et al., 2002). In these cells, CD95L colocalised with melanosomal markers (e.g. gp100) and lysosomal markers (e.g. CD63). The intracellular localisation of CD95L was confirmed within melanoma cells using immunocytochemistry, immunoelectron microscopy (identifying CD95L within melanosomes, contained within multivesicular bodies) and using Western blot analysis of the cytoplasmic fractions of melanoma cells; all of these techniques utilised the G247-4 antibody. The MVBs were found to degranulate extracellularly releasing CD95L-containing microvesicles. Microvesicular CD95L maintains its function as it was found to induce apoptosis in lymphoid cells. Interestingly, no surface expression of CD95L was detected on melanoma cells

using flow cytometry (NOK-1 mAb) or immunoprecipitation of the cell surface proteins (NOK-1 and G247-4).

Similarly, ascites-derived epithelial ovarian cancer cells isolated from late stage ovarian cancer patients have been reported to lack cell surface CD95L but secrete full length, CD95L from an intracellular compartment via the release of microvesicles (Abrahams et al., 2003). A heavily glycosylated form of sCD95L was also found to be associated with microvesicles, isolated from the ascites fluid of ovarian cancer patients (Abrahams et al., 2003) The presence of CD95L was confirmed by Western blot (using G247-4) and both forms of CD95L, released from the microvesicles, was found to induce apoptosis of Jurkat T cells. Intracellular CD95L staining was found to be colocalised with Lamp-1, a lysosomal membrane marker, however, the antibody used for this staining (clone N-20) had already been shown to lack specificity, so these data may not be correct (Sträter et al., 2001).

In contrast to this, surface expression of CD95L has been detected in murine glioma cell line SMA-560 via flow cytometry (using the anti-murine CD95L mAb MFL3), but only following intracranial implantation indicating a possible requirement of tumour/host interaction for expression (Kleber et al., 2008). This suggests that the form of CD95L found on, or secreted by, a cancer cell could be cell-type and environment specific.

MDA-MB-231 cells are a highly invasive, oestrogen-receptor negative, adenocarcinoma cell line that is often used as a model for triple negative breast cancer, for which there are few treatment options (see section 1.1.5). MDA-MB-231 cells have been widely reported to express CD95L (Malleter et al., 2013, Hsu et al., 2006, Kunigal et al., 2008) although the validity of this evidence is questionable, as will be discussed later. This cell line is therefore, a good candidate to test a targeted treatment on, such as drug delivery using CD95R-Fc coated microparticles. The targeting effect of CD95R-Fc coated microparticles, which may explain the enhanced uptake already seen (Chapter 3), depends on CD95L being present and on the surface of MDA-MB-231 cells, allowing the CD95R to interact with CD95L specifically. In this chapter I therefore set out to investigate CD95L expression at the protein and mRNA level in the target cells of interest, MDA-MB-231s, as well as using siRNA knockdown to confirm the results. Given the controversies in the field, it was important to first validate the antibodies to be used. For this purpose, I transiently expressed CD95L in HEK293T (human embryonic kidney) cells. These CD95L-expressing HEK293T cells, with or without CD95L-sheddase inhibitors, were also tested to determine whether they could be used as a tool to investigate the mechanism of CD95R-coated MP internalisation.

4.1.7. Aims of Chapter 4

- Transiently express CD95L in HEK293T cells to validate anti-CD95L antibodies
- Characterise and localise recombinant CD95L expression in HEK293T cells
- Test the effect of CD95L-sheddase inhibitors on CD95L plasma membrane expression in HEK293T cells
- Investigate CD95L protein and mRNA expression in MDA-MB-231 cells

4.2. Results

4.2.1. Validation of mAb G247-4 by transient expression of CD95L in HEK293T cells

The antibodies used in the past to detect CD95L have been critically analysed and many have been found to lack specificity (Sträter et al., 2001). Therefore, it is important to validate any anti-CD95L antibodies used here. To do this, HEK293T cells were seeded on 6-well plates and transfected with pCMV6-FasLG (coding for Myc-DDK-tagged human CD95L; OriGene; section 2.6.1). The construct encodes a C-terminally tagged (Myc and FLAG tag; Myc-DDK), CD95L protein. As CD95L is a type II transmembrane protein, the C-terminus of CD95L is extracellular after the protein has been trafficked to the plasma membrane.

Forty-eight hours post-transfection, transfected and untransfected HEK293T cells were lysed and different fractions of lysate (0.0002%, 0.0004% and 0.002%) were run on a 10% polyacrylamide gel (section 2.7.6, 2.7.7 & 2.7.8). The protein was transferred onto a PVDF membrane and probed using mouse anti-human CD178 (CD95L) clone G247-4 (BD Pharmingen) (section 2.7.11; Figure 4.2A). In the untransfected samples, no CD95L was detected which suggested no (or at least very low) endogenous CD95L expression. The strongest signal demonstrates the presence of recombinant CD95L-Myc-DDK at the expected molecular weight of 40kDa (most easily resolved as a discrete band in the lowest loading of 0.0002% of whole cell lysate). The lack of CD95L in untransfected cells and detection of the 40kDa species in the transfected samples shows that the transient transfection was successful. The lower molecular weight signals at 26kDa and 28kDa could be degradation products or they could potentially correspond to

soluble CD95L-Myc-DDK which has been reported previously in the cell lysates of CD95L-transfected COS cells (Tanaka et al., 1995) and HEK293T cells (Lettau et al., 2014). These two smaller molecular weight proteins could both be soluble CD95L-Myc-DDK but with differential glycosylation, leading to differences in protein mobility on the gel. A higher molecular weight species migrating between approximately 100kDa and 150kDa is also present at lower abundance (being most noticeable with the heaviest loading of cell lysate). To better resolve the higher molecular weight species seen in Figure 4.2A, 0.002% of the cell lysate was run on an 8% gel (Figure 4.2B). The higher molecular weight species has a mobility corresponding to 80kDa.

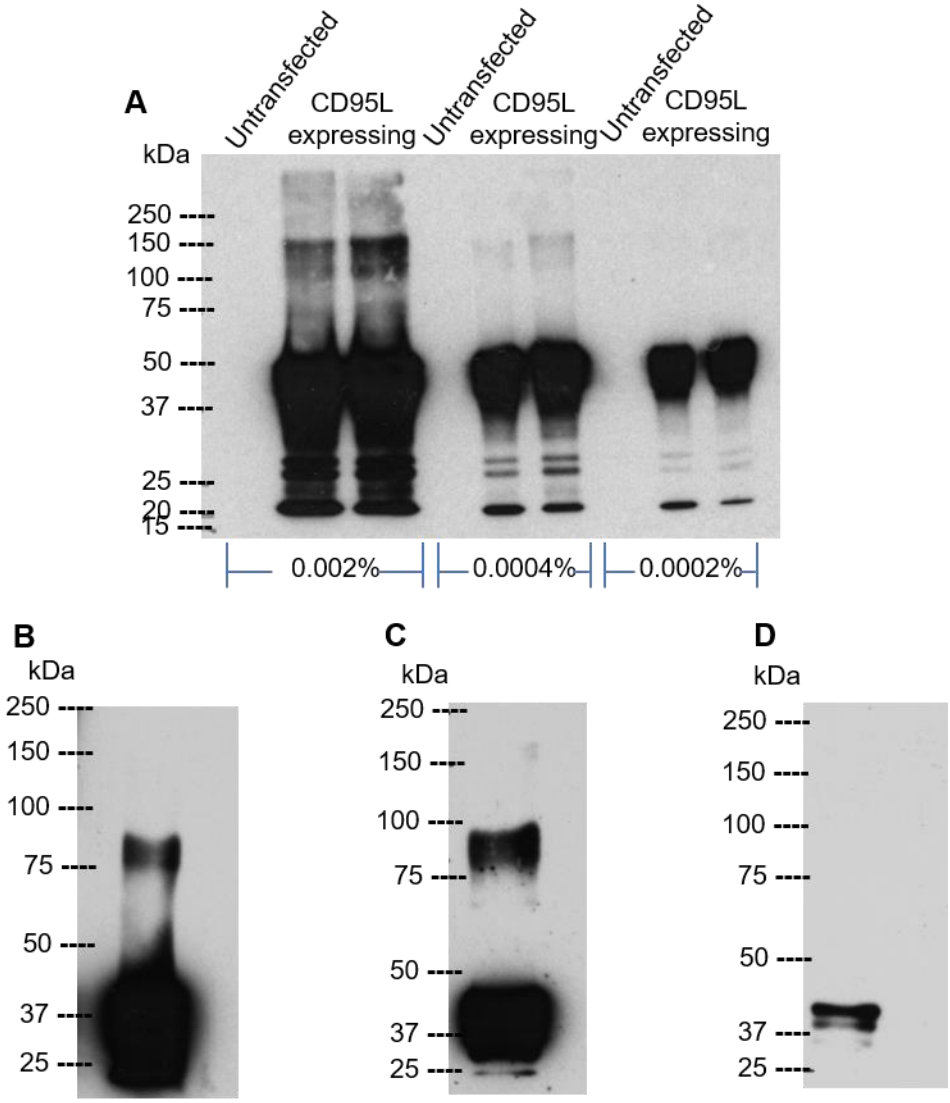

Figure 4.2. Validation of mAb G247-4 by transient expression of recombinant CD95L-Myc-DDK in HEK293T cells.
HEK293T cells were seeded on 6-well plates and transfected with a vector coding for CD95L-Myc-DDK. Samples were harvested 48 h post-transfection; cells lysed and different fractions of the total volume (0.002%, 0.0004% and 0.0002%) were reduced, denatured and separated by SDS-PAGE on a 10% polyacrylamide gel (**A**) or 0.002% was separated on an 8% polyacrylamide gel (**B - D**). Equivalent fractions of whole cell lysates from untransfected HEK293T cells were also blotted for comparison (**A**). The blots were prepared on a PVDF membrane and probed using anti-human CD95L mAb G247-4 (BD Pharmingen; **A**, **B**), anti-FLAG (Sigma; **C**) or anti-c-MYC (Sigma; **D**).

To further confirm that the protein detected by G247-4 is the recombinant CD95L-Myc-DDK protein, the HEK293T cell lysates were analysed on separate Western blots probed with anti-FLAG (Figure 4.2C) and anti-c-MYC (Sigma; Figure 4.2D) antibodies which should recognise the C-terminal -DDK (FLAG) and -MYC tags on the recombinant CD95L, respectively. Both antibodies detected protein and the anti-FLAG antibody detected protein migrating at the same molecular weights as G247-4 (Figure 4.2B). The anti-c-MYC antibody also detected the 40kDa monomeric CD95L-Myc-DDK (Figure 4.2D), however three protein species can clearly be seen with similar mobility, which may correspond to differing glycosylation of the protein, as described previously (Tanaka et al., 1995). The least abundant, higher molecular weight, species were not detected by the anti-c-MYC antibody (Figure 4.2D). This could be due to the high dilution of antibody used and this result would need to be confirmed by running the blot with a higher anti-c-MYC concentration.

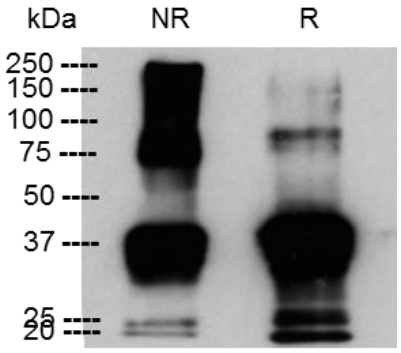

Figure 4.3. 2-mercaptoethanol reduces the presence of high-order CD95L species. HEK293T cells were seeded on 6-well plates and transfected with a vector coding for CD95L-Myc-DDK. Samples were harvested 48 h post-transfection, cells lysed and loaded onto an SDS polyacrylamide gel in non-reducing (NR – without 2-mercaptoethanol) or reducing (R – with 2-mercaptoethanol) conditions. Proteins were separated by electrophoresis. The blot was prepared on a PVDF membrane and probed using anti-human CD95L mAb G247-4 (BD Pharmingen).

It is possible that the 80kDa band corresponds to a CD95L-Myc-DDK aggregate, or a higher order oligomer. CD95L functions as an oligomer and the ECD has been crystallised as a trimer (Liu et al., 2014). The cell lysate from HEK293T cells was run on a gel under non-reducing (without 2-mercaptoethanol) and reducing (with 2-mercaptoethanol) conditions; blotted and probed with G247-4 (Figure 4.3). In the presence of 2-mercaptoethanol, a significant fraction of the higher molecular weight species disappears and more of the 40kDa and 25kDa species are observed, strongly suggesting that the 80kDa species is a complex that contains CD95L-Myc-DDK. Additionally, the reduction of the higher molecular weight species suggests that the disulphide bond is present in the ECD (Figure 4.1), as shown in the crystal structure of CD95L ECD (Liu et al., 2014) (see Figure 1.2). It is likely therefore that CD95L-Myc-DDK has been trafficked through an appropriate oxidative environment, such as through the ER, to allow the disulphide bridge to form although it remains a possibility that a non-physiological disulphide bond has formed after cell lysis.

4.2.2. Glycosylation status of recombinant CD95L-Myc-DDK expressed by HEK293T cells

Although Western analysis shows the presence of CD95L-Myc-DDK, it does not indicate whether the protein is at the cell surface. Plasma membrane expression of CD95L-Myc-DDK is required to allow interaction with the CD95R on CD95R-Fc coated microparticles. The glycosylation status of an expressed protein can provide some indication of its subcellular localisation. To identify any differences in glycosylation between the lower and higher molecular weight species of CD95L-Myc-DDK, whole-cell lysates were treated with Endoglycosidase-H

(Endo-H) or Peptide-N-glycosidase-F (PNGase-F) and analysed by Western blot (section 2.7.12 & 2.7.11; Figure 4.4) using the G247-4 antibody. Endo-H-sensitive, high mannose, *N*-glycans are added to proteins at the amide nitrogen of asparagine residues, within the sequon Asn-X-Ser/Thr (where X is any amino acid except proline) in the endoplasmic reticulum (Adrain et al., 2012). These sugars are then modified in the Golgi apparatus, by a wide variety of glycosyltransferases with the use of soluble precursors such as nucleotide sugars (Hirschberg et al., 1998), making them resistant to deglycosylation by Endo-H (Adrain et al., 2012). PNGase-F is an endoglycosidase capable of removing all N-linked glycans (Tretter et al., 1991) by cleavage of the amino acid side chain which converts the glycosylated asparagine into an aspartic acid. Differences in sensitivity to these two enzymes can therefore help to indicate the location of a protein; whether it is in the endoplasmic reticulum with high mannose glycans or it has passed through the Golgi and contains mature glycans. To investigate the glycosylation status of CD95L-Myc-DDK, a small fraction (0.0002%) of the HEK293T cell lysate from a confluent 3cm well, was incubated with each enzyme, loaded onto a 10% polyacrylamide gel and analysed by Western blot (Figure 4.4A). Digestion of CD95L-Myc-DDK with both Endo-H and PNGase-F resulted in resolution of the three smaller molecular weight forms, into one form with increased electrophoretic mobility, that migrated as a 34kDa protein.

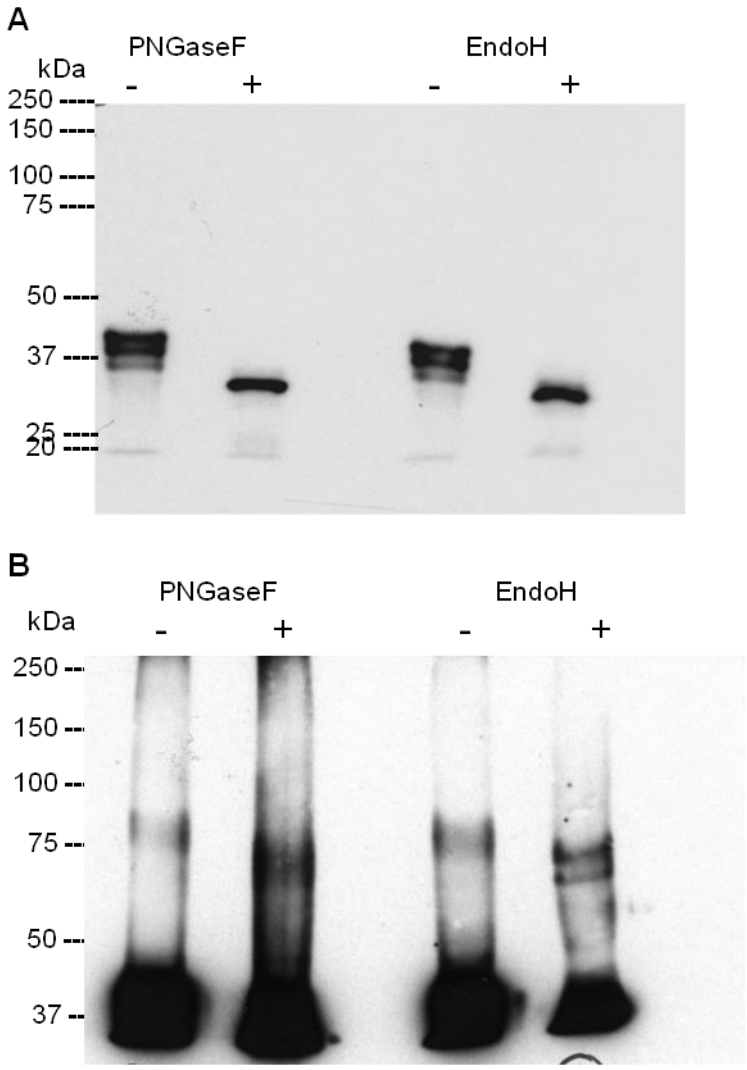

Figure 4.4. Deglycosylation by Endo-H and PNGase-F suggest that the higher molecular weight species of recombinant CD95L-Myc-DDK has differentially matured glycans. Fractions of cell lysate from transfected HEK293T cells, 0.0002% of total volume (see Figure 4.2) for (**A**) and 0.002% for (**B**) were reduced, denatured and treated with 500U of PNGase-F (+ samples) or 1000U of Endo-H (+ samples) for 2 hours at 37°C. Control samples were also loaded, without any PNGase-F or Endo-H (- samples). Samples were loaded onto a 10% (**A**) and 8% (**B**) SDS polyacrylamide gel and the proteins separated by electrophoresis. The blots were prepared on a PVDF membrane and probed using mouse, anti-human CD95L mAb G247-4 (BD Pharmingen).

These data indicate that the glycans on the 34kDa form of CD95L-Myc-DDK (which likely represents the monomer peptide) are likely to be of the high mannose variety, sensitive to both Endo-H and PNGase-F. This suggests that monomeric CD95L is resident in the endoplasmic reticulum and has not passed through the Golgi apparatus.

This experiment was repeated with a focus on the higher molecular weight species (Figure 4.4B); 0.02% of the HEK293T cell lysate was incubated with each enzyme and separated on an 8% polyacrylamide gel for improved separation and analysed by Western blot. Again, digestion with both Endo-H and PNGase-F resulted in an increase in electrophoretic mobility, from approximately 80kDa to around 70kDa when treated with PNGase-F, and from 80kDa to two distinct signals of around 75kDa and 70kDa when treated with Endo-H. This difference in patterns produced by Endo-H and PNGase-F deglycosylation suggest that the glycans on the higher molecular weight species could be differentially matured. Some glycans are high mannose and sensitive to Endo-H while some appear to be resistant. It is likely therefore that those species with mature glycans have, at least, passed through the Golgi apparatus. However, it is still not clear whether this material is present on the plasma membrane or retained in an intracellular compartment.

4.2.3. Expression of CD95L-Myc-DDK at the plasma membrane of transiently-transfected HEK293T cells

The higher molecular weight species has some Endo-H resistant, but PNGase-F sensitive glycans suggesting that the protein has passed through the Golgi apparatus, however this does not necessarily mean that the protein is present on the PM. Flow cytometry was therefore used to assess cell-surface expression of the recombinant CD95L-Myc-DDK. HEK293T cells were transfected as previously described with pCMV6-FasLG (coding for Myc-DDK-tagged Human CD95L; section 2.6.1) or the plasmid pTracer which expresses a green fluorescent protein (GFP; to measure transfection efficiency). Forty-eight hours

post transfection CD95L-Myc-DDK expressing cells were incubated with a different anti-CD95L primary antibody; mouse, anti-human CD178 (CD95L) NOK-1 clone (BioLegend) that is reported to recognise native CD95L and secondary antibody, donkey, anti-mouse IgG-FITC (Santa Cruz Biotechnology). The epitope of the NOK-1 antibody is located in the ECD of CD95L, between amino acid residues 196 and 240. NOK-1 recognises the epitope in the native fold of CD95L (Nisihara et al., 2001), and is therefore suitable for use in flow cytometry of intact cells. Untransfected cells were also incubated with the antibodies, to control for non-specific binding. Analysis by flow cytometry detected fluorescence emitted by the secondary antibody or GFP. Patterns of fluorescence from representative experiments were overlain on a histogram (Figure 4.5).

Seventy percent of the cell population transfected with pTracer were positive for GFP (as marked by the gate on Figure 4.5) and the median fluorescence of the entire cell population was 99.4 AFU, demonstrating that transfection conditions were efficient. The median fluorescence of the entire population of untransfected cells was 3.15 and cells transfected with pCMV6-FasLG, 4.12. The percentage of positive cells (the percentage of cells in the population with fluorescence levels above 10 AFU) was 5% for untransfected cells and 6% for pCMV6-FasLG transfected cells. This suggests that there is no, or little, detectable CD95L-Myc-DDK on the surface of the transfected HEK293T cells. There is a slight shift in median fluorescence in CD95L-Myc-DDK-expressing cells which might suggest a few molecules of CD95L-Myc-DDK on the cell surface or could potentially be an artefact as a result of the transfection procedure. To test this, mock-transfected cells should be used as a further negative control. This result could

be due to the concentration of antibody used being sub-optimal however, the concentration used was as per manufacturers recommendations (≤ 1 µg per 10^6 cells in 100 µl volume).

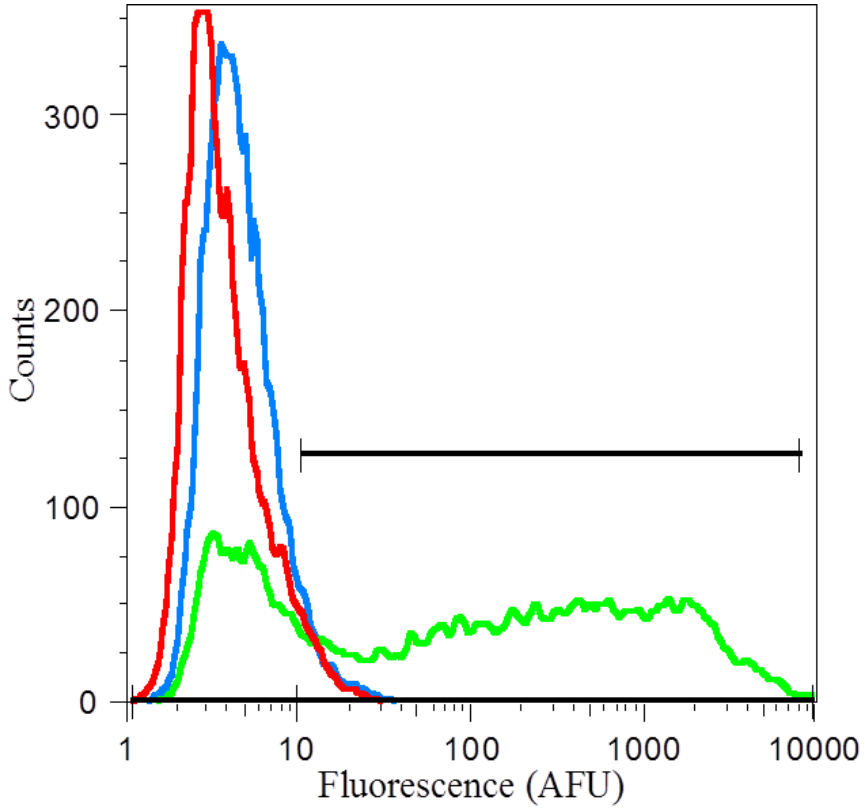

Figure 4.5. Histogram displays little or no plasma membrane expression of CD95L-Myc-DDK in HEK293T cells, detected using NOK-1 mAb.
HEK293T cells were seeded on 6-well plates and transfected with a vector (pCMV6-FasLG) coding for CD95L-Myc-DDK, green fluorescence protein (GFP) or left untransfected. Cells were harvested 48h post-transfection and pCMV6-FasLG transfected cells incubated with mouse, anti-human CD95L, NOK-1 clone (BioLegend) and secondary antibody, donkey, anti-mouse IgG-FITC (Santa Cruz Biotechnology). Untransfected cells were also incubated with the same antibodies, as a negative control. 10,000 cells of normal size and granularity were gated to eliminate cell debris and focus on healthy cells. Results from representative experiments were overlain on the histogram, displaying distribution of fluorescence (arbitrary fluorescence units; AFU) against number of cells (counts) for all conditions. GFP expressing cells (green) were gated (black bar) showing a 70% transfection efficiency. Percentage of positive cells and median fluorescence for entire cell populations; untransfected cells (red) 5% and 3.15 AFU, for pCMV6-FasLG transfected cells (blue) 6% and 4.12 AFU and GFP expressing cells (green) 99.4 AFU.

4.2.4. Cellular localisation of recombinant CD95L-Myc-DDK transiently expressed in HEK293T cells

Confocal microscopy was used to further investigate the expression and sub-cellular localisation of CD95L-Myc-DDK, HEK293T cells were seeded onto glass coverslips and transfected with pCMV6-FasLG (section 2.6.1, 2.6.2 & 2.10).

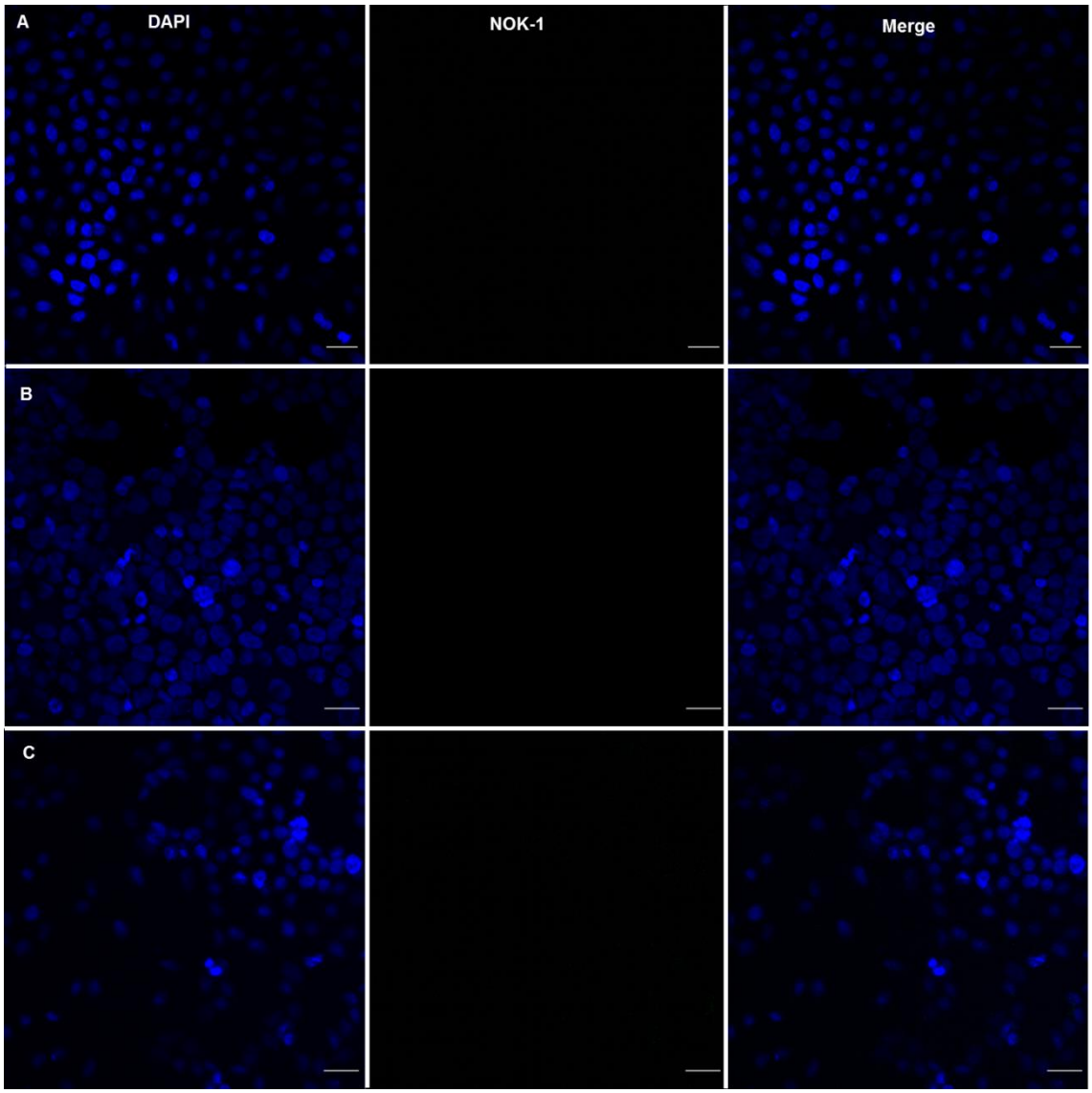

Figure 4.6. No CD95L-Myc-DDK is detected in HEK293T cells using NOK-1.
(**A**) Untransfected HEK293T cells or HEK293T cells transfected with pCMV6-FasLG (**B** and **C**) were fixed using 3.7% (w/v) paraformaldehyde (PFA). Cells were left non-permeabilised (**B**) or permeabilised with 0.1% (v/v) Triton X-100 (**A** and **C**). In order to detect CD95L-Myc-DDK by immunofluorescence, mouse, anti-human CD95L NOK-1 clone (BioLegend) and goat, anti-mouse Alexa Fluor® 488 (Invitrogen) was used. Cell nuclei were stained with DAPI (4',6-diamidino-2-phenylindole; Invitrogen). Scale bars, 20µm. Images representative of the whole population are shown in each case. There is no positive staining in (**A**), (**B**) and (**C**).

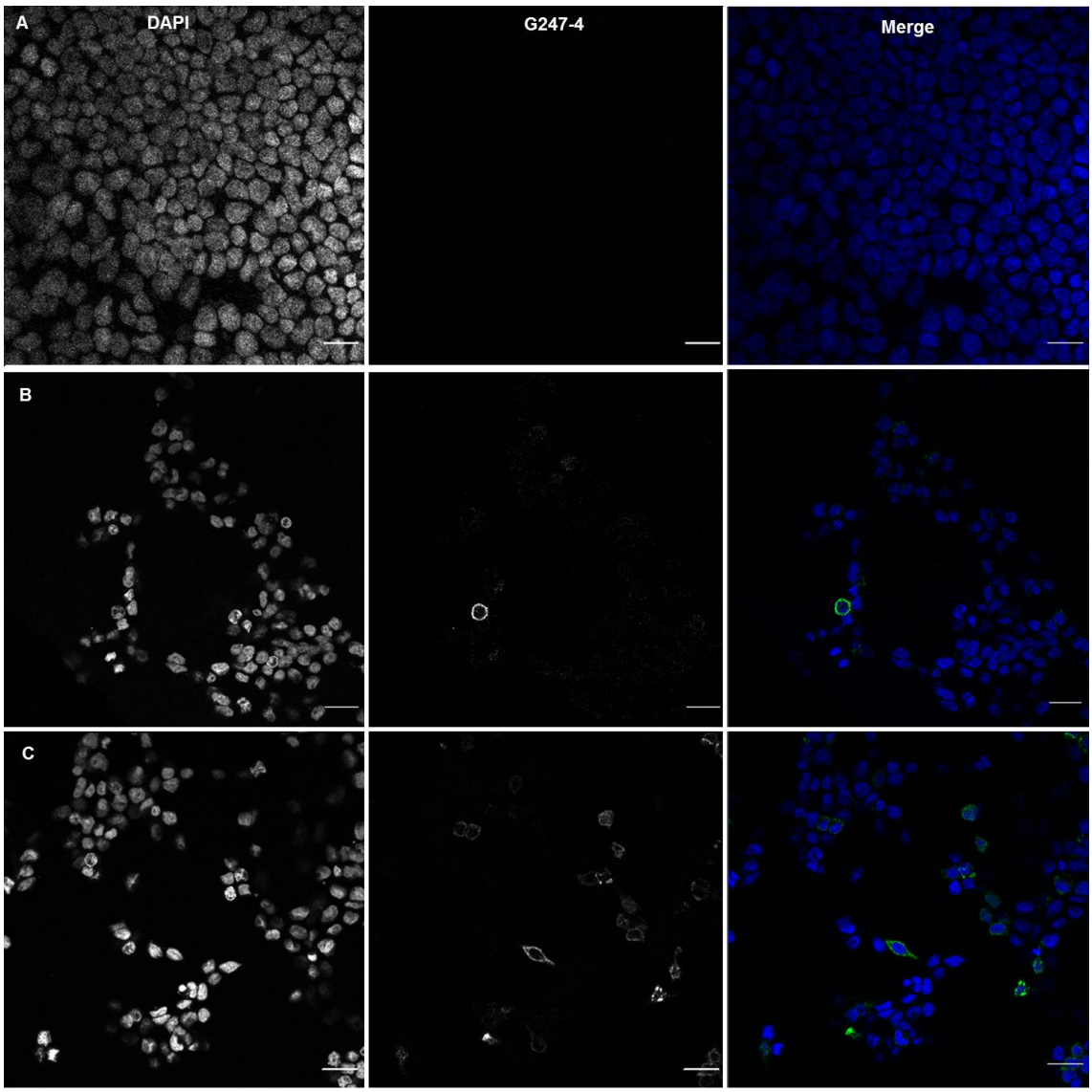

Figure 4.7. CD95L-Myc-DDK is detected in HEK293T cells using G247-4.
(**A**) Untransfected HEK293T cells or HEK293T cells transiently expressing CD95L-Myc-DDK (**B** and **C**) were fixed using 3.7% (w/v) paraformaldehyde (PFA). Cells were left non-permeabilised (**B**) or permeabilised with 0.1% (v/v) Triton X-100 (**A** and **C**). CD95L-Myc-DDK was detected by immunofluorescence using mouse, anti-human CD95L G247-4 clone (BD Pharmingen) and goat, anti-mouse Alexa Fluor® 488 (Invitrogen). Cell nuclei were stained with DAPI (4',6-diamidino-2-phenylindole; Invitrogen). DAPI and G247-4 staining shown in greyscale, merged images in colour (DAPI; blue, G247-4; green). Scale bars, 20µm. Images representative of the whole population are shown in each case. (**A**) Untransfected cells have no positive staining, (**B**) 3% of cells have positive, plasma membrane (PM) staining and (**C**) 18% of permeabilised cells show positive staining.

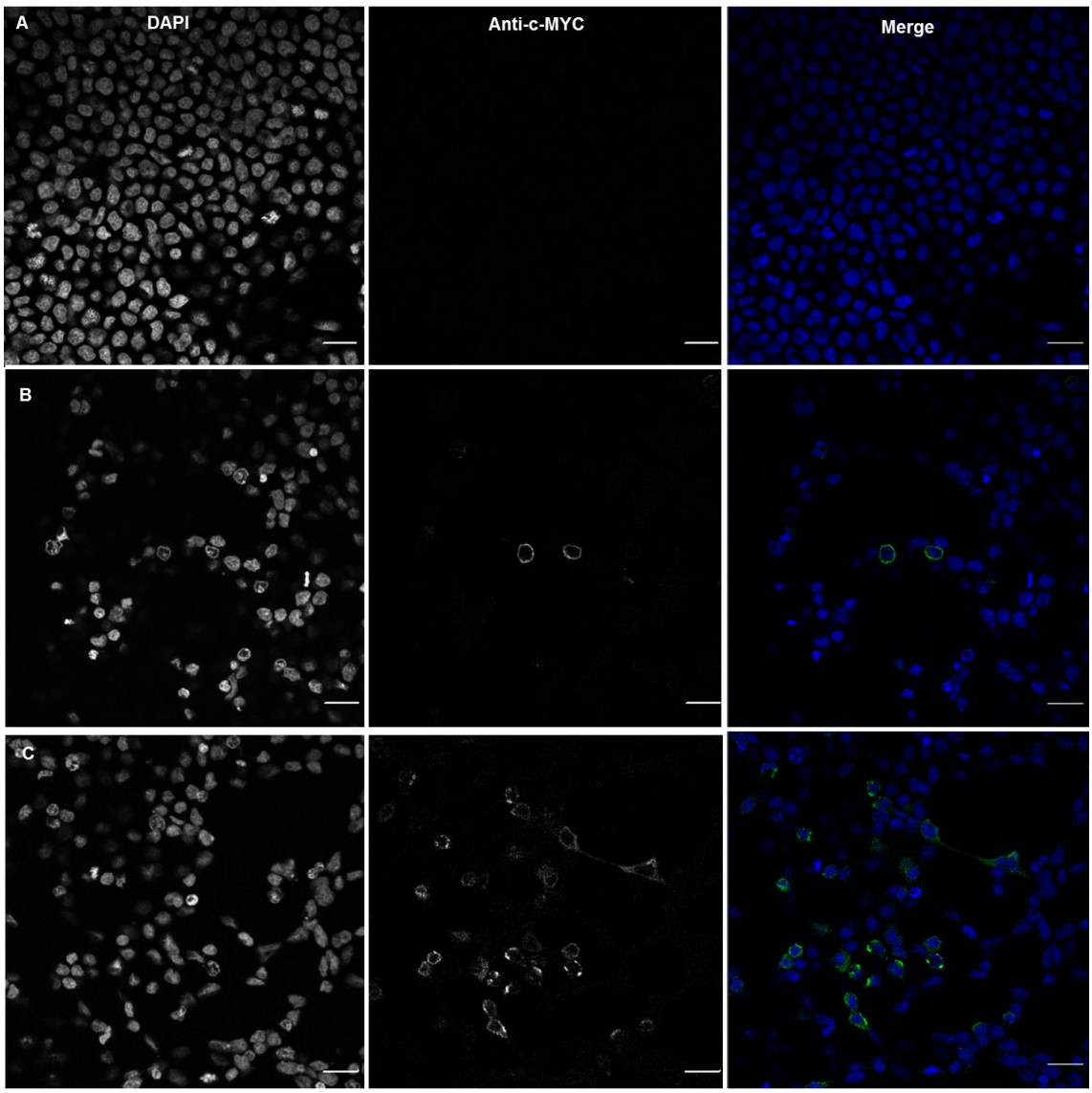

Figure 4.8. CD95L-Myc-DDK is detected in HEK293T cells using anti-c-MYC.
(**A**) Untransfected HEK293T cells or HEK293T cells transiently expressing CD95L-Myc-DDK (**B** and **C**) were fixed using 3.7% (w/v) paraformaldehyde (PFA). Cells were left non-permeabilised (**B**) or permeabilised with 0.1% (v/v) Triton X-100 (**A** and **C**). CD95L was detected by immunofluorescence using mouse, anti-c-MYC (Sigma) and goat, anti-mouse Alexa Fluor® 488 (Invitrogen). Cell nuclei were stained with DAPI (4',6-diamidino-2-phenylindole; Invitrogen). DAPI and c-MYC staining shown in greyscale, merged images in colour (DAPI; blue, c-MYC; green). Scale bars, 20µm. Images representative of the whole population are shown in each case. (**A**) Untransfected cells have no positive staining, (**B**) 2% of cells have positive, plasma membrane (PM) staining and (**C**) 15% of permeabilised cells show positive staining.

Forty-eight hours post transfection, cells were fixed and incubated with either mouse, anti-human CD95L, NOK-1 clone (BioLegend; Figure 4.6), mouse anti-c-MYC (Sigma; Figure 4.8) or mouse, anti-human CD95L clone G247-4 (BD Pharmingen; Figure 4.7) primary antibodies and secondary antibody, goat, anti-mouse Alexa Fluor® 488 (Invitrogen). Cell nuclei were stained with DAPI (4',6-diamidino-2-phenylindole; Invitrogen). Prior to staining, cells were either permeabilised (to also view possible intracellular protein) or left non-permeabilised (to view PM expression). Untransfected cells were also permeabilised to expose all possible antigens and incubated with the antibodies, as a negative control. Immunofluorescence was studied using a confocal, laser scanning microscope.

No fluorescence was detected in the untransfected cells showing that under the conditions used there was no non-specific binding of the primary or secondary antibodies (Figures 4.6A, 4.7A and 4.8A). This is also consistent with the conclusions from the Western analyses (section 4.2.1) that HEK293T cells do not express CD95L endogenously. No fluorescence was detected when the cells were incubated with the NOK-1 antibody (Figure 4.6). The epitope of the NOK-1 antibody is on the ECD (Nisihara et al., 2001) as is the epitope of the G247-4 antibody and the -myc tag is C-terminal, so a signal should be detect. This antibody is recommended for immunofluorescence and has previously been used to detect CD95L in melanoma cells (Andreola et al., 2002). The melanoma cells were fixed using 70% ethanol rather than PFA so perhaps the fixation method affects functionality of this antibody.

In contrast, cells transiently-transfected, permeabilised and stained using the G247-4 antibody (Figure 4.7C) and the anti-c-MYC antibody (Figure 4.8C), a distinct fluorescent signal was detected in the permeabilised samples (18% and 15% of cells, respectively), demonstrating expression of CD95L-Myc-DDK. Fewer positive cells were detected in non-permeabilised cells (Figure 4.7B, 3% of cells and figure 4.8B, 2% of cells), suggesting that in only a small fraction of the transfected population CD95L-Myc-DDK is present on the PM. There is a noticeable reduction in the number of cells after transfection, compared to the untransfected sample. For example, there are 65% and 41% fewer cells in Figure 4.7B & C respectively, and a 63% and 53% decrease in cell number in Figure 4.8B & C respectively. The precise intracellular localisation of CD95L-Myc-DDK has not yet been determined but co-localisation with an organelle-specific antibody such as calnexin (an endoplasmic reticulum marker) or Golgi matrix protein (GM130; a Golgi marker), would help to identify the subcellular compartment of the protein.

4.2.5. Use of inhibitors to improve plasma membrane expression of CD95L-Myc-DDK transiently expressed in HEK293T cells

The levels of detection of intracellular (~20% of cells) and PM CD95L (~2%) are low, despite the transfection efficiency being around 70% (Figure 4.5). It is possible that CD95L is being cleaved from the PM, since it is known to be a substrate of MMP-7 and ADAM10. The effects of two inhibitors of these endopeptidases were tested to determine if PM expression of CD95L-Myc-DDK could be stabilised. GM1006 (Merck), a cell permeable, broad spectrum MMP

inhibitor (of MMP - 1, 2, 3, 7, 8, 9, 12, 14, 26) and GI254023X (Sigma-Aldrich), which is marketed as selective ADAM10 inhibitor, were tested for inhibition of the MMP-7 and ADAM10, respectively. HEK293T cells were seeded onto glass coverslips and transfected with pCMV6-FasLG (encoding human CD95L-Myc-DDK)\; section 2.6.1, 2.6.2 & 2.10). Twenty-four hours after transfection, cells were incubated with 20µM GM1006 or 20µM GI254023X, or both inhibitors in combination, in FBS-free media. Forty-eight hours post transfection, cells were fixed and incubated with mouse, anti-human CD95L mAb G247-4 and secondary antibody, goat, anti-mouse Alexa Fluor® 488. Cell nuclei were stained with DAPI. Cells were non-permeabilised to view CD95L-Myc-DDK PM expression and immunofluorescence was studied using a confocal laser, scanning microscope.

Transfected cells incubated with the ADAM10 inhibitor GI254023X were 10% positive for CD95L-Myc-DDK staining (Figure 4.9A) and 12% of cells were positive when incubated with GM1006 (Figure 4.9B). When both inhibitors were used in combination, 18% of cells expressed CD95L-Myc-DDK at the cell surface (Figure 4.9C). However, cells were observed to be less healthy, which may be an additive effect of using both inhibitors. The use of inhibitors seems to have increased the amount of CD95L-Myc-DDK present on the PM, when comparing this staining to cells transfected without inhibitors (Figure 4.7B, 3% of cells and figure 4.8B, 2% of cells). Despite the apparent effects however, the amount of positive staining of CD95L-Myc-DDK on the PM is still low, in comparison to the transfection efficiency.

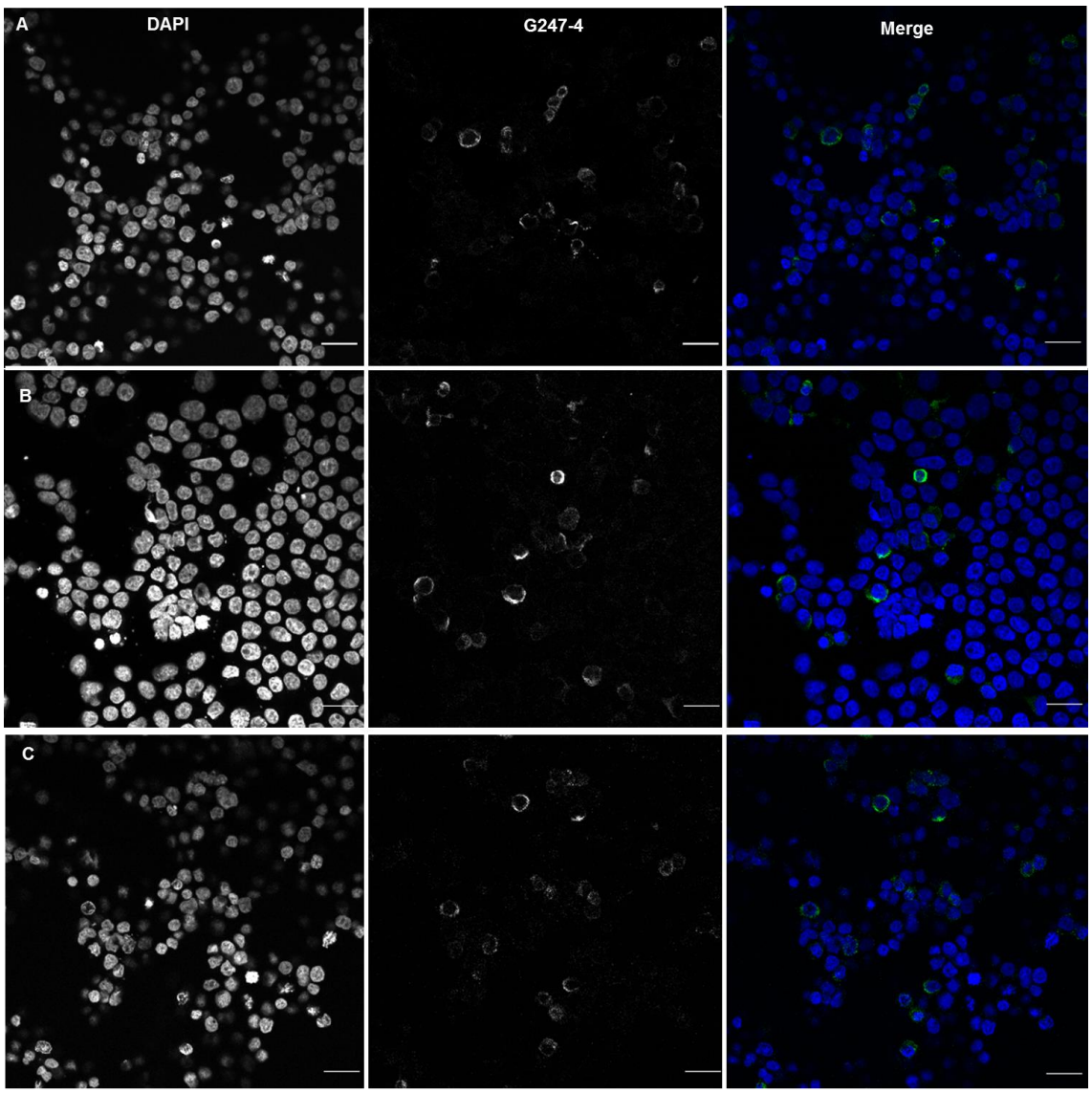

Figure 4.9. PM expression of CD95L-Myc-DDK in HEK293T cells is improved with inhibitors of MMP-7 and/or ADAM10.
HEK293T cells transiently expressing CD95L-Myc-DDK (**A**, **B** and **C**) which were incubated with inhibitors 24 hours before being fixed using 3.7% (w/v) paraformaldehyde (PFA). CD95L was detected by immunofluorescence using mouse, anti-human CD95L G247-4 clone (BD Pharmingen) and goat, anti-mouse Alexa Fluor® 488 (Invitrogen). Cell nuclei were stained with DAPI (4',6-diamidino-2-phenylindole; Invitrogen). DAPI and G247-4 staining shown in greyscale, merged images in colour (DAPI; blue, G247-4; green) Scale bars, 20µm. Images representative of the whole population are shown in each case. (**A**) Cells incubated with 20µM GI254023X (Sigma-Aldrich) with 10% of cells with positive staining, (**B**) Cells incubated with 20µM GM1006 (Merck) with 12% of cells with positive staining and (**C**) Cells incubated with 20µM of both inhibitors with 18% of cells with positive staining.

Flow cytometry was used to more accurately quantify the effect of the inhibitors and determine the amount of PM CD95L-Myc-DDK on a larger sample of cells. The epitope of the G274-4 antibody is located on the ECD of CD95L although the exact location is unknown (personal communication, BD Pharmingen), however, this antibody is not usually recommended for flow cytometry. Due to the success of this antibody in staining and Western blot however, its use was optimised for use in flow. Firstly, the antibody was titrated against untransfected HEKs (Appendix 1 - Supplementary Figure 1), as was the anti-c-MYC antibody (to validate the results since the -myc tag is C-terminal; Appendix 1 - Supplementary Figure 3) to ensure there was no non-specific binding of these antibodies. The secondary antibody was also bound alone to ensure no non-specific binding (Appendix 1 – Supplementary Figure 2). Secondly, transfected HEKs (expressing CD95L-Myc-DDK) were incubated with 20µM GM1006 and working concentrations of both antibodies titrated against the cells (Appendix 1 – Supplementary Figures 5 & 6). This demonstrated that both the G274-4 and anti-Myc antibodies detect the same population of transfected cells, and an appropriate working concentration (1µg mAb per 10^6 cells) was selected for both.

HEK293T cells were transfected with pCMV6-FasLG or with pCINeoCD36-12His (mock transfection) or a plasmid which expresses a green fluorescent protein (GFP; to measure transfection efficiency; section 2.6.1). Twenty-four hours after pCMV6-FasLG transfection, cells were incubated with 20µM GM1006, in FBS-free media. A well of pCMV6-FasLG transfected cells were also left without any inhibitor to compare the effects on PM expression.

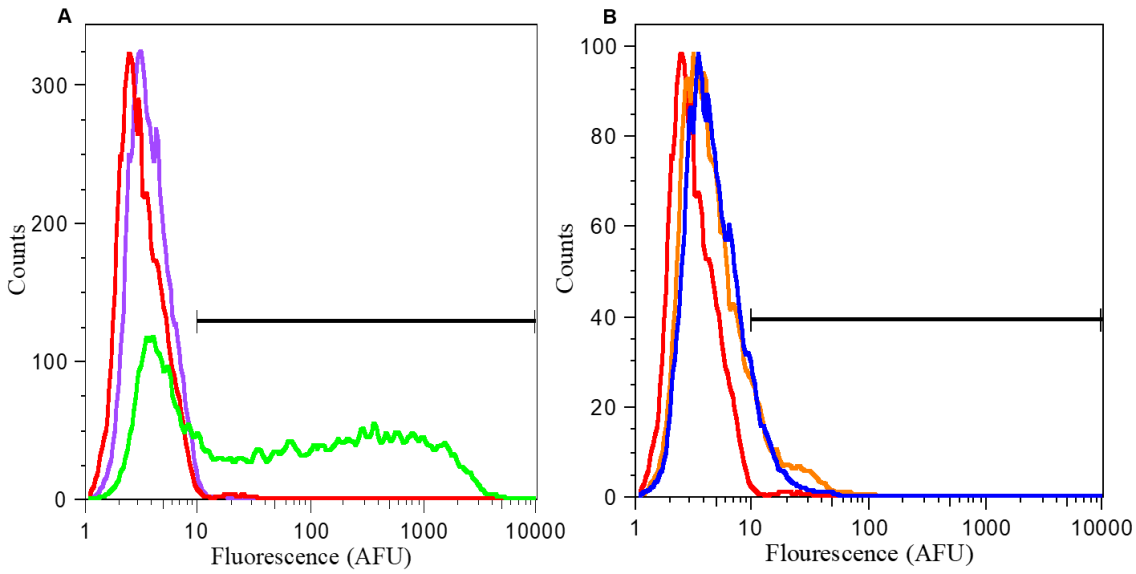

Figure 4.10. Histograms displaying plasma membrane expression of CD95L-Myc-DDK in HEK293T cells incubated with GM1006.
HEK293T cells were seeded on 6-well plates and transfected with a vector (pCMV6-FasLG) coding for CD95L-Myc-DDK, CD36-12His (mock-transfected), green fluorescence protein (GFP) or left untransfected. CD95L-Myc-DDK expressing cells were incubated with 20µM GM1006 (Merck) inhibitor in FBS free media, 24 hours before harvesting. Untransfected, mock-transfected (negative controls) and CD95L-Myc-DDK expressing cells were incubated with primary antibody mouse, anti-human CD95L G247-4 clone (BD Pharmingen) and goat, anti-mouse Alexa Fluor® 488 (Invitrogen). 10,000 cells of normal size and granularity were gated to eliminate cell debris. Results from representative experiments were overlain on the histogram, displaying distribution of fluorescence (arbitrary fluorescence units; AFU) against number of cells (counts) for all conditions. Cells were gated (black bar) to give percentage of positive cells and median fluorescence for the entire population was also calculated. (**A**) Untransfected cells (red) were 1.1% positive which had a median green fluorescence of 2.8 AFU, mock-transfected (purple) 0.8% positive with 3.41 AFU and GFP expressing cells (green) were 64% positive with 42 AFU. (**B**) Untransfected cells (red) were 1.1% positive with 2.8 AFU, pCMV6-FasLG transfected cells (blue) 10% positive with 4.14 AFU and pCMV6-FasLG transfected cells with GM1006 (orange) 12% positive with 3.9 AFU.

The concentration of GM1006 had previously been titrated from 1 - 100 µM on transfected HEKs to ensure 20µM was the most appropriate concentration (Appendix 1 - Supplementary Figure 4). Forty-eight hours post transfection, cells were incubated with mouse, anti-human CD95L mAb G247-4 and Alexa Fluor® 488 (section 2.9.3). Untransfected and mock transfected cells were also incubated with the antibodies, as negative controls. Analysis by flow cytometry detected fluorescence emitted by the secondary antibody or GFP. Patterns of fluorescence from representative experiments were overlain on histograms

(Figure 4.10). The percentage of positive cells and median fluorescence over the whole cell population for each condition, was analysed by ANOVA for 3 independent, repeat experiments (section 2.15; Figure 4.11).

In Figure 4.10A, cells were mock-transfected to ensure that the shift in median fluorescence (as first observed in Figure 4.5) for pCMV6-FasLG transfected cells was not an artefact. The negative control conditions shift from 2.8 AFU (untransfected) and 3.41 AFU (mock-transfected; Figure 4.10A) to 4.14 AFU (pCMV6-FasLG transfected) and 3.9 AFU (pCMV6-FasLG and GM1006; Figure 4.10B). There is also a change in percentage of positive cells. The gate was positioned such that fewer than 2% of the cells were positive in the controls (Figure 4.10A). CD95L-Myc-DDK positivity was detected in 10% and 12% in the transfected cells and in transfected cells treated with GM1006, respectively (Figure 4.10B). These data suggest that the peak shift in CD95L-Myc-DDK expressing cells is not an artefact and there are a few molecules of CD95L-Myc-DDK detectable on the cell surface (as was also seen using the NOK-1 antibody; Figure 4.5). Furthermore, GM1006 increased the percentage of positive cells suggesting that it prevented cleavage of CD95L-Myc-DDK from the PM. This population of cells is noticeable as a small shoulder around 20 – 50 AFU in CD95L-Myc-DDK expressing cells treated with GM1006 (Figure 4.10B; orange) and similar patterns were seen when the anti-C-MYC antibody was used in to detect CD95L-Myc-DDK in flow (Appendix 1 – Supplementary Figure 6).

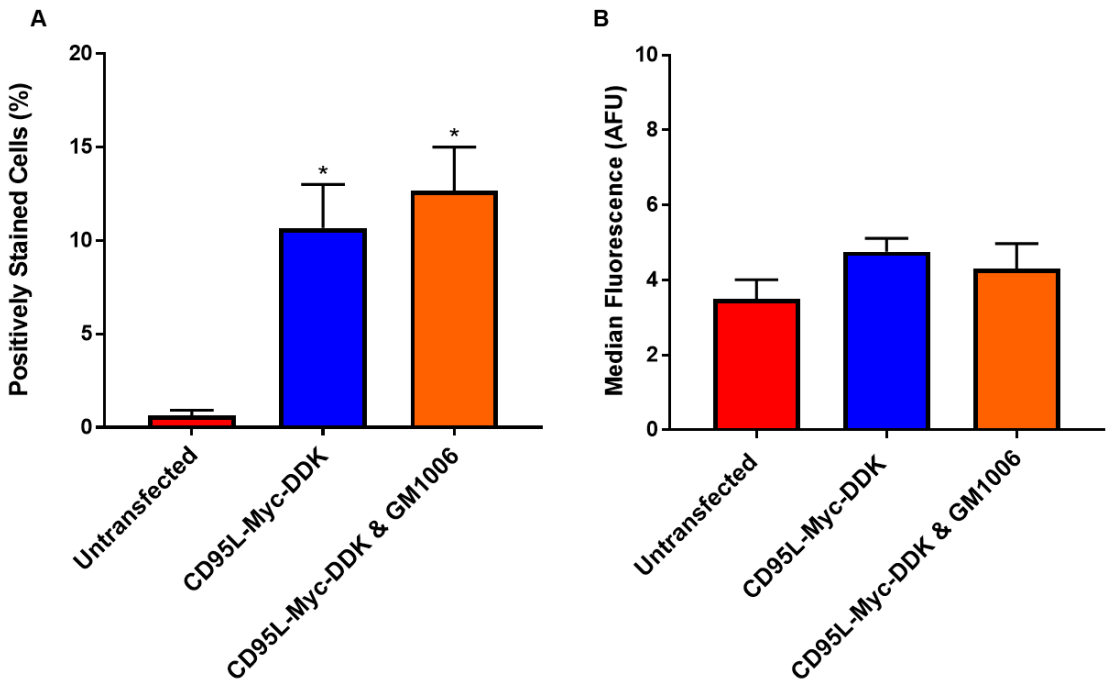

Figure 4.11. Statistical analysis demonstrates little plasma membrane expression of CD95L-Myc-DDK in HEK293T cells incubated with GM1006.
HEK293T cells were seeded on 6-well plates and transfected with a vector coding for CD95L-Myc-DDK or left untransfected. CD95L-Myc-DDK expressing cells were incubated with 20µM GM1006 (Merck) inhibitor in FBS free media, 24 hours before harvesting. Protein was detected using primary antibody mouse, anti-human CD95L G247-4 clone (BD Pharmingen) and goat, anti-mouse Alexa Fluor® 488 (Invitrogen). 10,000 cells of normal size and granularity were gated to eliminate cell debris. Mean and SEM values are from three independent, repeat experiments (n=3). Significance was calculated by one-way ANOVA; * $P \leq 0.05$. (**A**) Mean percentage of positive cells (CD95L-Myc-DDK expressing) without and with inhibitor, in comparison to untransfected cells. CD95L-Myc-DDK cells alone and with GM1006 inhibitor had statistically significant staining in comparison to untransfected cells. (**B**) Median fluorescence of cells untransfected, expressing CD95L-Myc-DDK without and with GM1006. There was no statistical difference between conditions.

The percentage of positive cells and median cell fluorescence over the whole cell population for untransfected cells, CD95L-Myc-DDK expressing cells and CD95L-Myc-DDK expressing cells incubated with GM1006 was analysed by ANOVA for 3 independent, repeat experiments (section 2.15; Figure 4.11).

The percentage of cells expressing CD95L-Myc-DDK averaged 11 +/- 2%, which increased to 13 +/- 2% when incubated with GM1006 (Figure 4.11A). Both values were statistically different ($P \leq 0.05$) to untransfected cells (0.6 +/- 0.3%). Despite there being a trend towards increased PM staining when using the inhibitor, there was no statistical difference between CD95L-Myc-DDK cells with or without GM1006 ($P > 0.05$). Although there is a significant increase in percentage staining with transfected cells however, the increase is not enough to shift the median fluorescence of the entire cell population (Figure 4.11B). There is therefore no statistical difference between the conditions, regardless of CD95L expression (median fluorescence of the untransfected cells, 3.5 +/- 0.5 AFU; CD95L-Myc-DDK, 5 +/- 0.4 AFU; and CD95L-Myc-DDK treated with GM1006; 4 +/- 0.7 AFU). In conclusion, these data fit with what was seen by flow cytometry using the NOK-1 antibody and the confocal staining data using anti-C-MYC and G247-4. There is very little detectable PM expression of CD95L-Myc-DDK, even with the use of inhibitors to prevent surface cleavage of the protein. This makes the use of transfected HEKs for further study of uptake of CD95R-Fc coated particles impractical since there is not a large enough population of CD95L positive cells and it is difficult to distinguish the increase in abundance of CD95L-Myc-DDK at the PM over the non-expressing cells. However, the antibodies used to detect native CD95L, particularly G247-4, have been validated. The anti-C-MYC, anti-FLAG and G247-4 antibodies gave comparable results when used in western. G247-4 can also be used for immunofluorescent staining and flow cytometry, as was validated by using the anti-C-MYC antibody, (which was tested in IF against a positive control, myc-tagged PGP, data not shown). The G247-4 antibody could be further validated by testing it with a positive control; a cell line or tissue with endogenous CD95L expression.

4.2.6. Detecting message for CD95L in MDA-MB-231 cells by RT-qPCR

The targeting effect of CD95R-Fc coated microparticles depends on CD95L being present and on the surface of MDA-MB-231 cells, allowing the CD95R to interact with CD95L specifically. Messenger RNA (mRNA) is required to produce protein, so to test for the presence of CD95L mRNA, real-time quantitative PCR (RT-qPCR) was utilised. RNA was extracted from MDA-MB-231 cells, and from untransfected HEKs and transfected HEKs expressing CD95L-Myc-DDK as negative and positive controls, respectively (section 2.11.1 & 2.11.2). Copy DNA was synthesised and diluted to the same concentration (200ng/µl; section 2.11.3). CD95L primers (forward and reverse; Sigma, table 2.4) and GAPDH primers (housekeeping gene control; EuroFins Genomics) were mixed with each cDNA sample and SYBR™ Green master mix (Thermo Scientific; section 2.11.4). Samples were amplified in triplicate for 40 cycles on a 7500 Real Time PCR system (Applied Biosystems) and Ct (cycle threshold) values were calculated using the 7500 software version 2.3 (Applied Biosystems). Amplification plots for CD95L expression and the house-keeping gene control (GAPDH) are shown (Figure 4.12). The Ct mean for CD95L-Myc-DDK expressing HEKs was 13.34 demonstrating the abundant presence CD95L mRNA in the transfected cells (Figure 4.12A). This Ct mean was much higher from MDA-MB-231 cells (30.65) suggesting that CD95L mRNA was lower in the MDA-MB-231 cells than the untransfected HEK293T negative control (27.88).

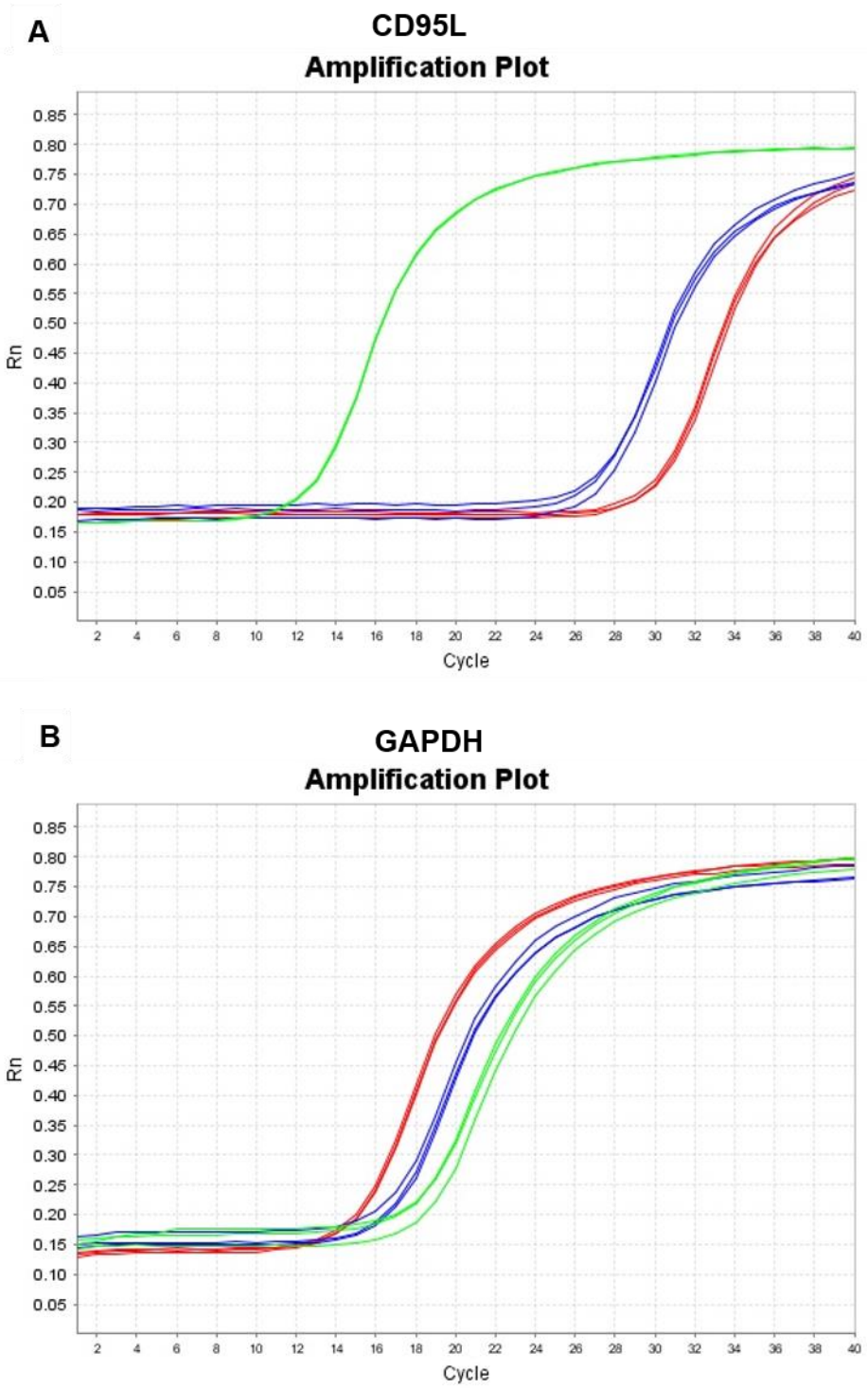

Figure 4.12. RT-qPCR analysis demonstrates little CD95L mRNA in MDA-MB-231 cells. Representative amplification plots showing delta Rn (normalised reporter value; fluorescent signal) against cycle number for detection of CD95L in triplicate for (**A**) CD95L-Myc-DDK expressing HEK293T cells (positive control; green), Ct (threshold cycle) mean 13.34, untransfected HEK293T cells (negative control; blue) Ct mean 27.88 and MDA-MB-231 cells (red) Ct mean 30.65. (**B**) Detection of GAPDH mRNA in HEK293T cells expressing CD95L-Myc-DDK (green) Ct mean 18.84, untransfected HEK293T cells (blue) Ct mean 17.15 and MDA-MB-231 cells (red) Ct mean 15.40.

The Ct mean for GAPDH (housekeeping gene control) was 18.84 for HEK293T cells expressing CD95L-Myc-DDK and 17.15 for untransfected HEK293Ts. For MDA-MB-231s, the Ct mean for GAPDH was 15.40. Therefore, there is very little CD95L mRNA present in MDA-MB-231 cells, in comparison to the house-keeping control (GAPDH).

4.2.7. Endogenous expression of CD95L in MDA-MB-231 cells

A gene's mRNA level does not always predict its protein level. For example, the low amount of CD95L mRNA detected in MDA-MB-231 cells does not mean there is low amounts of protein. Therefore, it is important to also investigate protein expression levels. To detect any CD95L protein, MDA-MB-231 cells were harvested using versene to avoid cleavage of any plasma membrane CD95L (section 2.7.5). Cells were lysed and whole-cell extracts run on an 8% SDS-polyacrylamide gel (section 2.7.8). The protein was transferred onto a PVDF membrane and probed using the G247-4 antibody for detection of CD95L (section 2.7.11; Figure 4.13). The blot shows a faint signal at the correct molecular weight of 40kDa for monomeric CD95L, however, a strong signal can be seen at 120kDa. Potentially, this could be the membrane bound, trimeric form of CD95L, however this has only been observed previously in non-reducing conditions in HEp-2 cells (Meza-Lamas et al., 2006). Higher molecular weight species of protein were detected with CD95L-Myc-DDK expressing HEK293T cells, however the mobility corresponded to 80kDa (Figure 4.2B). A comparison is required to ensure these bands have different mobilities, by running the lysates of MDA-MB-231 cells with untransfected and transfected HEK293T cells on the same gel, and analysing protein expression by Western blot. Furthermore, siRNA knockdown of CD95L in

MDA-MB-231 cells can be used to test whether the 120kDa signal is a trimer of CD95L (Figure 4.14).

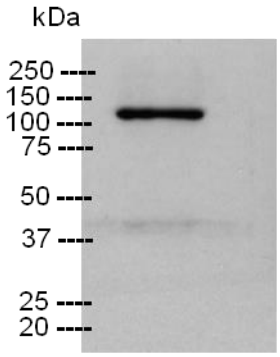

Figure 4.13. Endogenous expression of CD95L in MDA-MB-231 cells.
MDA-MB-231 cells (2 x 10^6) were lysed and 0.02% of the total volume was reduced, denatured and loaded onto an 8% SDS polyacrylamide gel and proteins separated by electrophoresis. The blot was prepared on a PVDF membrane and probed using mouse, anti-human CD95L G247-4 clone (BD Pharmingen).

4.2.8. siRNA knockdown of CD95L in MDA-MB-231 cells

In Figure 4.13, Western blot analysis on MDA-MB-231 cell lysate shows a faint signal at the correct molecular weight of 40kDa for monomeric CD95L, however, a strong signal can be seen at 120 kDa. The antibody used, G247-4, has been validated on CD95L-Myc-DDK expressing HEK cells. The absence of an appropriate negative control for the expression of CD95L in MDA-MB-231 cells makes these data difficult to interpret. However, if the 40kDa species is monomeric CD95L and the apparent 120 kDa species a higher order multimer, it should be possible to knock down their expression using two *CD95L* siRNAs targeted to different locations in the open reading frame (ORF) (Figure 4.14).

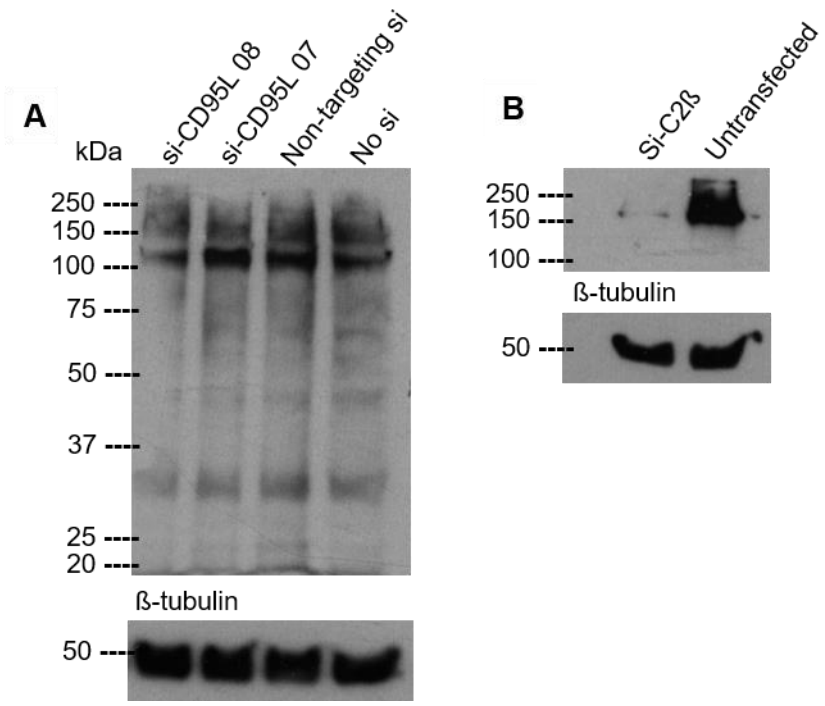

Figure 4.14. siRNA knockdown of CD95L in MDA-MB-231 cells.
MDA-MB-231 cells were seeded on 6-well plates and transfected using Oligofectamine (Invitrogen) with 20µM (**A**) *CD95L*/*FasLG* targeting siRNAs (si-CD95L 08 & si-CD95L 07; Dharmacon), a non-targeting siRNA (as a negative control; Dharmacon), a transfection agent only control (no siRNA) and (**B**) a siRNA against C2β (as a procedural control). 48 hours post transfection cells were harvested, lysed and equal amounts of lysate denatured, loaded onto an 8% SDS polyacrylamide gel and proteins separated by electrophoresis. The blots were prepared on a PVDF membrane and probed using primary antibodies, mouse, anti-human CD95L G247-4 clone (BD Pharmingen), anti-β-tubulin (Sigma) or mouse, anti-human PI3-Kinase C2β (BD Biosciences). There has been successful knockdown of C2β (**B**).

Cells were seeded in a 6-well dish and 24 hours later, transfected using oligofectamine (Invitrogen) with siRNAs (table 2.6) against CD95L (si-CD95L 08 and si-CD95L 07; Dharmacon), a non-targeting siRNA pool (as a negative control; Dharmacon), and a transfection agent only control (no siRNA; section 2.12.1). Another siRNA against another known expressed protein, PI3-Kinase C2β, in MDA-MB-231 cells (si-C2β) was also used as a procedural control. Forty-eight hours post transfection, cells were harvested, lysed and whole-cell extracts

run on a 10% gel. The protein was transferred onto a PVDF membrane and probed using mouse, anti-human CD95L mAb G247-4, anti-β-tubulin (Sigma), or mouse, anti-human PI3-Kinase C2β (BD Biosciences; Figure 4.14; section 2.12.2). There was no change in the intensity of the bands at 120kDa with either of the CD95L siRNAs (si-CD95L 07 and 08) in comparison to the controls (Figure 4.14A). However, C2β was successfully knocked down (Figure 4.14B) indicative of efficient siRNA transfection. These data do not support the hypothesis that the 120kDa band corresponds to the trimeric, membrane bound form of CD95L and this signal could be due to non-specific binding of the primary antibody. Again, a faint band around 40kDa was observed. This may be indicative of a small amount of monomeric CD95L and a reduction may have occurred with knockdown using si-CD95L 08, however this could be an artefact due to bad transfer during Western blot analysis, so this result is inconclusive. The 40kDa band may also represent non-specific binding of the primary antibody or a degradation product of the 120kDa protein which is either much more abundant or has more avidity with the antibody, or another non-specific interaction.

4.2.9. Investigating presence of CD95L in MDA-MB-231 cells using immunofluorescent staining

siRNA knockdown results show that the 120kDa band detected when probing for CD95L is likely due to non-specific binding of the primary antibody. However, the result for the faint band at 40kDa, which may be indicative of a small amount of monomeric CD95L, is inconclusive. The expression of CD95L was investigated using immunofluorescent staining along with GM1006, to prevent any cleavage of CD95L from the PM (section 2.10).

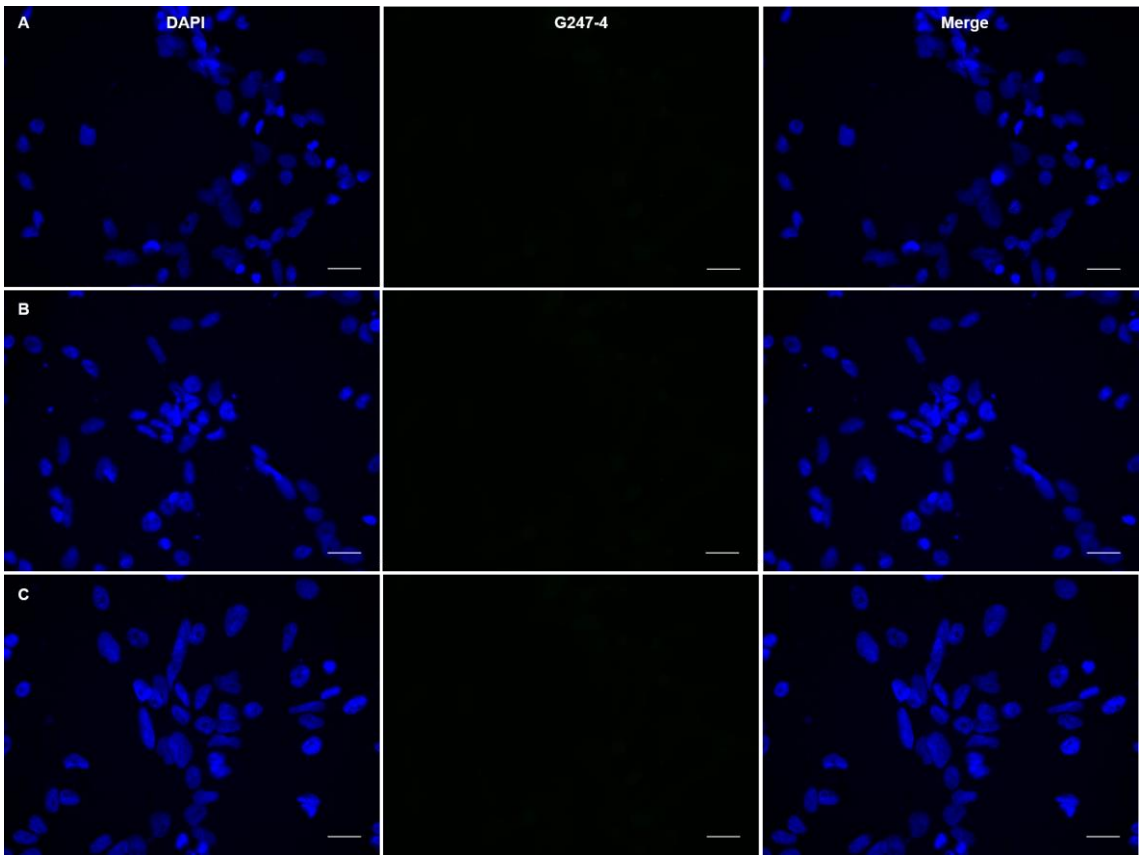

Figure 4.15. No CD95L is detected in MDA-MB-231 cells using G247-4, with or without an MMP-7 inhibitor.
MDA-MB-231 cells were seeded and incubated with GM1006 (**C**) 24 hours before being fixed using 3.7% (w/v) paraformaldehyde (PFA). Cells were left non-permeabilised (**B** and **C**) or permeabilised with 0.1% (v/v) Triton X-100 (**A**). The presence of CD95L was investigated by immunofluorescence using mouse, anti-human CD95L G247-4 clone (BD Pharmingen) and goat, anti-mouse Alexa Fluor® 488 (Invitrogen). Cell nuclei were stained with DAPI (4',6-diamidino-2-phenylindole; Invitrogen). Scale bars, 20µm. Images representative of the whole population are shown in each case. There is no positive staining in (**A**), (**B**) and (**C**).

MDA-MB-231 cells were seeded onto glass coverslips. Twenty-four hours later, cells were incubated with 20µM GM1006 in FBS-free media. Forty-eight hours post transfection, cells were fixed and incubated with mouse, anti-human CD95L mAb G247-4 (Figure 4.15) and secondary antibody, goat, anti-mouse Alexa Fluor® 488. Cell nuclei were stained with DAPI. Prior to staining, cells were either permeabilised (to also view possible intracellular protein) or non-permeabilised

(to view PM expression). Immunofluorescence was studied using an epi-fluorescent microscope (Leica).

No fluorescence was detected when the cells were incubated with the G247-4 antibody, either when the cells are permeabilised (Figure 4.15A) or non-permeabilised, without GM1006 (Figure 4.15B) or with GM1006 (Figure 4.15C). This antibody has been validated in transfected HEK293T cells, and the GM1006 inhibitor has been found to improve PM expression of CD95L-Myc-DDK. It is therefore likely that there is no detectable expression of CD95L in MDA-MB-231 cells, especially on the plasma membrane, where its presence is required to demonstrate any interaction with CD95R-Fc on a coated microparticle.

4.3. Discussion

CD95L has been previously described as critical for cancer survival (Hadji et al., 2014) and its expression in tumour endothelial tissue provides a counterattack against the immune system (Motz et al., 2014). It would therefore be possible to exploit CD95L expression by cancer cells as a therapeutic target if it is present on the plasma membrane of cancer cells, providing a targeted delivery of chemotherapeutic agents to prevent the side-effects associated with many cancer treatments (Ateh et al., 2011). However, recent publications have suggested that there is little or no CD95L in most tumours or cancer cell lines (Motz et al., 2014, Glukhova et al., 2018). In this chapter, methods to detect surface expression of CD95L were optimised, using HEK293T cells, transiently transfected to express CD95L-Myc-DDK. The endogenous expression of CD95L in MDA-MB-231 cells was then investigated.

The antibodies used in the past to detect CD95L have been critically analysed and many have been found to lack specificity (Sträter et al., 2001). It was therefore necessary to validate the antibody used here to detect CD95L (G247-4). HEK293T cells were successfully transfected with pCMV6-FasLG, and the expression of recombinant CD95L-Myc-DDK was demonstrated via Western blot using not only G274-4, but anti-flag and anti-C-MYC antibodies, which detect the two, C-terminal tags linked to CD95L. The G247-4 antibody failed to detect endogenous CD95L expression in HEK293T cells providing potential negative and positive controls to investigate the CD95R/L targeting theory. Higher molecular weight species detectable by G247-4 and anti-FLAG antibodies were also observed by Western blot of the transfected HEK293T cells. These were

resolved almost completely (even with heavily overloaded samples), to the monomeric form following reduction by the addition of a high volume of 2-mercaptoethanol. The reduction of these higher molecular weight species suggests the presence of the disulphide bond found in CD95L (Figure 4.1); also shown in the crystal structure of CD95L ECD (Liu et al., 2014) (Figure 1.2). It is likely that CD95L-Myc-DDK has been trafficked through an appropriate oxidative environment, such as through the endoplasmic reticulum, to allow the disulphide bridge to form. It is also possible however, that a non-physiological bond has formed between proteins after cell lysis or during denaturation since without prevention, these processes can lead to the creation of new disulphide bonds with other thiols to yield non-physiological complexes (Poole, 2015). This can be prevented or blocked, with the addition of a thiol-alkylating agent in the lysis buffer for example, which covalently bonds to the thiol group of cysteine residues to prevent the formation of any disulphide bonds, within or between proteins (Poole, 2015).

CD95L has 3 N-linked glycosylation sites in the ECD (Voss et al., 2008). Deglycosylation experiments showed that the monomeric form of CD95L-Myc-DDK is equally sensitive to PNGase-F and Endo-H, suggesting that these are high mannose glycans and the protein may be localised to the endoplasmic reticulum. Deglycosylation experiments on the higher molecular weight species of CD95L-Myc-DDK demonstrated differential sensitivity of these species to PNGase-F and Endo-H with Endo-H unable to fully degylcosylate the higher molecular weight species. This suggests that some of the glycans have been matured, which occurs in the Golgi apparatus. Immunocytochemistry

experiments using anti-CD95L and anti-C-MYC showed that there is a small amount of detectable CD95L-Myc-DDK at the PM, however a much stronger signal for CD95L was detected inside the cell following permeabilisation. CD95L can be shed from the PM to form soluble CD95L (sCD95L) by ADAM10 and MMP7. It therefore seemed possible that some of the matured CD95L-Myc-DDK has reached the PM, but little is detected using IF staining because it has been shed by these proteases. The proteases may be produced (ADAM10; (Lammich et al., 2010)) or secreted (MMP-7; (Liu and Wu, 2006)) by the HEK293T cells themselves or could already be present in the cell media from additives, such as Fetal bovine serum (FBS) for example (Hu and Beeton, 2010). The use of inhibitors improved PM retention of CD95L, however, not significantly enough to enable these cells to be used in uptake experiments (i.e. it would have been difficult to separate the CD95L-Myc-DDK expressing cells from the background by flow cytometry in order to test whether they were more proficient at CD95R-Fc-coated MP uptake).

Despite the sensitivity of monomeric form and higher molecular weight species of CD95L-Myc-DDK to deglycosidases, it is unknown whether all available sites for glycosylation on the recombinant CD95L have glycans attached. Mutation of the putative N-linked glycosylation sites correlates with reduced CD95L expression in COS-1 cell transfectants (detected using the mAb G247-4) (Orlinick et al., 1997) and glycosylation has been found to reduce CD95L aggregation, as has been shown by the mutagenesis of CD95L glycosylation sites with resulting aggregates eluted by size exclusion chromatography (Liu et al., 2014). If not glycosylated properly, the expressed protein in the HEK293T

cells may not traffic to the plasma membrane efficiently, which could help explain the lack of cell surface expression. Despite this, previous studies have demonstrated successful CD95L expression in HEK293T cells via Western blot and IF, using an anti-CD95L antibody, Fc2 (which was created with its epitope mapped in this study) (Lettau et al., 2014) and via Western blot of FLAG-tagged CD95L, detected using an anti-FLAG antibody (Schneider et al., 1997). One study has detected CD95L (using the anti-CD95L mAb NOK-1) on the cell surface of HEK293T cells using flow cytometry after a 24 hour incubation with G1254023X, the ADAM10 inhibitor used here (Kirkin et al., 2007). One observation of the data here was that the number of cells decreased when transfected with pCMV6-FasLG, which is most noticeable in the IF staining images. Normally, the level of CD95L expression in proliferating cells is low, since enhanced surface expression can lead to apoptosis of surrounding, CD95R-bearing cells (Glukhova et al., 2018) and most cells, including HEK293Ts as shown by flow cytometry, express CD95R (Larregina et al., 1998). Furthermore, along with siRNAs designed against CD95L being toxic to cancer cells (discussed further in section 4.3.1), the CD95L mRNA itself has also been reported to induce cell death in HeyA8 (ovarian cancer) cells, with enforced expression (Putzbach et al., 2017). Although this data has yet to be published and explained in full (as has been referred to in their paper; (Putzbach et al., 2017)) it suggests that it is possible that the overexpression of CD95L-Myc-DDK and so, presence of the CD95L mRNA, may be inducing cell death in HEK293T cells. To test this potential effect, it may be possible to prevent full length CD95L protein from being produced by the CD95L mRNA, by introducing a premature stop codon after the start codon in the pCMV6-FasLG vector. If this construct produces mRNA with no detectable CD95L protein, it’s effect on cell death and growth can be

determined in HEK293T cells, in comparison to transfection with unmodified pCMV6-FasLG.

Following validation of the anti-CD95L antibody, G247-4, in pCMV6-FasLG transfected HEK293T cells, CD95L expression in MDA-MB-231 cells was investigated. Firstly, very little mRNA was detected in the cells using RT-qPCR, in comparison to the housekeeping gene control. An abundance of CD95L was detected in transfected HEK293T cells however, demonstrating that the primers and experimental procedure was effective. Since a gene's mRNA level does not always predict its protein level, MDA-MB-231 cells were then lysed and CD95L expression investigated using Western blot. A strong signal was seen at 120kDa under reducing conditions. A protein species migrating with a similar apparent molecular weight, has been detected previously when investigating CD95L expression in human laryngeal carcinoma (HEp-2) cells, which they were able to fully reduce to the monomeric form (Meza-Lamas et al., 2006). Here, the protein has been analysed under strong, reducing conditions (8% (v/v) 2-mercaptoethanol), yet very little protein was detected corresponding to the 40kDa, monomeric form of CD95L. Furthermore, Meza-Lamas et al., only reported Western blot data and did not provide any further evidence to demonstrate the presence of homotrimeric CD95L, rather than a hetero-oligomeric form or CD95L aggregate, for example, by running the protein on a native gel, analytical centrifugation or mass spectrometry. When CD95L was knocked down by two separate siRNAs in the MDA-MB-231 cells, there was no detectable change in the abundance of the protein migrating at 120kDa, suggesting that it may not be CD95L. The effect of siRNA knockdown on the

40kDa protein however, which is barely detectable via Western blot, was inconclusive. Finally, the presence of CD95L was explored using IF, alongside GM1006, an MMP-7 inhibitor which was shown to improve detectable levels of CD95L-Myc-DDK at the PM of HEK293T cells. No intracellular or PM CD95L was detected, with or without GM1006. In conclusion, there is little or no evidence to suggest that CD95L protein is expressed by the MDA-MB-231s.

Previous papers which have stated presence of CD95L in breast cancer cell lines include IF detection using a CD95L antibody (polyclonal rabbit anti-human CD95L, Santa Cruz Biotechnology) which has now been discontinued (Müschen et al., 2000). Evidence for CD95L expression in MDA-MB-231 cells specifically include the use of an ELISA kit which has also been discontinued (Hsu et al., 2006) and detection via Western blot where the authors have not stated the antibody used (Kunigal et al., 2008). Therefore, there is a lack of clear evidence in the literature regarding CD95L expression in this cell line also. In 2013, Malleter et al., reported triggering of prometastatic signalling following CD95L cell surface cleavage in triple-negative breast cancer (TNBC) (Malleter et al., 2013). The study used an ELISA kit (Diaclone; antibody not specified) to detect serum CD95L in TNBC patients and found CD95L levels to be significantly higher in relapsed patients, which therefore correlated with a higher rate of metastasis (Malleter et al., 2013). More recent research (Motz et al., 2014) however, found CD95L to be expressed in endothelial cells of blood vessels surrounding tumour masses (using a validated anti-CD95L antibody), rather than the tumour cells themselves. Therefore, it cannot be assumed that the source of the soluble CD95L found in

the blood serum of some cancer patients comes from their tumour cells specifically.

If CD95L is not expressed by MDA-MB-231 cells, then it is likely that the enhanced uptake seen with CD95R-Fc coated MPs is not due to a CD95R/L interaction, but perhaps something else. If cells do not require CD95L for MP uptake, the technology lacks the targeted delivery which is hypothesised to reduce side effects of chemotherapy. This also raises questions about whether this is a cancer cell specific effect, which will be explored further in the next chapter. Uptake of CD95R-Fc modified particles in neuronal, medulloblastoma, breast and ovarian cancer cell lines was reported in 2011 (Ateh et al., 2011) with IF staining provided to demonstrate CD95L expression by these cell lines. However, the anti-CD95L antibody used for IF was not stated nor validated. Incubating Daoy medulloblastoma cells with CD95R-Fc before the addition of particles did prevent the enhanced uptake of coated particles (Ateh et al., 2011) but this could also occur if CD95R-Fc is binding to another target protein on the cell surface. There is prior evidence that brain cancer cells express CD95L (using the antibody G247-4), but these data were derived from tumour samples and may have been influenced by the tumour microenvironment including by endothelial cells of the tumour vasculature (Kleber et al., 2008). IGROV1 cells have been found to preferentially internalise CD95R-Fc modified MPs and in a orthotopic ovarian cancer xenograft model, created using IGROV1 cells, CD95R-Fc modification improved efficacy of paclitaxel-loaded MPs to reduce tumour bioluminescence (Ateh et al., 2011). However, there is evidence that ovarian cancer cells lack plasma membrane expression of CD95L (Abrahams et al.,

2003). Furthermore, the IGROV1 cell line has been found (by genotyping the cell line) to be hypermutated in comparison to ovarian tumours, and evidence suggests the cell line did not originate from a high-grade serous ovarian carcinoma (HGSOC) but from a different ovarian cancer subtype (endometrioid or clear cell carcinoma) (Domcke et al., 2013). There are examples of failed clinical trials conducted in HGSOC patients after preclinical studies in cell lines of endometrioid origin, among them IGROV1 (Coward et al., 2011) so these uptake experiments should be repeated using a more relevant cell line or model, to validate the effects seen with CD95R-modifed MPs.

4.3.1. Limitations and possible future directions

It is possible that incorrect glycosylation could affect trafficking of the expressed CD95L-Myc-DDK in HEK293T cells, explaining the abundance of intracellular CD95L, but lack of plasma membrane expression. Experiments here have indicated a level of glycosylation, yet do not indicate whether all available sites for glycosylation on the expressed CD95L have glycans attached. Mass spectrometry could be utilised to do so. Additionally, co-localisation of intracellular CD95L with an organelle-specific antibody such as calnexin (an endoplasmic reticulum marker), Golgi matrix protein (GM130; a Golgi marker) or Lamp-1/2 (lysosomal membrane markers) would identify the subcellular compartment of the protein. Co-staining PM CD95L with a marker of lipid rafts (such as caveolin-1; (Glukhova et al., 2018)) might also provide additional information to indicate whether there is CD95L translocation to lipid rafts in the cell membrane, as has been reported previously. However, if glycosylation and protein trafficking is not the issue regarding cell surface expression, it could be

that HEK293T cells expressing CD95L are inducing apoptosis in the surrounding cells. To overcome this, it may be possible to engineer cell lines with tetracycline-inducible CD95L expression, that are dominant negative in FADD/MORT1, to prevent cell death via CD95R signalling (Glukhova et al., 2018). This would prevent cell death becoming an issue while overexpressing CD95L. However, if the presence of *CD95L* mRNA itself is toxic to cells, as was suggested by Putzbach et al. recently (Putzbach et al., 2017), there may not be a way to prevent cell death during CD95L expression. However, the full details supporting this theory have yet to be described.

The siRNA experiment carried out on the MDA-MB-231 cells used two sequences from Dharmacon, targeting the *CD95L* ORF (table 2.6). The same two sequences were used to demonstrate the DISE effect of CD95L siRNAs in HeyA8 (ovarian cancer) cells (Putzbach et al., 2017). Previously, two lentiviral vectors targeting *CD95L* mRNA in MDA-MB-231 cells were tested and growth reduction and cell death was observed (supplementary information; (Hadji et al., 2014)). The siRNA experiment carried out here was performed before this evidence was published in 2017. Although no noticeable change in cell viability was specifically noted, it would be interesting to monitor this, for example, using propidium iodide to evaluate cell viability and cell cycle analysis in flow cytometry after *CD95L* siRNA knockdown. Furthermore, the use of a positive control, such as transfected HEK293Ts for CD95L knockdown, or a tissue or cell line that endogenously expresses CD95L (T-Cells, such as Jurkat cells) for RT-qPCR, would strengthen the conclusions of these experiments. The RT-qPCR experiment only provided CT mean data. This should be accompanied by an agarose gel with the RT-

qPCR products, displaying the presence or absence of *CD95L* cDNA, at the correct size, following the reaction. However, 3 different lines of evidence have been used to demonstrate that there are no detectable levels of CD95L in MDA-MB-231 cells (Western blot, siRNA knockdown and RT-qPCR), as well as negative IF experiments with and without CD95L-sheddase inhibitors.

There is evidence in a few tumour types that CD95L expression is induced by the tumour microenvironment, for example, SMA-560 (murine glioma) cells do not express CD95L on the cell surface but expression can be induced (as detected via Western blot using the antibody G247-4) by intracranial implantation suggesting a cross talk between host factions and the tumour cells (Kleber et al., 2008). Similarly, CD95L expression found in tumour endothelial tissue is upregulated when exposed to common metastatic tumour markers such as VEGF-A and PGE_2 (Motz et al., 2014). Therefore, the expression of CD95L in MDA-MB-231 cells could be investigated when used as a cancer orthotopic xenograft, in order to replicate more closely a breast tumour. Data inconsistency is a common issue however, and poor reproducibility between *in vitro* and *in vivo* models may be a complication here. Further evidence is required for CD95L expression in breast cancers, for example, IHC staining of patient tumours.

The observation of DISE in cancer cells by si/shRNAs designed against CD95L is now being explored as a potential therapy. The siRNAs have been coupled to templated lipoprotein nanoparticles (TLP) and found to induce cell death in ovarian cancer (HeyA8) cells and reduce tumour growth *in vivo* (HeyA8 cells injected into immunodeficient (NSG) mice) (Murmann et al., 2017). Since DISE

preferentially kills transformed cells and cancer stem cells (Putzbach et al., 2017), this could be a novel form of targeted treatment against cancer. Cells must also express scavenger receptor SR-B1, since uptake of TLPs has been found to depend on the presence of this receptor, which has been shown in human prostate cancer, breast cancer, and renal cell carcinoma among others (McMahon et al., 2016).

4.4. Summary

HEK293T cells were used to overexpress CD95L-Myc-DDK, in order to validate an anti-CD95L antibody. Plasma membrane expression of the protein was improved by using inhibitors of CD95L-sheddases. However, the level of cell surface expression was deemed too low to test uptake of CD95R-Fc coated MPs in the presence and absence of CD95L, which would have been useful to validate whether the target protein (CD95L) is necessary for uptake of CD95R-coated MPs. The reasons for low PM expression are unclear.

The expression of CD95L was investigated in MDA-MB-231 cells to examine the proposed targeting mechanism of CD95R-Fc coated MPs. It was concluded that there are very low or undetectable levels of the CD95L protein in MDA-MB-231s as shown by Western blot and validated using immunofluorescent staining. This is in agreement with recent literature stating that there is little or no CD95L in most tumours or cancer cell lines (Motz et al., 2014, Glukhova et al., 2018) and expression of CD95L, if it does indeed occur in tumours, may be reliant on factors in the tumour microenvironment (Motz et al., 2014, Kleber et al., 2008). Despite MDA-MB-231 cells lacking CD95L protein at the plasma membrane, they very efficiently take up CD95R-coated MPs. The reasons for this enhanced uptake are explored in Chapter 5.

5. Investigating the mechanism of CD95R-Fc coated microparticle internalisation

5.1. Introduction

Nanomedicine has the potential to improve the efficacy of cancer treatments. By combining nanotechnology and medicine, this field of research has enabled the development of small particle, therapeutic carriers such as microparticles (MPs) (Wang et al., 2012). MPs can be made from biodegradable polymers such as poly(lactic-co-glycolic acid) (PLGA) and loaded with chemotherapeutic agents. Upon internalisation, PLGA MPs degrade into lactic and glycolic acid and release their cytotoxic payload to kill the cancer cell. Functionalising the surface of particles can improve uptake levels into cells or target them to particular cells of interest, for example, by coating or opsonising with tumour-targeting proteins.

Micron-sized delivery systems have proved to be a good approach for drug delivery, allowing a high drug loading capacity, the use of poorly soluble therapeutics, improved bioavailability and sustained and controlled drug release within the target cell (Patiño et al., 2015, Kohane, 2007, Wang et al., 2012). In order to achieve high prognostic and treatment efficacy, the successful entry of MPs into cells plays a vital role (Zhao and Stenzel, 2018). Therefore, an understanding of MP interaction with the cell membrane during endocytosis is crucial in developing an efficient and “personalised” nanomedicine with minimal toxicity (Zhao and Stenzel, 2018).

The previous chapters have described the enhanced uptake of 0.5µm, CD95R-Fc coated, polystyrene MPs into triple negative breast cancer, MDA-MB-231, cells. The original hypothesis of a targeted interaction between CD95R-Fc on the particle and CD95L expressed by the cells has been disproved. Here, the mechanisms of uptake are investigated, and the possibility of any targeting discussed.

5.1.1. Uptake pathways into cells

There are two major pathways present in mammalian cells which allow the uptake of cargo; phagocytosis and pinocytosis. Phagocytosis is a process most associated with cells of the innate immune system such as macrophages, neutrophils and dendritic cells (Botelho and Grinstein, 2011), but is also present in other cells (see section 5.1.3 below). This is a receptor-mediated engulfment of large (≥0.5µm) particles, such as cellular debris and pathogens, into plasma-membrane derived vacuoles called phagosomes (Botelho and Grinstein, 2011).

Pinocytosis consists of uptake mechanisms that are present in all cells and can be categorised as dynamin-dependent (such as clathrin, caveolae and RhoA-mediated endocytosis) or dynamin-independent (such as macropinocytosis) (Mayor et al., 2014). Dynamin, the founding member of a family of dynamin-like proteins (DLPs) is a GTPase implicated in membrane remodelling (Ferguson and De Camilli, 2012). Dynamin-independent pinocytosis mechanisms and phagocytosis however, are dependent on large-scale actin-mediated reshaping of the plasma membrane (Mayor and Pagano, 2007). These large-scale pathways may share some of the same molecular machinery as the dynamin-

dependent processes, especially those utilizing actin machinery in membrane remodelling (Mayor et al., 2014). Uptake pathways have also been defined depending on the size of the particles they can internalise; large micrometre-scale pathways include macropinocytosis (0.2 to 10µm) and phagocytosis, with pinocytic pathways restricted to those that internalise smaller particles (<200nm) (Mayor et al., 2014).

5.1.2. Mechanisms of phagocytosis

Macrophages actively probe their microenvironment for particulate targets by extending highly dynamic membrane extensions (Botelho and Grinstein, 2011). RAC GTPases and CDC42 are required for maintaining the dynamic actin cytoskeleton for the formation of membrane protrusions (Botelho and Grinstein, 2011). Phagocytosis is induced by the interaction between ligands on the particle surface and receptors on the phagocytic membrane. For example, particles opsonised (coated) by immunoglobulins are ingested via an interaction with their specific Fc receptors. These are a well-known group of phagocytic receptors, which bind the Fc portion on antibodies. Other receptors include scavenger receptors, complement receptors and integrin receptors (see table 5.1).

Receptor	Ligands
FC Receptors:	
FcγRI (CD64)	IgG-, CRP-, SAP-opsonized particles
FcγRII* (CD32)	IgG-, CRP-, SAP-opsonized particles
FcγRIII (CD16)	IgG-, CRP-, SAP-opsonized particles
FcεRI	IgE-opsonized particles
FcεRII (CD23)	IgE-opsonized particles
FcαRI (CD89)	IgA-opsonized particles
Complement Receptors:	
CR1 (CD35)	MBL-, C1q-, C4b-, C3b-opsonized particles
CR3 (αMβ2, CD11b/CD18, Mac1)	iC3b-opsonized particle
CR4 (αXβ2, CD11c/CD18, gp150/95)	iC3b-opsonized particles
Various integrins:	
α5β1 (CD49e/CD29)	Fibronectin/Vitronectin-opsonized particles
α4β1 (CD49d/CD29)	
αvβ3 (CD51/CD61)	
Scavenger receptors:	
SRA	Bacteria, LPS, Lipoteichoic Acid
MARCO	Bacteria
Mannose receptor (CD206)	Mannan
Dectin-1	β1,3-glucan
CD14	LPS, peptidoglycan,
C1qR(P)	C1q, MBL, SPA

Table 5.1. Receptors expressed by phagocytes and their binding ligands, adapted from Underhill and Ozinsky, 2002.
*In humans, FcγRIIA is an activating phagocytic receptor, and FcγRIIB is an inhibitory receptor. Mice express only FcγRIIB. CRP, C-reactive protein; SAP, Serum amyloid P.

The receptor/ligand interaction triggers intracellular signalling pathways which result in efficient particle internalisation. Members of the Rho family of GTPases, Rac1 and CDC42, and Wiskott-Aldrich syndrome protein (WASP) family act as molecular scaffolds and mediate the polymerisation and assembly of actin at the base of the phagosome to form a phagocytic cup. Additionally, phosphatidylinositol-4,5-biphosphate (PIP_2) is believed to play a major role in cytoskeletal modification, by driving actin polymerisation (Botelho and Grinstein, 2011). This results in the circumferential projection of the cytoplasmic membrane as pseudopodia, which fuse around the particle to form a phagosome (Kumar and Clark, 2005). Phagocytosis is completed when pseudopods reach the apex of the particle and contract, via myosin X and perhaps myosin II, to sever the newly formed vacuole from the surface membrane (Botelho and Grinstein, 2011).

5.1.3. Non-professional phagocytes

Phagocytosis is well known and studied within “professional” phagocytes of the immune system. However, other cell types can also exhibit phagocytotic activity or “non-professional” phagocytosis. Examples of this have been found in a range of different cell types. MDA-MB-231 cells have been shown to locally degrade and phagocytose the extracellular matrix. Activation of alpha 3 beta 1 integrin was found to be necessary for initiating this phagocytosis (Coopman et al., 1996) (table 5.1). Airway epithelial cells can engulf neighbouring cells that undergo apoptosis after encountering environmental allergens; deletion of *Rac1* in these cells resulted in defective engulfment (Juncadella et al., 2013).

In embryo development, apoptosis is a key tool to sculpt body shape. Apoptosed cells are not only phagocytosed and cleared by macrophages, but also by mesenchymal cells (albeit with less efficiency) as has been shown in a 'macrophage-less' mouse embryo (Wood et al., 2000). Similarly, neural progenitor cells have been shown to elicit a phagocytic role during neurogenesis. This was found to be modulated by intracellular engulfment protein ELMO1, which promotes Rac activation downstream of phagocytic receptors (Lu et al., 2011). Disruption of ELMO1 *in vivo* (*Elmo1*-null mice) or pharmacologically in wild-type mice, led to reduced phagocytosis, the accumulation of apoptotic nuclei and impaired neurogenesis (Lu et al., 2011).

Following an injury, the clearance of apoptotic and necrotic cells is necessary for tissue repair. Kidney injury molecule–1 (KIM-1) is an immunoglobulin superfamily cell-surface protein highly upregulated on the surface of injured kidney epithelial cells, which transforms epithelial cells into semi-professional phagocytes (Ichimura et al., 2008). KIM-1 was able to specifically recognize apoptotic cell surface-specific epitopes phosphatidylserine, and oxidized lipoproteins, leading to the phagocytosis of apoptotic bodies after injury in rat kidney tubules *in vivo* (Ichimura et al., 2008). Furthermore, KIM-1 was directly responsible for phagocytosis in cultured primary rat tubule epithelial cells, porcine and canine epithelial cell lines (Ichimura et al., 2008).

Interestingly, macrophages can communicate with non-professional phagocytes (such as epithelial cells) and influence their phagocytic activity. Through the release of soluble growth factors and microvesicles, macrophages can alter the

type of particles engulfed by non-professional phagocytes and influence their inflammatory response (Han et al., 2016). For example, macrophages release insulin like growth factor 1 (IGF-1) during phagocytosis of apoptotic cells or in response to inflammation. The binding of IGF-1 to its receptor on the surface of LR73 fibroblasts and BEAS-2B (human lung epithelial) cells, non-professional phagocytes, redirected their phagocytosis such that the uptake of larger apoptotic cells was reduced, whereas the engulfment of liposomes was increased (Han et al., 2016).

5.1.4. Mechanisms of pinocytosis

Macropinocytosis can internalise large particles (perhaps even up to 10µm) and extracellular fluid through cell surface membrane protrusions, often called ruffles, that curve into cup-like structures to from vesicles, via actin polymerisation (Swanson, 2008). These vesicles, called macropinosomes, often form spontaneously or 'non-selectively', however there is some evidence of formation in response to activation of cell-surface receptors. For example, coating extracellular vesicles (EVs; 30 – 200nm) in an octaarginine peptide (an arginine-rich cell-penetrating peptide) initiates macropinocytosis in CHO-K1 (Chinese hamster ovary) cells by inducing proteoglycan clustering, resulting in uptake of EVs (Nakase et al., 2017). Common signalling mechanisms organise the construction of the cup-shaved invaginations of the plasma membrane, actin-filament assembly, disassembly and contractions including guanosine triphosphates (GTPases) of the Ras superfamily and membrane phospholipids (Swanson, 2008). Macropinocytosis has been found to be an important pathway of protein acquisition in cancer cells, particularly those with activated Ras, such as pancreatic and colon cancer (Redelman-Sidi et al., 2018). Ras activation (by

growth factor stimulation or oncogenic mutation) leads to increased membrane ruffling and so macropinocytosis via activation of Rac1 and CDC42 (Recouvreux and Commisso, 2017). This in turn, stimulates p21-activated kinase 1 (Pak 1), which has been shown to co-localise with macropinosomes in 3T3 fibroblasts, to induce actin polymerisation (Dharmawardhane et al., 1997).

Clathrin/receptor-mediated endocytosis generates small vesicles (60 – 120nm) to transport cargo molecules from the plasma membrane to the cytoplasm. Specific ligands are required to activate receptors in order for endocytosis to occur, so the pinocytosis in this case is not spontaneous. The iron chelation protein, transferrin, is a good marker for clathrin-mediated uptake, because once it has bound iron, it gains affinity for the transferrin receptor on the plasma membrane and is internalised (Vercauteren et al., 2010). After initiation, endocytic coat proteins including clathrin are recruited from the cytosol to cluster on the inner leaflet of the plasma membrane (Kaksonen and Roux, 2018). Clathrin forms a lattice-like coat around the nascent vesicle, promoting membrane bending, which transforms the flat plasma membrane into a ‘clathrin-coated pit’ (Kaksonen and Roux, 2018). In addition to clathrin, the coat is composed of many other proteins, including clathrin-adaptor proteins, such as the heterotetrameric adaptor protein AP2 complex, and scaffold proteins (Kaksonen and Roux, 2018). After the coat has assembled, a network of actin filaments polymerizes at the endocytic site, forming the actin module (Kaksonen and Roux, 2018), that enables the movement of the vesicle away from the plasma membrane i.e. via myosin motor proteins (Sun et al., 2006). The constriction and scission of the invagination neck is mediated by BAR domain (Bin, amphiphysin

and Rvs) proteins which interact with dynamin to mediate scission (Kaksonen and Roux, 2018).

In comparison, caveolar endocytosis is a process which mediates uptake of smaller, 50 – 60nm, vesicles via bulb-shaped plasma membrane invaginations called caveolae. Caveolae are enriched in cholesterol and sphingolipids, and their formation is driven by integral membrane proteins called caveolins and coat proteins called cavins (Mayor and Pagano, 2007). Similar to clathrin endocytosis, constriction and scission of caveolae from the plasma membrane is mediated by BAR domain proteins and dynamin. The actin-binding protein Filamin A plays a crucial role in trafficking of caveolae linked to actin (Muriel et al., 2011). Interestingly, caveolae can flatten in response to membrane stretch and this mechanosensitive response is thought to prevent membrane rupture, as well as activating protective downstream signalling responses (Parton and Del Pozo, 2013). Often this pathway is utilised by pathogens to enter cells, such as the SV40 virus and cholera toxin subunit B, a protein complex secreted by the bacterium *Vibrio Cholerae*; the latter is often used as a marker for caveolar endocytosis (Vercauteren et al., 2010).

Additional endocytic pathways that do not use clathrin, cavin or any other characterised coat proteins, have begun to be recognised. Some of these pathways are constitutive, whereas others are triggered by specific signals and are also exploited by pathogens (Mayor et al., 2014). RhoA-dependent, IL-2 receptor endocytosis is a well-characterised example of a non-clathrin, non-caveolin route (Gesbert et al., 2004). Electron-microscopy studies confirm that

IL-2 receptors are concentrated on the plasma membrane and then internalised via small invaginations (Mayor et al., 2014). Both the specific concentration of the receptors and uniform size (50 –100nm) of the endocytic vesicle indicate the presence of an, as yet, unidentified protein coat that may aid in the recruitment of these proteins to the site of endocytosis and form the endocytic pit (Mayor et al., 2014). Flotillin-dependent endocytosis has also been characterised as a dynamin-, caveolin- and clathrin- independent process. Internal and immuno-electron microscopy has shown flotillin-1-containing regions of the plasma membrane budding into COS-7 (green monkey kidney) cells (Glebov et al., 2006). Cargo including fluid phase and a glycosyl-phosphatidylinositol (GPI)-anchored protein, CD59, are also endocytosed via this pathway in HeLa cells (Glebov et al., 2006).

5.1.5. Elucidating the mechanisms of cellular uptake

Endocytic inhibitors are commonly used to assess how particles are being internalised into cells since they are simple, reliable and affordable tools, however, the specificity of these inhibitors and possible side effects are frequently overlooked and need to be considered (Zhao and Stenzel, 2018).

In this chapter, a series of inhibitors have been introduced to block different endocytosis pathways. Cytochalasin D is an inhibitor of F-actin polymerisation commonly used to block macropinocytosis and phagocytosis (Thompson et al., 2012), since these uptake pathways are dependent on large-scale actin-mediated reshaping of the plasma membrane (Mayor and Pagano, 2007). Amiloride also inhibits macropinocytosis. Amiloride is used clinically to treat high

blood pressure or oedema due to heart failure (Baer et al., 1967) because it inhibits Na^+/H^+ exchange. This generates a submembranous acidic microenvironment that prevents the activation of GTPases that promote actin remodelling, and so macropinosome formation is also inhibited (Koivusalo et al., 2010).

Two commonly used inhibitors of clathrin-mediated endocytosis are chlorpromazine and dynasore. Chlorpromazine, a cationic, amphiphilic drug, prevents assembly of clathrin-coated pits at the cell membrane by translocating clathrin and AP2 from the cell surface to intracellular endosomes (Zhao and Stenzel, 2018). However, there is evidence that chlorpromazine may interfere with other forms of uptake, such as has been shown in four different cell lines, resulting in an increase of lactosylceramide (LacCer) uptake; a glycosphingolipid that partitions to lipid rafts, which is a marker of caveolae-mediated endocytosis (Vercauteren et al., 2010). Dynasore inhibits the GTPase activity of dynamin in the formation of clathrin-coated vesicles, preventing scission and membrane fission of vesicles (Macia et al., 2006) however it can also affect the involvement of dynamin in caveolae formation.

Caveolae and lipid raft internalisations are known to be inhibited by the polyene antibiotics, nystatin and filipin (Ivanov, 2008). These are a class of antibiotics produced by *Streptomyces* that are toxic to fungi but not bacteria, which work via depletion of the cholesterol from the cell membrane by forming inclusion complexes with cholesterol (Kuhn et al., 2014). As a result, at high concentrations, these antibiotics can induce a profound distortion of the structure

and function of cholesterol-rich membrane domains resulting in cell toxicity (Milhaud, 1992). Fortunately, these effects can be minimised by lowering the drug concentration (Ivanov, 2008).

Other inhibitors used here are mannan, which binds to the mannose-receptor, a competitive inhibitor which prevents mannose-receptor initiated internalisation (like phagocytosis, see table 5.1) (Cui et al., 2003). Mannan has been shown to block receptor-mediated, but not fluid-phase uptake of horseradish peroxidase (Lang and De Chastellier, 1985) and inhibit phagocytosis of zymosan by mouse peritoneal macrophages (Sung et al., 1983). Nocodazole is also used, which is a microtubule-disrupting agent that has been shown to affect MP internalisation and localisation of latex beads in B16 (melanoma) cells (Rejman et al., 2004). The effect of Nocodazole is non-specific however and could potentially affect many other cellular processes.

Since the use of pharmacological inhibitors can have nonspecific effects on a cell (Ivanov, 2008) complementary techniques can be used to study uptake mechanisms, such as microscopy. Novak *et al.* used scanning ion conductance microscopy to allow high-speed topographical and fluorescence imaging of the interactions between red-fluorescent 200nm polystyrene particles and human lung cells (Novak et al., 2014). By transfecting the cells with actin-binding, green-fluorescence protein (GFP) or clathrin-enhanced GFP, they were able to follow the 3D dynamics of topographic features of the membrane with 2D dynamics of the GFP labelled proteins, and the red fluorescent particles (Novak et al., 2014). Interestingly, they found that an initial interaction occurred between clathrin-

coated pits and the particles, however, the particle was ultimately engulfed by a large membrane protrusion following disappearance of the GFP clathrin (Novak et al., 2014). The appearance of a large membrane protrusion suggests a macropinocytotic or phagocytotic route of uptake. This highlights a more complex relationship between uptake pathways and cell sensing of external particles and provides more detail regarding an internalisation mechanism than 2D imaging or inhibitor use alone.

5.1.6. Factors affecting microparticle internalisation

Uptake of microparticles or nanoparticles (NPs) is cell-type dependent, for example, HeLa cells internalise lipid NPs (~60nm) via macropinocytosis while NIH 3T3 fibroblasts take them up in clathrin-mediated endocytosis (Gilleron et al., 2013). Uptake is known to be affected by the characteristics including size, shape, surface charge and material composition (Wang et al., 2012, Sun et al., 2014, Zhao and Stenzel, 2018).

Particle size can affect uptake efficiency, kinetics, internalisation mechanism and subcellular distribution (Shang et al., 2014). Different sized particles are preferentially internalised by certain cell types. For example, small diameter MPs (0.1 μm) are taken up more efficiently than larger MPs (1 and 10 μm) in Caco-2 cells (Desai et al., 1997). This is likely due to an internalisation pathway preference in this cell type for one of the several pinocytic pathways that internalise particles <200nm. Höekstra *et al.* used a range of fluorescent latex beads of different sizes (50 – 1000nm) to investigate the effect of NP size on entry in B16 (murine melanoma) cells. Internalisation of particles <200nm

involved clathrin-coated pits, however as particle size increased, internalisation became caveolae-mediated; this was the predominant route of uptake for 500nm particles (Rejman et al., 2004). This is a surprising result since the size of a single flask-shape caveolae is too small for accommodating particles as large as 500nm. It was speculated that electrostatic interactions may localise the particles to caveolin-coated domains of the cell membrane but the recruitment of an internalisation machinery would be needed to accommodate particles that extend beyond the actual size of a caveolae domain (Rejman et al., 2004).

In addition to size, particle surface charge can be a major factor affecting cellular and tumour uptake (Wang et al., 2012). In the case of nanoparticles, positively-charged NPs are rapidly taken up by tumour cells but can lead to significant immune reactions (Wang et al., 2012, Gratton et al., 2008). Thus, neutral and negatively charged particles are preferable for clinical applications (Gratton et al., 2008). A similar trend has been found with microparticle uptake into SK-BR-3 (human breast cancer) cells. IgG functionalised, 3µm, polystyrene microparticles were coated with positively charged polyethyleneimine (PEI) of two different molecular weights, 25 and 750kDa (Patiño et al., 2015). Non-coated particles were negatively charged, and PEI coated particles were positively charged; the most positively charged particles were those with a 750 kDa PEI coating. This difference in charge affected uptake into SK-BR-3 cells in comparison to normal breast epithelial cell line MCF-10A, with the cancer cells preferentially internalising the more positively charged particles and the epithelial cells preferentially internalising the negatively-charged, non-coated particle. The mechanisms of uptake in each different cell line were investigated and the cancer

cells internalised all particles, regardless of charge, via macropinocytosis (as inhibited by Cytochalasin D). MCF-10A cells however showed different mechanisms of internalisation, depending on the microparticle type (Patiño et al., 2015). Non-coated particle uptake was inhibited by both cytochalasin D and dynasore, suggesting they are internalised by macropinocytosis and a form of dynamin-dependent endocytosis. In contrast, the uptake of PEI-25K and PEI-750K coated MPs was not affected by either inhibitor, suggesting an alternative mechanism of uptake (Patiño et al., 2015). Therefore, coating particles can affect surface charge, which may be internalised via different uptake pathways in different types of cell.

The MPs used thus far in the current study are polystyrene and 0.5µm in size. The use of polystyrene particles is convenient as they are uniform in size and not broken down within the cell, allowing uptake to be easily quantified. The target MDA-MB-231 cells also showed a preference for the 0.5µm particles; CD95R-Fc coated, 0.5µm particles were preferentially internalised compared to CD95R-Fc coated, 1µm particles (70% compared to 40% uptake, respectively) (Ateh et al., 2011). Whilst there has been a wide range of particle-cell interaction studies conducted with nanoparticles (Sun et al., 2014, Shang et al., 2014, Treuel et al., 2013, Zhao and Stenzel, 2018), less is known about the interaction of larger micrometre-sized particles with cells. In this chapter I aim to investigate the mechanisms of uptake of CD95R-Fc coated MPs in MDA-MB-231 cells. Since there is no CD95L protein expressed on the plasma membrane, I test whether enhanced uptake is a cancer-cell specific effect by testing uptake in primary cells. Confocal imaging is used to confirm that the particles are internalised and

visualise the internalisation process, and coated MPs are characterised using dynamic light scattering (DLS). Finally, inhibitors of key internalisation pathways are used to explore the mechanisms of cellular uptake.

5.1.7. Aims of Chapter 5

- Investigate CD95R-Fc coated MP uptake in a non-cancerous cell line, primary dermal fibroblasts
- Use confocal imaging to complement flow data, ensure MPs are internalised and live-cell imaging to visualise internalisation dynamics
- Characterise differentially coated MPs using DLS
- Use inhibitors to elucidate the key mechanisms involved in CD95R-Fc coated MP uptake

5.2. Results

5.2.1. Investigating uptake of CD95R-Fc modified MPs in primary dermal fibroblasts

In the previous chapter, it was concluded that there is no CD95L expression on the plasma membrane of MDA-MB-231 cells, suggesting that uptake does not occur via a CD95R-Fc/CD95L interaction. In order to see whether the enhanced uptake of CD95R-Fc coated particles is a cancer-cell specific effect, uptake was tested in primary dermal fibroblasts, sourced from facial skin. Dermal fibroblasts are an essential component of skin, producing and organising the extracellular matrix of the dermis and communicating with each other and other cell types, playing a crucial role in regulating skin physiology (Sorrell and Caplan, 2004). Primary cells were used to avoid any bias due to selection for growth in tissue culture which might alter the uptake properties of cancer or immortalised cell lines. MDA-MB-231 cells and primary dermal fibroblasts (passage number 15) were seeded to the same density and incubated with CD95R-Fc coated particles for 24 hours (section 2.9.1). Non-bound particles were washed off before analysis using flow cytometry. Control cells were also incubated with no particles (PBS only, negative control), non-coated particles, particles coated with human IgG Fc fragment (Abcam; to control for the Fc portion of CD95R-Fc) and particles coated with an excess of BSA. The population of cells was analysed by flow cytometry, gating on cells with normal size but including a large range of granularity because polystyrene particle uptake makes the cells appear more granular. Fluorescence emitted by the fluorescein label of the MP was detected in the FL-1 channel.

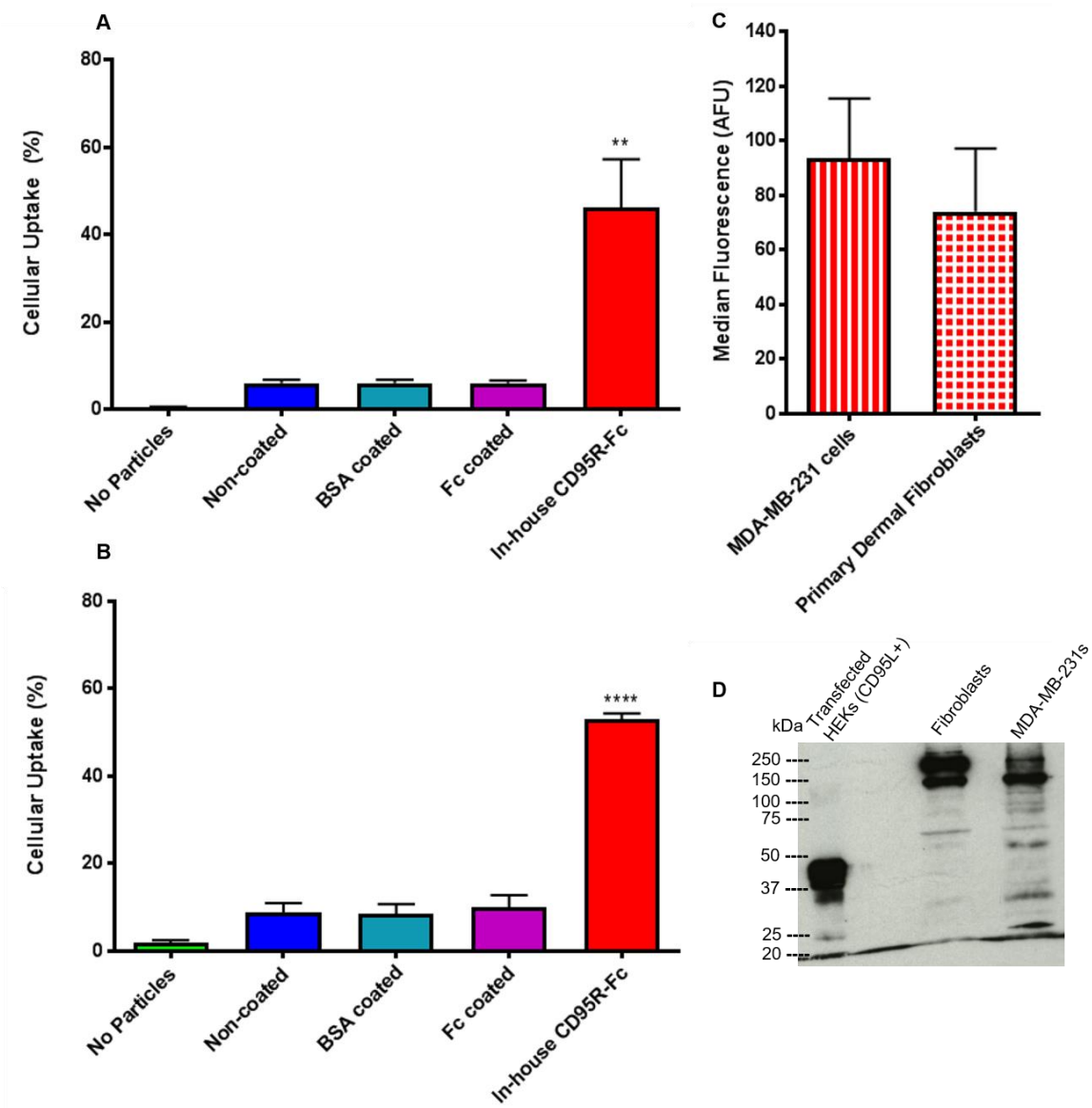

Figure 5.1. CD95R-Fc improves uptake of microparticles in primary dermal fibroblasts, as well as MDA-MB-231 cells.

Cells were incubated with fluorescent, 0.5µm MPs for 24 hrs and analysed by flow cytometry. Cells were gated to eliminate cell debris and 10,000 gated cells were analysed. Mean and SEM values are from three independent, repeat experiments (n=3). Significance was calculated by one-way ANOVA; **** $P \leq 0.0001$ and ** $P \leq 0.01$. (**A**) Mean percentage uptake by MDA-MB-231 cells incubated with no particles (negative control), non-coated particles, BSA-coated, Fc-coated and in-house-purified CD95R-Fc coated particles. In-house-purified CD95R-Fc coated MP uptake was statistically different to non-coated MPs, BSA and Fc coated MPs. (**B**) Mean percentage uptake of the same particles by primary dermal fibroblasts. In-house-purified CD95R-Fc coated MP uptake was statistically different to non-coated MPs, BSA and Fc coated MPs. (**C**) Means of the median fluorescence of cells (a measure of the number of particles internalised per cell over three independent experiments), incubated with in-house CD95R-Fc coated particles. There was no statistical difference between the two cell lines ($P > 0.05$; Mann-Whitney U test). (**D**) Fractions of cell lysate from transfected HEK293T cells (positive control, CD95L+; 0.0002% of total volume), primary dermal fibroblasts (4% of total volume) and MDA-MB-231 cells (negative control; 4% of total volume), were loaded onto an SDS polyacrylamide gel and the proteins separated by electrophoresis. The blot was prepared on PVDF membrane and probed for CD95L.

Efficiency of MP uptake was determined by measuring the percentage of the gated cells with a fluorescence level above the autofluorescence of cells in the absence of particles. The percentage uptake for each condition in MDA-MB-231 cells and the primary fibroblasts was analysed by ANOVA for 3 independent repeat experiments (section 2.15; Figure 5.1A & B respectively).

The percentage uptake of MPs in primary dermal fibroblasts coated with in-house CD95R-Fc was 53 +/- 1% (Figure 5.1B) and was found to be statistically different ($P \leq 0.0001$) to the mean uptake of 9 +/- 2% for non-coated particles, 9 +/- 2% for BSA coated particles, and 10 +/- 3% for Fc coated particles. The percentage uptake of MPs opsonised with BSA or Fc protein was not statistically different to each other ($P > 0.05$), and neither of these proteins improved particle uptake (in comparison to non-coated particles). MP uptake by fibroblasts was the same as in MDA-MB-231 cells (and consistent with that previously observed in Chapter 3). Uptake for in-house CD95R-Fc coated particles was 46 +/- 11% and was found to be statistically different ($P \leq 0.01$) to the mean uptake of 6 +/- 1% for non-coated particles, 6 +/- 1% for BSA coated particles, and 6 +/- 1% for Fc coated particles. The median fluorescence of cells with particles, coated with in-house CD95R-Fc, from 3 independent, repeat experiments was analysed to explore any differences in the number of particles internalised per cell, for each cell line (Figure 5.1C). The mean of these median fluorescence levels over three independent experiments for MDA-MB-231 cells was 94 +/- 22 AFU and for the fibroblasts it was 74 +/- 23 AFU. There was no statistical significance between the two cell lines ($P > 0.05$). Therefore, primary fibroblasts and MDA-MB-231 cells have a similar number of particles internalised per cell.

To assess expression of CD95L, cells were lysed and whole-cell extracts run on a 10% polyacrylamide gel (section 2.7.5, 2.7.7 & 2.7.8). HEK293T cells transfected with pCMV6-FasLG (coding for Myc-DDK-tagged Human CD95L; OriGene) was loaded as a positive control for CD95L (0.0002% of total lysate, from a 500µl stock created from a confluent well of a six well dish, see section 2.7.6). Maximal loading volumes of lysate from primary dermal fibroblasts and MDA-MB-231 cells (negative control; both 4% of total lysate volume, as before) were loaded in order to detect even minimal amounts of CD95L. The protein was transferred onto a PVDF membrane and probed using mouse anti-human CD95L, clone G247-4 (BD Pharmingen; Figure 5.1D; section 2.7.11), which was validated in Chapter 4. For the positive control, a strong signal at the correct molecular weight of 40kDa for monomeric CD95L. A strong signal was also observed in the fibroblasts at around 120 kDa and 170kDa, which is also seen in the MDA-MB-231 cells that was previously determined to have no CD95L in the plasma membrane (see Chapter 4) suggesting non-specific binding of the antibody. There is further background binding of the antibody for both fibroblasts and MDA-MB-231 cells, which is likely due to over-loading of the gel, however neither cell shows any CD95L at the expected molecular weight for the monomer, 40kDa.

In summary, CD95R-Fc coating enhances the uptake of MPs in primary dermal fibroblasts, a non-cancerous cell line, suggesting that the uptake pathway is not a cancer-cell specific. Furthermore, the lack of CD95L expression in primary dermal fibroblasts suggests that uptake does not result from a CD95R/CD95L interaction, as with MDA-MB-231 cells.

5.2.2. Confocal imaging to determine microparticle internalisation

As discussed in Chapter 3, steps are taken in the uptake procedure to ensure that non-internalised particles are washed from cells before flow cytometry. This includes repeatedly washing adhered cells with PBS and tapping the sides of the plate to dislodge any unbound particles, before cells are trypsinised and collected for flow analysis. The FACScan detects the level of fluorescence emitted by a microparticle, however cannot discriminate between surface bound and internalised particles. Since no evidence for CD95R interaction with CD95L was found to be required for microparticle uptake, and because CD95R-Fc also enhanced uptake in a non-cancerous cell line, it was important to ensure that the particles were internalised and not simply stuck to the cell surface. To test this, MDA-MB-231 cells were seeded onto a 6-well dish and incubated with CD95R-Fc coated particles for 24 hours (section 2.13.1). Cells were also incubated with no particles (PBS only), non-coated particles, particles coated with human IgG – Fc fragment and particles coated with BSA. The cells were washed with PBS to removed unbound particles and two hours prior to imaging, the live, adhered cells were stained with Hoechst (Thermo Scientific), a cell-permanent nuclear counterstain that emits blue fluorescence when bound to double-stranded, (ds)DNA, washed again with PBS, and then incubated with CellMask™ deep red plasma membrane stain (Thermo Scientific) for 20 minutes, before imaging on the IN Cell Analyser 6000 (GE Healthcare). The plasma membrane of each cell was imaged using the confocal aperture and a 3D, Z-stack of 6 x 1.7µm slices (excluding the top of the cell) was taken in order to capture all particles within the cell. The Z-stack was then collapsed into 2D allowing all particles to be seen. Representative images are shown of cells with no particles, non-coated particles

and in-house CD95R-Fc coated particles (Figure 5.2A, B & C respectively). 'FITC' shows the fluorescence of green particles only and 'Merge' overlays fluorescence from the nucleus, cell membrane and particles. To see each fluorescent channel separately, go to Appendix 2 – Supplementary Figure 8.

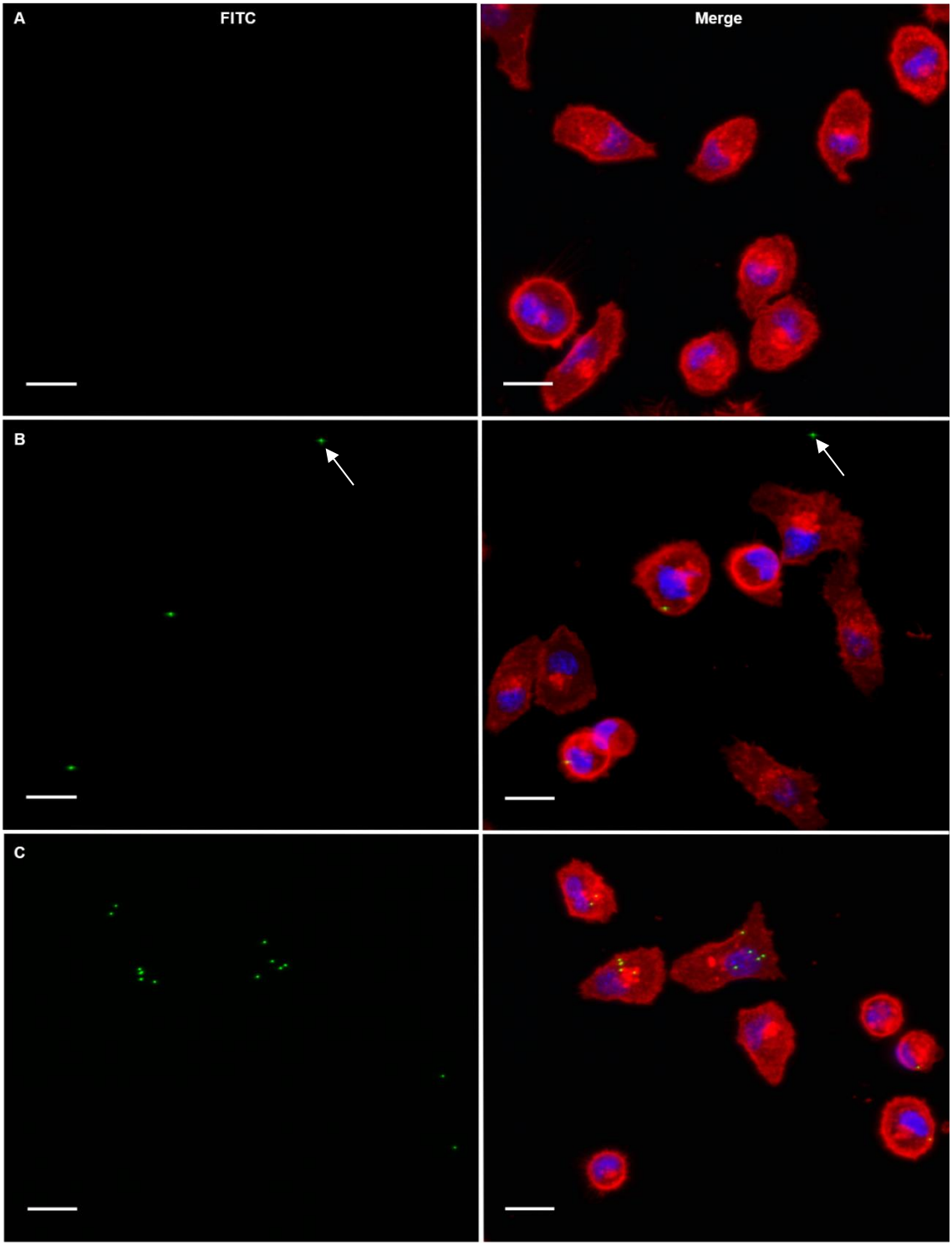

Figure 5.2. CD95R-Fc coated particles are internalised by MDA-MB-231 cells, and not bound to the plasma membrane.
MDA-MB-231 cells were incubated with no particles (PBS; negative control) (**A**) non-coated particles (**B**) or in-house CD95R-Fc coated particles (**C**) for 24 hours. Cells were then washed to remove non-internalised particles. Live, adhered cells were then stained for imaging. Cell nuclei were stained with Hoechst (blue) and cellular membranes with CellMask™ (red). Particles are fluorescent green and detected in the FITC channel and 'Merge' overlays fluorescence from the nucleus, cell membrane and particles. White arrows show a particle which has not been internalised by a cell or washed away. Scale bars, 20µm. Images representative of the whole population are shown in each case (see section 2.13.1).

The live cell staining shows that the particles are internalised. For non-coated particles, the field of view shows two cells that have each internalised one particle, and one further particle can be seen which has not been internalised or washed away using PBS (white arrow). Few particles were found adhered to the dish in this manner, suggesting that the washing procedure was effective. For CD95R-Fc coated particles, more cells have internalised particles, and there are more particles per cell (two cells with 3 or more particles, one cell with 2 particles and two cells with one particle).

Image quantitation and processing was performed using the Developer software version 1.9.1 (GE Healthcare) as described in section 2.13.1. Briefly, the software identifies the nucleus and the cell membrane based on size and fluorescence (blue pixels for the nucleus and red for the membranes). The two are linked together to determine the number of cells per well. The particles are also identified using similar parameters, and the number of cells with particles determined by linking particles (or foci) to the nucleus and membrane of a cell. Furthermore, each particle is counted separately, allowing the analyses to calculate the number of particles internalised by each distinct cell. Further stringencies were introduced to ensure only internalised particles were counted including that a particle should be 100% surrounded by the cell membrane; even if one pixel of a particle is not, the particle is not counted. The outer edge of the membrane was excluded during processing, so particles close to outside of the cell were also excluded from the count.

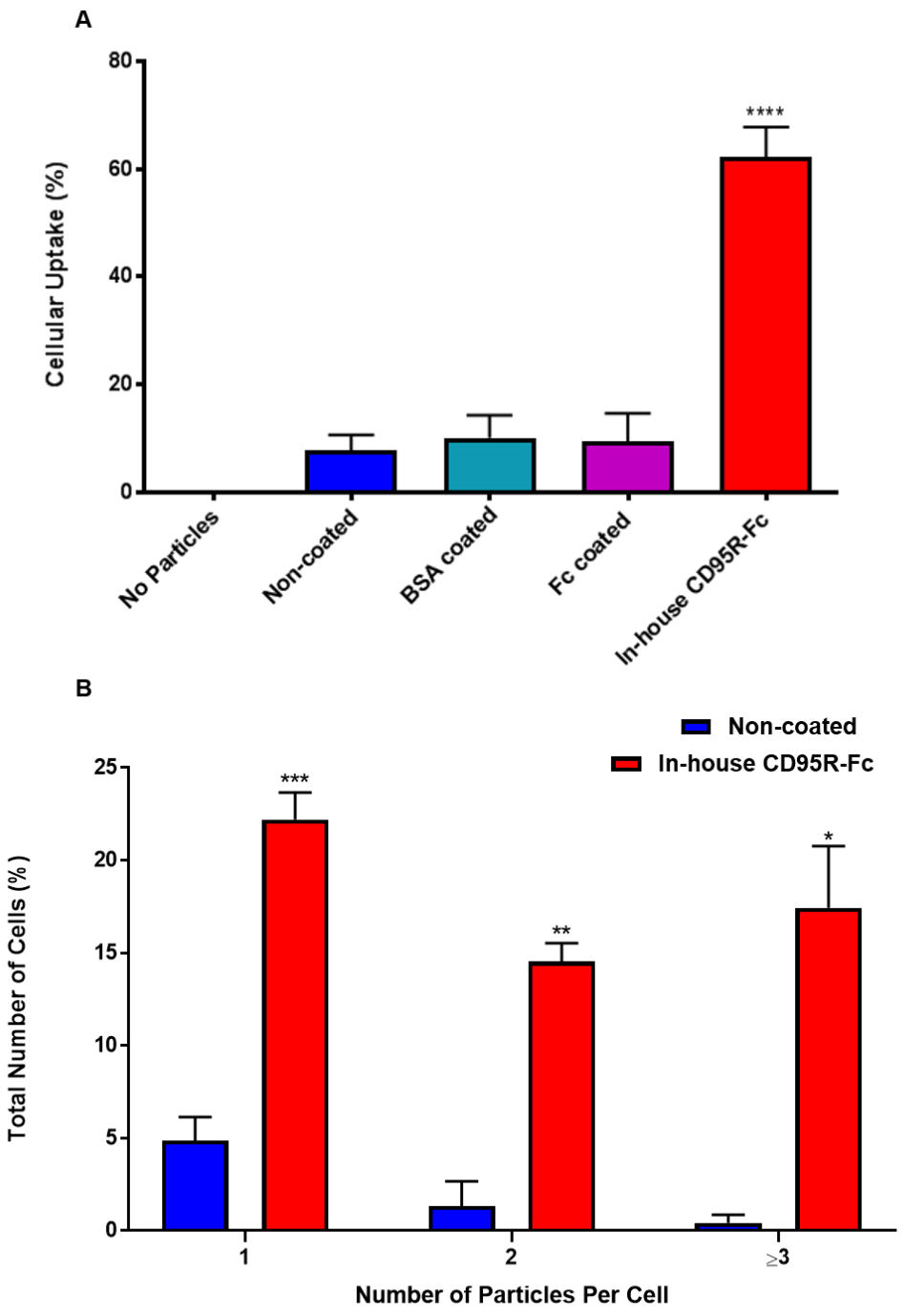

Figure 5.3. Confocal imaging demonstrates enhanced CD95R-Fc coated MP uptake in MDA-MB-231 cells, with more cells internalising a higher number of particles.
Cells were incubated with green-fluorescent, 0.5µm MPs for 24 hrs. Live, adhered cells were then stained for imaging on an IN Cell Analyser 6000 (GE Healthcare). Cell nuclei were stained with Hoechst (blue) and plasma membranes with CellMask™ (red). Mean and SEM values are from three independent, repeat experiments (n=3). (**A**) Mean percentage uptake of MDA-MB-231 cells incubated with no particles (negative control), non-coated particles, particles coated with BSA, particles coated with Fc and particles coated with in-house-purified CD95R-Fc. Uptake of particles coated with in-house-purified CD95R-Fc was statistically different to uptake of non-coated MPs, BSA- and Fc- coated MPs. Significance was calculated by one-way ANOVA; **** $P \leq 0.0001$. (**B**) The number of particles internalised by each cell (1, 2 or ≥3), expressed as a percentage of total cell number, was compared for non-coated particles (blue) and in-house CD95R-Fc coated particles (red). Significance was calculated by Welch's t test and the difference between conditions for each particle number was found to be statistically significant; 1 particle *** ($P \leq 0.001$), 2 particles ** ($P \leq 0.01$) and ≥3 particles * ($P \leq 0.05$).

The uptake experiment was repeated independently 3 times, images quantified, and percentage uptake statistically compared by ANOVA (section 2.15; Figure 5.3A).

The percentage uptake of MPs coated with in-house CD95R-Fc was 62 +/- 6% (Figure 5.3A) and was found to be statistically different ($P \leq 0.0001$) to the mean uptake of 7 +/- 3% for non-coated particles, 10 +/- 4% for BSA coated particles, and 9 +/- 5% for Fc coated particles. The percentage uptake of MPs opsonised with BSA or Fc protein was not statistically different to each other ($P > 0.05$), and neither of these proteins was statistically different in comparison to non-coated particles. Uptake of MPs by cells incubated with non-coated particles was not statistically different ($P > 0.05$) to the level of cellular fluorescence recorded in the absence of particles. This data complements the results obtained by flow cytometry (Figure 5.1A) even when far fewer cells are being analysed (150 – 200 cells per condition here compared to 10,000 cells for flow analysis). It is therefore very likely that the particles are internalised by the cells, rather than simply peripherally attached to the cell surface. Furthermore, with a CD95R-Fc coating, significantly more cells internalise particles, and significantly more particles are internalised per cell (Figure 5.3B). For cells with one particle per cell, the mean population uptake was 5 +/- 1% for non-coated particles, compared to 22 +/- 1% for CD95R-Fc coated particles ($P \leq 0.001$), for two particles per cell, the respective values were 1 +/- 1% compared to 15 +/- 1% ($P \leq 0.01$), and for three or more particles per cell the respective values were 0.4 +/- 0.4% compared to 17 +/- 3% ($P \leq 0.05$). This confirms the data obtained by flow cytometry, which showed that the median green fluorescence of cells that had taken up particles

was higher when the particle was coated with CD95R-Fc, in comparison to all other conditions (Chapter 3), indicative of a higher number of particles internalised by each cell. See Appendix 2 – Supplementary Figure 9 for a more detailed breakdown of particle number, for each MP coating condition.

5.2.3. Time-lapse imaging of particle internalisation

The use and staining of adherent, live cells worked very well, opening the possibility of using the IN Cell 6000 for time-lapse imaging (section 2.13.2). This includes taking a series of images of the same cells in a time dependent manner, which may provide insights into the mechanisms of uptake. MDA-MB-231 cells were therefore seeded and stained with Hoechst. After two hours, the cells were washed with PBS to remove any excess stain. Cells were then incubated with CellMask™ deep red plasma membrane stain for 20 minutes, washed again and media added along with the CD95R-Fc coated MPs, for 30 minutes before imaging. The plate was sealed with a membrane and supplied with 5% CO_2 and kept at 37°C whilst the cells were imaged on the IN Cell Analyser 6000 detecting Hoechst, CellMask™ and green fluorescence emitted by the MPs. Nine fields of view were imaged, every 15 minutes for 5 hours.

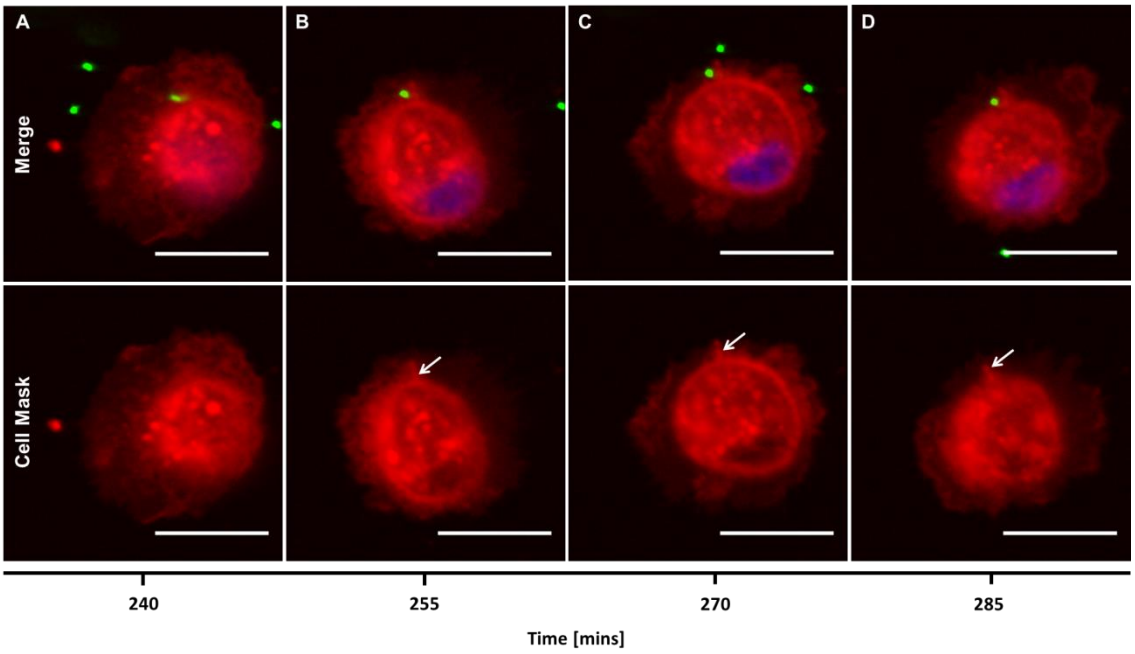

Figure 5.4. Live-cell, confocal imaging demonstrates a single microparticle interacting with a membrane protrusion.
MDA-MB-231 cells were incubated with in-house CD95R-Fc coated particles for 30 minutes and imaged every 15 minutes for 5 hours (300 minutes in total). Cell nuclei were stained with Hoechst (blue) and plasma membranes with CellMask™ (red). Particles are fluorescent green and detected in the FITC channel. (**A**) - (**D**) show a cell in 15-minute time frames, starting at 240 minutes. White arrows show a membrane protrusion stained with Cell Mask, which forms at 255 minutes, and which may be interacting with the green MP (Merge) potentially prior to internalisation. Scale bars, 20µm.

Frames are shown from 240 - 285 minutes (Figure 5.4.). From 255 - 285 minutes (and at 300 minutes, frame not shown) a single particle was seen interacting with a membrane protrusion (white arrow, Figure 5.4B - D). Imaging was completed before the particle was internalised. Potentially, this indicates an interaction between the coated MP and the plasma membrane of the MDA-MB-231, which might be important to initiate internalisation. The involvement of a membrane protrusion in 200nm particle uptake has been shown in lung cells using topographical imaging and GFP labelled actin (Novak et al., 2014) and may indicate a macropino- or phagocytotic mechanism of internalisation.

5.2.4. Characterisation of microparticles using dynamic light scattering (DLS)

Previous studies have shown that coating polystyrene microparticles in different chemicals can impart a distinct surface charge or zeta (ζ)-potential and this has been suggested to influence uptake. For example, coating polystyrene particles in polyethyleneimine (PEI) imparts a positive surface charge on the otherwise negatively-charged, non-coated particles. By using two different PEI polymers of 25 and 750kDa, particles can be made less or more positive, respectively (Patiño et al., 2015). The surface charge affected the internalisation of particles differentially in cancerous and non-cancerous epithelial cells, with cancer cells internalising more particles with increasing positive surface charge. The non-cancerous epithelial cells however, internalised more negatively-charged, non-coated particles.

To investigate the surface charge of the polystyrene particles used and whether it changes with the different coats, dynamic light scattering (DLS) was measured in a Zetasizer Nano ZS (Malvern; section 2.14). DLS is a non-invasive technique for measuring the size and size distribution (polydispersity index, PDI) of molecules and particles typically in the submicron range. Typical applications of DLS are the characterization of particles, emulsions and molecules, which have been dispersed or dissolved in a liquid (Ganguly, 2018). The Brownian motion of the particles or molecules in suspension causes laser light to be scattered at different intensities. Analysis of these intensity fluctuations is a measure of the velocity of the Brownian motion and hence the particle size using the Stokes-Einstein relationship (see section 2.14, equation 2.2). The Zetasizer can also

measure the zeta potential of particles; the electrostatic potential at the electrical double layer surrounding a particle in solution (Clogston and Patri, 2011). A charge is applied across the solution, leading to electrophoresis of the particles. The velocity with which particles move is dependent on factors such as dielectric constant and viscosity of the medium, and the zeta potential. The Zetasizer measures electrophoresis using the Doppler effect, in which a laser beam is passed through a sample undergoing electrophoresis to measure the scattered light from the moving particles.

Particles were coated by passive adsorption (section 2.8). Briefly, proteins were incubated with particles at a ratio of 0.5µg protein:1µg MP (except BSA, where an excess of protein is used) in PBS, for 90 minutes at 37°C, with mixing every 20 minutes. Adsorption occurs based on hydrophobic attractions between the hydrophobic portions of the adsorbed protein and the polymeric surface of the microspheres (Bangs, 2008a). Samples were then diluted to 1ml and triplicate size measurements were recorded; the z-average diameter (d.nm); PDI (a measure of the breadth of the size distribution within a sample); and surface charge (ζ-potential) measurements (section 2.14). These measurements were recorded for each of the non-coated, BSA coated, Fc-coated and CD95R-Fc coated (with and without BSA) samples. The mean size and zeta potential for each coating condition was analysed by ANOVA for 3 independent repeat experiments (section 2.15; Figure 5.5A & B respectively).

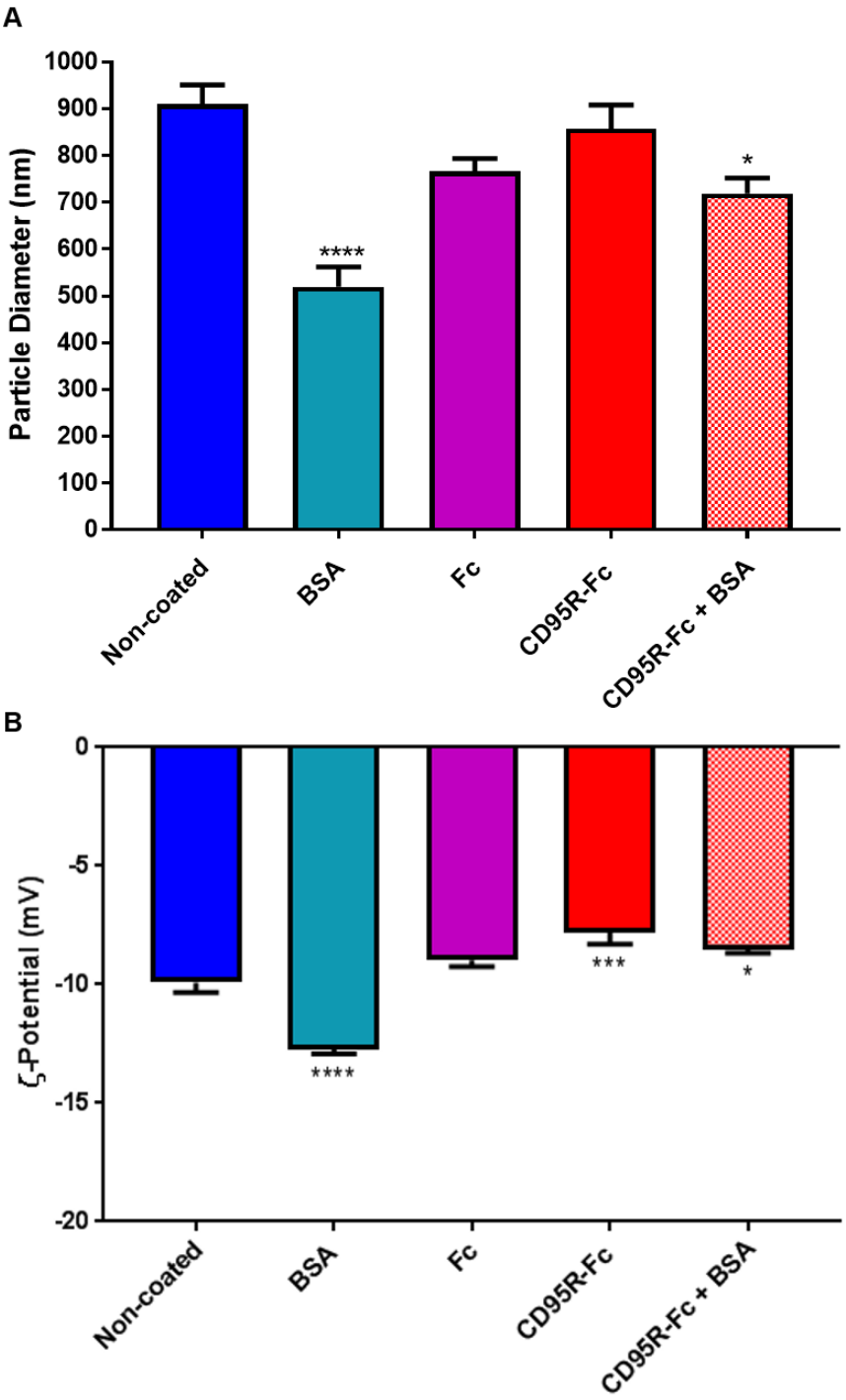

Figure 5.5. Characterisation of Microparticles with and without protein coats.
Microparticles (MPs) were diluted to 1ml in PBS and triplicate readings for each condition taken using a Zetasizer Nano ZS (Malvern). Significance was calculated by one-way ANOVA; **** $P \leq 0.0001$, *** $P \leq 0.001$ and * $P \leq 0.5$. (**A**) Mean z-average Diameter (particle diameter; nanometres (nm)) for each condition; Non-coated (mean polydispersity index (PDI) value: 0.321 ± 0.053), BSA coated (PDI: 0.468 ± 0.044), Fc coated (PDI: 0.300 ± 0.035), CD95R-Fc coated (PDI: 0.294 ± 0.059) and CD95R-Fc + BSA coated (PDI: 0.488 ± 0.074). The size of particles coated in BSA and CD95R-Fc + BSA was statistically different to non-coated MPs. (**B**) Mean ζ-potential (millivolts; mV) measurement of each condition; Non-coated, BSA coated, Fc coated, CD95R-Fc coated and CD95R-Fc + BSA coated MPs. The ζ-potential of particles coated in BSA, CD95R-Fc and CD95R-Fc + BSA was significantly different to non-coated MPs. There was no statistical significance between the ζ-potentials of non-coated and Fc coated MPs ($P > 0.05$).

The mean particle diameter of non-coated particles is 909 +/- 41nm, larger than the expected mean diameter of 530nm, which may be due to the presence of aggregates. The fluorescent MPs which have been coated and characterised here, and previously used for uptake, are commercially available and purchased at a specific size range. The quality control data states the mean diameter of this batch is 0.53µm (530nm). However, the particles can aggregate in solution depending on several factors including temperature, particle size or concentration (Bangs, 1999). Coating in BSA gave a mean particle size that is expected, 520 +/- 42nm, which is statistically different ($P \leq 0.0001$) to the mean size of non-coated particles. This could be because BSA blocks the exposed hydrophobic surfaces of the MPs, reducing nonspecific binding and self-aggregation (Bangs, 2008a). This effect is seen to a lesser extent when particles are coated in CD95R-Fc with additional BSA (which was initially included as a cryoprotectant; see Chapter 3), with a mean particle diameter of 719 +/- 33nm which is also statistically different (* $P \leq 0.5$) to the size of non-coated particles. This suggests a further advantage to adding BSA to the in-house expressed CD95R-Fc used for coating. There was no statistical difference in particle diameter ($P > 0.05$), in comparison to non-coated particles, when using Fc (767 +/- 27nm) or CD95R-Fc (857 +/- 51nm) to coat particles. There was no statistically significant difference between the PDI values for each condition, which range from 0.3 – 0.5, suggesting that the particles in all samples are polydisperse.

BSA coating decreased the surface charge of particles to the greatest extent, with a mean zeta potential of -12.7 +/- 0.2 mV, which is statistically significant ($P \leq 0.0001$) in comparison to non-coated particles (-9.9 +/- 0.4 mV). However, since

neither the non-coated particles nor BSA-coated particles are readily internalised by MDA-MB-231 cells, this imparted negative charge doesn't affect uptake, but it does show that the surface charge on the particle can be changed (albeit subtly) by protein absorption. Coating particles in CD95R-Fc with additional BSA slightly increases the surface charge, -8.5 +/- 0.1 mV, which is also statistically different (* $P \leq 0.5$) to non-coated particles. CD95R-Fc coating reduces the negative surface charge of particles to the greatest extent, with a zeta potential of -7.8 +/- 0.5 mV which is also statistically different (*** $P \leq 0.001$) to non-coated particles. However, there is no statistical difference ($P > 0.05$) between the surface charge of Fc coated particles (-8.9 +/- 0.3 mV) and non-coated particles, or Fc coated particles and CD95R-Fc coated particles (with or without BSA). Fc coated particles are internalised to a similar extent to non-coated particles, however, there is a large difference in the percentage uptake of Fc coated particles compared to CD95R-Fc coated particles (with or without BSA).

In conclusion, these small changes in surface charge don't consistently reflect the differences observed in uptake. The size and zeta potential difference of the BSA coated particles suggests that the absorption technique results in modification of the particle surface. When particles are coated with CD95R-Fc with BSA, this BSA-effect is not apparent or perhaps is prevented by the CD95R-Fc. This suggests both that the CD95R-Fc functionalises the particle surface and has a higher avidity for the particles than the BSA, since there is 50x more BSA in the coating mix than CD95R-Fc.

5.2.5. Chemical inhibition of CD95R-Fc coated microparticle internalisation

Previous studies have suggested that breast cancer cells internalise 3µm, polystyrene particles via macropinocytosis, regardless of particle surface charge (Patiño et al., 2015). This conclusion was based on almost complete inhibition of particle internalisation by 20µM cytochalasin D. The uptake of 200nm polystyrene particles into human lung cells has been suggested to involve actin-supported membrane protrusions, as imaged using fast ion conductance microscopy (Novak et al., 2014) which could be a form of macropinocytosis or phagocytosis. I therefore applied a range of known endocytosis inhibitors to investigate the role of different endocytic pathways in the uptake of CD95R-Fc coated MPs.

MDA-MB-231 cells were pre-treated with inhibitors for 1 hour prior to incubation with CD95R-Fc coated MPs (section 2.5.3 & 2.9.2). Two inhibitors of each pathway were used; cytochalasin D and amiloride to inhibit macropinocytosis, chlorpromazine and dynasore to inhibit clathrin-dependent endocytosis and nystatin and filipin to inhibit caveolin-dependent endocytosis. Mannan was used to inhibit mannose-receptor mediated endocytosis. Nocodazole, was also tested to investigate the involvement of microtubules in uptake. Non-treated cells were incubated with non-coated particles (negative control) and CD95R-Fc coated particles (positive control). After 12 hours, unbound particles were washed off before analysis using flow cytometry. Efficiency of MP uptake was determined by measuring the percentage of the gated cells with a fluorescence level above the autofluorescence of cells in the absence of particles. The percentage uptake over

the gated population for each condition was analysed using a paired t test for 3 independent repeat experiments (section 2.15; Figure 5.6A).

Only amiloride, which prevents the activation of macropinocytosis (Dangoria et al., 1996), caused a statistically significant reduction in uptake of particles (43 +/- 5%; $P \leq 0.05$), compared to CD95R-Fc coated MP uptake in non-treated cells (61 +/- 7%; Figure 5.6A). There was a statistical difference between non-coated particle uptake (17 +/- 3%) and CD95R-Fc coated particle uptake (61 +/- 7%; $P \leq 0.01$) in non-treated cells. There was also a statistical difference between non-coated particle uptake and all inhibitor conditions; $P \leq 0.05$ for filipin; $P \leq 0.01$ for amiloride, cytochalasin D, dynasore, nystatin and nocodazole; $P \leq 0.001$ for chlorpromazine and mannose. There was a trend toward reduced percentage uptake (45 +/- 5%) when cells were incubated with cytochalasin D, an inhibitor of actin polymerisation (Thompson et al., 2012) which is also required for macropinocytosis. There was also a consistent trend toward increased uptake when cells were treated with Chlorpromazine (117 +/- 12 %) an inhibitor of clathrin-dependant endocytosis. Further experimental repeats may determine whether these trends are significant or not.

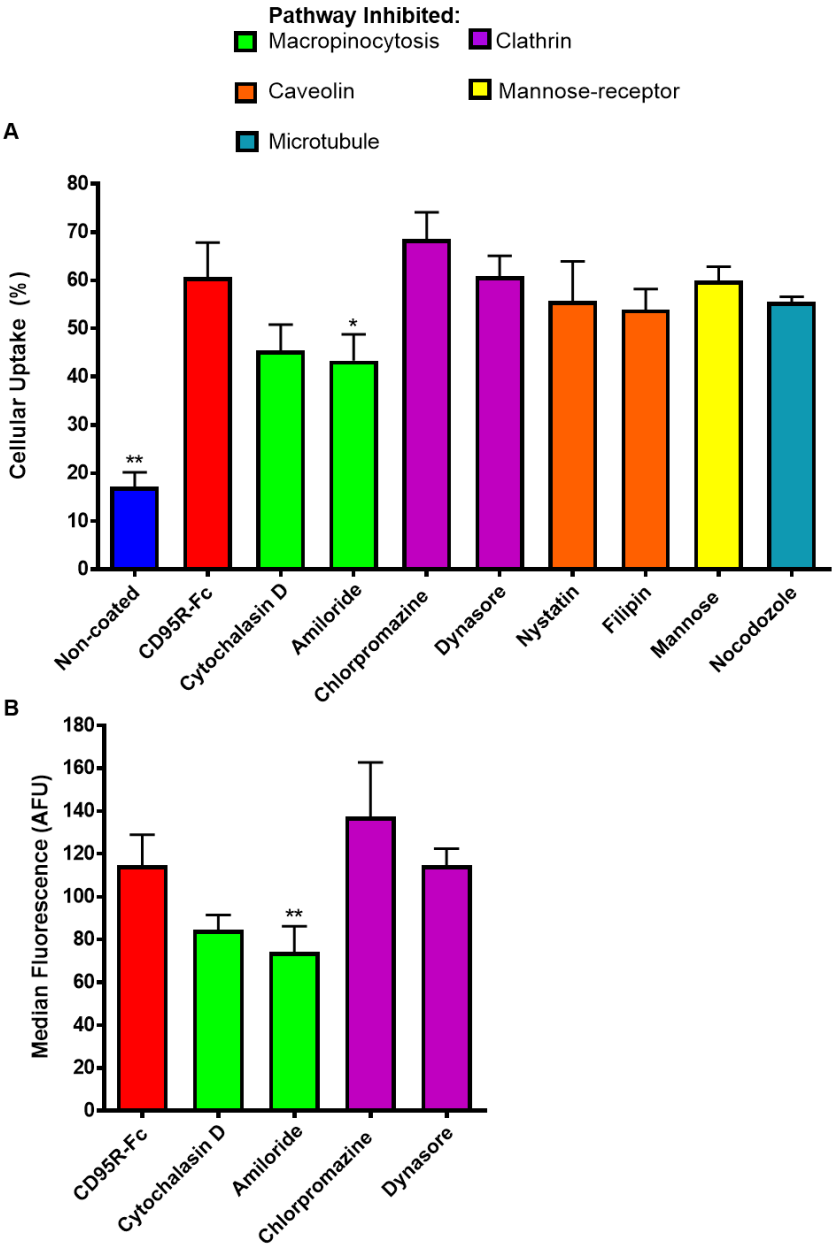

Figure 5.6. Effects of endocytic pathway inhibitors on CD95R-Fc coated microparticle uptake in MDA-MB-231 cells.
Cells were pre-treated for 1 hour with the indicated inhibitor prior to the addition of CD95R-Fc coated MPs. Non-treated cells were incubated with non-coated particles (blue, negative control) and CD95R-Fc coated particles (red, positive control). After 12 hours, cells were washed and analysed by flow cytometry. Cells were gated to eliminate cell debris and 10,000 gated cells were analysed. Mean and SEM values are from three independent, repeat experiments (n=3). Significance was tested using a paired t test; ** $P \leq 0.01$, * $P \leq 0.5$. (**A**) Percentage uptake of CD95R-Fc coated MPs in MDA-MB-231 cells with different inhibitors. Treatment of cells with amiloride statistically reduced uptake of CD95R-Fc coated MPs, compared to non-treated cells. Non-coated particle uptake in non-treated cells was statistically different to CD95R-Fc uptake in non-treated cells. Non-coated particle uptake in non-treated cells was also statistically different to all inhibitor treatments, (not shown on graph; $P \leq 0.05$ for filipin; $P \leq 0.01$ for amiloride, cytochalasin D, dynasore, nystatin and nocodazole; $P \leq 0.001$ for chlorpromazine and mannose) (**B**) Mean median fluorescence (AFU) of cells with particles (a measure of the number of particles internalised per cell over three independent experiments) treated with different inhibitors. Treatment with amiloride statistically reduced median fluorescence of cells compared to non-treated cells incubated with CD95R-Fc coated MPs.

These trends can also be seen when comparing the median fluorescence of cells with particles (Figure 5.6B). There was a statistically significant, lower median fluorescence (and so fewer particles per cell) when cells were treated with amiloride (74 +/- 12 AFU) compared to non-treated cells incubated with CD95R-Fc coated particles (115 +/- 14 AFU; $P \leq 0.01$). There was a trend toward lower median fluorescence with cytochalasin D (85 +/- 7 AFU) and with chlorpromazine, there is an increase in median fluorescence (137 +/- 25 AFU) indicating that cells internalised more particles. This trend is not as pronounced with Dynasore (114 +/- 8 AFU). Further experimental repeats could determine whether these trends are significant or not.

5.3. Discussion

CD95R-Fc enhances the uptake of MPs into MDA-MB-231 cancer cells, however the mechanisms involved in targeting and uptake were not known. Since the use of micro- and nanosystems for drug delivery has shown a strong potential for biomedical applications, a deeper understanding of their interaction with cells is needed for more efficient design of drug delivery systems (Patiño et al., 2015). In this chapter, the mechanisms of uptake of CD95R-Fc coated particles were investigated using confocal microscopy, live-cell imaging, endocytic inhibitors and DLS characterisation of coated MPs.

It was hypothesised that enhanced uptake of CD95R-Fc coated particles was due to an interaction of this protein with its natural ligand, CD95L, which had been reported to be expressed on the surface of cancer cells and so should be present on MDA-MB-231 cells. In Chapter 4, this hypothesis was tested and rejected because no evidence for plasma membrane, CD95L expression in this cell line was found (or by cancerous cells in general). Nevertheless, coating in CD95R-Fc stimulated high level uptake of the particles in MDA-MB-231 cells. In order to test whether the enhanced uptake is a cancer-cell specific effect, CD95R-Fc coated MP uptake was measured in primary dermal fibroblasts sourced from facial skin. Primary cells were used to avoid any bias due to selection for growth in tissue culture which might alter the uptake properties of cancer or immortalised cell lines. A statistically significant improvement in uptake (53 +/- 1%) of CD95R-Fc coated MPs was recorded in comparison to several control particle preparations, which is similar to the levels observed in MDA-MB-231 cells. The controls included Fc coated and BSA coated particles, which did not improve uptake to

the extent of CD95R-Fc coated particles, showing that the CD95R ECD is responsible for the enhanced uptake. There was no statistical difference in the median fluorescence of cells with particles, between the two cell lines, suggesting that they have internalised a similar number of particles per cell. These data suggest that the CD95R-Fc enhanced uptake effect is not specific to cancer cells. However, as described in the introduction, some cells exhibit the phagocytic activity similar to immune cells, classed as “non-professional” phagocytes. Indeed, a mechanism has been described where phagocytes can alter and dampen the phagocytic activity of neighbouring cells via IGF-1, including LR73 cells, which are a type of Chinese hamster ovary fibroblast cells (Han et al., 2016). These fibroblasts have a phagocytic activity and are classed as “non-professional” phagocytes, with the potential to clear apoptotic cells and particles (Gregory and Pound, 2010). Similarly, human dermal fibroblasts have the ability to phagocytose the apoptotic bodies of neutrophils which are recognised by the fibroblast via the vitronectin receptor and a mannose/fucose-specific lectin (Hall et al., 1994). Fibroblasts in the wound sites of rats have also been found to internalise non-coated, IgG coated and collagen coated fluorescent beads (1µm) (Arlein et al., 1998). Therefore, it is perhaps not particularly surprising that the primary dermal fibroblasts used here have internalised MPs.

The expression of CD95L was investigated via Western blot, however, none was detected in the fibroblasts. Even though CD95L doesn’t seem to play a role in uptake in primary dermal fibroblasts or the MDA-MB-231 cells, the uptake mechanisms active in these two cell lines are not necessarily identical. Internalisation pathways are often cell-type specific. For example, in breast

cancer cells, non-coated, negatively charged particles appear to be internalised via macropinocytosis but in breast epithelial cells, they are internalised via two pathways; macropinocytosis and a dynamin-dependent endocytosis method (clathrin or caveolae-mediated endocytosis) (Patiño et al., 2015). The uptake pathway in primary dermal fibroblasts would need to be determined and compared to MDA-MB-231 cells; potentially the two cell lines share a common receptor, which is recognising the CD95R coat or the particle itself to trigger uptake, but this would need to be investigated. In terms of clinical application, a CD95R-Fc coated MP for cancer drug-delivery, given intravenously, risks inducing side-effects if non-cancerous cells are able to internalise the MPs as demonstrated here.

When working with MPs it is important to distinguish between MPs that have been completely internalised by cells from those that are simply membrane-attached, since they are utilised for intracellular drug delivery. Several methods have been developed to address this. For example, when using polystyrene particles that are surface-labelled with fluorescent antibodies (such as Alexa488-IgG), the fluorescence can be quenched using trypan blue. Since trypan blue is not capable of penetrating live cells, the quenching effect only occurs in the extracellular space, so the fluorescence of MPs bound to the membrane can be quenched, whereas internalised MPs, separated from the quencher, fluoresce intracellularly (Patiño et al., 2015). An added benefit of using trypan blue is that it can also determine cell viability since it can only enter cells with damaged plasma membranes (Patiño et al., 2015). However, the polystyrene particles used here are internally labelled with dragon green fluorescence using dye

diffusion/entrapment. This involves the swelling of polymeric microspheres in an organic solvent or dye solution where the water-insoluble dye diffuses into the polymer matrix and is entrapped when the solvent is removed from the microspheres (Bangs, 2013). This means that fluorescence cannot be quenched using a substance like trypan blue because the dye is inaccessible to the quencher.

The FACscan used for flow cytometry cannot discriminate between surface bound and internalised particles. Some forms of flow cytometry can do this, such as an ImageStream (Merck) which can provide low to medium resolution images of every cell analysed, allowing the user to assess whether a particle is membrane bound or internalised, although the analysis remains subjective and the resolution is limiting. For analysis of live cells, the approach adopted here, making use of an IN Cell 6000 provides an excellent compromise. Confocal imaging of adhered cells at medium to high resolution can be automated and quantified to provide high throughput analyses. Such an approach proved useful to demonstrate the effectiveness of the washing procedures used to remove non-internalised particles from cells. With analysis stringencies in place to ensure non-bound particles were not counted, CD95R-Fc coated MP uptake was found to be statistically different with more cells internalising particles, and more particles per cell than the control conditions. This technique allowed discrete numbers of particles internalised by cells to be seen and complements the uptake and median fluorescence data obtained by flow, even when far fewer cells were analysed (150 – 200 cells per condition here compared to 10,000 cells for flow analysis). There is however, a margin of error when using confocal imaging to

take optical slices throughout a cell, since the slice (the Z-intensity profile) is not sharp but has a Gaussian profile and is shaped like a bell. The practical thickness of each slice may therefore deviate from theoretical estimation. The exact Z-intensity profile, or optical slice thickness, can vary with objective (numerical aperture; NA), size of confocal aperture and wavelength of light. The confocal slices for the experiment here were taken at 40x, NA=0.6 at 1 AU (airy unit), meaning that the theoretical 1.7µm slices may include light over a 5µm slice. Confocal settings can be optimised by using an objective with a higher numerical aperture, improving the resolution, however the amount of time required to image each cell in focus would increase, which may be impractical. Another way to optimise confocal settings is via sample preparation, for example, by seeding the MDA-MB-231 cells onto thin, glass bottomed wells, ensuring the entirety of the cells are included in the confocal slice. The plate curvature of typical 6-well plate (as was used) means part of the sample may not be included or imaged since confocality does not solve the issue of light scattering caused by plate bottom curvature, it only removes out of focus light. To help counteract this, multiple 3D Z-images were flattened into one, 2D image, hoping to get all cells in focus.

Protein-coated particles were characterised using dynamic light scattering (DLS). Even though the particles used are purchased at a discrete size (quality control suggests 0.53µm diameter), the presence of aggregates in solution distorts the particle size reading obtained for most samples, and likely explains the larger values obtained than 530nm. Aggregation was reduced by coating particles in BSA, which is recommended technique to reduce nonspecific binding and self-aggregation since BSA blocks the exposed hydrophobic surfaces of the MPs

(Bangs, 2008a). Other methods to reduce particle aggregation include sonication, (particularly by using a bath sonicator with samples in a glass vial), vortexing and pipetting which provide shear forces to break up particle masses (Bangs, 1999). These techniques however are not recommended after passively absorbing a ligand to the surface of non-functionalised MPs, since the shear forces involved can dislodge protein adsorbed to the particle surface (Bangs, 1999). Despite this, they may be useful prior to coating. Having a monodisperse population will mean more free, single particles are available for cells to internalise, as large aggregates are not as readily taken up by cells.

A combination of electrophoresis and DLS was also utilised to measure the surface charge of non-coated versus protein-coated particles, since this is a factor that can affect particle uptake. Previous studies have suggested that tumour and cancer cells preferentially internalise positively-charged nanoparticles and 3µm polystyrene particles (section 5.1.6.) (Patiño et al., 2015, Wang et al., 2012, Gratton et al., 2008). The size and zeta potential difference of the BSA coated particles suggests that the absorption technique results in modification of the particle surface. When particles are coated with CD95R-Fc with BSA, this BSA-effect is not apparent or perhaps is prevented by the CD95R-Fc. This suggests both that the CD95R-Fc functionalises the particle surface and has a higher avidity for the particles than the BSA. However, the difference in charge caused by coating in different proteins did not correlate well with the differences in uptake seen, for example, there was no statistical difference in surface charge of Fc-coated MPs and CD95R-Fc coated MPs (with or without BSA), yet there was a pronounced and statistically significant difference between

these conditions when uptake was tested. It is therefore unlikely that a difference in surface charge explains the differences in uptake. Although subtle differences in surface charge were seen here, particles with a zeta potential between -10 and +10mV are considered approximately neutral, while particles with zeta potentials of greater than +30mV or less than -30mV are considered strongly cationic and strongly anionic, respectively (Clogston and Patri, 2011). All particles, coated or non-coated, had a zeta-potential that would be considered close to neutral, (perhaps excluding BSA coated MPs which are slightly anionic with a surface charge of -12.7 +/- 0.2mV). *In vivo*, the BSA coated particles would be considered advantageous, because negatively-charged particle therapies have been shown to be less likely to induce an immune reaction. This may be explained by the display of negatively charged sialic acids by macrophages, that readily interact with cationic substances (Chellat et al., 2005). Uptake by macrophages can then lead to the release of inflammatory cytokines, as shown by Lucarelli et al., who exposed human macrophages to non-toxic concentrations of different nanoparticles that triggered distinct inflammatory responses (Lucarelli et al., 2004). Silicon dioxide (SiO2) nanoparticles, for example, induced the production of inflammatory cytokines interleukin 1 beta (IL-1β) and tumour necrosis factor alpha (TNF-α) (Lucarelli et al., 2004).

Preliminary investigations of the uptake mechanism of CD95R-Fc coated MPs was also investigated, using a panel of commonly used inhibitors. Two inhibitors for each pathway were used to maximise confidence in the conclusion. Since endocytic inhibitors can induce cellular side-effects and are prone to act non-specificity, use of two inhibitors helps to ensure that any observed effect

genuinely impacts a particular uptake pathway since inhibitors of the same pathway tend to work via different mechanisms and on different targets. A statistically significant reduction in uptake and number of particles per cell was discovered with amiloride treatment. Amiloride inhibits macropinocytosis by affecting Na^+/H^+ exchange, which has been linked to macropinosome formation. By inhibiting this exchange, Amiloride acidifies the submembranous pH of a cell and so, prevents the activation of GTPases (Rac1 and CDC42) that promote actin remodelling, since they have been found to be extremely sensitive to these pH changes (Koivusalo et al., 2010). Selective inhibitors of the Na^+/H^+ exchange (such as amiloride) may have the fewest side effects and may be considered as a first choice for the pharmacological probing of macropinocytosis (Ivanov, 2008). However, possible endocytosis-unrelated effects on ion transport and the cytoskeleton may still be an issue, affecting the viability of tested cells. A similar reduction in cellular uptake and median fluorescence was seen when cells were treated with cytochalasin D, however this did not reach statistical significance. Cytochalasin D blocks actin polymerisation by occupying the faster-growing “barbed” end of actin filaments (Ivanov, 2008). It was predominantly used here as an inhibitor of macropinocytosis, but it can affect the formation of large F-actin-coated vesicles (phagosomes and macropinosomes) associated with both phagocytosis and macropinocytosis. It is possible that MDA-MB-231 cells may possess a “non-professional” phagocytic activity to internalise the MPs since they have been shown to locally degrade and phagocytose the extracellular matrix (Coopman et al., 1996). However, the actin cytoskeleton is involved in endocytosis for nearly all internalisation pathways, such as the formation of the actin module, which enables movement of vesicles away from the plasma membrane irrespective of vesicle-coat protein. As a result, cytochalasin D might

be considered as a global and nonselective inhibitor of all internalisation pathways, rather than a specific blocker of macropino- and phagocytosis (Ivanov, 2008). Despite this, particle size also has a large part to play in the pathways of cellular uptake. Since phagocytosis (≥0.5µm) and macropinocytosis (0.2 to 10µm) are capable of internalising micrometre-scale particles, it is logical to assume that one or both of these pathways are in effect to internalise the 0.5µm, CD95R-Fc coated MPs. Additionally, none of the inhibitors of small-scale endocytosis mechanisms (which usually internalise particles <200nm), had any noticeable reduction on particle uptake. More investigation is required to determine whether uptake is due to macropinocytosis, phagocytosis (alone or combined), or whether the CD95R-Fc protein coat has any targeting or activating effect on uptake (see section 5.3.1.).

Interestingly, chlorpromazine seemed to have a positive effect on particle uptake and number of particles internalised (as reproducible trends which did not reach statistical significance) by the MDA-MB-231 cells. Potentially, this could be an off-target effect since chlorpromazine is an amphipathic molecule, which can incorporate into the lipid bilayers and can increase lipid fluidity within the plasma membrane (Ogiso et al., 1981). Such gross changes of the membrane are likely to have knock-on effects on the endocytic pathways. However, there is also some prior evidence suggesting that inhibition of clathrin-coated uptake upregulates other pathways. When chlorpromazine was used on ARPE-19 (human retinal epithelial), HuH-7 (human liver), Vero (monkey kidney epithelial) and COS-7 (monkey kidney fibroblast) cells, it enhanced uptake of lactosylceramide

(LacCer); a glycosphingolipid that resides preferably in lipid rafts, which is a marker of caveolae-mediated endocytosis (Vercauteren et al., 2010).

In contrast, a study by Novak *et al*. found a potential link between clathrin-dependent uptake and uptake via membrane protrusions (potentially indicating macropino- or phagocytosis). They used scanning ion conductance microscopy to allow high-speed topographical and fluorescence imaging of the interactions between 200nm polystyrene particles and human lung cells (Novak et al., 2014). A particle was imaged being engulfed by a large membrane protrusion, but prior to this, there was an initial interaction between fluorescently-tagged clathrin pits and the particle. It was hypothesised that the disproportion in diameters of the pits (~100nm) to the particles led to failure in uptake and may reflect a form a 'cell-sensing', allowing the cell to test whether or not a particle is the correct size for a particular internalisation pathway. Perhaps, removing a cells' ability to internalise via clathrin-mediated endocytosis and this cell-sensing procedure, speeds up or leads to a reliance on actin-only forms of uptake and the increase in MP uptake seen with chlorpromazine. Time-lapse, live-cell imagining demonstrated an interaction between a CD95R-Fc coated MP and a membrane protrusion from MDA-MB-231 cells. Further testing of uptake of CD95R-Fc coated MPs using a scanning ion conductance microscopy and fluorescently labelled clathrin and actin, might elucidate more detailed information regarding the mechanism of particle internalisation.

5.3.1. Limitations and possible future directions

Although DLS measurements found that different protein coats affect particle size and surface charge, the experiments were undertaken in the coating buffer, PBS. After coating, the particles are added to cells which are growing in DMEM supplemented with 2% (reduced) FBS. Ideally, particle properties should be measured again, after suspension in this medium. Medium contains many different biomolecules, such as proteins, which can adsorb onto the particle surface to produce a protein corona (Shang et al., 2014). The reduced FBS component of the media (2% rather than a standard 10% FBS (v/v) component) was to reduce the amount of free protein that can interact with the particle and form a corona. The likely presence of a protein corona will change the properties of the particles, including important factors that affect uptake, such as surface charge and aggregation. Potentially, the initial protein coat could affect the characteristics of this protein corona, thus modulating particle/cell interactions. Furthermore, the CD95R-Fc used for coating could interact with proteases in the cell media and it is unknown whether it is cleaved or modified during particle incubation with the cells. This could be difficult to determine, however, the CD95R-Fc used for coating could be incubated in spent media (from the MDA-MB-231 cells) for 24 hours, and its stability determined by Western blot.

It is likely that the particles are being internalised via macropino- or phagocytosis because of their size. The results of the inhibitor experiments may also indicate this; however, some important factors were not tested in this experiment. This includes cell viability in response to the inhibitor concentrations used, which has been found to be cell type-dependent. For example, high chlorpromazine

concentrations (12µg/ml, ~38µM and above) have very little effect on ARPE-19 and D407 (human retinal epithelial) cells but are toxic to COS-7 cells at 5µg/ml, 16µM (Vercauteren et al., 2010). Chlorpromazine was used at 15µM for the experiments described here yet the effect of this concentration on MDA-MB-231 cells is not known. Furthermore, the use of positive controls, to ensure that specific endocytic pathways had been inhibited, would have improved this experiment. Some markers of uptake pathways have already been described such as human transferrin, which is a good specific marker for clathrin-mediated uptake and LacCer or cholera toxin subunit B as a marker of caveolae-mediated endocytosis. DMSO only controls would also be useful, i.e. cells incubated with matching volumes of DMSO and then non-coated and CD95R-Fc coated particles, since many of the inhibitors were solubilised in DMSO and this can be toxic to cells. To elucidate the specific pathways further and complement the inhibitor experiment data (without the complications associated with using endocytic inhibitors) siRNA experiments could be utilised. This has been used to determine the uptake of folate-functionalised glycol chitosan nanogels (Pereira et al., 2015). Knockdown of specific proteins of each pathway, such as clathrin and caveolin, is possible. For macropinocytosis, Pereira *et al.*, knocked down CDC42 and p21-activated kinase (Pak-1), since it is associated with growth-factor-induced macropinosomes and can be activated by CDC42 and Rac1; well-known GTPases involved in macropinocytosis (Pereira et al., 2015).

Since MDA-MB-231 cells have been shown to elicit a “non-professional” phagocytic capability, it is possible that they internalise MPs this way. Phagocytosis is induced by interaction between ligands on the particle surface

and receptors on the phagocytic membrane. Therefore, knockdown of known scavenger, complement and integrin receptors (see table 5.1) that are present in MDA-MB-231 cells, would be a good strategy to determine whether the CD95R-Fc protein coat or perhaps, the resulting protein corona, is initiating uptake. Previous reports of the phagocytic ability of MDA-MB-231 cells showed that it was dependent on alpha 3 beta 1 integrin (Coopman et al., 1996). Since CD95L is likely not involved in uptake, this would be crucial in determining whether there is any specific effect due to the CD95R coat, for preferential internalisation by MDA-MB-231 cells and primary dermal fibroblasts.

Finally, along with the uptake mechanisms, it would be important to determine the intracellular fate of internalised particles. This could be determined by incubating the cells with an endosomal (such as EEA1) or lysosomal (LAMP-1) markers, and analysing uptake of CD95R-Fc MPs over time, using the IN Cell 6000. Both end point and live-cell imaging could be utilised where possible. The 3µm polystyrene particles internalised by SKBR-3 and MCF-10A were found to localise to lysosomes, regardless of coat or surface charge (Patiño et al., 2015).

5.4. Summary

CD95R-Fc coated MPs are more readily internalised by MDA-MB-231 cells but not via a CD95L interaction as was previously hypothesised. In Chapter 5, the mechanisms involved in particle uptake were investigated. Uptake was tested in non-cancerous cells and again, CD95R-Fc coated MPs were preferentially internalised. This effect therefore, is not specific to cancer cells. Confocal imaging

showed that the particles are fully internalised, and not simply bound to the cell surface. Particles were characterised by dynamic light scattering (DLS) which suggested that the protein absorption technique results in modification of the particle surface, which is most noticeable when coating with BSA. Although coating in different proteins affects particle size and surface charge, the subtle differences measured suggest that it is unlikely that these are responsible for the enhanced uptake of CD95R-Fc coated MPs. Finally, common endocytic pathways were inhibited. There was a statistically significant reduction in uptake when treating cells with amiloride and a similar trend when treating with cytochalasin D, inhibitors of macropinocytosis, however no inhibitor fully blocked uptake. Due to particle size, MP uptake likely occurs via macropino- or phagocytosis. More investigation is required to determine which pathway is preferred in this cell type, and whether or not the CD95R is binding to a specific receptor or lipid on the cell surface to initiate the process.

6. General Discussion

The aim of this study was to develop an expression and purification system for CD95R-Fc to allow the mechanisms of coated microparticle (MP) uptake in cancer cells to be investigated. In Chapter 3, a baculoviral system was optimised for expression of recombinant CD95R, fused to the Fc region of human IgG1, in Sf21 and Hi5 cells. The protein was purified by affinity chromatography with a potential yield of 1.2mg per 100ml culture and a purity of 90%. The purified CD95R-Fc was used to coat microparticles that were efficiently taken up by MDA-MB-231 (triple negative breast cancer) cells, in comparison to non-coated particles. It had been suggested that this enhanced uptake was due to a CD95L/CD95R interaction. Stability of the in-house CD95R-Fc was tested, and long-term storage conditions were optimised. In Chapter 4, anti-CD95L antibodies (many of which have been critically appraised and found to lack specificity) were validated by overexpressing CD95L-Myc-DDK in HEK293T cells, with and without CD95L-sheddase inhibitors. The expression of supposed target ligand CD95L was then tested in MDA-MB-231 cells to examine the proposed targeting mechanism of CD95R-Fc coated MPs. It was concluded that there are undetectable levels of the CD95L protein in MDA-MB-231s, as shown by Western blot and immunocytochemistry. Despite MDA-MB-231 cells lacking CD95L protein at the plasma membrane, they very efficiently take up CD95R-coated MPs. In Chapter 5, the reasons for this enhanced uptake were explored and mechanisms of particle uptake examined. Uptake was tested in a non-cancerous cell line and CD95R-Fc enhanced uptake was also found in primary dermal fibroblasts and so the effect is not cancer-cell specific. Confocal imaging demonstrated that the particles are fully internalised, and not simply bound to the

cell surface. Particles were characterised by dynamic light scattering (DLS) and electrophoresis and notable differences in surface charge, due to coating in CD95R-Fc, were not apparent. Finally, common endocytic pathways were inhibited which suggested that MP uptake likely occurs via macropino- or phagocytosis and may involve membrane protrusions as seen via time-lapse microscopy.

In the following sections, the findings of this study are discussed in relation to the data in the literature, and possible further work is considered that may lead to fuller understanding of whether this delivery system is plausible for use as a cargo delivery system.

6.1. Targeted chemotherapeutics for triple negative breast cancer

The main cell line used in this study was MDA-MB-231 cells, a triple negative breast cancer cell line. Triple negative breast cancers, which represent ~15 - 20% of breast carcinomas, lack the three main breast cancer biomarkers; oestrogen, progesterone or HER2 (human epidermal growth factor receptor 2) receptors (Denkert et al., 2017). Patients with triple negative breast cancer do not benefit from any endocrine or anti-HER2 therapy (such as Herceptin, a mAb), and chemotherapy is the only established therapeutic option (Denkert et al., 2017). Chemotherapies such as the taxane, paclitaxel, are associated with common off-target toxicities including neutropenia, leukopenia, anaemia, neuropathy and fatigue (Wood et al., 1995) and tumours often develop resistance to such

cytotoxic compounds (Longley and Johnston, 2005). Furthermore, taxanes are poorly soluble in water and the agents in which they are solubilised in (such as cremophor) can lead to hypersensitivity reactions in patients (Wang et al., 2012). Therefore, there is a need for targeted treatments for triple negative breast tumours, which can deliver cytotoxic compounds directly to the cancerous cells to reduce systemic toxicity. Abraxane is one example of a solvent-free treatment for breast cancer, a 130 nm, albumin-bound particle form of paclitaxel (Miele et al., 2009). This treatment option utilises the natural uptake pathway of albumin, which binds to a cell surface, 60kDa glycoprotein (gp60) receptor called albondin. The gp60/ligand complex interacts with caveolin-1 to form vesicles which transcytose the albumin (and bound paclitaxel) into the cell cytoplasm (Miele et al., 2009). This results in a higher penetration of Abraxane into tumour cells with an increased anti-tumour activity, compared to an equal dose of standard paclitaxel (Miele et al., 2009). Despite the improved solubility, uptake and reduced toxicity seen with Abraxane, it doesn't actively target cancer cells for treatment.

A study in 2011 found a novel use for CD95R in targeted drug delivery; when used to coat microparticles, >0.5µm in diameter, they were preferentially internalised by neurons, medulloblastoma, breast and ovarian cancer cells *in vitro* (Ateh et al., 2011). When biodegradable MPs, made from PLGA and loaded with paclitaxel, were coated in CD95R-Fc, they were significantly more effective compared to conventional paclitaxel therapy (taxol) at the same dose in subcutaneous medulloblastoma and orthotopic ovarian cancer xenograft models (Ateh et al., 2011). This drug delivery system potentially represented a way to

improve function of cytotoxics in cancer by increasing drug targeting and efficacy whilst reducing toxicity, without the need for any toxic solvents. This study has provided some further evidence to support this previous data, showing that CD95R modifies the surface of particles and is responsible for the increase in uptake into MDA-MB-231 cells. However, the precise mechanisms behind this are still not known, although it has been shown not to involve CD95L. Initially, this improved uptake suggested a potential cancer targeting mechanism of drug delivery however, it was then seen in a non-cancerous cell line which alludes to potential off-target toxicities. This puts into question the conclusions of the 2011 paper, and more study is required in cellular systems (see section 6.4) before further testing in *in vitro* models. Animal models are an important tool to test drug delivery systems on since they can more closely mimic the tumour microenvironment in a way that is not possible using 2D, cellular systems. Considerable efforts have been made to develop more clinically relevant models, for example, by use of orthotopic transplantation of tumour material in rodents (Bibby, 2004). It has been shown that transplanting tumour material from a variety of tumour types into the appropriate anatomical site results in tumours that will metastasise in a similar manner and to similar locations as the same tumour type will in human cancer (Bibby, 2004). An animal model like this could prove more relevant than the orthotopic model used by Ateh et al. in 2011, since this was developed using IGROV1 cells rather than real tumour material.

6.2. The use of micron-sized particles for drug delivery

0.5µm MPs, coated in CD95R-Fc, were found to be internalised to a greater extent than 1µm, CD95R-Fc coated MPs in MDA-MB-231 cells (Ateh et al., 2011)

which is why 0.5µm particles were selected for the current study. There has been extensive study into nanoparticle systems for drug delivery since nanoparticles are easily internalised by cells (by either active or passive uptake) (Shang et al., 2014). However, there are advantages of using a large or micron-sized particle for drug delivery, rather than nano-scale methods, including providing a greater volume for drug loading. For example, the volume of 1µm diameter particles is 125-fold greater than their 200nm counterparts, enabling more drug molecules to be packaged and potentially allowing more to be delivered directly to the cytoplasm of cancer cells (Ateh et al., 2011). Particle size however can also affect drug loading efficiency and drug release profiles. A very large particle, for example, 20µm compared to 1µm, may have a lower drug loading efficiency. Dawes et al., found this when comparing drug loading and release profiles of differently sized PLGA particles. The drug loading efficiency was tested by dissolving particles in acetonitrile and measuring encapsulated drug release by High Performance Liquid Chromatography (HPLC); for 1µm particles, the efficiency was 11% compared to 1% for 20µm particles (Dawes et al., 2009). Additionally, over a 550 hour release period, where particles were placed in PBS at 37°C with drug release measured again by HPLC, the larger particles were found to release 90% of encapsulated drug in a linear fashion, whereas the 1µm particles released only 30%; 20% within the first 25 hours (Dawes et al., 2009). This demonstrates a biphasic, ‘burst effect’ release profile, where an initial bolus of drug is released before the release rate reaches a stable profile (Huang and Brazel, 2001). Both of these effects can be attributed to the higher surface area per unit volume of the 1µm particles. During formulation, the level of polymer-water interface is increased in the smaller particle allowing more drug to be encapsulated by the emerging polymer spheres (Dawes et al., 2009). Similarly,

during drug release, the rate of inclusion of water into the polymer increases, permitting faster diffusion of the loaded drug (Dawes et al., 2009). In addition to particle size, the type of PLGA used to create particles can affect how encapsulated drug is released. The hydrophilicity of PLGA (as defined by the lactide:glycolide ratio) and the polymer molecular weight are the key factors influencing drug release. The rate of degradation is inversely proportional to the proportion of lactide monomer in the polymer strands (Anderson and Shive, 2012) and the rate of diffusion of drugs through the polymer matrix is inversely proportional to the molecular weight of the PLGA polymer (Dawes et al., 2009). These examples describe the advantages of using PLGA microparticles for drug delivery, since their size and polymer characteristics allow tuneable drug loading and release profiles. Furthermore, micron-based systems can be loaded with more drug and provide a sustained release for longer periods of time than nanoparticle drug delivery methods. Microscale spheres have been typically used in applications where the drugs can be delivered to a particular site without diffusing away; the most effective size range for this has been quoted as 10 – 200µm (Dawes et al., 2009). Particles smaller than 10µm can be phagocytosed by immune cells. The downsides of this not only include potential side-effects (as is discussed in section 6.4) but the immune cells will transport the particles away from their intended site of action. Using microspheres larger than 200µm can disrupt the tissue structure of the implantation site, leading to an increased immune response and unnecessary inflammation (Dawes et al., 2009). Additionally, due to the increased radius and decreased surface area, the rate of water permeation into these particles would reduce significantly, reducing the maximum possible rate of drug release (Dawes et al., 2009).

6.3. Potential advantages of using microparticles in a clinical setting

In a clinical setting, micron-sized PLGA particle therapies may reduce a patients' visits to hospital to receive treatment. A standard chemotherapy regime for triple-negative breast cancer is FEC-T (**F**luorouracil, **E**pirubicin, **C**yclophosphamide and doce**T**axel) in which there are 3 or 4 cycles of FEC and then 3 or 4 cycles of T, each cycle lasting for 21 days (Roché et al., 2006). This means that a patient may visit a hospital 6 - 8 times, potentially more if there are bad reactions and side-effects to the chemotherapy. Dutta et al., tested the release period of differently sized PLGA particles, loaded with BSA (Dutta et al., 2016). Lyophilised particles were resuspended in PBS and incubated at 37°C under constant agitation. At specified time points, the particle suspensions were centrifuged, and supernatants removed and replaced with fresh PBS. The release media samples (supernatants) were quantified for protein content using a BCA assay and for particles with an average diameter of 541nm, the total release period was 72 days (Dutta et al., 2016). In relation to the FEC-T regime, a microparticle-based treatment may have the potential to reduce hospital visits by a patient, to 2 – 3 visits for example, which is more convenient for a patient and could reduce the burden on hospital resources. With successful targeting, a MP treatment could also reduce the adverse side-effects to improve a patient's quality of life throughout their treatment.

6.4. Lack of active targeting by CD95R-Fc coated MPs

The potential of CD95R-Fc coated MPs for use as a delivery system for chemotherapeutic treatments relies on the successful targeting of these MPs

directly to the cancer cells. In the paper by Ateh et al, when discussing the success of the CD95R-Fc MP treatment in an orthotopic ovarian cancer xenograft model, it is stated that any immune cell involvement as a side-effect of this treatment (uptake by peritoneal macrophages or NK cells for example), would need to be determined further (Ateh et al., 2011). Not only do immune cells have a natural phagocytotic activity for particles (≥0.5 µm), but it was thought that off-target effects may also be induced by the CD95R-Fc on the particle binding to CD95L or an Fc receptor endogenously expressed on the surface of immune cell. The targeting mechanism of the CD95R-Fc drug delivery system was investigated in the current study for targeting potential to MDA-MB-231 cells, and despite increased uptake of CD95R-Fc modified MPs, there was no convincing evidence to suggest this cell line expresses CD95L. Furthermore, the enhanced uptake of CD95R-Fc coated MPs was found in a non-cancerous cell line; primary dermal fibroblasts. Primary cells were used to avoid any bias due to selection for growth in tissue culture which might alter the uptake properties of cancer or immortalised cell lines. The potential for CD95R-Fc to interact with another protein to initiate uptake is discussed below in ‘future work’ (see section 6.8), but it seems likely that this system lacks a sufficient targeting mechanism. This could present problems if a future treatment was administered systemically, as chemotherapeutics often are. It means that potential off-target effects could include not only MP uptake by innate immune phagocytes, but any cells that have phagocytic activity; non-professional phagocytes (such as fibroblasts). Uptake of MPs by non-cancerous cells means that patients could still suffer the side effects associated with standard chemotherapeutics.

6.5. Passive targeting of cancer nanomedicines

Not all nano/microparticle therapies rely on active targeting, such as functionalising the particle surface with a natural ligand or biological marker (Kohane, 2007). Passive targeting involves using a specific physiological parameter to act as a filter. In the case of cancer, many nanoparticle therapies rely on the EPR (enhanced permeability and retention) effect, whereby molecules of a certain size range tend to accumulate in tumour tissues more than healthy tissues. This is due to the blood vessels in the tumour system having leaky walls and generally the lymphatic system in a tumour is absent or dysfunctional, therefore insufficient drainage leads to particle accumulation within the tumour tissue (Sun et al., 2014). The effect results from dysregulated tumour angiogenesis, whereby the rapid growth of blood vessels surrounding the tumour leads to the reduced density of endothelial cells and thus loss of tight junctions and formation of large gaps between the cells (Sun et al., 2014). Furthermore, the underlying basement membrane of the blood vessels is mostly abnormal or missing (Baban and Seymour, 1998). The openings in the tumour vasculature are typically in the size range of 100 – 800nm, and vary depending on the tumour type (Sun et al., 2014). When liposomes of different mean sizes were tested, the cut off size for extravasation into tumours was approximately 400nm, whereas particles with diameters smaller than 200nm were found to work most effectively (Yuan et al., 1995). This is because particles larger than 200nm were cleared from the blood stream more rapidly by the spleen, as it contains a tight reticular mesh which preferentially clears particles of ≥200nm (Sun et al., 2014). Experiments have shown for example, that 50% of polystyrene nanoparticles with a diameter of 250nm and coated in poloxamine 908 (a hydrophobic, block co-polymer) accumulate in the spleen within 24 hours of injection because of this

physical filtration effect (Moghimi et al., 1993). Taken together, this evidence suggests that CD95R-Fc modified, 0.5µm MPs may not be suitable for passive targeting, since they could be too large to extravasate into tumours, and their size means they would likely be cleared systemically by the spleen.

6.6. Intratumoral injection

A potential way to counteract the lack of active targeting would be to inject CD95R-Fc coated MPs directly into the target tumour. In the peritoneal ovarian cancer xenograft model, where CD95R-Fc modified PLGA particles were more effective than free paclitaxel at the same dose, the particles were injected directly into the peritoneum of the mice (Ateh et al., 2011). Potentially this effect may be partially due to the microparticles staying where they have been placed; they are retained within the tumour environment allowing local release of the cytotoxic. The difference between micro- and nanoparticles has been described in the abdominal cavity (Kohane, 2007). PLGA microparticles, 5, 25, 60 and 250µm in diameter, injected into the peritoneum of mice, remained there for at least two weeks, whereas an equal mass of nanoparticles (265nm) of the same material showed almost complete clearance in the same time frame (Kohane et al., 2006). The nanoparticles were sequestered in the spleen and liver, with 'foamy' macrophages noted, likely due to the accumulation of a large amount of polymeric material (Kohane et al., 2006). This could also apply to the tumour microenvironment since microparticles injected directly into a tumour may be more likely to be retained with their larger size preventing redistribution. This approach has been utilised recently, using microparticles within an injectable hydrogel, to treat TNBC (Davoodi et al., 2017). Core-shell microparticles (ranging

from 12 – 18µm), encapsulating cisplatin and paclitaxel, were embedded into an injectable hydrogel (Davoodi et al., 2017). The use of the hydrogel serves many advantages such as providing a diffusion barrier to prevent premature release of the loaded drugs, preventing surgical site infection due to its inherent antibacterial properties, but most importantly, it retains the particles in the tumour resected cavity during the injection, following debulking (tumour removal) surgery (Davoodi et al., 2017) thus ensuring a localised delivery of the loaded drugs. The performance of the microparticle/hydrogel carrier was tested using three-dimensional, MDA-MB-231 spheroids. These *in vitro* tumour models are thought to more accurately recapitulate human solid tumour architecture and biology (Sant and Johnston, 2017). The microparticle/hydrogel carrier was found to provide a superior efficacy and reduction on spheroid growth compared to free-drug treatment (Davoodi et al., 2017). This demonstrates the use of microparticles in injectables, which do not rely on systemic delivery. Perhaps there is a use for CD95R-Fc in these sorts of treatments since coating particles could target them for cellular uptake, ensuring better intracellular drug delivery within the localised environment.

6.7. CD95R-Fc microparticles for transfection

Despite the implications discussed, a CD95R-Fc coated MP system could be useful as a method of transfection, since these particles have been shown here to be efficiently taken up by different cell types. PLGA microparticles can be loaded with many different types of cargo, not just toxic chemotherapeutics. For example, siRNAs, miRNAs or peptides. The system described here may provide useful for delivering such agents successfully into cells, without the toxicity and

cell death that standard transfection reagents can induce. An example of this has been shown by Haggag et al., who have used pegylated PLGA nanoparticles to deliver anti-Ran-GTPase peptides to MDA-MB-231 cells. Ran is a small RAS-related GTPase which is highly expressed in aggressive breast carcinoma, and these peptides were predicted to prevent Ran hydrolysis and activation by blocking activity of RCC1, which catalyses the exchange of GDP for GTP on the nucleotide binding pocket of Ran (Haggag et al., 2017). Although these peptides have suggested anti-Ran activity *in silico*, peptide activity was limited *in vitro* due to poor delivery and reduced bioavailability. Delivery of these peptides, enclosed in pegylated PLGA nanoparticles however (with a mean diameter of 182 – 227nm), led to 56.8 +/- 12.7% uptake by MDA-MB-231 cells and caused greater cell cycle arrest after 24 hours, compared to cells incubated with free peptide only (38% compared to 0.1% respectively) (Haggag et al., 2017). Western blot analysis confirmed the mechanism was via inhibition of Ran-GTP formation, which is essential for tumorigenesis and metastasis (Haggag et al., 2017).

6.8. Perspectives for Future Work

It has been demonstrated here that uptake of MPs into MDA-MB-231 cells does not occur via cell surface expression of CD95L. However, it would be important to test cell lines which have previously shown enhanced uptake of CD95R-Fc coated MPs, to further validate this finding. In the paper by Ateh et al., enhanced uptake was shown in human Daoy (medulloblastoma), human IGROV1 (ovarian cancer) and primary DRG sensory neurons (Ateh et al., 2011). An antibody for detecting CD95L has been validated here for use in Western blot, immunohistochemistry and flow cytometry, which could allow this to be done.

Additionally, the use of a positive control, such as Jurkat cells which endogenously express CD95L, would be a useful tool for comparison.

Finally, a global siRNA screen would be useful using the CD95R-Fc coated MP system in MDA-MB-231 cells to identify how the CD95R coat drives uptake into cells. Systematically knocking down genes in the human genome provides a powerful way to investigate the mechanism MP uptake and to identify any genes which aid or hinder uptake. Furthermore, it may identify any potential surface scavenger, complement or integrin receptors (see table 5.1) that may play a part in initialising uptake of these particles into cells. This is a key piece of information to discover and would allow this system to be tailored for uses outside of delivering chemotherapeutics.

Appendices

Appendix 1

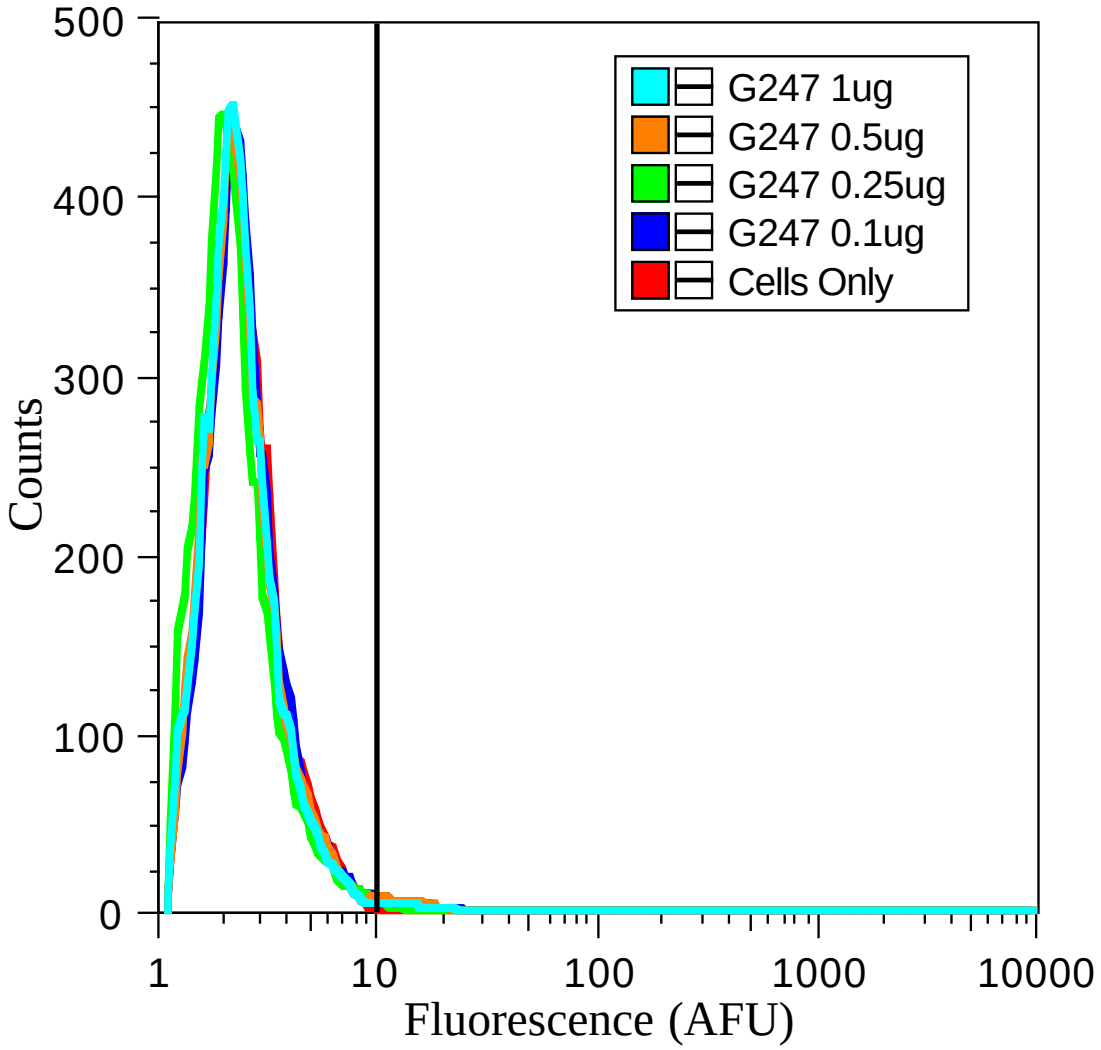

Supplementary Figure 1. Histogram displaying G247-4 antibody titration against untransfected HEK cells.
HEK293T cells were seeded on 6-well plates and left untransfected. Cells were harvested 48h later and 1 x 106 cells were incubated with different concentrations (0.1 – 1 µg) of primary antibody, mouse, anti-human CD95L G247-4 clone (BD Pharmingen), and goat, anti-mouse Alexa Fluor® 488 (Invitrogen). 10,000 cells of normal size and granularity were gated to eliminate cell debris. Results from representative experiments were overlain on the histogram, displaying distribution of fluorescence (arbitrary fluorescence units; AFU) against number of cells (counts) for all conditions. Cells were gated (black bar) to give percentage of positive cells and median fluorescence for the entire population was also calculated. Results for cells only (red) was 0.04% and 2.22 AFU, for 0.1 µg (blue) 1.6% and 2.25 AFU, 0.25 µg (green) 0.6% and 2.01 AFU, 0.5 µg (orange) 1.6% and 2.19 AFU and 1 µg (turquoise) 1.2% and 2.16 AFU. This demonstrates no non-specific binding of the primary antibody.

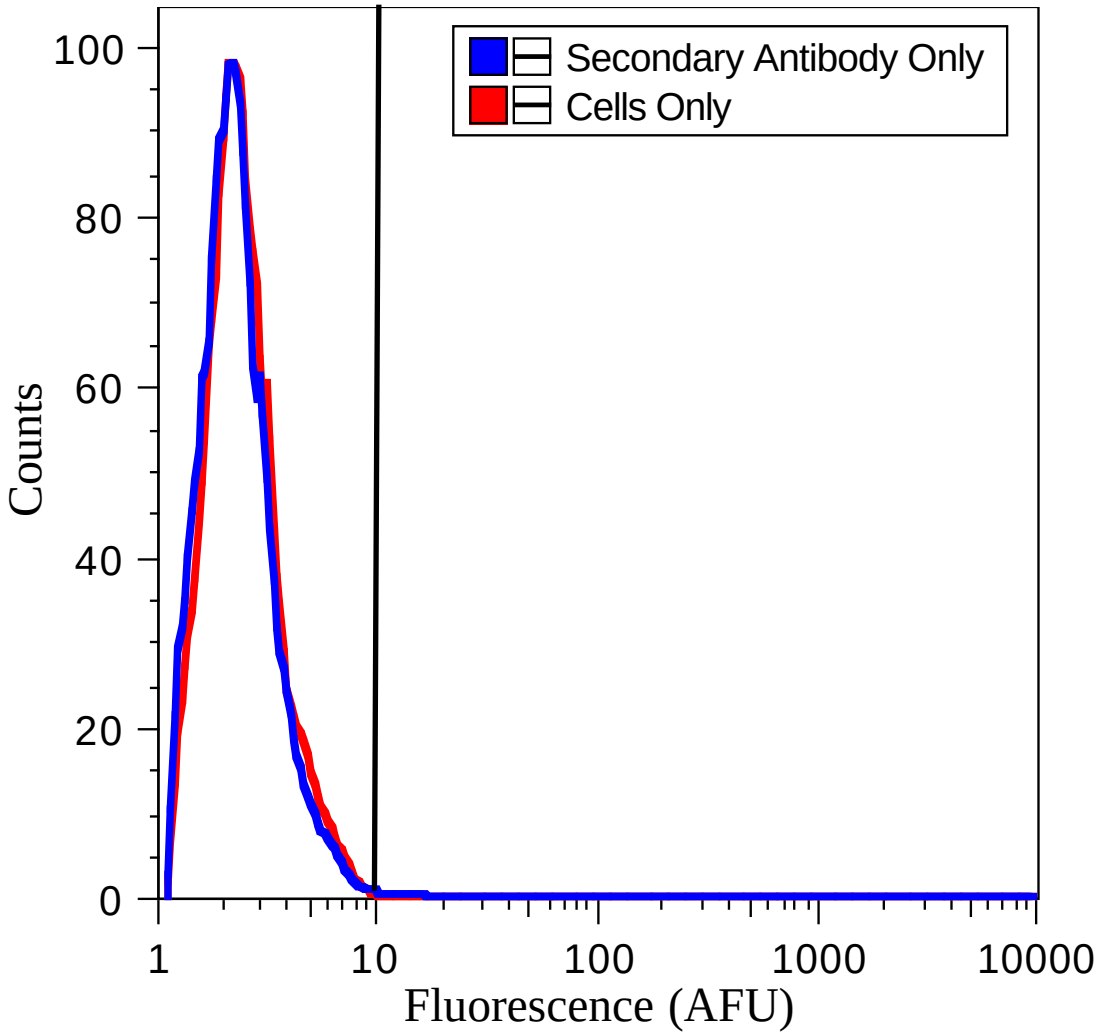

Supplementary Figure 2. Histogram displaying secondary antibody only control.
HEK293T cells were seeded on 6-well plates and left untransfected. Cells were harvested 48h later and 1 x 10^6 cells were incubated with goat, anti-mouse Alexa Fluor® 488 (Invitrogen). 10,000 cells of normal size and granularity were gated to eliminate cell debris. Results from representative experiments were overlain on the histogram, displaying distribution of fluorescence (arbitrary fluorescence units; AFU) against number of cells (counts) for all conditions. Cells were gated (black bar) to give percentage of positive cells and median fluorescence for the entire population was also calculated. Results for cells only (red) was 0.04% and 2.22 AFU, for secondary only (blue) 0.5% and 2.12 AFU. This demonstrates no non-specific binding of the secondary antibody.

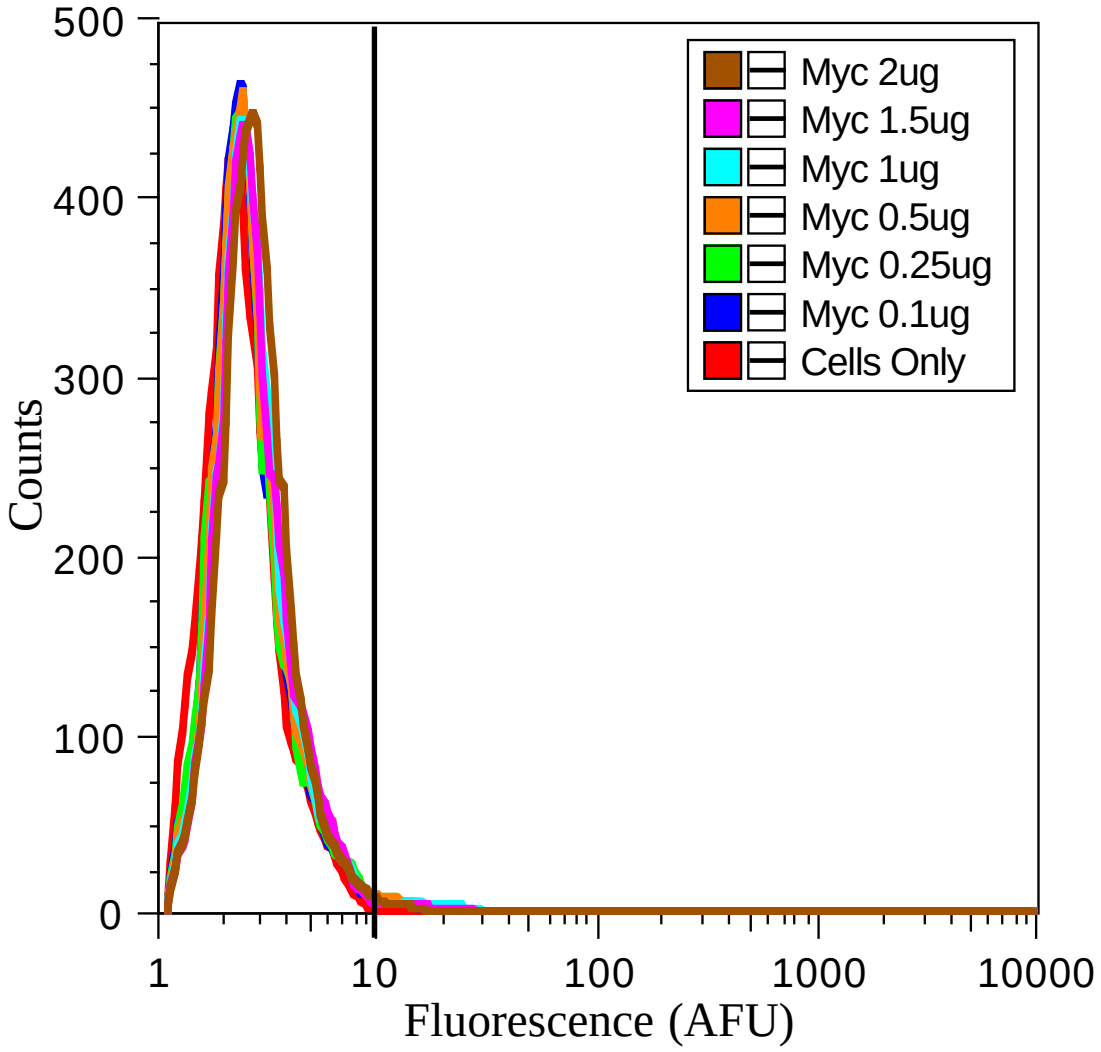

Supplementary Figure 3. Histogram displaying anti-c-MYC antibody titration against untransfected HEK cells.
HEK293T cells were seeded on 6-well plates and left untransfected. Cells were harvested 48h later and 1 x 10^6 cells were incubated with different concentrations (0.1 – 2 µg) of primary antibody mouse, anti-c-MYC (Sigma) and goat, anti-mouse Alexa Fluor® 488 (Invitrogen). 10,000 cells of normal size and granularity were gated to eliminate cell debris. Results from representative experiments were overlain on the histogram, displaying distribution of fluorescence (arbitrary fluorescence units; AFU) against number of cells (counts) for all conditions. Cells were gated (black bar) to give percentage of positive cells and median fluorescence for the entire population was also calculated. Results for cells only (red) was 0.04% and 2.22 AFU, for 0.1 µg (blue) 1% and 2.33 AFU, 0.25 µg (green) 1.3% and 2.35 AFU, 0.5 µg (orange) 1.3% and 2.39 AFU, 1 µg (turquoise) 1.7% and 2.47 AFU, 1.5 µg (pink) 1.3% and 2.49 AFU and 2 µg (brown) 1.1% and 2.59 AFU. This demonstrates no non-specific binding of the primary antibody.

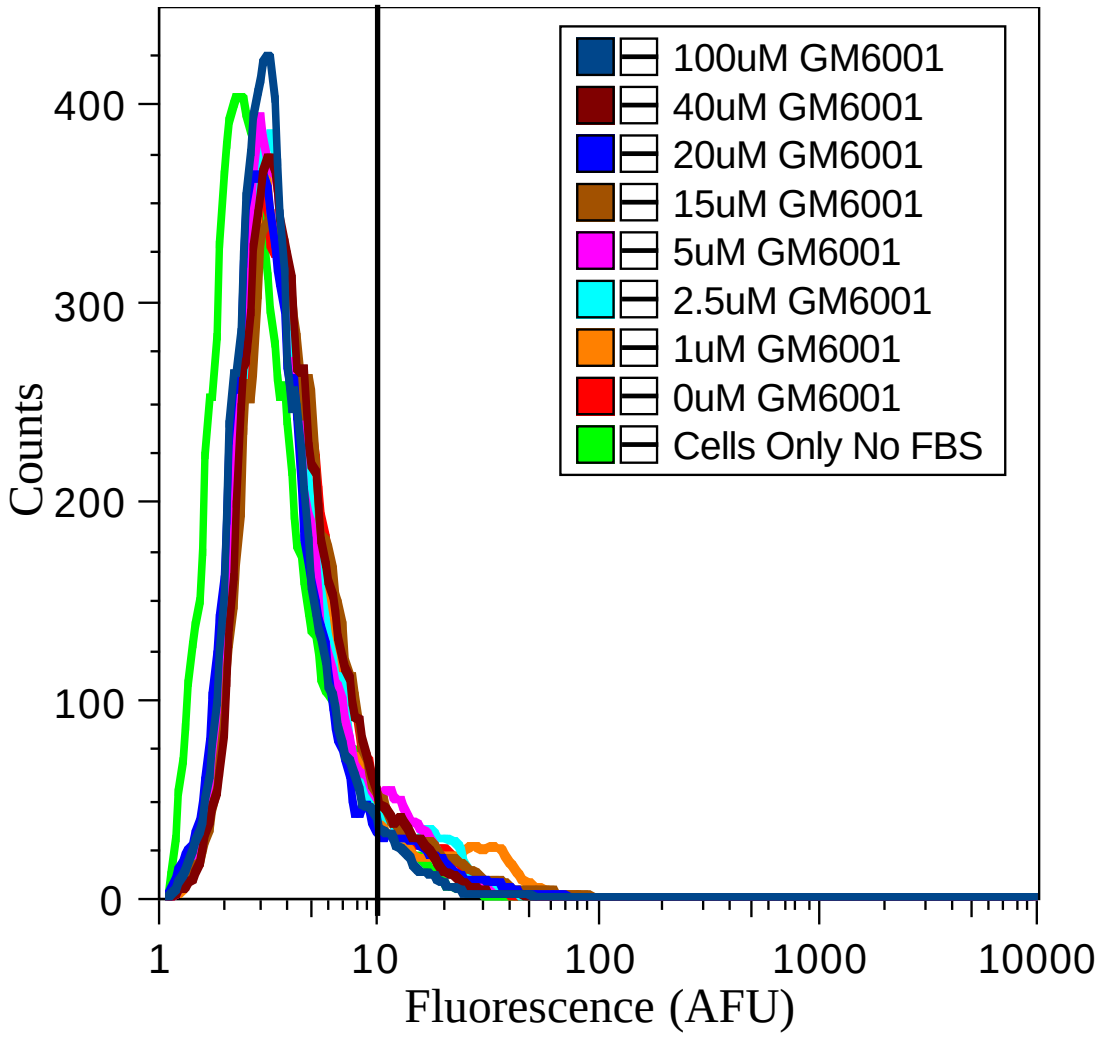

Supplementary Figure 4. Histogram displaying GM1006 inhibitor titration against CD95L-Myc-DDK expressing HEK cells.

HEK293T cells were seeded on 6-well plates, transfected with a vector coding for CD95L-Myc-DDK and incubated with different concentrations (0 µM – 100 µM) of GM1006 (Merck) inhibitor in FBS free media, 24 hours before harvesting. 1 x 10^6 cells were incubated with primary antibody mouse, anti-human CD95L G247-4 clone (BD Pharmingen) and goat, anti-mouse Alexa Fluor® 488 (Invitrogen). 10,000 cells of normal size and granularity were gated to eliminate cell debris. Results from representative experiments were overlain on the histogram, displaying distribution of fluorescence (arbitrary fluorescence units; AFU) against number of cells (counts) for all conditions. Cells were gated (black bar) to give percentage of positive cells and median fluorescence for the entire population was also calculated. Results for cells only (green) was 0.1% and 2.49 AFU, for 0 µM (red) 7% and 3.55 AFU, 1 µM (orange) 10% and 3.49 AFU, 2.5 µM (turquoise) 9% and 3.44 AFU, 5 µM (pink) 9% and 3.36 AFU, 15 µM (brown) 9% and 3.75 AFU, 20 µM (blue) 8% and 3.15 AFU, 40 µM (mauve) 7% and 3.57 AFU and 100 µM (dark blue) 5% and 3.13 AFU. 20 µM of GM1006 was selected, as recommended and used previously. GFP expressing cells were 60% positive (transfection efficiency; not shown).

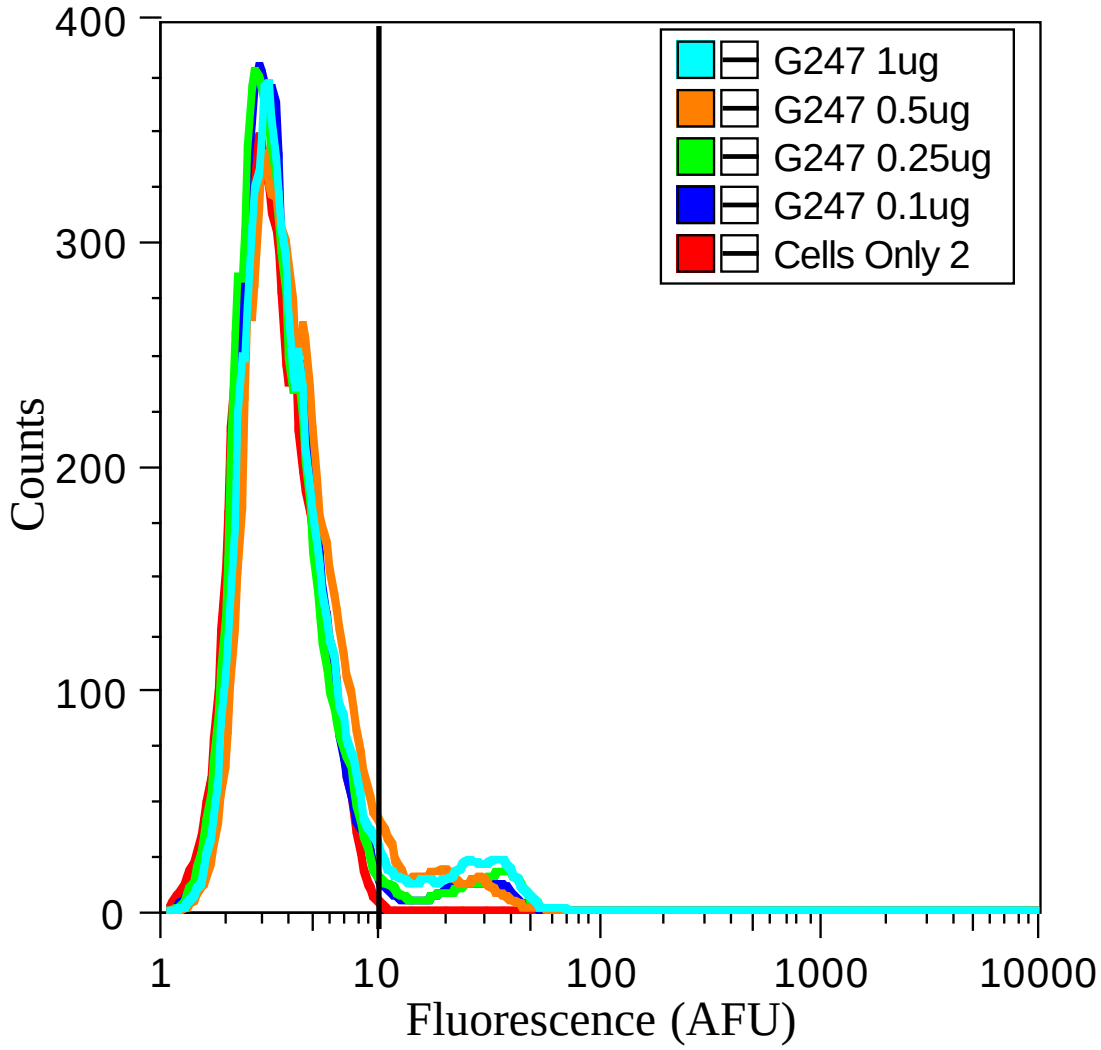

Supplementary Figure 5. Histogram displaying G247-4 antibody titration against CD95L-Myc-DDK expressing HEK cells, incubated with GM1006.

HEK293T cells were seeded on 6-well plates, transfected with a vector coding for CD95L-Myc-DDK and incubated with 20 µM GM1006 (Merck) inhibitor in FBS free media, 24 hours before harvesting. 1 x 10^6 cells were incubated with different concentrations (0.1 – 1 µg) of primary antibody, mouse, anti-human CD95L G247-4 clone (BD Pharmingen) and goat, anti-mouse Alexa Fluor® 488 (Invitrogen). 10,000 cells of normal size and granularity were gated to eliminate cell debris. Results from representative experiments were overlain on the histogram, displaying distribution of fluorescence (arbitrary fluorescence units; AFU) against number of cells (counts) for all conditions. Cells were gated (black bar) to give percentage of positive cells and median fluorescence for the entire population was also calculated. Results for cells only (red) was 0.1% and 3.22 AFU, for 0.1 µg (blue) 7% and 3.21 AFU, 0.25 µg (green) 5% and 3.14 AFU, 0.5 µg (orange) 7% and 3.64 AFU and 1 µg (turquoise) 8% and 3.39 AFU. 1 µg G247-4 was selected for further experiments. Population of positive cells detected is the same as the anti c-MYC antibody (Supp. Figure 6). GFP expressing cells were 51% positive (transfection efficiency; data not shown)

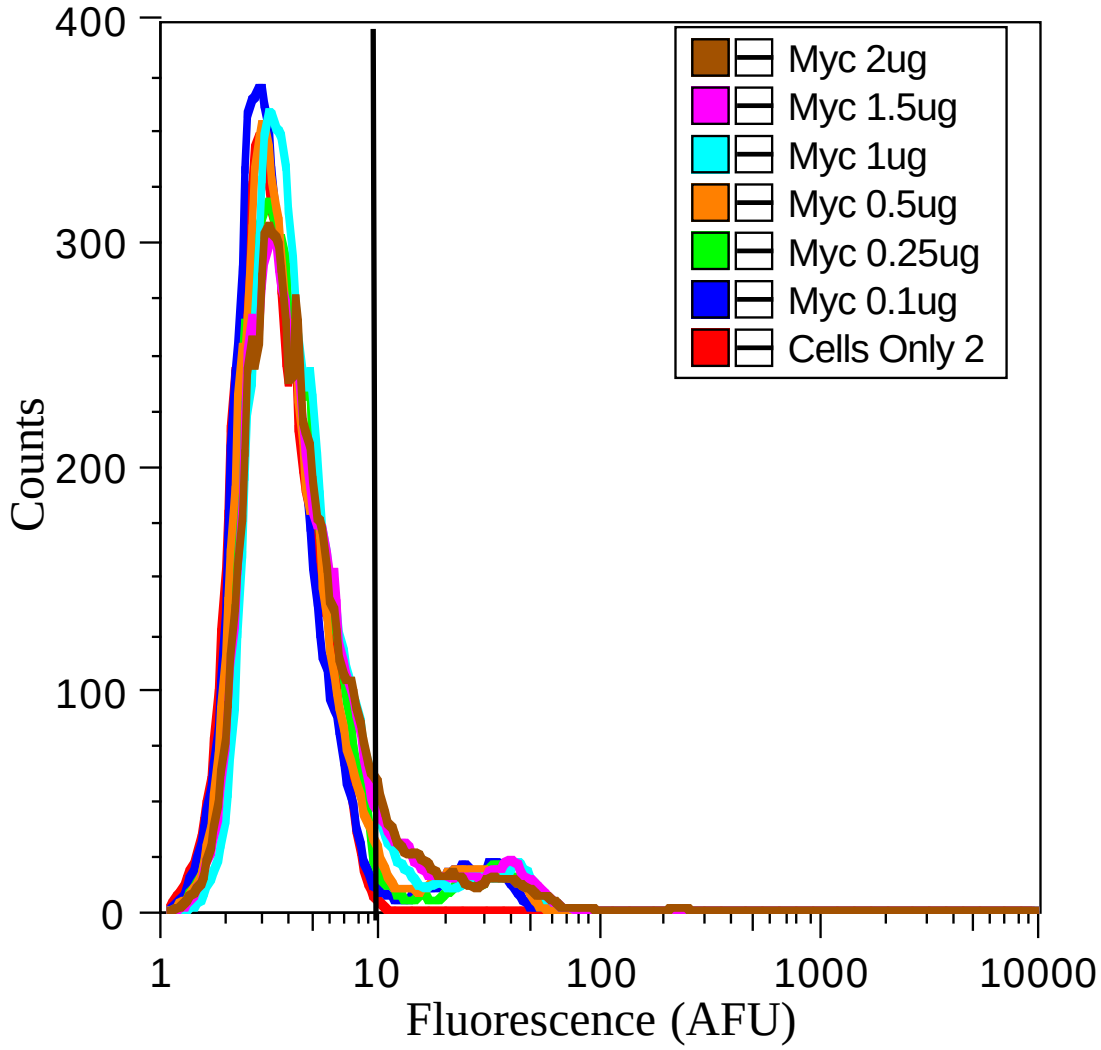

Supplementary Figure 6. Histogram displaying anti-c-MYC antibody titration against CD95L-Myc-DDK expressing HEK cells, incubated with GM1006.
HEK293T cells were seeded on 6-well plates, transfected with a vector coding for CD95L-Myc-DDK and incubated with 20 µM GM1006 (Merck) inhibitor in FBS free media, 24 hours before harvesting. 1 x 10^6 cells were incubated with different concentrations (0.1 – 2 µg) of primary antibody mouse, anti-c-MYC (Sigma) and goat, anti-mouse Alexa Fluor® 488 (Invitrogen) and goat, anti-mouse Alexa Fluor® 488 (Invitrogen). 10,000 cells of normal size and granularity were gated to eliminate cell debris. Results from representative experiments were overlain on the histogram, displaying distribution of fluorescence (arbitrary fluorescence units; AFU) against number of cells (counts) for all conditions. Cells were gated (black bar) to give percentage of positive cells and median fluorescence for the entire population was also calculated. Results for cells only (red) was 0.1% and 3.22 AFU, for 0.1 µg (blue) 6% and 3.12 AFU, 0.25 µg (green) 6% and 3.46 AFU, 0.5 µg (orange) 7% and 3.34 AFU, 1 µg (turquoise) 9% and 3.74 AFU, 1.5 µg (pink) 11% and 3.74 AFU and 2 µg (brown) 11% and 3.76 AFU. 1 µg anti-C-MYC was selected for further experiments, since non-specific binding was occurring with high concentrations (data not shown). Population of positive cells detected is the same as the G247-4 antibody (Supp. Figure 5). GFP expressing cells were 51% positive (transfection efficiency; data not shown).

CD95L Protein Sequence				
10	20	30	40	50
MQQPFNYPYP	QIYWVDSSAS	SPWAPPGTVL	PCPTSVPRRP	GQRRPPPPPP
60	70	80	90	100
PPPLPPPPPP	PPLPPLPLPP	LKKRGNHSTG	LCLLVMFFMV	LVALVGLGLG
110	120	130	140	150
MFQLFHLQKE	LAELRESTSQ	MHTASSLEKQ	IGHPSPPPEK	KELRKVAHLT
160	170	180	190	200
GKSNSRSMPL	EWEDTYGIVL	LSGVKYKKGG	LVINETGLYF	VYSKVYFRGQ
210	220	230	240	250
SCNNLPLSHK	VYMRNSKYPQ	DLVMMEGKMM	SYCTTGQMWA	RSSYLGAVFN
260	270	280		
LTSADHLYVN	VSELSLVNFE	ESQTFFGLYK L		

Supplementary Figure 7. Protein sequence of Human CD95L.
In blue – CD95L cytoplasmic domain, residues 1 to 80, green – transmembrane domain, residues 81 to 102 and red – extracellular domain, residues 103 to 281.

Appendix 2

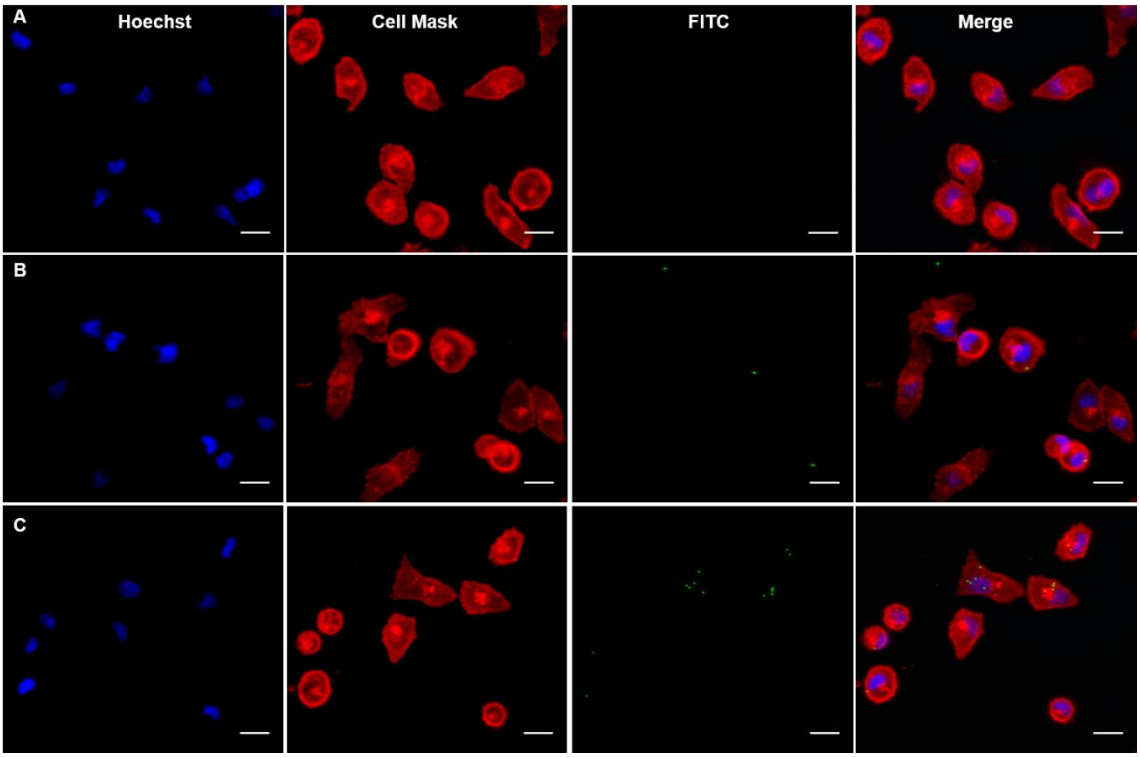

Supplementary Figure 8. MDA-MB-231 cells internalise more CD95R-Fc coated particles. MDA-MB-231 cells were incubated with no particles (PBS; negative control) (**A**) non-coated particles (**B**) or in-house CD95R-Fc coated particles (**C**) for 24 hours. Cells were then washed to remove non-internalised particles. Live, adhered cells were then stained for imaging. Cell nuclei were stained with Hoechst (blue) and plasma membranes with CellMask™ (red). Particles are fluorescent green and detected in the FITC channel. Scale bars, 20µm. Images representative of the whole population are shown in each case.

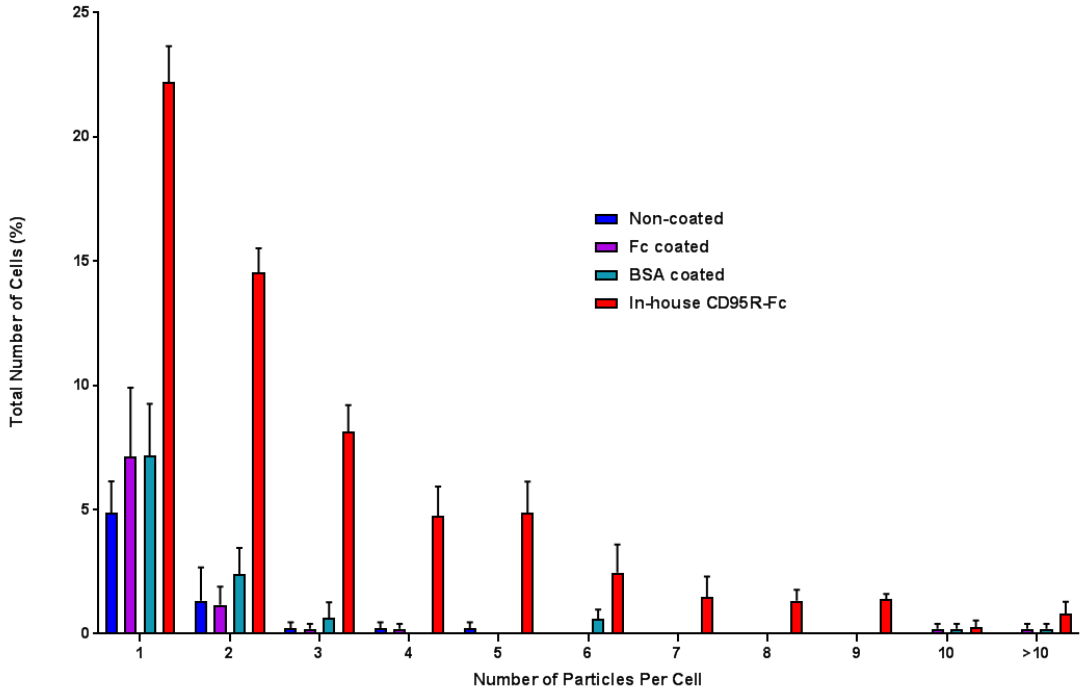

Supplementary Figure 9. Confocal imaging demonstrates enhanced CD95R-Fc coated MP uptake in MDA-MB-231 cells, with more cells internalising a higher number of particles. Cells were incubated with fluorescent, 0.5µm MPs for 24 hrs. Live, adhered cells were then stained for imaging on an IN Cell Analyser 6000 (GE Healthcare). Cell nuclei were stained with Hoechst (blue) and plasma membranes with CellMask™ (red). Particles are fluorescent green and detected in the FITC channel. Mean and SEM values are from three independent, repeat experiments (n=3). The number of particles internalised by each cell (1, 2, 3, 4, 5, 6, 7, 8, 9, 10 or ≥ 10), expressed as a percentage of total cell number, was compared for non-coated particles (blue), Fc coated particles (purple), BSA coated particles (green) and in-house CD95R-Fc coated particles (red). With a CD95R-Fc coating, cells internalise more particles, and more particles per cell across all particle numbers.

Bibliography

Abrahams, V. M., Straszewski, S. L., Kamsteeg, M., Hanczaruk, B., Schwartz, P. E., Rutherford, T. J. and Mor, G. (2003) 'Epithelial ovarian cancer cells secrete functional Fas ligand', *Cancer research,* 63(17), pp. 5573-5581.

Adams, A. J., Warram, J. M., Chaudhuri, T. R. and Zinn, K. R. (2006) 'Fc receptors (FcR) on the surface of human breast cancer cells may facilitate the cytotoxic effects of hTRA-8, a new humanized apoptosis-inducing antibody', *Proceedings of the American Association for Cancer Research,* 2006(1), pp. 1291.

Adrain, C., Zettl, M., Christova, Y., Taylor, N. and Freeman, M. (2012) 'Tumor necrosis factor signaling requires iRhom2 to promote trafficking and activation of TACE', *Science,* 335(6065), pp. 225-228.

Andersen, J. T. and Sandlie, I. J. D. m. a. p. (2009) 'The versatile MHC class I-related FcRn protects IgG and albumin from degradation: implications for development of new diagnostics and therapeutics', 24(4), pp. 318-332.

Anderson, J. M. and Shive, M. S. (2012) 'Biodegradation and biocompatibility of PLA and PLGA microspheres', *Advanced drug delivery reviews,* 64, pp. 72-82.

Andreola, G., Rivoltini, L., Castelli, C., Huber, V., Perego, P., Deho, P., Squarcina, P., Accornero, P., Lozupone, F. and Lugini, L. (2002) 'Induction of lymphocyte apoptosis by tumor cell secretion of FasL-bearing microvesicles', *The Journal of experimental medicine,* 195(10), pp. 1303-1316.

Arlein, W. J., Shearer, J. D. and Caldwell, M. D. (1998) 'Continuity between wound macrophage and fibroblast phenotype: analysis of wound fibroblast phagocytosis', *American Journal of Physiology-Regulatory, Integrative and Comparative Physiology,* 275(4), pp. R1041-R1048.

Ashkenazi, A. (2008) 'Targeting the extrinsic apoptosis pathway in cancer', *Cytokine & growth factor reviews,* 19(3), pp. 325-331.

Askenasy, N., Yolcu, E. S., Yaniv, I. and Shirwan, H. (2005) 'Induction of tolerance using Fas ligand: a double-edged immunomodulator', *Blood,* 105(4), pp. 1396-1404.

Ateh, D. D., Leinster, V. H., Lambert, S. R., Shah, A., Khan, A., Walklin, H. J., Johnstone, J. V., Ibrahim, N. I., Kadam, M. M. and Malik, Z. (2011) 'The intracellular uptake of CD95 modified paclitaxel-loaded poly (lactic-co-glycolic acid) microparticles', *Biomaterials,* 32(33), pp. 8538-8547.

Baban, D. F. and Seymour, L. W. (1998) 'Control of tumour vascular permeability', *Advanced drug delivery reviews,* 34(1), pp. 109-119.

Baer, J., Jones, C., Spitzer, S. and Russo, H. (1967) 'THE POTASSIUM-SPARING AND NATRIURETIC ACTIVITY OF N-AMIDINO-3, 5-DIAMINO-6-CHLOROPYRAZINECAR-BOXAMIDE HYDROCHLORIDE DIHYDRATE (AMILORIDE HYDROCHLORIDE)', *Journal of Pharmacology and Experimental Therapeutics,* 157(2), pp. 472-485.

Bai, C., Connolly, B., Metzker, M. L., Hilliard, C. A., Liu, X., Sandig, V., Soderman, A., Galloway, S. M., Liu, Q. and Austin, C. P. (2000) 'Overexpression of M68/DcR3 in human gastrointestinal tract tumors independent of gene amplification and its location in a four-gene cluster', *Proceedings of the National Academy of Sciences,* 97(3), pp. 1230-1235.

Bangs (1999) 'Technote 202: Microsphere Aggregation', *Bangs Laboratories: Fishers, IN*.

Bangs (2008a) 'Technote 204: Adsorption to Microspheres', *Bangs Laboratories: Fishers, IN*.
Bangs (2008b) 'Technote 205: Covalent Coupling', *Bangs Laboratories: Fishers, IN*.
Bangs (2013) 'Technote 103: Fluorescent / Dyed Microspheres', *Bangs Laboratories: Fishers, IN*.
Barnhart, B. C., Legembre, P., Pietras, E., Bubici, C., Franzoso, G. and Peter, M. E. (2004) 'CD95 ligand induces motility and invasiveness of apoptosis-resistant tumor cells', *The EMBO journal,* 23(15), pp. 3175-3185.
Bibby, M. (2004) 'Orthotopic models of cancer for preclinical drug evaluation: advantages and disadvantages', *European journal of cancer,* 40(6), pp. 852-857.
Blott, E. J., Bossi, G., Clark, R., Zvelebil, M. and Griffiths, G. M. (2001) 'Fas ligand is targeted to secretory lysosomes via a proline-rich domain in its cytoplasmic tail', *Journal of Cell Science,* 114(13), pp. 2405-2416.
Bornhorst, J. A. and Falke, J. J. (2000) '[16] Purification of proteins using polyhistidine affinity tags', *Methods in enzymology*: Elsevier, pp. 245-254.
Botelho, R. J. and Grinstein, S. (2011) 'Phagocytosis', *Current Biology,* 21(14), pp. R533-R538.
Bray, F., Ferlay, J., Soerjomataram, I., Siegel, R. L., Torre, L. A. and Jemal, A. (2018) 'Global cancer statistics 2018: GLOBOCAN estimates of incidence and mortality worldwide for 36 cancers in 185 countries', *CA: a cancer journal for clinicians*.
Brondyk, W. H. (2009) 'Selecting an appropriate method for expressing a recombinant protein', *Methods in enzymology*: Elsevier, pp. 131-147.
Byrne, J. A., Strautnieks, S. S., Ihrke, G., Pagani, F., Knisely, A., Linton, K. J., Mieli-Vergani, G. and Thompson, R. J. J. H. (2009) 'Missense mutations and single nucleotide polymorphisms in ABCB11 impair bile salt export pump processing and function or disrupt pre-messenger RNA splicing', 49(2), pp. 553-567.
Cahuzac, N., Baum, W., Kirkin, V., Conchonaud, F., Wawrezinieck, L., Marguet, D., Janssen, O., Zörnig, M. and Hueber, A.-O. (2006) 'Fas ligand is localized to membrane rafts, where it displays increased cell death–inducing activity', *Blood,* 107(6), pp. 2384-2391.
Carter, P. J. J. E. c. r. (2011) 'Introduction to current and future protein therapeutics: a protein engineering perspective', 317(9), pp. 1261-1269.
Ceppi, P., Hadji, A., Kohlhapp, F. J., Pattanayak, A., Hau, A., Liu, X., Liu, H., Murmann, A. E. and Peter, M. E. (2014) 'CD95 and CD95L promote and protect cancer stem cells', *Nature communications,* 5.
Chellat, F., Merhi, Y., Moreau, A. and Yahia, L. H. (2005) 'Therapeutic potential of nanoparticulate systems for macrophage targeting', *Biomaterials,* 26(35), pp. 7260-7275.
Chen, J.-J., Sun, Y. and Nabel, G. J. (1998) 'Regulation of the proinflammatory effects of Fas ligand (CD95L)', *Science,* 282(5394), pp. 1714-1717.
Chen, L., Park, S.-M., Tumanov, A. V., Hau, A., Sawada, K., Feig, C., Turner, J. R., Fu, Y.-X., Romero, I. L. and Lengyel, E. (2010) 'CD95 promotes tumour growth', *Nature,* 465(7297), pp. 492-496.
Cheng, J., Zhou, T., Liu, C., Shapiro, J. P., Brauer, M. J., Kiefer, M. C., Barr, P. J. and Mountz, J. D. (1994) 'Protection from Fas-mediated apoptosis by a soluble form of the Fas molecule', *Science,* 263(5154), pp. 1759-1762.
Chodorge, M., Züger, S., Stirnimann, C., Briand, C., Jermutus, L., Grütter, M. and Minter, R. (2012) 'A series of Fas receptor agonist antibodies that

demonstrate an inverse correlation between affinity and potency', *Cell Death & Differentiation,* 19(7), pp. 1187-1195.

Clogston, J. D. and Patri, A. K. (2011) 'Zeta potential measurement', *Characterization of nanoparticles intended for drug delivery*: Springer, pp. 63-70.

Contreras-Gómez, A., Sánchez-Mirón, A., García-Camacho, F., Molina-Grima, E. and Chisti, Y. (2014) 'Protein production using the baculovirus-insect cell expression system', *Biotechnology progress,* 30(1), pp. 1-18.

Coopman, P., Thomas, D., Gehlsen, K. and Mueller, S. (1996) 'Integrin alpha 3 beta 1 participates in the phagocytosis of extracellular matrix molecules by human breast cancer cells', *Molecular biology of the cell,* 7(11), pp. 1789-1804.

Coward, J., Kulbe, H., Chakravarty, P., Leader, D. A., Vassileva, V., Leinster, D. A., Thompson, R., Schioppa, T., Nemeth, J. A. and Vermeulin, J. (2011) 'Interleukin-6 as a therapeutic target in human ovarian cancer', *Clinical cancer research*, pp. clincanres. 0945.2011.

Cruz, P. E., Martins, P. C., Alves, P. M., Peixoto, C. C., Santos, H., Moreira, J. L. and Carrondo, M. J. (1999) 'Proteolytic activity in infected and noninfected insect cells: Degradation of HIV-1 Pr55gag particles', *Biotechnology and bioengineering,* 65(2), pp. 133-143.

Cui, Z., Hsu, C.-H. and Mumper, R. J. (2003) 'Physical characterization and macrophage cell uptake of mannan-coated nanoparticles', *Drug development and industrial pharmacy,* 29(6), pp. 689-700.

Czajkowsky, D. M., Hu, J., Shao, Z. and Pleass, R. J. (2012) 'Fc-fusion proteins: new developments and future perspectives', *EMBO molecular medicine,* 4(10), pp. 1015-1028.

Dangoria, N. S., Breau, W. C., Anderson, H. A., Cishek, D. M. and Norkin, L. C. (1996) 'Extracellular simian virus 40 induces an ERK/MAP kinase-independent signalling pathway that activates primary response genes and promotes virus entry', *Journal of general virology,* 77(9), pp. 2173-2182.

Danhier, F., Feron, O. and Préat, V. (2010) 'To exploit the tumor microenvironment: Passive and active tumor targeting of nanocarriers for anti-cancer drug delivery', *Journal of Controlled Release,* 148(2), pp. 135-146.

Davoodi, P., Ng, W. C., Srinivasan, M. P. and Wang, C. H. (2017) 'Codelivery of anti-cancer agents via double-walled polymeric microparticles/injectable hydrogel: A promising approach for treatment of triple negative breast cancer', *Biotechnology and bioengineering,* 114(12), pp. 2931-2946.

Dawes, G., Fratila-Apachitei, L., Mulia, K., Apachitei, I., Witkamp, G.-J. and Duszczyk, J. (2009) 'Size effect of PLGA spheres on drug loading efficiency and release profiles', *Journal of Materials Science: Materials in Medicine,* 20(5), pp. 1089-1094.

De Laurentiis, M., Cancello, G., D'Agostino, D., Giuliano, M., Giordano, A., Montagna, E., Lauria, R., Forestieri, V., Esposito, A. and Silvestro, L. (2008) 'Taxane-based combinations as adjuvant chemotherapy of early breast cancer: a meta-analysis of randomized trials', *Journal of clinical oncology,* 26(1), pp. 44-53.

de Weger, V. A., Beijnen, J. H. and Schellens, J. H. (2014) 'Cellular and clinical pharmacology of the taxanes docetaxel and paclitaxel–a review', *Anti-cancer drugs,* 25(5), pp. 488-494.

Denkert, C., Liedtke, C., Tutt, A. and von Minckwitz, G. (2017) 'Molecular alterations in triple-negative breast cancer—the road to new treatment strategies', *The Lancet,* 389(10087), pp. 2430-2442.

Desai, M. P., Labhasetwar, V., Walter, E., Levy, R. J. and Amidon, G. L. (1997) 'The mechanism of uptake of biodegradable microparticles in Caco-2 cells is size dependent', *Pharmaceutical research,* 14(11), pp. 1568-1573.

Dhankhar, R., Vyas, S. P., Jain, A. K., Arora, S., Rath, G. and Goyal, A. K. (2010) 'Advances in novel drug delivery strategies for breast cancer therapy', *Artificial Cells, Blood Substitutes, and Biotechnology,* 38(5), pp. 230-249.

Dharmawardhane, S., Sanders, L. C., Martin, S. S., Daniels, R. H. and Bokoch, G. M. (1997) 'Localization of p21-activated kinase 1 (PAK1) to pinocytic vesicles and cortical actin structures in stimulated cells', *The Journal of cell biology,* 138(6), pp. 1265-1278.

Dhein, J., Walczak, H., Bäumler, C., Debatin, K.-M. and Krammer, P. H. (1995) 'Autocrine T-cell suicide mediated by APO-1/(Fas/CD95)', *Nature,* 373(6513), pp. 438-441.

Domcke, S., Sinha, R., Levine, D. A., Sander, C. and Schultz, N. (2013) 'Evaluating cell lines as tumour models by comparison of genomic profiles', *Nature communications,* 4, pp. 2126.

Dougherty, W. G., Cary, S. M. and Dawn Parks, T. (1989) 'Molecular genetic analysis of a plant virus polyprotein cleavage site: a model', *Virology,* 171(2), pp. 356-364.

Dutta, D., Salifu, M., Sirianni, R. W. and Stabenfeldt, S. E. (2016) 'Tailoring sub-micron PLGA particle release profiles via centrifugal fractioning', *Journal of Biomedical Materials Research Part A,* 104(3), pp. 688-696.

Faulkner, P., Kuzio, J., Williams, G. V. and Wilson, J. A. (1997) 'Analysis of p74, a PDV envelope protein of Autographa californica nucleopolyhedrovirus required for occlusion body infectivity in vivo', *Journal of General Virology,* 78(12), pp. 3091-3100.

Ferguson, S. M. and De Camilli, P. (2012) 'Dynamin, a membrane-remodelling GTPase', *Nature reviews Molecular cell biology,* 13(2), pp. 75.

Fletcher, J. I., Haber, M., Henderson, M. J. and Norris, M. D. (2010) 'ABC transporters in cancer: more than just drug efflux pumps', *Nature Reviews Cancer,* 10(2), pp. 147-156.

Frykberg, E. R. (1999) 'Lobular carcinoma in situ of the breast', *The breast journal,* 5(5), pp. 296-303.

Fulda, S. and Debatin, K. (2006) 'Extrinsic versus intrinsic apoptosis pathways in anticancer chemotherapy', *Oncogene,* 25(34), pp. 4798-4811.

Ganguly, B. N. 'Nanomaterials in Bio-Medical Applications: A Novel approach'. Materials Research Forum LLC.

Gesbert, F., Sauvonnet, N. and Dautry-Varsat, A. (2004) 'Clathrin-independent endocytosis and signalling of interleukin 2 receptors', *Signalling from Internalized Growth Factor Receptors*: Springer, pp. 119-148.

Ghose, S., Zhang, J., Conley, L., Caple, R., Williams, K. P. and Cecchini, D. J. B. p. (2014) 'Maximizing binding capacity for protein A chromatography', 30(6), pp. 1335-1340.

Gilleron, J., Querbes, W., Zeigerer, A., Borodovsky, A., Marsico, G., Schubert, U., Manygoats, K., Seifert, S., Andree, C. and Stöter, M. (2013) 'Image-based analysis of lipid nanoparticle–mediated siRNA delivery, intracellular trafficking and endosomal escape', *Nature biotechnology,* 31(7), pp. 638.

Glebov, O. O., Bright, N. A. and Nichols, B. J. (2006) 'Flotillin-1 defines a clathrin-independent endocytic pathway in mammalian cells', *Nature cell biology,* 8(1), pp. 46.

Glukhova, X. A., Trizna, J. A., Proussakova, O. V., Gogvadze, V. and Beletsky, I. P. (2018) 'Impairment of Fas-ligand–caveolin-1 interaction inhibits Fas-ligand translocation to rafts and Fas-ligand-induced cell death', *Cell death & disease,* 9(2), pp. 73.

Gluzman, Y. (1981) 'SV40-transformed simian cells support the replication of early SV40 mutants', *Cell,* 23(1), pp. 175-182.

Gratas, C., Tohma, Y., Meir, E. G. V., Klein, M., Tenan, M., Ishii, N., Tachibana, O., Kleihues, P. and Ohgaki, H. (1997) 'Fas ligand expression in glioblastoma cell lines and primary astrocytic brain tumors', *Brain pathology,* 7(3), pp. 863-869.

Gratton, S. E., Ropp, P. A., Pohlhaus, P. D., Luft, J. C., Madden, V. J., Napier, M. E. and DeSimone, J. M. (2008) 'The effect of particle design on cellular internalization pathways', *Proceedings of the National Academy of Sciences,* 105(33), pp. 11613-11618.

Gregory, C. D. and Pound, J. D. (2010) 'Microenvironmental influences of apoptosis in vivo and in vitro', *Apoptosis,* 15(9), pp. 1029-1049.

Griffith, T. S., Brunner, T., Fletcher, S. M., Green, D. R. and Ferguson, T. A. (1995) 'Fas ligand-induced apoptosis as a mechanism of immune privilege', *Science,* 270(5239), pp. 1189-1192.

Hadji, A., Ceppi, P., Murmann, A. E., Brockway, S., Pattanayak, A., Bhinder, B., Hau, A., De Chant, S., Parimi, V. and Kolesza, P. (2014) 'Death Induced by CD95 or CD95 Ligand Elimination', *Cell reports,* 7(1), pp. 208-222.

Hage, D. S., Anguizola, J. A., Bi, C., Li, R., Matsuda, R., Papastavros, E., Pfaunmiller, E., Vargas, J. and Zheng, X. J. J. o. p. a. b. a. (2012) 'Pharmaceutical and biomedical applications of affinity chromatography: recent trends and developments', 69, pp. 93-105.

Hage, D. S. J. C. c. (1999) 'Affinity chromatography: a review of clinical applications', 45(5), pp. 593-615.

Haggag, Y. A., Matchett, K. B., Dakir, E.-H., Buchanan, P., Osman, M. A., Elgizawy, S. A., El-Tanani, M., Faheem, A. M. and McCarron, P. A. (2017) 'Nano-encapsulation of a novel anti-Ran-GTPase peptide for blockade of regulator of chromosome condensation 1 (RCC1) function in MDA-MB-231 breast cancer cells', *International journal of pharmaceutics,* 521(1-2), pp. 40-53.

Hall, S. E., Savill, J. S., Henson, P. M. and Haslett, C. (1994) 'Apoptotic neutrophils are phagocytosed by fibroblasts with participation of the fibroblast vitronectin receptor and involvement of a mannose/fucose-specific lectin', *The Journal of Immunology,* 153(7), pp. 3218-3227.

Han, C. Z., Juncadella, I. J., Kinchen, J. M., Buckley, M. W., Klibanov, A. L., Dryden, K., Onengut-Gumuscu, S., Erdbrügger, U., Turner, S. D. and Shim, Y. M. (2016) 'Macrophages redirect phagocytosis by non-professional phagocytes and influence inflammation', *Nature,* 539(7630), pp. 570.

Harris, G., Pinder, S. and Ellis, I. (2004) 'Ductal carcinoma in situ: diagnosis and classification', *Current Diagnostic Pathology,* 10(3), pp. 204-210.

Harrison, R. L. and Jarvis, D. L. (2006) 'Protein N-Glycosylation in the Baculovirus–Insect Cell Expression System and Engineering of Insect Cells to Produce “Mammalianized” Recombinant Glycoproteins', *Advances in virus research,* 68, pp. 159-191.

Hawtin, R. E., Arnold, K., Ayres, M. D., de A. Zanotto, P. M., Howard, S. C., Gooday, G. W., Chappell, L. H., Kitts, P. A., King, L. A. and Possee, R. D. (1995) 'Identification and preliminary characterization of a chitinase gene in the Autographa californica nuclear polyhedrosis virus genome', *Virology,* 212(2), pp. 673-685.

Hawtin, R. E., Zarkowska, T., Arnold, K., Thomas, C. J., Gooday, G. W., King, L. A., Kuzio, J. A. and Possee, R. D. (1997) 'Liquefaction ofAutographa californicaNucleopolyhedrovirus-Infected Insects Is Dependent on the Integrity of Virus-Encoded Chitinase and Cathepsin Genes', *Virology,* 238(2), pp. 243-253.

He, Y., Wang, K. and Yan, N. (2014) 'The recombinant expression systems for structure determination of eukaryotic membrane proteins', *Protein & cell,* 5(9), pp. 658-672.

Healthcare, G. 2007. PD-10 Desalting Columns. Uppsala, Svíþjóð: GE Healthcare.

Hirschberg, C. B., Robbins, P. W. and Abeijon, C. 1998. Transporters of nucleotide sugars, ATP, and nucleotide sulfate in the endoplasmic reticulum and Golgi apparatus. Annual Reviews 4139 El Camino Way, PO Box 10139, Palo Alto, CA 94303-0139, USA.

Hitchman, R. B., Possee, R. D., Crombie, A. T., Chambers, A., Ho, K., Siaterli, E., Lissina, O., Sternard, H., Novy, R. and Loomis, K. (2010) 'Genetic modification of a baculovirus vector for increased expression in insect cells', *Cell biology and toxicology,* 26(1), pp. 57-68.

Hitchman, R. B., Possee, R. D. and King, L. A. (2009) 'Baculovirus expression systems for recombinant protein production in insect cells', *Recent patents on biotechnology,* 3(1), pp. 46-54.

Hober, S., Nord, K. and Linhult, M. (2007) 'Protein A chromatography for antibody purification', *Journal of Chromatography B,* 848(1), pp. 40-47.

Hom, L., Ohkawa, T., Trudeau, D. and Volkman, L. (2002) 'Autographa californica M nucleopolyhedrovirus ProV-CATH is activated during infected cell death', *Virology,* 296(2), pp. 212-218.

Hsu, Y., Kuo, P., Tzeng, W. and Lin, C. (2006) 'Chalcone inhibits the proliferation of human breast cancer cell by blocking cell cycle progression and inducing apoptosis', *Food and chemical toxicology,* 44(5), pp. 704-713.

Hu, X. and Beeton, C. (2010) 'Detection of functional matrix metalloproteinases by zymography', *Journal of visualized experiments: JoVE,* (45).

Huang, X. and Brazel, C. S. (2001) 'On the importance and mechanisms of burst release in matrix-controlled drug delivery systems', *Journal of controlled release,* 73(2-3), pp. 121-136.

Ichimura, T., Asseldonk, E. J., Humphreys, B. D., Gunaratnam, L., Duffield, J. S. and Bonventre, J. V. (2008) 'Kidney injury molecule–1 is a phosphatidylserine receptor that confers a phagocytic phenotype on epithelial cells', *The Journal of clinical investigation,* 118(5), pp. 1657-1668.

Igney, F. H. and Krammer, P. H. (2005) 'Tumor counterattack: fact or fiction?', *Cancer Immunology, Immunotherapy,* 54(11), pp. 1127-1136.

Ivanov, A. I. (2008) 'Pharmacological inhibition of endocytic pathways: is it specific enough to be useful?', *Exocytosis and Endocytosis*: Springer, pp. 15-33.

Iverson, S. L. and Orrenius, S. (2004) 'The cardiolipin–cytochrome< i> c</i> interaction and the mitochondrial regulation of apoptosis', *Archives of biochemistry and biophysics,* 423(1), pp. 37-46.

Jain, R. A., Rhodes, C. T., Railkar, A. M., Malick, A. W. and Shah, N. H. (2000) 'Controlled release of drugs from injectable in situ formed biodegradable PLGA microspheres: effect of various formulation variables', *European journal of pharmaceutics and biopharmaceutics,* 50(2), pp. 257-262.

Je, Y. H., Chang, J. H., Choi, J. Y., Roh, J. Y., Jin, B. R., O'reilly, D. R. and Kang, S. K. J. B. l. (2001) 'A defective viral genome maintained in Escherichia coli for the generation of baculovirus expression vectors', 23(8), pp. 575-582.

Jehle, J. A., Blissard, G., Bonning, B., Cory, J., Herniou, E., Rohrmann, G., Theilmann, D., Thiem, S. and Vlak, J. (2006) 'On the classification and nomenclature of baculoviruses: a proposal for revision', *Archives of virology,* 151(7), pp. 1257-1266.

Juncadella, I. J., Kadl, A., Sharma, A. K., Shim, Y. M., Hochreiter-Hufford, A., Borish, L. and Ravichandran, K. S. (2013) 'Apoptotic cell clearance by bronchial epithelial cells critically influences airway inflammation', *Nature,* 493(7433), pp. 547.

Kaba, S. A., Salcedo, A. M., Wafula, P. O., Vlak, J. M. and van Oers, M. M. (2004) 'Development of a chitinase and v-cathepsin negative bacmid for improved integrity of secreted recombinant proteins', *Journal of virological methods,* 122(1), pp. 113-118.

Kaksonen, M. and Roux, A. (2018) 'Mechanisms of clathrin-mediated endocytosis', *Nature Reviews Molecular Cell Biology*.

Kalimutho, M., Parsons, K., Mittal, D., López, J. A., Srihari, S. and Khanna, K. K. (2015) 'Targeted therapies for triple-negative breast cancer: combating a stubborn disease', *Trends in pharmacological sciences,* 36(12), pp. 822-846.

Kanno, S., Furuyama, A. and Hirano, S. (2007) 'A murine scavenger receptor MARCO recognizes polystyrene nanoparticles', *Toxicological sciences,* 97(2), pp. 398-406.

Kassahn, D., Nachbur, U., Conus, S., Micheau, O., Schneider, P., Simon, H.-U. and Brunner, T. (2009) 'Distinct requirements for activation-induced cell surface expression of preformed Fas/CD95 ligand and cytolytic granule markers in T cells', *Cell death and differentiation,* 16(1), pp. 115.

Kirkin, V., Cahuzac, N., Guardiola-Serrano, F., Huault, S., Lückerath, K., Friedmann, E., Novac, N., Wels, W., Martoglio, B. and Hueber, A. (2007) 'The Fas ligand intracellular domain is released by ADAM10 and SPPL2a cleavage in T-cells', *Cell Death & Differentiation,* 14(9), pp. 1678-1687.

Kitts, P. A., Ayres, M. D. and Possee, R. D. (1990) 'Linearization of baculovirus DNA enhances the recovery of recombinant virus expression vectors', *Nucleic Acids Research,* 18(19), pp. 5667-5672.

Kitts, P. A. and Possee, R. (1993) 'A method for producing recombinant baculovirus expression vectors at high frequency', *Biotechniques,* 14(5), pp. 810-817.

Kleber, S., Sancho-Martinez, I., Wiestler, B., Beisel, A., Gieffers, C., Hill, O., Thiemann, M., Mueller, W., Sykora, J. and Kuhn, A. (2008) 'Yes and PI3K bind CD95 to signal invasion of glioblastoma', *Cancer cell,* 13(3), pp. 235-248.

Koda, N., Asaeda, T., Yamade, K., Kawahara, H. and Obata, H. (2001) 'A novel cryoprotective protein (CRP) with high activity from the ice-nucleating bacterium, Pantoea agglomerans IFO12686', *Bioscience, biotechnology, and biochemistry,* 65(4), pp. 888-894.

Kohane, D. S. (2007) 'Microparticles and nanoparticles for drug delivery', *Biotechnology and bioengineering,* 96(2), pp. 203-209.

Kohane, D. S., Tse, J. Y., Yeo, Y., Padera, R., Shubina, M. and Langer, R. (2006) 'Biodegradable polymeric microspheres and nanospheres for drug delivery in the peritoneum', *Journal of Biomedical Materials Research Part A: An Official Journal of The Society for Biomaterials, The Japanese Society for Biomaterials, and The Australian Society for Biomaterials and the Korean Society for Biomaterials,* 77(2), pp. 351-361.

Koivusalo, M., Welch, C., Hayashi, H., Scott, C. C., Kim, M., Alexander, T., Touret, N., Hahn, K. M. and Grinstein, S. (2010) 'Amiloride inhibits macropinocytosis by lowering submembranous pH and preventing Rac1 and Cdc42 signaling', *The Journal of cell biology,* 188(4), pp. 547-563.

Korkola, J. E., DeVries, S., Fridlyand, J., Hwang, E. S., Estep, A. L., Chen, Y.-Y., Chew, K. L., Dairkee, S. H., Jensen, R. M. and Waldman, F. M. (2003) 'Differentiation of lobular versus ductal breast carcinomas by expression microarray analysis', *Cancer research,* 63(21), pp. 7167-7175.

Kuhn, D. A., Vanhecke, D., Michen, B., Blank, F., Gehr, P., Petri-Fink, A. and Rothen-Rutishauser, B. (2014) 'Different endocytotic uptake mechanisms for nanoparticles in epithelial cells and macrophages', *Beilstein journal of nanotechnology,* 5, pp. 1625.

Kumar, P. and Clark, M. (2005) 'Clinical Medicine. 2005', *Edinburgh: WB Saunders,* 5.

Kundra, R. and Kornfeld, S. (1999) 'Asparagine-linked oligosaccharides protect Lamp-1 and Lamp-2 from intracellular proteolysis', *Journal of Biological Chemistry,* 274(43), pp. 31039-31046.

Kunigal, S., Lakka, S. S., Joseph, P., Estes, N. and Rao, J. S. (2008) 'Matrix metalloproteinase-9 inhibition down-regulates radiation-induced nuclear factor-κB activity leading to apoptosis in breast tumors', *Clinical Cancer Research,* 14(11), pp. 3617-3626.

Kuzio, J., Pearson, M. N., Harwood, S. H., Funk, C. J., Evans, J. T., Slavicek, J. M. and Rohrmann, G. F. (1999) 'Sequence and Analysis of the Genome of a Baculovirus Pathogenic forLymantria dispar', *Virology,* 253(1), pp. 17-34.

Laemmli, U. (1970) 'Most commonly used discontinuous buffer system for SDS electrophoresis', *Nature,* 227, pp. 680-685.

Lammich, S., Buell, D., Zilow, S., Ludwig, A.-K., Nuscher, B., Lichtenthaler, S. F., Prinzen, C., Fahrenholz, F. and Haass, C. (2010) 'Expression of the anti-amyloidogenic secretase ADAM10 is suppressed by its 5′-untranslated region', *Journal of Biological Chemistry*, pp. jbc. M110. 110742.

Lang, T. and De Chastellier, C. (1985) 'Fluid phase and mannose receptor-mediated uptake of horseradish peroxidase in mouse bone marrow-derived macrophages. Biochemical and ultrastructural study', *Biology of the Cell,* 53(2), pp. 149-154.

Larregina, A., Morelli, A., Dewey, R., Castro, M., Fontana, A. and Lowenstein, P. (1998) 'FasL induces Fas/Apo1-mediated apoptosis in human embryonic kidney 293 cells routinely used to generate E1-deleted adenoviral vectors', *Gene Therapy,* 5(4), pp. 563.

Legembre, P., Barnhart, B. C., Zheng, L., Vijayan, S., Straus, S. E., Puck, J., Dale, J. K., Lenardo, M. and Peter, M. E. (2004a) 'Induction of apoptosis and activation of NF-κB by CD95 require different signalling thresholds', *EMBO reports,* 5(11), pp. 1084-1089.

Legembre, P., Schickel, R., Barnhart, B. C. and Peter, M. E. (2004b) 'Identification of SNF1/AMP kinase-related kinase as an NF-κB-regulated anti-apoptotic kinase involved in CD95-induced motility and invasiveness', *Journal of Biological Chemistry,* 279(45), pp. 46742-46747.

Lettau, M., Voss, M., Ebsen, H., Kabelitz, D. and Janssen, O. (2014) 'Differential protein–protein interactions of full length human FasL and FasL fragments generated by proteolysis', *Experimental cell research,* 320(2), pp. 290-301.

Licari, P. and Bailey, J. (1991) 'Factors influencing recombinant protein yields in an insect cell–bacuiovirus expression system: Multiplicity of infection and intracellular protein degradation', *Biotechnology and bioengineering,* 37(3), pp. 238-246.

Linkermann, A., Qian, J., Lettau, M., Kabelitz, D. and Janssen, O. (2005) 'Considering Fas ligand as a target for therapy', *Expert opinion on therapeutic targets,* 9(1), pp. 119-134.

Liu, C.-H. and Wu, P.-S. (2006) 'Characterization of matrix metalloproteinase expressed by human embryonic kidney cells', *Biotechnology letters,* 28(21), pp. 1725-1730.

Liu, W., Zhan, C., Nathenson, S. and Almo, S. (2014) 'Crystal structures of FasL: DcR3 and LIGHT: DcR3 complexes reveal the molecular basis for the broad specificity of DcR3 (CCR5P. 255)', *The Journal of Immunology,* 192(1 Supplement), pp. 181.9-181.9.

Locksley, R. M., Killeen, N. and Lenardo, M. J. (2001) 'The TNF and TNF receptor superfamilies: integrating mammalian biology', *Cell,* 104(4), pp. 487-501.

Loibl, S. and Gianni, L. (2017) 'HER2-positive breast cancer', *The Lancet,* 389(10087), pp. 2415-2429.

Longley, D. and Johnston, P. (2005) 'Molecular mechanisms of drug resistance', *The Journal of Pathology: A Journal of the Pathological Society of Great Britain and Ireland,* 205(2), pp. 275-292.

Lu, Z., Elliott, M. R., Chen, Y., Walsh, J. T., Klibanov, A. L., Ravichandran, K. S. and Kipnis, J. (2011) 'Phagocytic activity of neuronal progenitors regulates adult neurogenesis', *Nature cell biology,* 13(9), pp. 1076.

Lucarelli, M., Gatti, A. M., Savarino, G., Quattroni, P., Martinelli, L., Monari, E. and Boraschi, D. (2004) 'Innate defence functions of macrophages can be biased by nano-sized ceramic and metallic particles', *European cytokine network,* 15(4), pp. 339-346.

Lückerath, K., Kirkin, V., Melzer, I. M., Thalheimer, F. B., Siele, D., Milani, W., Adler, T., Aguilar-Pimentel, A., Horsch, M. and Michel, G. (2010) 'Immune modulation by Fas ligand reverse signaling: lymphocyte proliferation is attenuated by the intracellular Fas ligand domain', *Blood*, pp. blood-2010-07-292722.

Macauley-Patrick, S., Fazenda, M. L., McNeil, B. and Harvey, L. M. (2005) 'Heterologous protein production using the Pichia pastoris expression system', *Yeast,* 22(4), pp. 249-270.

Macia, E., Ehrlich, M., Massol, R., Boucrot, E., Brunner, C. and Kirchhausen, T. (2006) 'Dynasore, a cell-permeable inhibitor of dynamin', *Developmental cell,* 10(6), pp. 839-850.

Malleter, M., Tauzin, S., Bessede, A., Castellano, R., Goubard, A., Godey, F., Levêque, J., Jézéquel, P., Campion, L. and Campone, M. (2013) 'CD95L cell surface cleavage triggers a prometastatic signaling pathway in triple-negative breast cancer', *Cancer research,* 73(22), pp. 6711-6721.

Matsen, C. B. and Neumayer, L. A. (2013) 'Breast cancer: a review for the general surgeon', *JAMA surgery,* 148(10), pp. 971-980.
Mayor, S. and Pagano, R. E. (2007) 'Pathways of clathrin-independent endocytosis', *Nature reviews Molecular cell biology,* 8(8), pp. 603.
Mayor, S., Parton, R. G. and Donaldson, J. G. (2014) 'Clathrin-independent pathways of endocytosis', *Cold Spring Harbor perspectives in biology,* 6(6), pp. a016758.
McMahon, K. M., Plebanek, M. P. and Thaxton, C. S. J. A. f. m. (2016) 'Properties of native high-density lipoproteins inspire synthesis of actively targeted in vivo siRNA delivery vehicles', 26(43), pp. 7824-7835.
Merrington, C. L., Bailey, M. J. and Possee, R. D. (1997) 'Manipulation of baculovirus vectors', *Molecular biotechnology,* 8(3), pp. 283-297.
Meza-Lamas, E., Ramírez-Sandoval, R., Sánchez-Rodríguez, S., López-Robles, E., Avalos-Díaz, E. and Herrera-Esparza, R. (2006) 'Camptothecin induces the transit of FasL trimers to the cell surface in apoptotic HEp-2 cells', *Cellular and Molecular Biology Letters,* 11(3), pp. 299-311.
Miele, E., Spinelli, G. P., Miele, E., Tomao, F. and Tomao, S. (2009) 'Albumin-bound formulation of paclitaxel (Abraxane® ABI-007) in the treatment of breast cancer', *International journal of nanomedicine,* 4, pp. 99.
Milhaud, J. (1992) 'Permeabilizing action of filipin III on model membranes through a filipin-phospholipid binding', *Biochimica et Biophysica Acta (BBA)-Biomembranes,* 1105(2), pp. 307-318.
Moghimi, S. M., Muir, I., Illum, L., Davis, S. S. and Kolb-Bachofen, V. (1993) 'Coating particles with a block co-polymer (poloxamine-908) suppresses opsonization but permits the activity of dysopsonins in the serum', *Biochimica et Biophysica Acta (BBA)-Molecular Cell Research,* 1179(2), pp. 157-165.
Motz, G. T., Santoro, S. P., Wang, L.-P., Garrabrant, T., Lastra, R. R., Hagemann, I. S., Lal, P., Feldman, M. D., Benencia, F. and Coukos, G. (2014) 'Tumor endothelium FasL establishes a selective immune barrier promoting tolerance in tumors', *Nature medicine,* 20(6), pp. 607-615.
Muraki, M. and Honda, S. (2010) 'Efficient production of human Fas receptor extracellular domain–human IgG1 heavy chain Fc domain fusion protein using baculovirus/silkworm expression system', *Protein expression and purification,* 73(2), pp. 209-216.
Muriel, O., Echarri, A., Hellriegel, C., Pavón, D. M., Beccari, L. and Del Pozo, M. A. (2011) 'Phosphorylated filamin A regulates actin-linked caveolae dynamics', *J Cell Sci,* 124(16), pp. 2763-2776.
Murmann, A. E., McMahon, K. M., Haluck-Kangas, A., Ravindran, N., Patel, M., Law, C. Y., Brockway, S., Wei, J.-J., Thaxton, C. S. and Peter, M. E. J. O. (2017) 'Induction of DISE in ovarian cancer cells in vivo', 8(49), pp. 84643.
Müschen, M., Moers, C., Warskulat, U., Even, J., Niederacher, D. and Beckmann, M. (2000) 'CD95 ligand expression as a mechanism of immune escape in breast cancer', *Immunology,* 99(1), pp. 69-77.
Nakase, I., Noguchi, K., Aoki, A., Takatani-Nakase, T., Fujii, I. and Futaki, S. (2017) 'Arginine-rich cell-penetrating peptide-modified extracellular vesicles for active macropinocytosis induction and efficient intracellular delivery', *Scientific reports,* 7(1), pp. 1991.
Nisihara, T., Ushio, Y., Higuchi, H., Kayagaki, N., Yamaguchi, N., Soejima, K., Matsuo, S., Maeda, H., Eda, Y. and Okumura, K. (2001) 'Humanization and epitope mapping of neutralizing anti-human Fas ligand monoclonal

antibodies: structural insights into Fas/Fas ligand interaction', *The Journal of Immunology,* 167(6), pp. 3266-3275.

Nounou, M. I., ElAmrawy, F., Ahmed, N., Abdelraouf, K., Goda, S. and Syed-Sha-Qhattal, H. (2015) 'Breast cancer: conventional diagnosis and treatment modalities and recent patents and technologies', *Breast cancer: basic and clinical research,* 9, pp. BCBCR. S29420.

Novak, P., Shevchuk, A., Ruenraroengsak, P., Miragoli, M., Thorley, A. J., Klenerman, D., Lab, M. J., Tetley, T. D., Gorelik, J. and Korchev, Y. E. (2014) 'Imaging single nanoparticle interactions with human lung cells using fast ion conductance microscopy', *Nano letters,* 14(3), pp. 1202-1207.

Ober, R. J., Martinez, C., Vaccaro, C., Zhou, J. and Ward, E. S. J. T. J. o. I. (2004) 'Visualizing the site and dynamics of IgG salvage by the MHC class I-related receptor, FcRn', 172(4), pp. 2021-2029.

Ofek, I., Goldhar, J., Keisari, Y. and Sharon, N. (1995) 'Nonopsonic phagocytosis of microorganisms', *Annual Reviews in Microbiology,* 49(1), pp. 239-276.

Ogiso, T., Iwaki, M. and Mori, K. (1981) 'Fluidity of human erythrocyte membrane and effect of chlorpromazine on fluidity and phase separation of membrane', *Biochimica et Biophysica Acta (BBA)-Biomembranes,* 649(2), pp. 325-335.

Orlinick, J. R., Elkon, K. B. and Chao, M. V. (1997) 'Separate domains of the human fas ligand dictate self-association and receptor binding', *Journal of Biological Chemistry,* 272(51), pp. 32221-32229.

Parton, R. G. and Del Pozo, M. A. (2013) 'Caveolae as plasma membrane sensors, protectors and organizers', *Nature reviews Molecular cell biology,* 14(2), pp. 98.

Patiño, T., Soriano, J., Barrios, L., Ibáñez, E. and Nogués, C. (2015) 'Surface modification of microparticles causes differential uptake responses in normal and tumoral human breast epithelial cells', *Scientific reports,* 5, pp. 11371.

Pereira, P., Pedrosa, S. S., Wymant, J. M., Sayers, E., Correia, A., Vilanova, M., Jones, A. T. and Gama, F. M. (2015) 'siRNA inhibition of endocytic pathways to characterize the cellular uptake mechanisms of folate-functionalized glycol chitosan nanogels', *Molecular pharmaceutics,* 12(6), pp. 1970-1979.

Peter, M., Hadji, A., Murmann, A., Brockway, S., Putzbach, W., Pattanayak, A. and Ceppi, P. (2015) 'The role of CD95 and CD95 ligand in cancer', *Cell Death & Differentiation,* 22(4), pp. 549-559.

Poole, L. B. (2015) 'The basics of thiols and cysteines in redox biology and chemistry', *Free Radical Biology and Medicine,* 80, pp. 148-157.

Possee, R. and Howard, S. (1987) 'Analysis of the polyhedrin gene promoter of the Autographa californica nuclear polyhedrosis virus', *Nucleic acids research,* 15(24), pp. 10233-10248.

Possee, R. D., Sun, T.-P., Howard, S. C., Ayres, M. D., Hill-Perkins, M. and Gearing, K. L. (1991) 'Nucleotide sequence of the Autographa californica nuclear polyhedrosis 9.4 kbp EcoRI-I and-R (polyhedrin gene) region', *Virology,* 185(1), pp. 229-241.

Putzbach, W., Gao, Q. Q., Patel, M., Van Dongen, S., Haluck-Kangas, A., Sarshad, A. A., Bartom, E. T., Kim, K.-Y. A., Scholtens, D. M. and Hafner, M. (2017) 'Many si/shRNAs can kill cancer cells by targeting multiple survival genes through an off-target mechanism', *Elife,* 6, pp. e29702.

Rabinovitch, M. (1995) 'Professional and non-professional phagocytes: an introduction', *Trends in cell biology,* 5(3), pp. 85-87.

Rankin, C., Ladin, B. F. and Weaver, R. F. (1986) 'Physical mapping of temporally regulated, overlapping transcripts in the region of the 10K protein gene in Autographa californica nuclear polyhedrosis virus', *Journal of virology,* 57(1), pp. 18-27.

Recouvreux, M. V. and Commisso, C. (2017) 'Macropinocytosis: A Metabolic Adaptation to Nutrient Stress in Cancer', *Frontiers in endocrinology,* 8, pp. 261.

Redelman-Sidi, G., Binyamin, A., Gaeta, I., Palm, W., Thompson, C. B., Romesser, P. B., Lowe, S. W., Bagul, M., Doench, J. G. and Root, D. E. (2018) 'The Canonical Wnt Pathway Drives Macropinocytosis in Cancer', *Cancer research*, pp. canres. 3199.2017.

Rejman, J., Oberle, V., Zuhorn, I. S. and Hoekstra, D. (2004) 'Size-dependent internalization of particles via the pathways of clathrin-and caveolae-mediated endocytosis', *Biochemical Journal,* 377(1), pp. 159-169.

Richman, D., Cleveland, P., Oxman, M. and Johnson, K. J. T. J. o. I. (1982) 'The binding of staphylococcal protein A by the sera of different animal species', 128(5), pp. 2300-2305.

Roché, H., Fumoleau, P., Spielmann, M., Canon, J.-L., Delozier, T., Serin, D., Symann, M., Kerbrat, P., Soulié, P. and Eichler, F. (2006) 'Sequential adjuvant epirubicin-based and docetaxel chemotherapy for node-positive breast cancer patients: the FNCLCC PACS 01 Trial', *Journal of Clinical Oncology,* 24(36), pp. 5664-5671.

Roopenian, D. C. and Akilesh, S. (2007) 'FcRn: the neonatal Fc receptor comes of age', *Nature Reviews Immunology,* 7(9), pp. 715-725.

Sanders, D., Nettleship, Zampronio, Cooper, Owens, Owen, Linton 2015. The Glycans of the Scavenger Receptor CD36 are not required for ligand binding. In preparation.

Sant, S. and Johnston, P. A. (2017) 'The production of 3D tumor spheroids for cancer drug discovery', *Drug Discovery Today: Technologies,* 23, pp. 27-36.

Saville, G. P., Patmanidi, A. L., Possee, R. D. and King, L. A. (2004) 'Deletion of the Autographa californica nucleopolyhedrovirus chitinase KDEL motif and in vitro and in vivo analysis of the modified virus', *Journal of general virology,* 85(4), pp. 821-831.

Sayers, T. J. (2011) 'Targeting the extrinsic apoptosis signaling pathway for cancer therapy', *Cancer Immunology, Immunotherapy,* 60(8), pp. 1173-1180.

Schmidt, E. V., Christoph, G., Zeller, R. and Leder, P. (1990) 'The cytomegalovirus enhancer: a pan-active control element in transgenic mice', *Molecular and Cellular Biology,* 10(8), pp. 4406-4411.

Schneider, P., Bodmer, J.-L., Holler, N., Mattmann, C., Scuderi, P., Terskikh, A., Peitsch, M. C. and Tschopp, J. (1997) 'Characterization of Fas (Apo-1, CD95)-fas ligand interaction', *Journal of Biological Chemistry,* 272(30), pp. 18827-18833.

Schneider, P., Holler, N., Bodmer, J.-L., Hahne, M., Frei, K., Fontana, A. and Tschopp, J. (1998) 'Conversion of membrane-bound Fas (CD95) ligand to its soluble form is associated with downregulation of its proapoptotic activity and loss of liver toxicity', *The Journal of experimental medicine,* 187(8), pp. 1205-1213.

Schottenfeld, D. and Fraumeni Jr, J. F. (2006) *Cancer epidemiology and prevention.* Oxford University Press.
Schwarz, F. and Aebi, M. (2011) 'Mechanisms and principles of N-linked protein glycosylation', *Current opinion in structural biology,* 21(5), pp. 576-582.
Shang, L., Nienhaus, K. and Nienhaus, G. U. (2014) 'Engineered nanoparticles interacting with cells: size matters', *Journal of nanobiotechnology,* 12(1), pp. 5.
Shatnyeva, O. M., Kubarenko, A. V., Weber, C. E., Pappa, A., Schwartz-Albiez, R., Weber, A. N., Krammer, P. H. and Lavrik, I. N. (2011) 'Modulation of the CD95-induced apoptosis: the role of CD95 N-glycosylation', *PloS one,* 6(5), pp. e19927.
Siegel, R. M., Frederiksen, J. K., Zacharias, D. A., Chan, F. K.-M., Johnson, M., Lynch, D., Tsien, R. Y. and Lenardo, M. J. (2000) 'Fas preassociation required for apoptosis signaling and dominant inhibition by pathogenic mutations', *Science,* 288(5475), pp. 2354-2357.
Simons, K. and Toomre, D. (2000) 'Lipid rafts and signal transduction', *Nature reviews Molecular cell biology,* 1(1), pp. 31.
Smith, I. E. and Dowsett, M. (2003) 'Aromatase inhibitors in breast cancer', *New England Journal of Medicine,* 348(24), pp. 2431-2442.
Sodoyer, R. (2004) 'Expression systems for the production of recombinant pharmaceuticals', *BioDrugs,* 18(1), pp. 51-62.
Sorrell, J. M. and Caplan, A. I. (2004) 'Fibroblast heterogeneity: more than skin deep', *Journal of cell science,* 117(5), pp. 667-675.
Strande, V., Canelle, L., Tastet, C., Burlet-Schiltz, O., Monsarrat, B. and Hondermarck, H. (2009) 'The proteome of the human breast cancer cell line MDA-MB-231: Analysis by LTQ-Orbitrap mass spectrometry', *PROTEOMICS-Clinical Applications,* 3(1), pp. 41-50.
Strasser, A., Jost, P. J. and Nagata, S. (2009) 'The many roles of FAS receptor signaling in the immune system', *Immunity,* 30(2), pp. 180-192.
Sträter, J., Walczak, H., Hasel, C., Melzner, I., Leithäuser, F. and Möller, P. (2001) 'CD95 ligand (CD95L) immunohistochemistry: a critical study on 12 antibodies', *Cell death and differentiation,* 8(3), pp. 273.
Suda, T., Takahashi, T., Golstein, P. and Nagata, S. (1993) 'Molecular cloning and expression of the Fas ligand, a novel member of the tumor necrosis factor family', *Cell,* 75(6), pp. 1169-1178.
Sun, T., Zhang, Y. S., Pang, B., Hyun, D. C., Yang, M. and Xia, Y. (2014) 'Engineered nanoparticles for drug delivery in cancer therapy', *Angewandte Chemie International Edition,* 53(46), pp. 12320-12364.
Sun, Y., Martin, A. C. and Drubin, D. G. (2006) 'Endocytic internalization in budding yeast requires coordinated actin nucleation and myosin motor activity', *Developmental cell,* 11(1), pp. 33-46.
Sung, S., Nelson, R. S. and Silverstein, S. C. (1983) 'Yeast mannans inhibit binding and phagocytosis of zymosan by mouse peritoneal macrophages', *The Journal of cell biology,* 96(1), pp. 160-166.
Swanson, J. A. (2008) 'Shaping cups into phagosomes and macropinosomes', *Nature reviews Molecular cell biology,* 9(8), pp. 639.
Swanson, J. A. and Hoppe, A. D. (2004) 'The coordination of signaling during Fc receptor-mediated phagocytosis', *Journal of leukocyte biology,* 76(6), pp. 1093-1103.
Takahashi, T., Tanaka, M., Brannan, C. I., Jenkins, N. A., Copeland, N. G., Suda, T. and Nagata, S. (1994a) 'Generalized lymphoproliferative disease in

mice, caused by a point mutation in the Fas ligand', *Cell,* 76(6), pp. 969-976.

Takahashi, T., Tanaka, M., Inazawa, J., Abe, T., Suda, T. and Nagata, S. (1994b) 'Human Fas ligand: gene structure, chromosomal location and species specificity', *International immunology,* 6(10), pp. 1567-1574.

Tanaka, M., Itai, T., Adachi, M. and Nagata, S. (1998) 'Downregulation of Fas ligand by shedding', *Nature medicine,* 4(1), pp. 31-36.

Tanaka, M., Suda, T., Takahashi, T. and Nagata, S. (1995) 'Expression of the functional soluble form of human Fas ligand in activated lymphocytes', *The EMBO Journal,* 14(6), pp. 1129.

Taticek, R., Choi, C., Phan, S. E., Palomares, L. and Shuler, M. (2001) 'Comparison of growth and recombinant protein expression in two different insect cell lines in attached and suspension culture', *Biotechnology progress,* 17(4), pp. 676-684.

Teng, S. F., Sproule, K., Husain, A. and Lowe, C. R. (2000) 'Affinity chromatography on immobilized “biomimetic” ligands: synthesis, immobilization and chromatographic assessment of an immunoglobulin G-binding ligand', *Journal of Chromatography B: Biomedical Sciences and Applications,* 740(1), pp. 1-15.

Thomas, C. J., Brown, H. L., Hawes, C. R., Lee, B. Y., Min, M.-K., King, L. A. and Possee, R. D. (1998) 'Localization of a baculovirus-induced chitinase in the insect cell endoplasmic reticulum', *Journal of virology,* 72(12), pp. 10207-10212.

Thompson, D. B., Villaseñor, R., Dorr, B. M., Zerial, M. and Liu, D. R. (2012) 'Cellular uptake mechanisms and endosomal trafficking of supercharged proteins', *Chemistry & biology,* 19(7), pp. 831-843.

Thornhill, P. B., Cohn, J. B., Stanford, W. L. and Desbarats, J. (2008) 'The adaptor protein Grb2 regulates cell surface Fas ligand in Schwann cells', *Biochemical and biophysical research communications,* 376(2), pp. 341-346.

Tretter, V., Altmann, F. and März, L. (1991) 'Peptide-N4-(N-acetyl-β-glucosaminyl) asparagine amidase F cannot release glycans with fucose attached α1→ 3 to the asparagine-linked N-acetylglucosamine residue', *European Journal of Biochemistry,* 199(3), pp. 647-652.

Treuel, L., Jiang, X. and Nienhaus, G. U. (2013) 'New views on cellular uptake and trafficking of manufactured nanoparticles', *Journal of The Royal Society Interface,* 10(82), pp. 20120939.

Turner, N. C., Neven, P., Loibl, S. and Andre, F. (2017) 'Advances in the treatment of advanced oestrogen-receptor-positive breast cancer', *The Lancet,* 389(10087), pp. 2403-2414.

van Regenmortel, M. H., Fauquet, C. M., Bishop, D. H., Carstens, E., Estes, M., Lemon, S., Maniloff, J., Mayo, M., McGeoch, D. and Pringle, C. (2000) *Virus taxonomy: classification and nomenclature of viruses. Seventh report of the International Committee on Taxonomy of Viruses.* Academic Press.

Vaughn, J., Goodwin, R., Tompkins, G. and McCawley, P. (1977) 'The establishment of two cell lines from the insectSpodoptera frugiperda (Lepidoptera; Noctuidae)', *In vitro,* 13(4), pp. 213-217.

Vercauteren, D., Vandenbroucke, R. E., Jones, A. T., Rejman, J., Demeester, J., De Smedt, S. C., Sanders, N. N. and Braeckmans, K. (2010) 'The use of inhibitors to study endocytic pathways of gene carriers: optimization and pitfalls', *Molecular Therapy,* 18(3), pp. 561-569.

Voss, M., Lettau, M., Paulsen, M. and Janssen, O. (2008) 'Posttranslational regulation of Fas ligand function', *Cell Communication and Signaling,* 6(1), pp. 1.

Wang, A. Z., Langer, R. and Farokhzad, O. C. (2012) 'Nanoparticle delivery of cancer drugs', *Annual review of medicine,* 63, pp. 185-198.

Watanaba, F., Brannan, I. and CopelandN, G. (1992) 'Lymphoproliferation disorder in m ice explained by defects in Fas antigen thatmediatedapoptosis', *Nature,* 356, pp. 314-317.

Wesselborg, S., Engels, I. H., Rossmann, E., Los, M. and Schulze-Osthoff, K. (1999) 'Anticancer drugs induce caspase-8/FLICE activation and apoptosis in the absence of CD95 receptor/ligand interaction', *Blood,* 93(9), pp. 3053-3063.

Wickham, T., Davis, T., Granados, R., Shuler, M. and Wood, H. (1992) 'Screening of insect cell lines for the production of recombinant proteins and infectious virus in the baculovirus expression system', *Biotechnology progress,* 8(5), pp. 391-396.

Wilde, M., Klausberger, M., Palmberger, D., Ernst, W. and Grabherr, R. (2014) 'Tnao38, high five and Sf9—evaluation of host–virus interactions in three different insect cell lines: baculovirus production and recombinant protein expression', *Biotechnology letters,* 36(4), pp. 743-749.

Wong, K. T., Peter, C. H., Greenfield, P. F., Reid, S. and Nielsen, L. K. (1996) 'Low multiplicity infection of insect cells with a recombinant baculovirus: the cell yield concept', *Biotechnology and bioengineering,* 49(6), pp. 659-666.

Wood, A. J., Rowinsky, E. K. and Donehower, R. C. (1995) 'Paclitaxel (taxol)', *New England Journal of Medicine,* 332(15), pp. 1004-1014.

Wood, W., Turmaine, M., Weber, R., Camp, V., Maki, R. A., McKercher, S. R. and Martin, P. (2000) 'Mesenchymal cells engulf and clear apoptotic footplate cells in macrophageless PU. 1 null mouse embryos', *Development,* 127(24), pp. 5245-5252.

Woodward, W. A. and Cristofanilli, M. 'Inflammatory breast cancer'. *Seminars in radiation oncology*: Elsevier, 256-265.

Yang, Z. and Zhang, C. (2012) 'Advances on BmNPV functional genomics', *J Biotechnol Biomaterial S,* 9, pp. 2.

Yuan, F., Dellian, M., Fukumura, D., Leunig, M., Berk, D. A., Torchilin, V. P. and Jain, R. K. (1995) 'Vascular permeability in a human tumor xenograft: molecular size dependence and cutoff size', *Cancer research,* 55(17), pp. 3752-3756.

Zhao, J. and Stenzel, M. H. (2018) 'Entry of nanoparticles into cells: the importance of nanoparticle properties', *Polymer Chemistry,* 9(3), pp. 259-272.

Ziegler, R. G., Hoover, R. N., Pike, M. C., Hildesheim, A., Nomura, A. M., West, D. W., Wu-Williams, A. H., Kolonel, L. N., Horn-Ross, P. L. and Rosenthal, J. F. (1993) 'Migration patterns and breast cancer risk in Asian-American women', *JNCI: Journal of the National Cancer Institute,* 85(22), pp. 1819-1827.